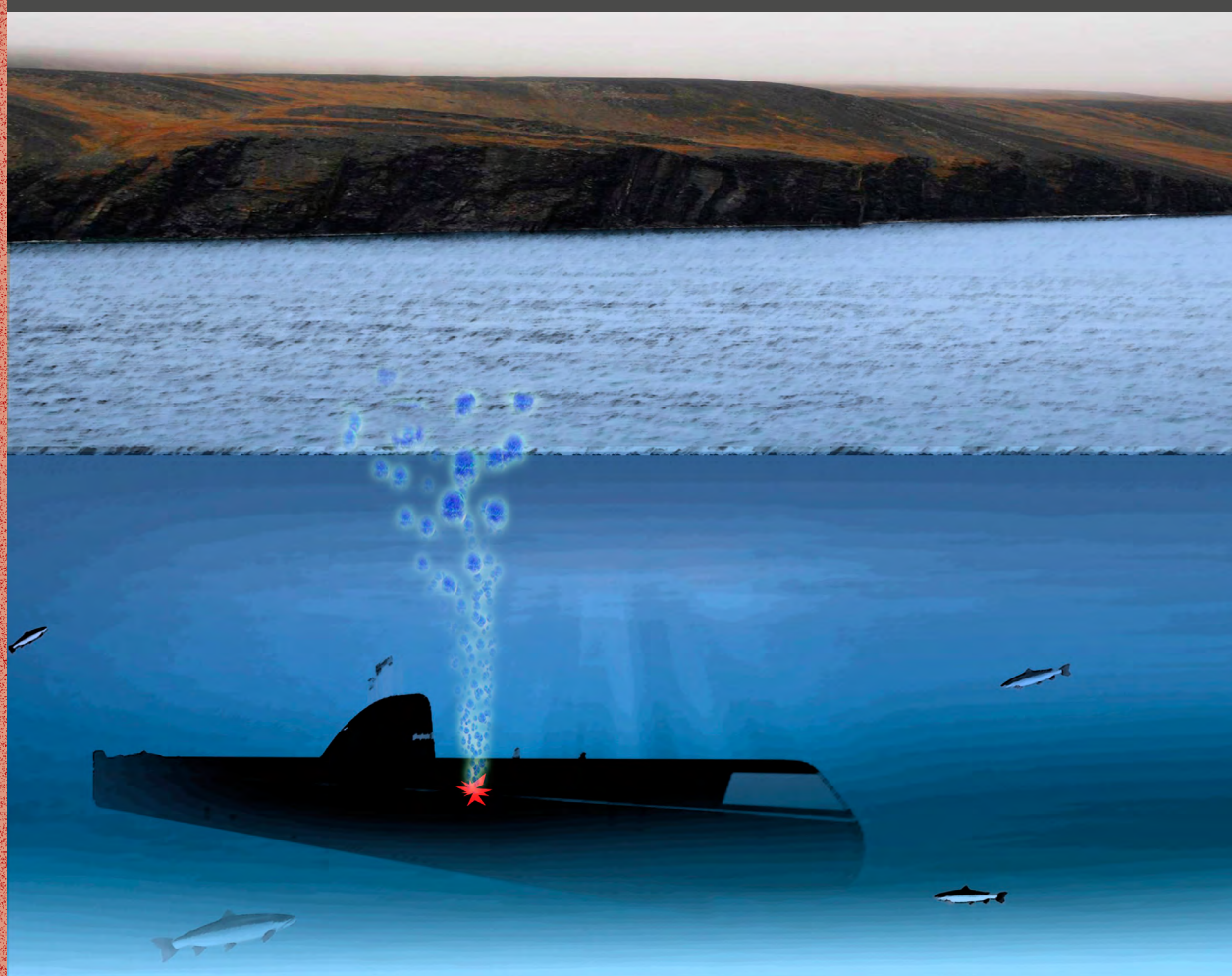


Statens strålevern
Norwegian Radiation Protection Authority



STRÅLEVERN RAPPORT 2016:8



**Environmental modelling and radiological
impact assessment associated with
hypothetical accident scenarios for
the nuclear submarine K-27**

Reference:

Hosseini A, Amundsen I, Bartnicki J, Brown J, Dowdall M, Dyve JE, Harm I, Karcher M, Kauker F, Klein H, Lind OC, Salbu B, Schnur R, Standring W. Environmental modelling and radiological impact assessment associated with hypothetical accident scenarios for the nuclear submarine K-27. StrålevernRapport 2016:8. Østerås: Statens strålevern, 2016.

Key words:

Dumped objects in the Arctic, Liquid Metal Reactor, LMR, Submarine K-27, Recovery of K-27, Contamination, Consequences, Concentration, Doses, Criticality scenarios,

Abstract:

The report presents the second part of the work related to radiological impact assessment of the dumped Russian nuclear submarine K-27. Broadly, the report can be divided into two parts; the first part focusing on the dispersion of radioactivity in the environment and its fate with regards to exposure situations relevant for environmental impact assessments and the second part focusing on the consequences of releases of radioactivity into the environment and calculation of doses.

Referanse:

Hosseini A, Amundsen I, Bartnicki J, Brown J, Dowdall M, Dyve JE, Harm I, Karcher M, Kauker F, Klein H, Lind OC, Salbu B, Schnur R, Standring W. Environmental modelling and radiological impact assessment associated with hypothetical accident scenarios for the nuclear submarine K-27. StrålevernRapport 2016:8. Østerås: Statens strålevern, 2016.

Emneord:

Dumpede objekter i Arktisk, LMR, atomubåt K-27, kritikalitet scenarier, løfting av K-27, konsekvensvurderinger, nedfall, radioaktivitet, doser

Resymé:

Rapporten presenterer resultater fra den siste delen av arbeidet knyttet til radiologisk konsekvensvurderinger av den russiske atomubåten K-27. I hovedsak består rapporten av to deler; den første delen fokuserer på potensiell spredning av radioaktivitet i miljøet med hensyn til forskjellige eksponeringssituasjoner og andre del fokuserer på konsekvensene av utslipp av radioaktivitet til miljøet og beregning av doser.

Head of project: Ali Hosseini

Approved:



Per Strand, director, Department of Department for Emergency Preparedness and Environmental Radioactivity.

134 pages.

Published 2016-09-02

Cover design: 07 Media.

Printed by 07 Media.

Printed number: 100 (09-16)

Cover photo: Ali Hosseini

Norwegian Radiation Protection Authority, P.O. Box 55, N-1332 Østerås, Norway.

Telephone +47 67 16 25 00, fax + 47 67 14 74 07.

E-mail: nrpa@nrpa.no

www.nrpa.no

ISSN 1891-5205 (online)

ISSN 0804-4910 (print)

StrålevernRapport 2016:8

**Environmental modelling and radiological
impact assessment associated with
hypothetical accident scenarios for the
nuclear submarine K-27**

Ali Hosseini

Statens strålevern
Norwegian Radiation
Protection Authority
Østerås, 2016

Table of contents

1.	Introduction	7
2.	Review of earlier works: Arctic marine dispersion modelling	9
2.1	Modelling marine radioactivity	9
	2.1.1 <i>Model set-up</i>	9
	2.1.2 <i>Model physics</i>	9
	2.1.3 <i>Model forcing</i>	10
2.2	Previous near field dispersion modelling for Stepovogo Fjord	10
2.3	New assessments of local dispersion from a potential K-27 recovery accident	11
	2.3.1 <i>Considerations for a worst case scenario</i>	11
	2.3.2 <i>Considerations for a continuous release scenario</i>	12
2.4	Far Field Assessment and transport of radioactivity by Arctic sea ice	13
3.	Marine dispersion modelling	14
3.1	Model description	14
3.2	Setup of the tracer release experiments	15
3.3	Motivation of the experimental set-up: Variability of circulation	15
	3.3.1 <i>The 1983 versus the 1988 flow field: Two different Arctic-wide circulations</i>	15
	3.3.2 <i>The 1998 flow regime: the reverse flow from Kara Sea to Barents</i>	16
3.4	Model Experiments: results	17
	3.4.1 <i>Instantaneous Release Experiments</i>	17
	3.4.2 <i>Continuous Release Experiments</i>	28
3.5	Selected sea water activity concentrations for estimation of doses	31
4.	Atmospheric dispersion	34
4.1	SNAP: the atmospheric dispersion model	34
4.2	Selection of the worst case meteorological scenario	35
4.3	Selection procedure	35
	4.3.1 <i>Source term for the selection procedure</i>	35
4.4	Worst case meteorological scenarios	37
	4.4.1 <i>Worst case scenario related to an accident at Stepovogo Fjord</i>	38
	4.4.2 <i>Worst case scenario related to an accident during transport</i>	39
	4.4.3 <i>Worst case scenario for a release at Gremikha</i>	41
4.5	Statistical analysis	43
	4.5.1 <i>Metrological cases which results in deposition in Norway</i>	43
	4.5.2 <i>Probability of arrival</i>	44
4.6	Source term for selected scenarios	46
	4.6.1 <i>Source term for the SNAP runs</i>	46
4.7	Model runs for the worst case scenarios	49
	4.7.1 <i>Accident at the Stepovogo Fjord</i>	49
	4.7.2 <i>Accident on the way to Gremikha</i>	49

4.7.3	<i>Release at Gremikha Bay - general worst case scenario</i>	52
4.7.4	<i>Depositions from individual components</i>	54
4.7.5	<i>Dynamics of transport</i>	54
4.7.6	<i>Time integrated concentrations</i>	55
4.7.7	<i>Comparison with Chernobyl Accident</i>	55
5.	New considerations regarding release scenarios	57
5.1	Release scenario for marine dispersion	57
5.2	New analysis of atmospheric dispersion based on different assumptions and more "realistic" considerations	58
5.2.1	<i>New source term</i>	60
5.2.2	<i>Considerations regarding the fire scenario at Gremikha</i>	60
5.2.3	<i>Considerations regarding maximum SCR scenario at Stepovogo Fjord</i>	62
6.	Considerations regarding dose assessment methodology	64
6.1	Quantifying exposures and consequent impacts to man and the environment	64
6.2	Modelling transfer of radionuclides through food-chains	65
6.3	Modelling doses to humans and the environment	66
6.3.1	<i>Models used for human dose assessment</i>	66
6.3.1.1	<i>Parametrisation of the human dose assessment models in relation to various exposed groups</i>	67
6.3.2	<i>Models used for environmental impact assessment</i>	71
6.3.2.1	<i>Parametrisation of the environmental dose assessment models</i>	72
6.4	Contextualising impacts to humans and the environment	73
6.4.1	<i>Humans</i>	73
6.4.2	<i>Environment</i>	74
7.	Results: Activity concentrations	76
7.1	Terrestrial ecosystem	76
7.2	Marine ecosystem	80
7.2.1	<i>Gremikha release scenario</i>	80
7.2.2	<i>Stepovogo release scenario</i>	82
8.	Results: Dose estimates	85
8.1	Estimation of doses to humans	85
8.1.1	<i>Human Dose estimates for Stepovogo</i>	85
8.1.2	<i>Human Dose estimates for Gremikha</i>	88
8.2	Dose estimation for non-human biota	89
8.2.1	<i>Terrestrial</i>	89
8.2.2	<i>Marine</i>	91
8.2.2.1	<i>Gremikha release scenario</i>	91
8.2.2.2	<i>Stepovogo release scenario</i>	92
9.	Dealing with uncertainties	94
10.	Summary and concluding remarks	96

11.	Acknowledgments	99
	Appendix A: Previous studies: Near and far field dispersion modelling	100
A1	Near field dispersion modelling	100
	<i>A1.1 Flushing time scenarios</i>	100
	<i>A1.2 Release rate scenarios with simplified forcing</i>	100
	<i>A1.3 Release rate scenarios with realistic forcing</i>	102
A2	Far Field Assessment: a perspective view	107
	<i>A2.1 Far field dispersion from radioactive sources in the Kara Sea</i>	107
	<i>A2.2 Release scenarios for the sunken submarine 'Kursk'</i>	108
	<i>A2.3 Transport of radioactivity by Arctic sea ice</i>	110
	Appendix B: Marine dispersion modelling	113
B1	Hydrodynamics	113
B2	Transport modelling	113
B3	Thermodynamics / Sea Ice	114
	Appendix C: Atmospheric dispersion modelling: SNAP model	115
C1	Parametrization of the source term	115
C2	Mixing Height	115
C3	Advection, diffusion and gravitational settling	115
C4	Boundary conditions	115
C5	Dry deposition	116
C6	Wet deposition	116
C7	Radioactive decay	117
	Appendix D: Modelling transfer of radionuclides through food-chains	118
D1	Marine food-chain model description	118
D2	Terrestrial food-chain Model description	120
	Glossary	127
	References	130

1. Introduction

There is increasing concern over potential radioactive contamination of the Arctic due to the presence of a wide range of nuclear sources within this region. Dumped radioactive waste contributes the greatest proportion to the total activity found in the Arctic followed by inputs from Sellafield and global fallout (Sarkisov et al., 2009). Of these, dumped objects containing Spent Nuclear Fuel (SNF) are of special importance.

Dumping of radioactive wastes into the world oceans was widespread in the decades following the Second World War. The first dumping was conducted by the USA in the Pacific Ocean in 1946 and the last one took place in the Sea of Japan in 1993 by the Russian Federation (IAEA, 1999a). Between 1959 and 1992, solid and liquid radioactive waste were dumped in the Arctic Seas first by the Former Soviet Union and then by the Russian Federation (Sarkisov et al., 2009).

After more than three decades of dispute, an agreement on the total banning of dumping of any radioactive waste to the marine environment was reached in 1993 by the London Convention member-states (IAEA, 1999a).

All objects and nuclear waste which have been dumped in the Arctic present a real and potential hazard that, given the unique and vulnerable Arctic ecosystem, give rise to concerns due to the effects of possible leakages of radioactivity.

Amongst dumped objects in the Arctic, the Russian submarine K-27 has received much attention due to particular concerns related to this vessel: it contains two reactors with highly enriched SNF and lies at a depth of about 30 m under water.

To address these concerns, the Norwegian Radiation Protection Authority (NRPA) initiated a study in 2013 to examine the radiological consequences of the dumped submarine K-27 for both humans and the environment. The dumped K-27 is also of particular interest to Norway, given its proximity and importance of northern sea areas for Norway and Norwegian economic interests.

The study is based on derivation of different hypothetical accident scenarios and evaluating possible associated consequences for humans and the environment. In general, three main scenarios seem plausible and thus appropriate for consideration. The first is the “zero- alternative”, i.e. investigate the current and future impact assuming no interventions. The second considers an accidental scenario involving the raising of the submarine and the third an accidental scenario related to the transportation of the submarine to shore for defueling.

With regards to the accidental scenarios related to raising and transportation of the submarine, two alternatives can be considered depending on where and how a hypothetical accident could take place and whether the subsequent releases occur underwater or at the water surface. The issue of an uncontrolled chain reaction occurring as a result of a potential recovery of the submarine is included in the assessment.

The work includes application of state of the art 3D hydrodynamic and atmospheric dispersion models to investigate the transport, distribution and fate of relevant radionuclides following hypothetical accidents that result in releases to aquatic and terrestrial ecosystems. The outputs from these dispersion models have been used as inputs to food-chain transfer and environmental dosimetry models such as ERICA (Brown et al., 2008) and other well developed models (exposure pathways-based models for humans). The resultant doses to human and biota have been calculated and associated consequences have been evaluated.

The first part of this work was completed in 2015 and its findings published as a NRPA report (Hosseini et al., 2015). The second and final part of the work is presented in this report. The first report's main focus was to provide an overview of the extant and available facts and information regarding the submarine, characterising the source term and considering the various conditions under which a spontaneous chain reaction might occur. Furthermore, the findings detailed in Hosseini et al. (2015) have been used as inputs for this second and final part of the work where the focus has been on the modelling of radionuclide

advection and dispersion in the environment and subsequent assessment of doses and associated consequences.

This report moves from compiling facts and relevant data to computer simulations using pre-defined scenarios. This necessitates application and parametrisation of several models as well as making use of various assumptions. All these have an impact on the obtained results and also the type and amount of uncertainty involved in them. To deal with uncertainty and consequently lend credibility to the outcomes of the modelling work, conservatism has been introduced at various points in the present study.

The report can be broadly divided into two parts; the first part focusing on the transport of radioactivity in the environment and its fate with regards to exposure situations relevant for environmental impact assessments and the second part focusing on the consequences of releases of radioactivity into the environment and calculation of doses.

The report starts by discussing issues relevant for marine dispersion in order to provide a background for subsequent sections which present the results of the marine dispersion modelling. Next, the results from atmospheric dispersion modelling will be presented. The outputs from dispersion modelling are used as inputs to the models which deal with estimation of activity concentrations in the environment including biological components important for human exposures. In the chapters that follow the methodology used is introduced and results obtained are presented - estimated activity concentrations and calculated doses for both humans and non-human biota.

The work reported here is financed with funding from the Norwegian government's Nuclear Action Plan with allocation from the Ministry of Foreign Affairs.

2. Review of earlier works: Arctic marine dispersion modelling

In order to have an overview of the published literature regarding the dispersion of radioactivity associated with dumped objects in the Kara Sea, a review of existing studies was conducted (see Appendix A). Before going further, we will first highlight some general aspects of oceanographic dispersion modelling (Harms and Karcher, 2003; Harms et al., 2003) and hence provide some basis to facilitate understanding and interpreting the outputs of such models.

2.1 Modelling marine radioactivity

2.1.1 Model set-up

The model systems applied in the studies referred to in the following sections are based on classical approaches in hydrodynamic and transport modelling which make use of numerical models. Such models consist of mathematical equations which are solved for discrete time steps on a regular or irregular grid that covers the model domain containing the region of interest. A model study requires the selection of a model domain, the definition of the model grid and the determination of the grid size. The regional focus and the spatial extent are the most obvious differences between various model studies. In the current case of dispersion scenarios for Kara Sea dump sites, the spatio-temporal aspect can be separated into three groups:

- **Near field or local scale applications** that deal with estuaries, fjords, bays or straits. Typical size of the model domain: 1-100 km, typical grid size: 0.01 – 5 kilometres.
- **Medium range or regional scale applications** that deal with shelf areas or semi-enclosed seas. Typical size of the model domain: 100 – 1000 km, typical grid size: 5 – 50 kilometres.
- **Far field or global / basin scale applications** that deal with large ocean basins or whole oceans. Typical size of the model domain: 1000 km – global scale, typical grid size: 10 – 50 kilometres.

Previous studies have used this model hierarchy to assess radiological contamination on all scales, from the North Atlantic, the Nordic Seas, the Arctic Ocean and down to the dump sites in the Kara Sea.

2.1.2 Model physics

Hydrodynamic model studies on dispersion of marine radioactivity involve basically two model types: a hydrodynamic circulation model and a transport model. The hydrodynamic model calculates the three-dimensional flow field, depending on model representations of external forcing and internal physics, whereas the transport model calculates the dispersion of a tracer according to a previously computed flow.

There are two basic approaches for dispersion modelling: the *Eulerian* approach that calculates the exchange of radionuclide concentrations between adjacent grid boxes in time and space and the *Lagrangian* approach that applies a particle tracking method which follows a trajectory in space and time.

In small scale applications, such as for the fjords of Novaya Zemlya, the Eulerian approach, which is the most common approach in numerical dispersion modelling, is used. It is frequently used for the dispersion of dynamically active variables like temperature and salinity. In principle, the transport algorithm for temperature or salinity is assigned to radioactivity as a third tracer. As long as no further sources or sinks are considered such an approach is appropriate for conservative and soluble radionuclides with relatively long half-lives.

However, radionuclides in the marine environment may also be particle reactive, adding a new physical process to the simple redistribution of the tracer by the flow field in a conservative, passive form. Particle

reactive radionuclides in turn tend to attach to particles or suspended material in the water column which constitutes a sink for the dissolved radioactive load in the water column. Where appropriate a simple non-conservative approach is applied for simulating radioactivity in both phases. Details on this approach are described in Appendix A2.

Ice transport can play a significant role in redistributing particle reactive radionuclides as well (Dethleff, et al., 2000). This effect is omitted for the local scale, however, the process is discussed with respect to large scale dispersion pathways in Appendix B3.

2.1.3 Model forcing

Depending on the task which a hydrodynamic circulation model is used to solve, different kinds of external driving forces can be applied. The external driving forces initiate the circulation which, in turn, is responsible for the advection and diffusion of the tracers. These driving forces are applied to the model via the setting of boundary conditions at the sea surface, at lateral boundaries or as a tide generating force on the entire volume. The details of the application of the external forcing via the boundary conditions is an essential part of the experimental design which is governed by the questions to be answered by the model experiment.

An important aspect in terms of model forcing is the temporal and spatial resolution of the meteorological input data. On very small spatial scales, the atmospheric forcing at the sea surface is determined by direct observation. For modelling over larger spatial scales, the use of meteorological observational data sets or the products of meteorological forecast models is more common.

Although the fjord simulations in earlier studies were performed for a very small scale, it was not possible to use direct observations as forcing data because such data were not available. Instead the fjord scenarios were forced with idealized wind situations such as on-shore or off-shore wind directions at different wind speeds. An exception was the use of atmospheric data from the European Centre for Medium-Range Weather Forecasts (ECMWF) reanalysis where explicitly noted.

Another important aspect is the presence of an ice cover. The fjord model accounts for the change in momentum transfer in the presence of an immobile ice sheet. During winter it can be assumed, that a land-fast ice cover is established at the surface that largely inhibits any transfer of momentum by wind at the sea surface. As a result, summer and winter circulation patterns differ considerably in dynamic intensity.

2.2 Previous near field dispersion modelling for Stepovogo Fjord

Realistic release rate scenarios for Stepovogo Fjord were performed by Koziy et al. (1998). These model simulations clearly confirmed previous findings concerning seasonality in circulation and dispersion as well as concerning accumulation of concentrations in the inner fjord. The study conducted by Koziy et al. (1998) investigated the release from a submarine, dumped at the fjord entrance at about 30 m depth. Figure 1 shows the distribution of ^{137}Cs in August, 6 months after release. Unfortunately, it was not possible to identify the release rate applied for this study. As with other simulations conducted for the case of Abrosimov Bay (Harms and Povinec, 1999), the vertical distribution is inhomogeneous, showing a maximum concentration in the inner part of the fjord, at the bottom. This accumulation might be attributed to the weak winter outflow (ice-cover) and the onset of the flushing at the surface in late summer (ice melt). A pronounced vertical stratification and the sill in Stepovogo Fjord contribute to this situation. Although the model configuration and forcing in Koziy et al. (1998) differs from the Hamburg model system used by Harms and Povinec (1999) the results concerning gradual release scenarios are very similar.

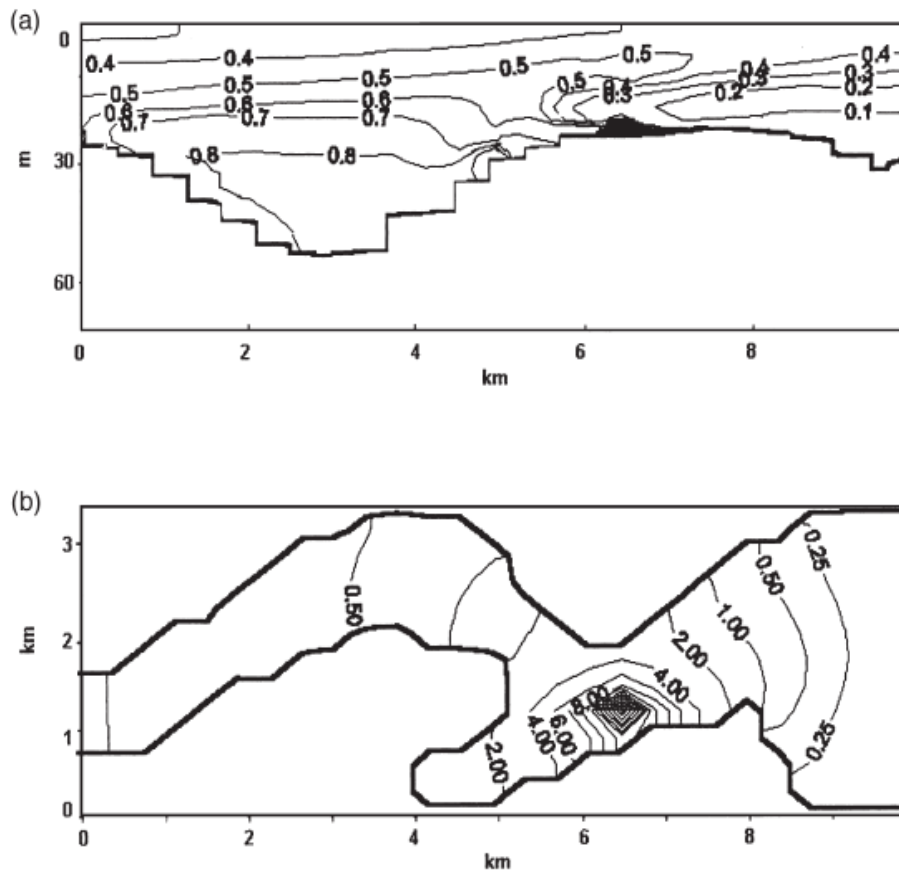


Figure 2.1. a) Concentration of ^{137}Cs on a longitudinal section through Stepovogo Fjord in August (Bq m^{-3}), six months after release; b) Concentration of ^{137}Cs in sediment (Bq kg^{-1}) of Stepovogo Fjord for the same situation. Figure from Koziy et al. (1998).

Information on the dumping sites of the Kara Sea, i.e. the bathymetry of the Stepovogo Fjord, its hydrography or relevant local meteorological data, is either very sparse or not easily available. In this respect, the present situation does not differ very much from the knowledge basis during the late 90's when most of the previous modelling work on local dispersion was performed (see Appendix A).

2.3 New assessments of local dispersion from a potential K-27 recovery accident

This section summarizes the findings from previously described model scenarios and puts them into a context relevant for the K-27 case. On a fundamental level, an accidental release during recovery of K-27 does not differ from previous model scenarios that were focused on sunken submarines, dumped reactors or waste containers. The results for a worst case (sudden release of high amounts of radioactivity) and a moderate case with a continuous release rate are summarised here. It has to be stressed that all evaluations for the local scale are based on the aforementioned existing model calculations. New information on the topography, the hydrography or any other forcing data regarding Stepovogo Fjord which exceed the state of knowledge at the time when those model experiments were performed were not available at the time of writing. Hence, no additional new model calculations for the local scale were undertaken.

2.3.1 Considerations for a worst case scenario

A worst case scenario would consist of an instantaneous underwater release of high amounts of radioactivity due to a failure during recovery or even reactor nuclear accident. The model findings from flushing time scenarios are pertinent in assessing such a situation. The sudden release of 1 TBq would give

rise to concentrations of radioactivity in the inner fjord waters in the range of at least $10^4 - 10^5$ Bq m^{-3} . This estimate is based on the volume of the fjord (approx. 10^7 m^3) and the assumption that the contamination disperses rapidly (i.e. within a few days) and more or less instantaneously all over the fjord. Contamination from higher release rates can easily be scaled using the same approach.

The assumption of an instantaneous dispersion throughout the fjord may be viewed as somewhat simplified. However, given the rapid release of very high amounts of radioactivity and the small size of the fjord, a differentiation in time and space on the fjord scale seems to be obsolete. Moreover, a severe accident or even an explosion may additionally disturb the stratification.

How and when the contamination will leave the fjord are important aspects which require consideration. The flushing time scenarios (see Appendix A1.1) suggest that concentrations in the inner fjord affect coastal waters of Novaya Zemlya within a month on average. Strong winds may shorten flushing times down to a few days. Under very calm conditions, the outflow of the contaminated plume may be prolonged up to 2-3 months. Very similar flushing rates were given by Koziy et al. (1998). In summer, Stepovogo Fjord can be flushed under favourable wind directions within 10 days.

It can be assumed that a recovery of the K-27 will likely be performed during late summer when weather conditions are favourable for this activity (i.e. no ice). It may, therefore, be assumed that an accidental release would happen during this period. Based on the evaluation of the existing model scenarios and in case of no sea ice cover in the fjord, it is arguable that the three dimensional circulation in the fjord would be considerably enhanced, in particular during late summer when autumn winds start getting stronger after weak summer winds. It is therefore presumed that an intense mixing in the fjord and a rapid outflow towards the Novaya Zemlya coast and the Kara Sea is the most probable consequence following a severe accident during remediation.

2.3.2 Considerations for a continuous release scenario

The second possible scenario for an assessment could be that the wreck is damaged during recovery, leading to an uncontrolled continuous release in the fjord. Simulation of such a situation requires model experiments covering longer time scales than instantaneous releases, in particular when realistic (i.e. transient) atmospheric forcing is applied.

For simplified atmospheric conditions (application of two prevailing wind directions) the resulting depth mean outflow of dissolved radioactivity (e.g. ^{137}Cs) will likely be below or in the range of 1000 Bq m^{-3} for a 1 TBq y^{-1} release. However, for previously published scenarios, the applied wind speeds were quite low and constant in time and space. They led to stationary radionuclide concentration patterns in the water. Based on these stationary solutions it is possible to evaluate the scavenging effect of particle reactive radionuclides. For such a case, calculated for a release of 1 TBq y^{-1} of the radionuclide ^{239}Pu , the highest simulated concentration in sediment are of the order of 500 Bq kg^{-1} . It must be stressed, however, that the particle reaction for many radionuclides, including ^{239}Pu , is difficult to estimate since the coefficients which determine the relative distribution between water and sediment are based on an equilibrium assumption (see Appendix B2) which may not adequately reflect the real conditions in case of variable wind and circulation. On the other hand, the strong mixing inside the fjord may lead to rather constant concentrations of the dissolved radionuclides at least over a long time period of the order of years, in case of a continuous release.

Temporal variability of the circulation has been taken into account in the results presented in Appendix A1.3, however subject to considerable constraints due to limited data availability. An important finding emerging from these model scenarios is the pronounced seasonality in circulation and hence dispersion. In general, the fjord circulation is most enhanced in late summer, when ice is still absent and intense autumn winds become established. Calm conditions occur in spring when the winds are weak and the ice cover shields the water surface from wind input. If a continuous release is applied over a couple of cyclo-stationary years, the tracer load in the fjord increases during spring and summer before a sudden highly contaminated outburst flushes large amounts of radioactivity out of the fjord in autumn.

2.4 Far Field Assessment and transport of radioactivity by Arctic sea ice

So far, the near field consequences have been considered. The issue of the far field dispersion of radionuclides will be the focus of the next chapter, some background information regarding the large scale dispersion of dissolved radioactivity from Kara Sea and Barents Sea sources as it already exists in literature being provided in Appendix A2. The case of long range transportation of contaminated sediment by sea ice is also reviewed (see Appendix A2.3). It is clear that realistic export rates of radioactively contaminated sea ice are difficult to deduce because of the significant lack of sedimentological data and uncertain parametrisations. In a simple conservative approach, Harms (1997) estimated that the possible radionuclide export rate by sea ice from the Kara Sea to the Arctic Ocean to be of the order of 0.03 TBq y^{-1} . This calculation assumes an ice volume flux from the Kara Sea into the Arctic Ocean of $150 \text{ km}^3/\text{y}$ (Pavlov and Pfirman, 1995), a sediment load in sea ice of 3 mg/l (IAEA, 1994) and a radionuclide concentration in sea ice sediment of 70 Bq kg^{-1} (Meese et al., 1997). The estimated export rate is at least one order of magnitude lower than the corresponding export rate through the water column but probably still overestimated.

A wide range of possible export rates was also presented in a more detailed study by Dethleff et al. (2000). Both publications confirm that, compared to the dissolved transport in the water column, drifting sea ice might be a very fast transport pathway. It might also be quite efficient due to the missing dilution / diffusion of radioactive concentration in the ice and the possibility of transporting 'hot spots', i.e. sediment patches of very high contamination. Integrated over time and space, however, the dominant pathway for an export of radioactivity from the Arctic Ocean is the transport in dissolved form in the water column, even if radionuclide concentrations in the water are much lower than in sea ice. The main reason for this is the large water volume transport compared to a much smaller sea ice transport.

3. Marine dispersion modelling

After characterization of the source term in first part of the present study (Hosseini et al. 2015) which included evaluation of the inventory of the contaminants available for release and quantification of time-varying release rates to the environment, the next step in the risk assessment was to evaluate the transport of hypothetically released radionuclides in Arctic waters using marine dispersion modelling.

An important output of such models is the prediction of the spatial and temporal distribution of radionuclide concentrations in the marine environment.

Following the input of radionuclides to the surface waters of a marine system, several immediate processes are likely to occur. A fraction of the radionuclide inventories will be advected by prevailing currents away from the input point and diluted and dispersed by diffusion processes. The remaining fraction of the radionuclide inventories will undergo interaction with suspended particulate material and / taken up by biota. The degree of particulate-phase interaction will depend on numerous factors including the physico-chemical form of the radionuclide, the availability of adsorption surfaces and the lithology and chemical attributes of the suspended material.

In the process of conducting the initial part of a marine impact assessment, the modelling of radionuclides fate can be arbitrarily split into 2 components namely (i) physical (abiotic) transfer processes and (ii) biological transfer through marine food-chains.

In order to simulate the physical transport of tracers or contaminants in marine environments, models with various considerations can be applied. These may range from uniform and instantaneous mixing models to 3D hydrodynamic models where the movement of contaminants can be simulated in the vertical and horizontal planes.

In the previous chapter, near field marine dispersion modelling, which is relevant for the assessment of local accidents, was discussed and some background materials for far field dispersion was provided. The latter type of dispersion modelling is the focus of this chapter.

The aim is to provide data on the dispersion of radioactivity in the Arctic marine environment from a number of scenario experiments which are performed for releases in the Kara Sea and the Barents Sea through the application of a large scale numerical model (see following section).

3.1 Model description

The numerical model used for the current set of experiments is a version of NAOSIM (North Atlantic/Arctic coupled Ocean Sea Ice Model) (Karcher et al., 2003a; Köberle and Gerdes (2003)). It is derived from the Geophysical Fluid Dynamics Laboratory modular ocean model MOM-2 (Pacanowski, 1995) and a dynamic-thermodynamic sea ice model with a viscous-plastic rheology (Hibler, 1979). NAOSIM has been used successfully in a number of applications focusing on Northern Sea circulation (Karcher et al. 2008, Gerdes et al. 2005) and tracer dispersion (Karcher et al. 2004; 2012).

The version used here has 30 unevenly spaced vertical levels, starting from 20 m thickness down to 100 m depth with the thickness gradually increasing with depth. The model domain covers the Nordic Seas, the Arctic Ocean and the northern North Atlantic down to about 50°N. The model has an open boundary in Bering Strait where a total inflow for the barotropic mode of 0.8 Sv is imposed to cover approximate amount of observed inflow of Pacific Water into the Arctic Ocean. It also has an open boundary in the south, where barotropic flow from a larger scale version of the model is prescribed. At both boundaries, the flow profiles can develop freely. The open boundary conditions have been implemented following Stevens (1991), thereby allowing the outflow of tracers and the radiation of waves. The initial hydrography, in January 1948, is adopted from the Polar science centre Hydrographic Climatology (PHC), winter climatology (Steele et al., 2001), while a yearly mean climatology is used as a reference for surface salinity restoring on a time scale of 180 days. The restoring of sea surface salinity is a common method used to prevent the ocean salinity from drastically drifting away from the observed ocean state (Steele et al., 2001). Sea surface salinity restoring compensates for a mismatch between freshwater forcing data

(e.g., precipitation and runoff) and model physics. Parametrization of river runoff is employed using negative salt fluxes proportional to seasonal climatologies of runoff for each of the major rivers which follows the Arctic Ocean Model Intercomparison Project (AOMIP protocol) (Holloway et al., 2007). The model is driven with daily atmospheric forcing from 1948 to 2010 (NCEP/NCAR reanalysis (Kalnay et al., 1996)).

The tracer release experiments began in July for each of the experiments, since summer is assumed to be the most likely season for a potential recovery of the submarine.

3.2 Setup of the tracer release experiments

The aim of the current set of experiments was to cover ocean circulation scenarios which represented extreme situations in terms of speed and range of dispersion of the pollutant. The basis for this decision has been earlier studies on the large scale changes of circulation in the Barents and Kara Sea as well as the Arctic Ocean (Gerdes et al., 2001; Harms and Karcher, 2005; Karcher et al., 2003b), and the effect of this on the dispersion of radionuclides (Gerdes et al., 2001; Karcher et al., 2004; 2006, 2010, 2012).

To evaluate the (large scale) marine dispersion of potentially released soluble radionuclides as a consequence of a possible recovery of K-27, the following assumptions have been made. The half life of the contaminant has been assumed to be much longer than the dispersion period of 10 years and sediment interaction is not considered. The time period envisaged for salvaging of the submarine is summer. The experiments being considered are as follows:

- A) "On-site"; one depth (at the surface),
- B) During transportation (past the "half way" point) two depths (surface and ~ 300 m),
- C) "Final destination" (i.e. at or very near Gremikha); one depth (surface),

For each location, three different large scale atmospheric and oceanic circulation scenarios were considered: weak and strong Kara→Barents flow and Transpolar Drift current (transporting radionuclides toward Fram Strait/Svalbard area), and a special case of a reverse flow period through Kara Gate, for two release scenarios each (i.e. instantaneous and continuous).

Data was collated as the weekly means of the tracer concentration and was stored on a server in the common NetCDF format. A web-based tool was generated which allowed access to the data based on geographical and temporal information for each of the experiments.

3.3 Motivation of the experimental set-up: Variability of circulation

As mentioned previously, three different circulation regimes were considered in this study. The reason for the selection of these circulation regimes was based on analyses of the large scale flow field and experience from earlier studies.

3.3.1 The 1983 versus the 1988 flow field: Two different Arctic-wide circulations

As part of the work on potential releases from the submarine Kursk in the Barents Sea, an analysis of the oceanic circulation on the entire western Siberian Shelves and beyond was performed (Gerdes et al., 2001).

Motivated by this analysis, two maximally different flow regimes, each lasting for three years, were selected. The periods selected were 1983–1986 and 1988–1991. During 1983–1986 a weak through-flow through the Barents Sea was dominant, while a strong through-flow was predominant during 1988–1991 (see Appendix A2.2). These periods also align with a low and a high phase, respectively, of an Arctic-wide atmospheric sea level pressure pattern named the Arctic Oscillation (AO). In its low phase, the AO leads to a location of the oceanic Transpolar Drift rather close to the Siberian shelves. In its high phase, as in the late 1980s/ early 1990s, it leads to a shift of the Transpolar Drift, oriented from the Chukchi Sea/Bering Strait to the Fram Strait, with large implications also for the dispersion of substances carried with the Atlantic derived waters passing the Barents Sea (e.g. Karcher et al. 2012). This means that a contaminated

water mass stemming from the western Siberian shelves, would spread far eastward into the central Arctic Ocean Basin before returning to Norwegian Waters with the Transpolar Drift. In contrast, during the earlier, weak Barents Sea throughflow (lower AO) period starting in 1983 would the location of the Transpolar Drift in the Eurasian basin, along the Siberian shelves, would favoured a rather quick return flow to the Fram Strait. Regionally, this translates into a longer flushing time of the Kara Sea and south-eastern Barents Sea in the 1983-1986 flow regime resulting in higher concentrations, compared to the 1988-1991 flow regime.

3.3.2 The 1998 flow regime: the reverse flow from Kara Sea to Barents

Based on an analysis of local flow regimes in the Kara Sea (Harms and Karcher, 2005), a third flow field was selected for further investigation. It was characterized by the exceptional situation of a return flow through Kara Gate which occurred in 1998/99, favouring dispersion of potential contamination from the Kara Sea back into the Barents Sea.

As highlighted by Harms and Karcher (2005), the atmospheric sea level pressure patterns (SLP) over the north-western Siberian shelves in the period 1948–2002 reveal a strong positive anomaly over the north-eastern Barents Sea and the Kara Sea in the years 1998 and 1999. This strong anomaly resulted in large scale wind stress forcing fields which forced drastic changes in the oceanic circulation over the shelves. Empirical Orthogonal Function (EOF) analysis of the simulated oceanic flow fields of the entire Barents and Kara Sea shelf over the period 1948–2002 revealed two dominant modes that explained 43% and 25% of the variability, respectively. This result was very similar to an analysis carried out for the shorter period of 1979 to 2002 (Karcher et al., 2003b). The first mode described a general increase of the through-flow from the Barents Sea Opening eastward, including the Kara Sea. The second mode described a northward shift of the through-flow through the Barents Sea, and a reduction of eastward flow through the Kara Strait and the Kara Sea (Figures 3.1a and 3.1b).

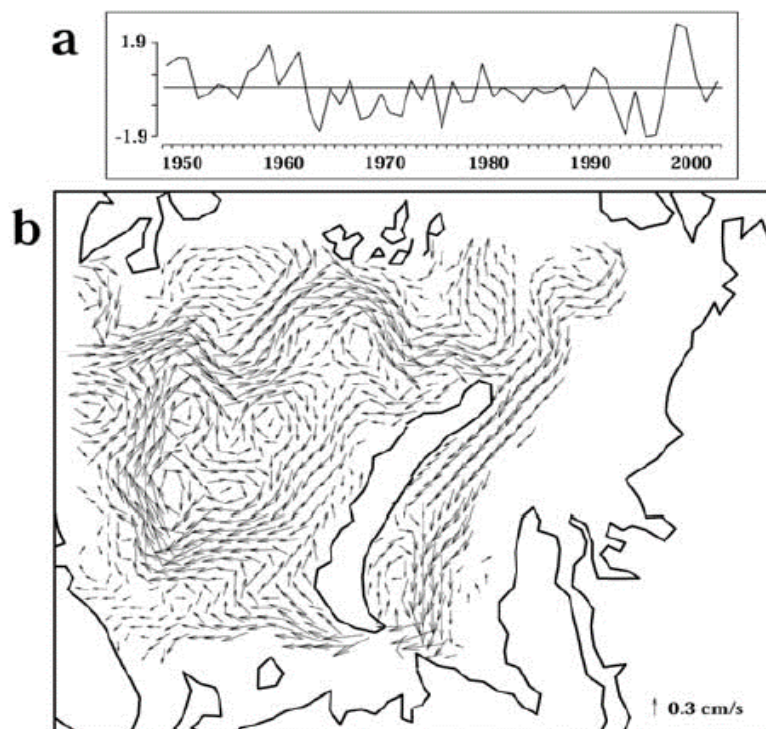


Figure 3.1. Second EOF mode of yearly mean velocities in 80 m depth on the Barents and Kara shelf for the period 1948–2002: (a) principal component and (b) circulation pattern.

The second mode was strongest in the years 1998/1999, when circulation and transport rates in the Kara Sea were completely reversed; i.e., the flow through Kara Gate, normally directed eastwards to the Kara Sea, was directed westwards towards the Barents Sea for a period of almost a year (Figure 3.2).

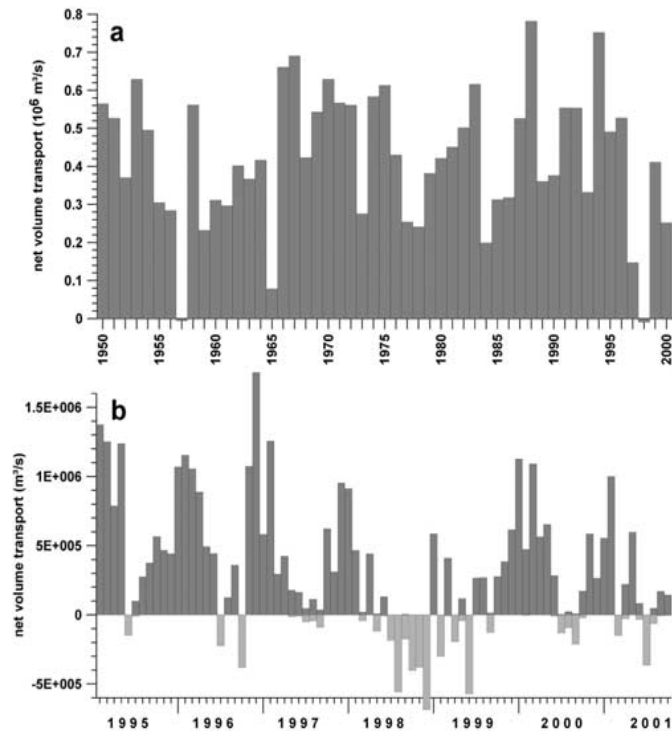


Figure 3.2. (a) Yearly mean Kara Strait throughflow from 1948–2001 and (b) monthly mean Kara Strait throughflow from 1995–2001, deduced from NAOSIM. (from Harms and Karcher, 2005).

3.4 Model Experiments: results

3.4.1 Instantaneous Release Experiments

In the following, a few examples will be presented for the results of dispersion experiment as far as the instantaneous releases are concerned. Figures 3.3–3.12 exhibit the surface concentration, based on an instantaneous release of 1 PBq (10^{15} Bq) at the 3 different release positions (Stepovogo Fjord, Barents Sea and Gremikha Bay). For each release location activity concentration in water is shown at various time after the release start in three different years; 1983, 1988 and 1998.

As expected, in all cases the advection of the contaminants generally occurs eastward via the Kara Sea and Laptev Sea and subsequently into the central Arctic Ocean. From here, the dispersion occurs mostly via the Transpolar Drift to Fram Strait and further south with the East Greenland Current and into the Labrador Sea. Part of the contaminants in the central Arctic, however, recirculate southward into the Barents Sea, dominantly on the east coast of Svalbard. In the Nordic Seas, low concentrations of the contaminant reach Norwegian waters, recirculating with the Jan Mayen Current and the East Icelandic Current, mixing into the Norwegian Atlantic Current and the Norwegian Coastal Current.

For the instantaneous release in 1983, shown in Figures 3.3, 3.6 and 3.9, the widespread contamination of the central Arctic is a consequence of the variability of circulation pathways on timescales of several years. The centre of mass for the contaminants 10 years after release is located in the Central Basin of the Arctic around the North Pole. Relatively, higher concentrations are still identifiable on the shelves, mostly

in the eastern Kara and the Laptev Seas. The north-western Barents Sea exhibits elevated concentrations, too, following a recirculation of Polar water from the central Arctic east of Svalbard. The patterns from the four different release positions show rather similar levels and form. Surface concentrations in the case of release at position C near Gremikha (Figure 3.9) are somewhat lower, following the longer advective pathway from the start to the central Arctic, but also likely due to a larger fraction being exported to depth with the formation of dense water occurring in the western Barents Sea.

As pointed out previously, 1988 and the following period of 5-6 years were characterized by a Transpolar Drift which carried water from the Siberian Shelves far eastward into the Amerasian/Canadian Basin, beyond the Lomonosov Ridge. This can be found in Figures 3.4, 3.7 and 3.10 for all release positions. The maximum concentrations after 10 years are found much further towards the Canadian coast than in the 1983 flow regime case. Also the fact that the circulation was strong over the shelves of the Barents and Kara Seas in the period after 1988 is emphasized by the fact that concentrations in the Kara Sea are considerably lower as compared to the flow regime of 1983. This is a consequence of strong flushing of the Barents and Kara Sea which has led to a replacement of contaminated water. High concentrations also reach the area north of Svalbard.

For the release in 1998, shown in Figures 3.5, 3.8 and 3.11, the overall large scale pattern is similar, but there are considerable regional differences. Most noticeably, the interior Canadian Basin is less affected by the contaminants, following obviously less variability of the Transpolar Drift path in the 10 years following 1998. This fits the fact that since 1996, the interior Arctic Ocean has been dominated by an anticyclonic circulation regime, favouring a large Beaufort Gyre and a Transpolar Drift from the Laptev Sea to the Fram Strait. As a consequence of the large and strong Beaufort Gyre, recirculation of contaminated water to the west, north of Greenland and the Canadian Archipelago can be found. This is congruent with the finding of Karcher et al. (2012). Furthermore, year 10 of the 1998 release case also indicates higher contamination of the waters around Svalbard and south into the western Barents Sea, as was the case in the 1983 flow regime release experiment. Higher surface concentrations can also be found in the Laptev and the East Siberian Sea, in comparison to the case of the 1983 flow regime.

To illustrate the impact of different flow-regimes on the resultant activity concentrations in water at a given location, a number of examples are shown in Figures 3.3-3.11. These maps also provide an overview of the dispersion of contamination as a function of time and place.

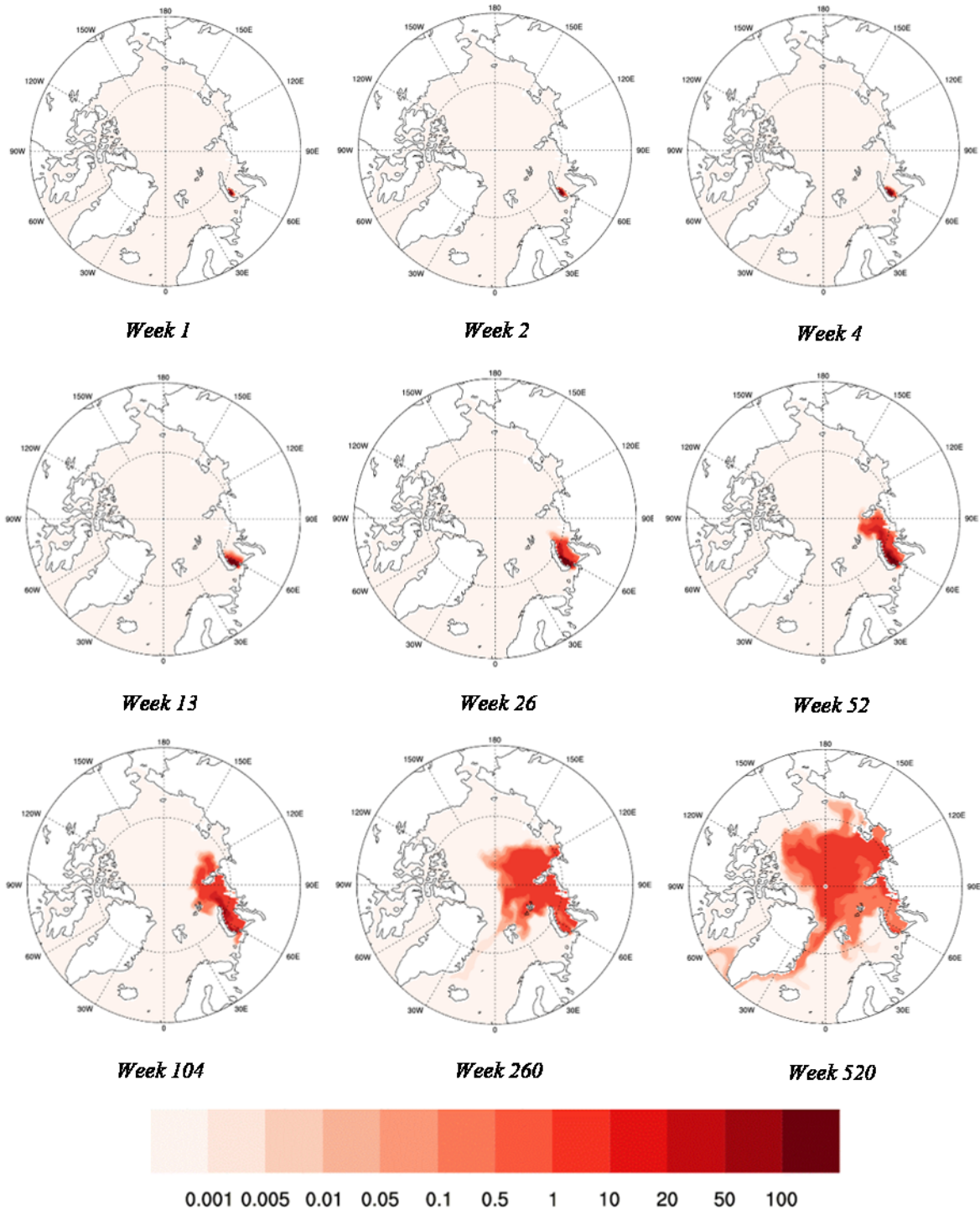


Figure 3.3. Tracer concentration (Bq m^{-3}) at the surface following an instantaneous release of 1 PBq at Stepovogo fjord. The maps illustrate the temporal development of contamination plume in Arctic Seas according to the 'weak' flow regime after 1983.

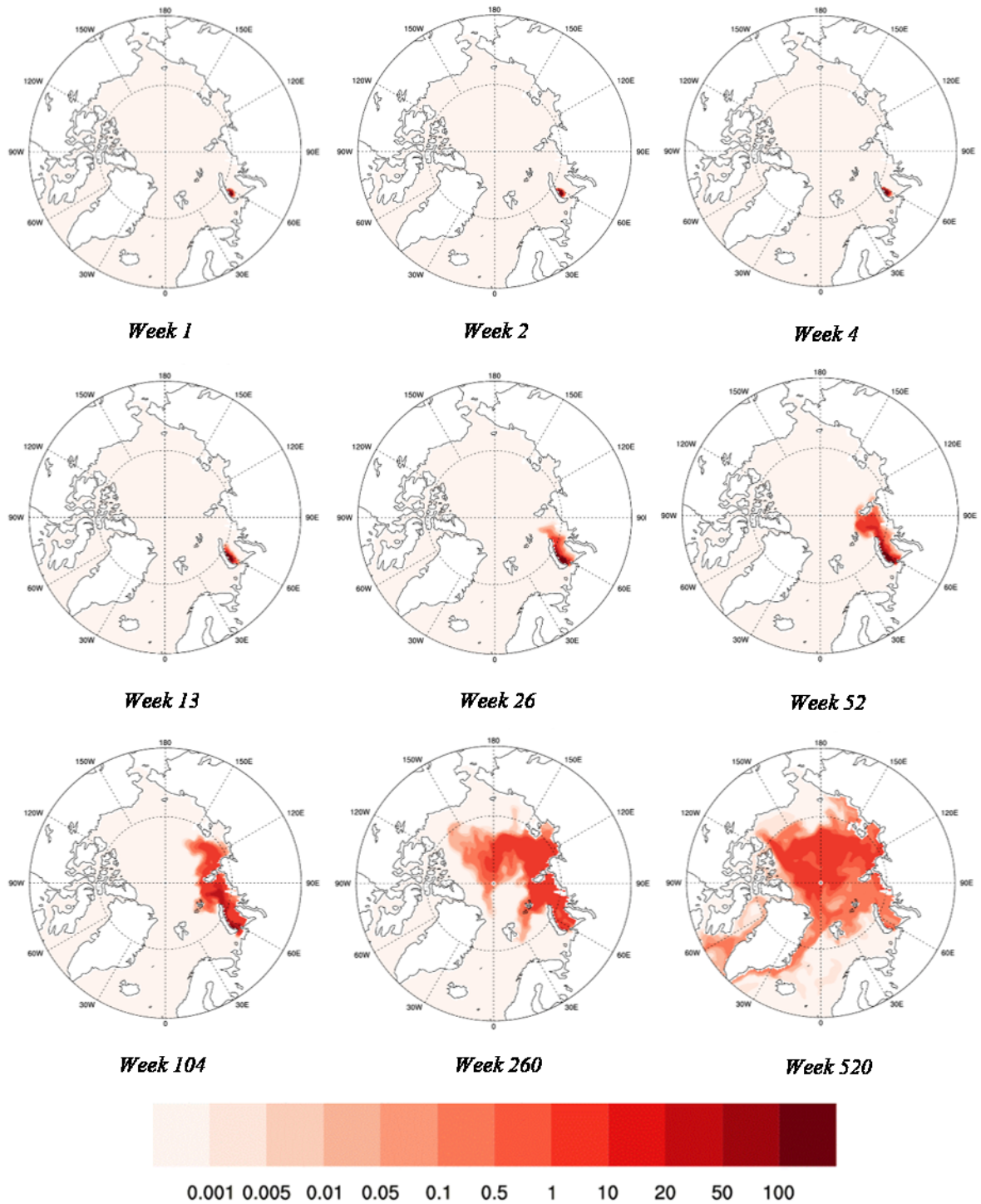


Figure 3.4. Tracer concentration (Bq m^{-3}) at the surface following an instantaneous release of 1 PBq at Stepovogo fjord. The maps illustrate the temporal development of contamination plume in Arctic Seas according to the 'strong' flow regime after 1988.

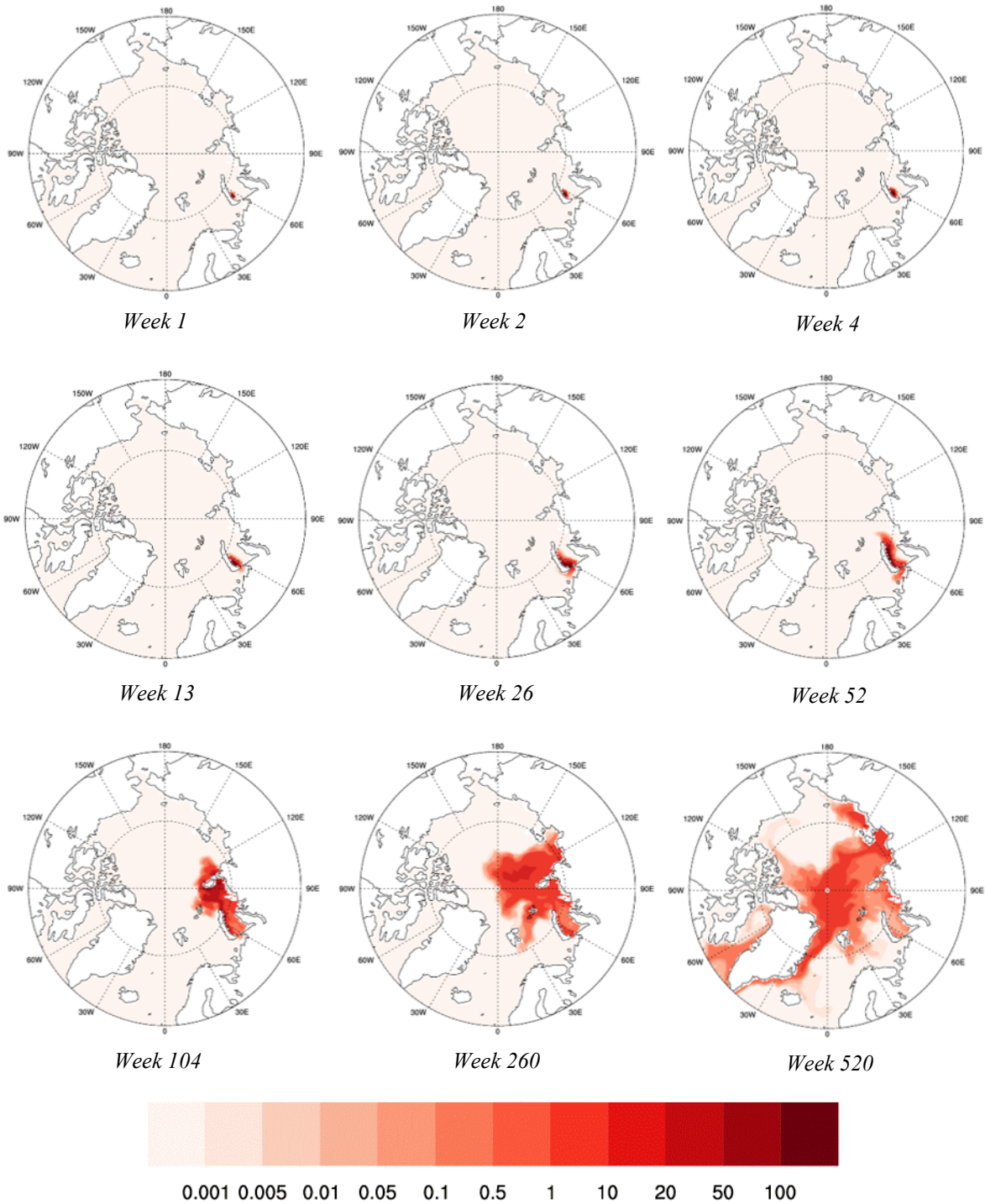


Figure 3.5. Tracer concentration (Bq m^{-3}) at the surface following an instantaneous release of 1 PBq at Stepovogo fjord. The maps illustrate the development of contamination plume in Arctic Seas according to the flow regime after 1998.

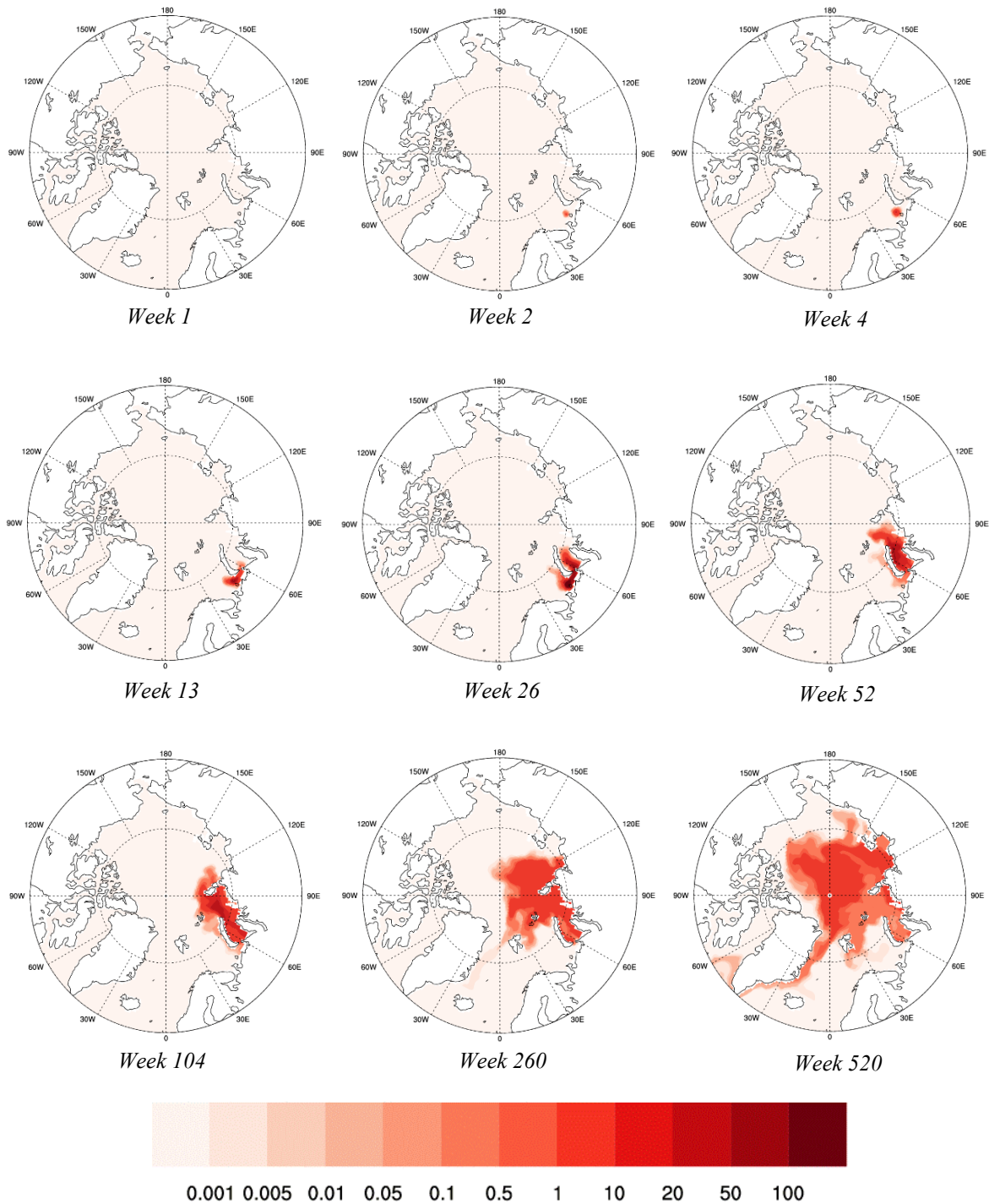


Figure 3.6. Tracer concentration (Bq m^{-3}) at the surface following an instantaneous release of 1 PBq at the bottom in Barents Sea. The maps illustrate the temporal development of contamination plume in Arctic Seas according to the flow regime after 1983.

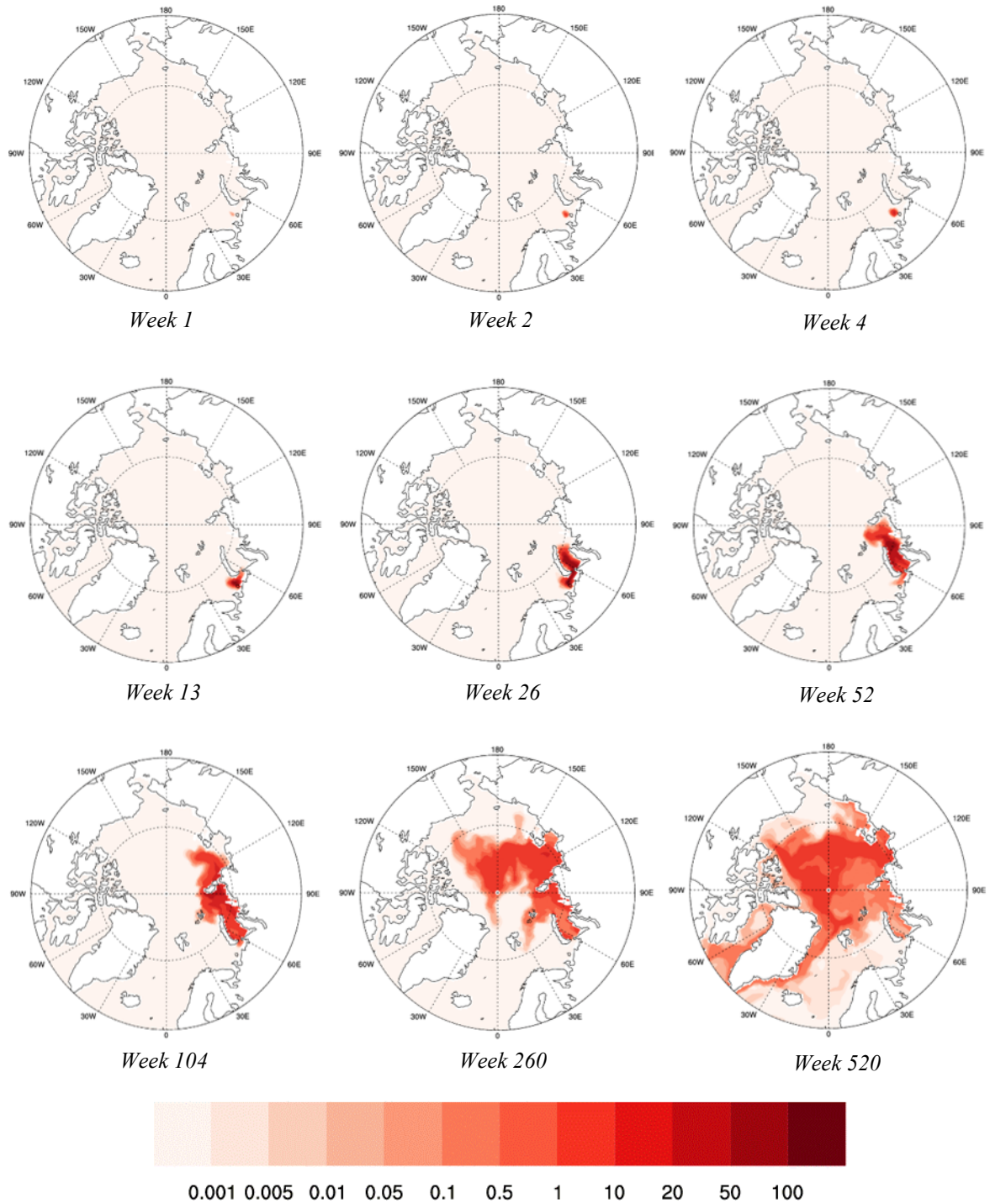


Figure 3.7. Tracer concentration (Bq m^{-3}) at the surface following an instantaneous release of 1 PBq at bottom in the Barents Sea. The maps illustrate the temporal development of contamination plume in Arctic Seas according to the flow regime after 1988.

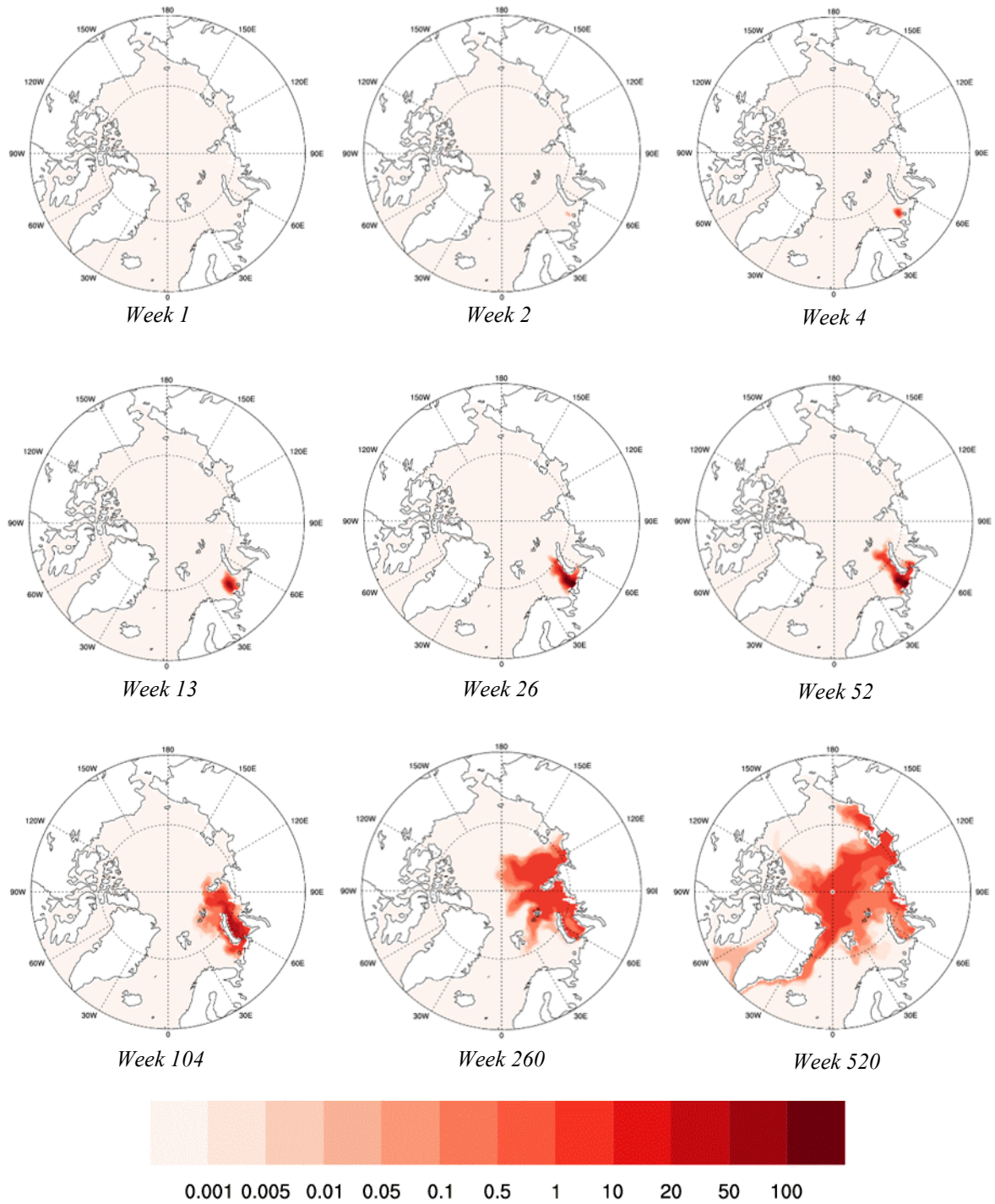


Figure 3.8. Tracer concentration (Bq m^{-3}) at the surface following an instantaneous release of 1 PBq at bottom in the Barents Sea. The maps illustrate the temporal development of contamination plume in Arctic Seas according to the flow regime after 1998.

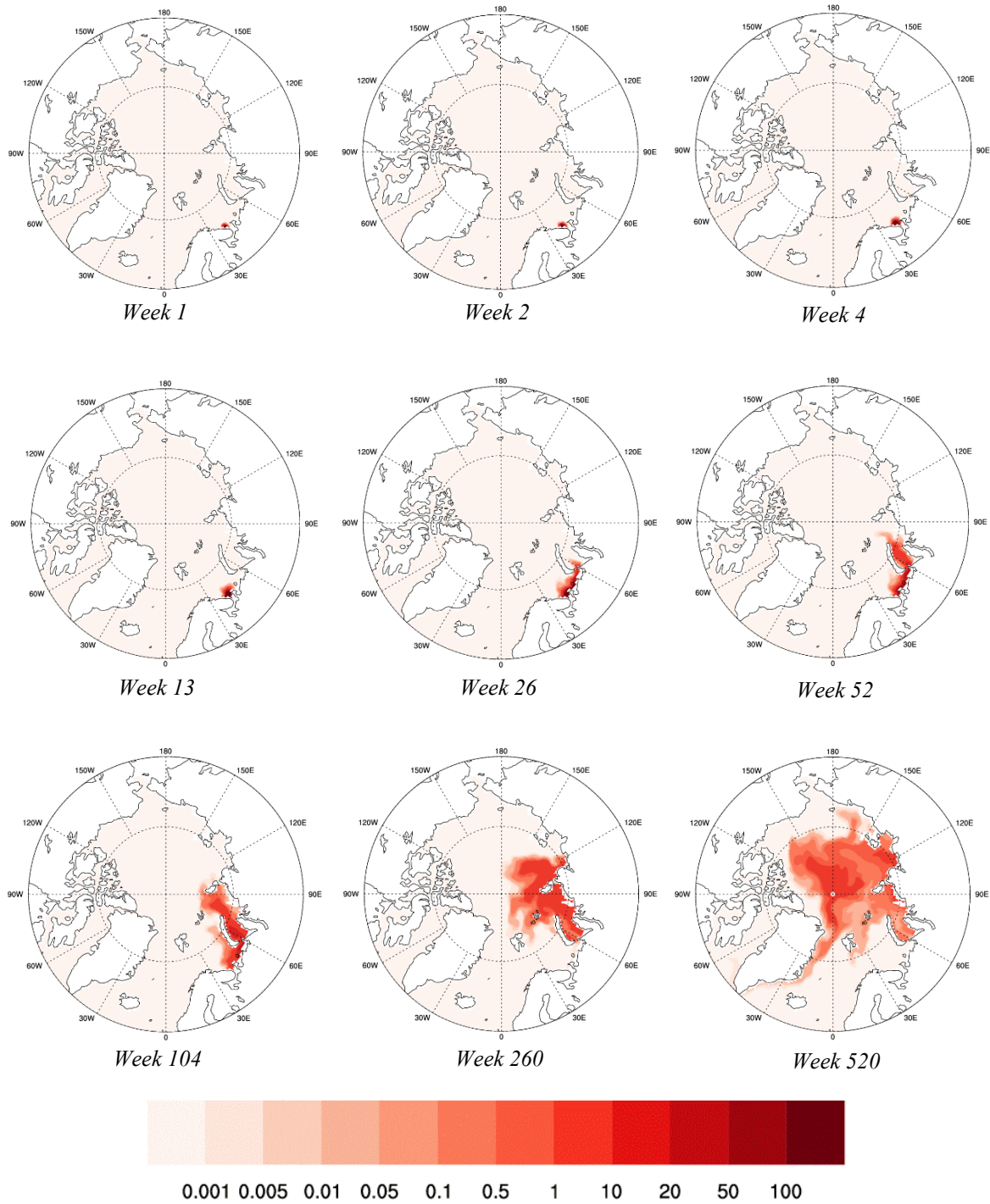


Figure 3.9. Tracer concentration (Bq m^{-3}) at the surface following an instantaneous release of 1 PBq at Gremikha Bay. The maps illustrate the temporal development of contamination plume in Arctic Seas according to the flow regime after 1983.

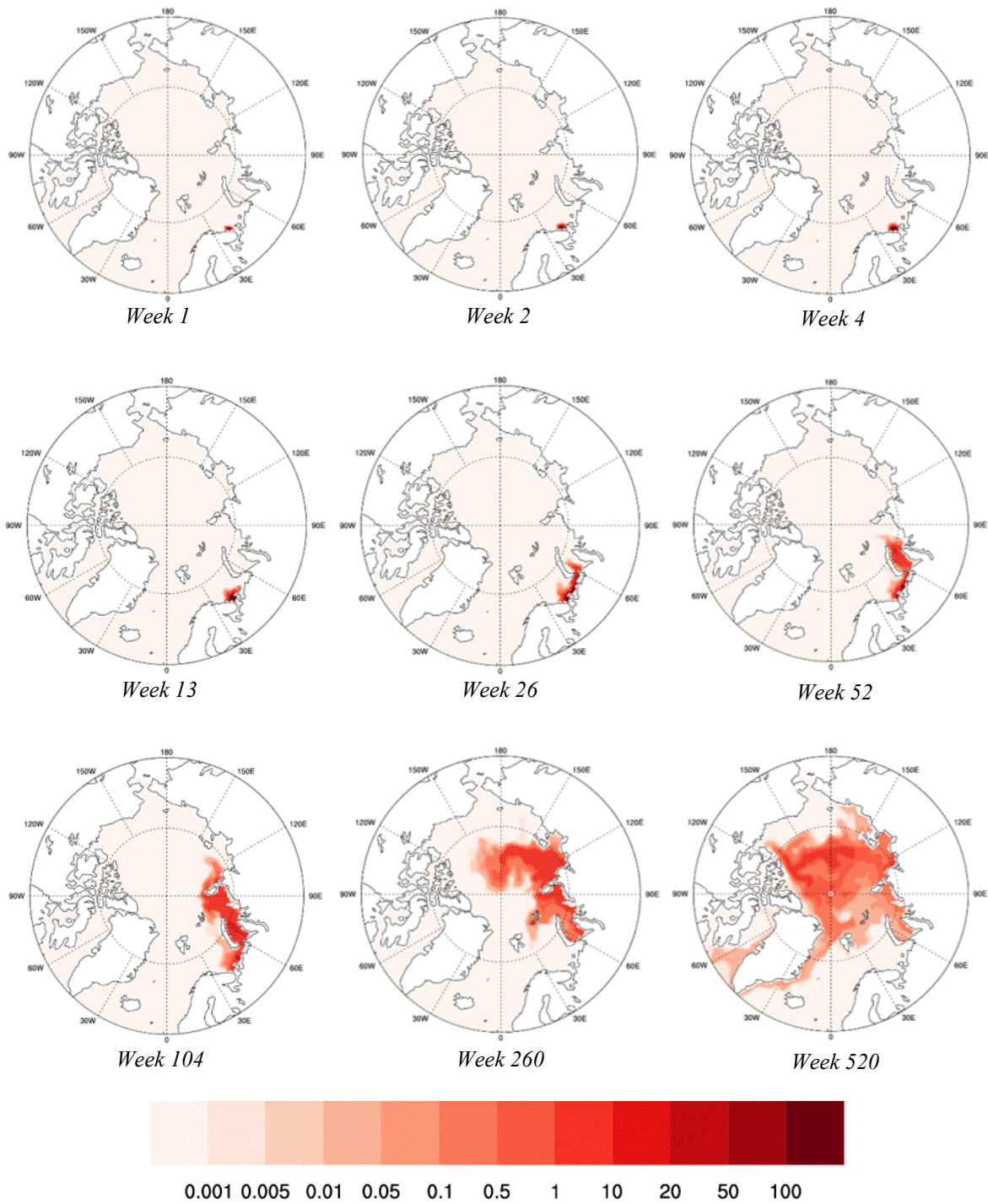


Figure 3.10. Tracer concentration (Bq m^{-3}) at the surface following an instantaneous release of 1 PBq at Gremikha Bay. The maps illustrate the temporal development of contamination plume in Arctic Seas according to the flow regime after 1988.

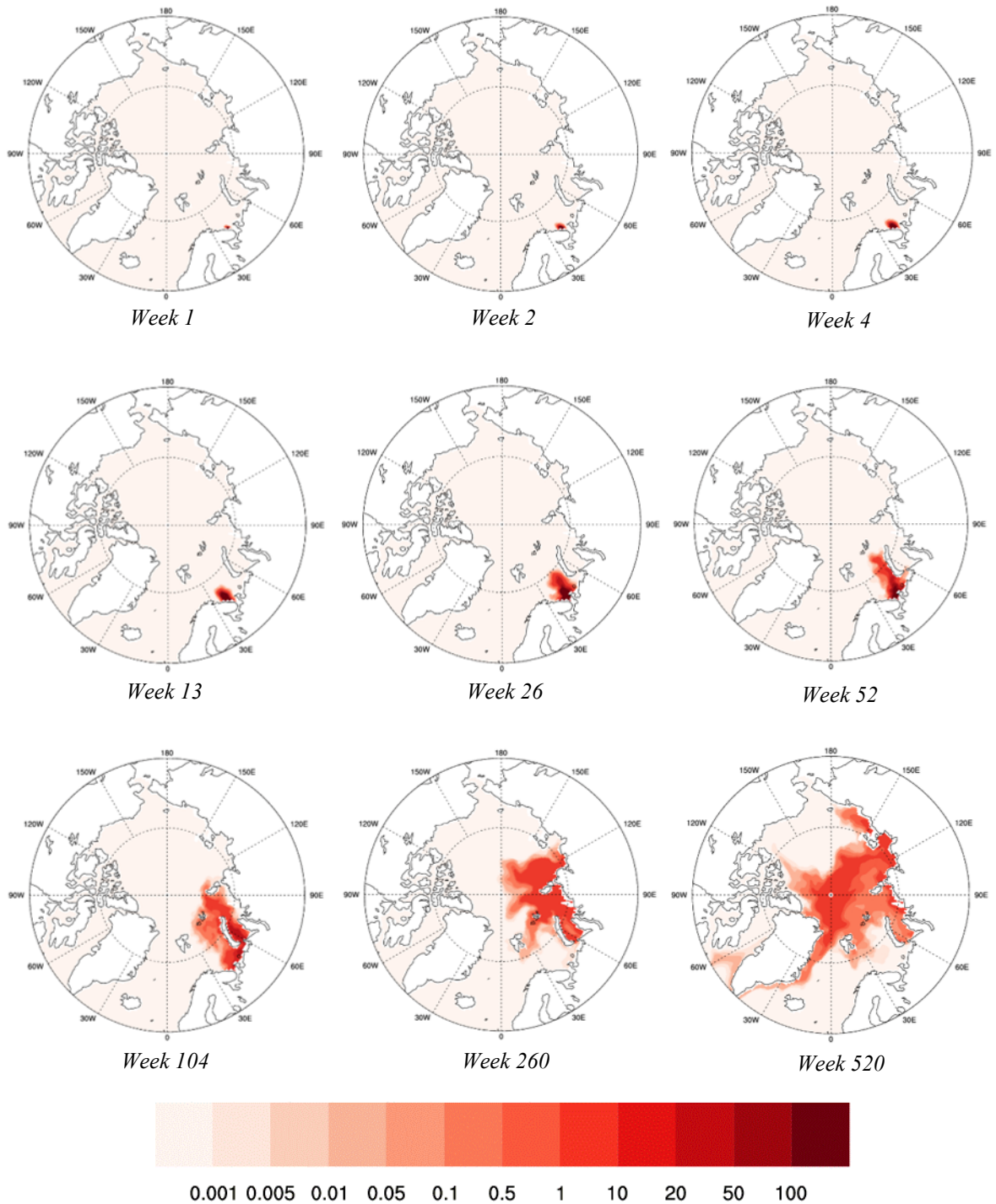


Figure 3.11. Tracer concentration (Bq m^{-3}) at the surface following an instantaneous release of 1 PBq at Gremikha Bay. The maps illustrate the temporal development of contamination plume in Arctic Seas according to the flow regime after 1998.

3.4.2 Continuous Release Experiments

Figures 3.12, 3.13 and 3.14 show the patterns of contaminant dispersion in year 10 after start of the continuous release of 1 TBq y^{-1} ($10^{12} \text{ Bq y}^{-1}$) in 1983, 1988 and 1998 for various release locations.

For the case of a continuous release starting in 1983 (Figure 3.12) the largest part of the central Arctic Basin is affected, as are the Kara and the Laptev Sea shelves. Since the end of the 10 year release period starting in 1983 is in the phase of the high Arctic Oscillation starting in 1989, we find the year 10 distribution covering also parts of the Canadian Basin.

Figure 3.13 shows the surface concentration after 10 years of continuous release starting in 1988. Most striking, in comparison to the release starting in 1983, is the narrower plume of high contamination spreading from the Kara Sea into the eastern Eurasian and the Canadian Basin, even reaching the Canadian Archipelago. Importantly, the transport southwards towards Svalbard is considerably weaker in that phase, leading to lower concentrations there in year 10. As was the case for the instantaneous releases, lower concentrations on the shelves in the period of the 1988 flow regime than in the period of 1983 are evident, likely due to the stronger flushing of the shelf seas in the 1988 flow regime phase.

In contrast to both earlier periods, the continuous release case for the start year 1998, shown in Figure 3.14, exhibits a narrow band of the Transpolar Drift stretched parallel to the Siberian Shelf break towards Fram Strait. The contaminant plume has reached the Fram Strait and Svalbard waters with higher concentrations than it is the case for the 1988 flow regime. Interestingly, as a consequence of the circulation, highest concentrations in the Svalbard vicinity are a consequence of the release in the Kara Sea (position A, Figure 3.14a), in contrast to the closer release position C near Gremikha in the Barents Sea (Figure 3.14b).

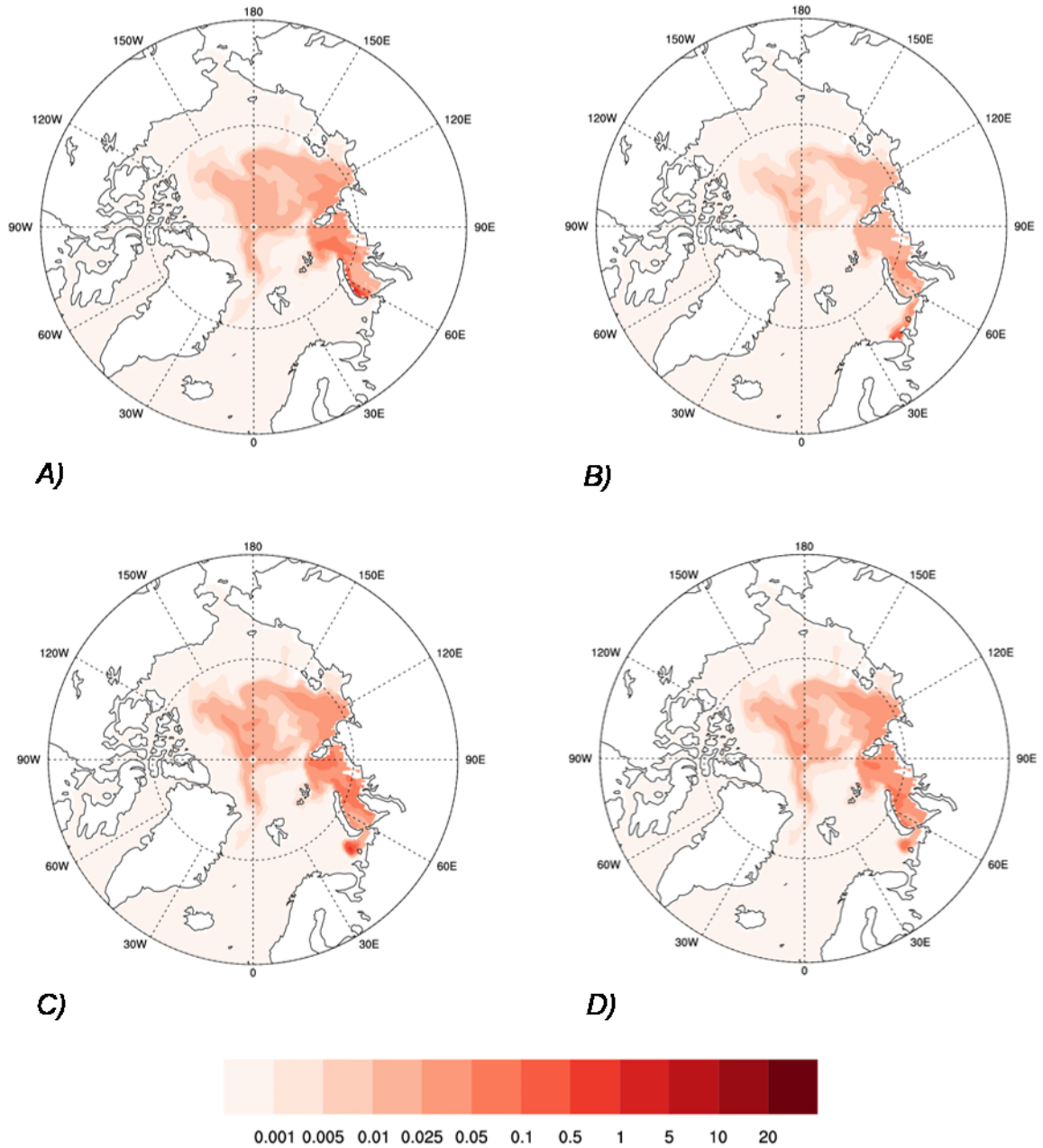


Figure 3.12. Tracer concentration in Bq m^{-3} at the surface 10 years after start of **continuous** release of $10^{12} \text{ Bq y}^{-1}$ in summer **1983** at position: A) Stepovogo, B) Gremikha, C) Barents Sea (surface), D) Barents Sea (bottom).

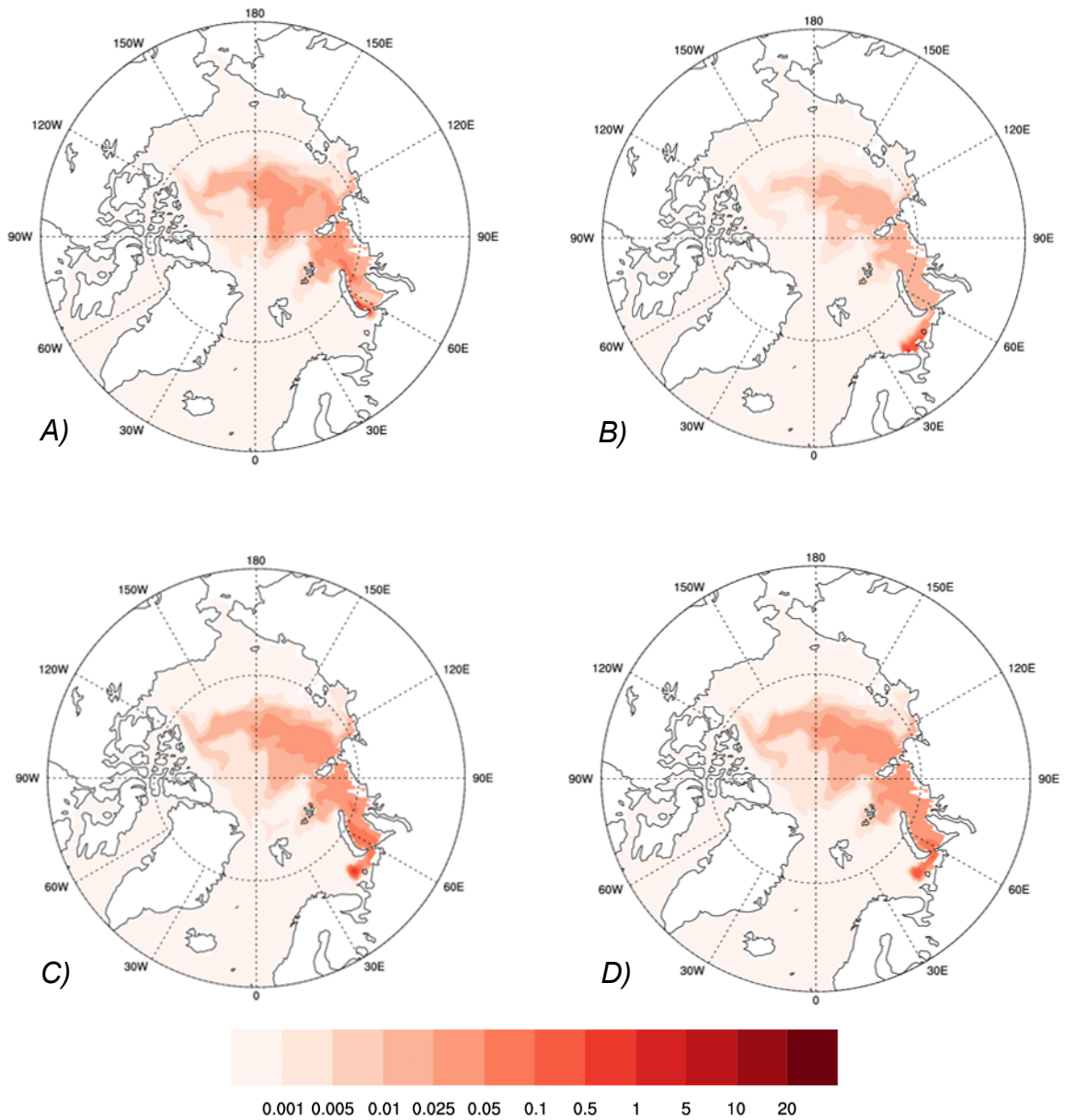


Figure 3.13. Tracer concentration in Bq m^{-3} at the surface 10 years after start of **continuous** release of $10^{12} \text{ Bq y}^{-1}$ in summer **1988** at position: A) Stepovogo, B) Gremikha, C) Barents Sea (surface), D) Barents Sea (bottom).

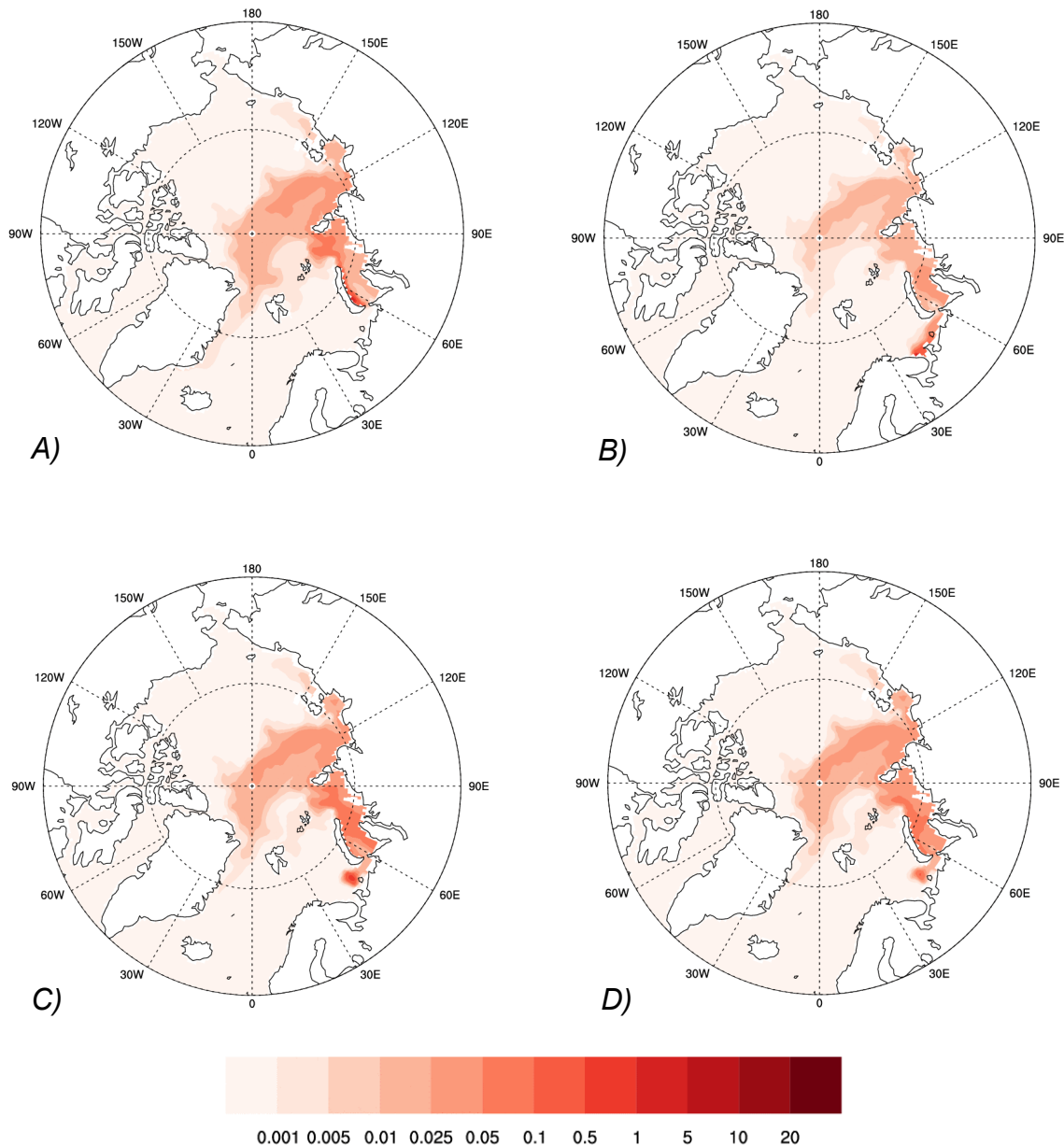


Figure 3.14. Tracer concentration in Bq m^{-3} at the surface 10 years after start of **continuous** release of $10^{12} \text{ Bq y}^{-1}$ in summer **1998** at position: A) Stepovogo, B) Gremikha, C) Barents Sea (surface), D) Barents Sea (bottom).

In summary, the results from a set of 24 experiments (2 release modes, 3 release locations and 4 depths, i.e. 24 experiments) have been presented in this chapter. The experiments were each performed for 10 years duration, with release start dates in summer 1983, 1988 and 1998 respectively.

3.5 Selected sea water activity concentrations for estimation of doses

Dispersion data for each release location and all considered current regimes has been scrutinised to identify regions of highest sea water activity concentrations.

In order to extract and average geographic areas from the NAOSIM model data, the grid boxes in a given longitude and latitude region were first transformed to the NAOSIM model domain, a $0.25^\circ \times 0.25^\circ$ rotated-pole coordinate system with its equator corresponding to the true $30^\circ \text{ W}/150^\circ \text{ E}$ meridian and its

North Pole located at a true 0° N, 60° E. Mean time series of concentrations were then computed as area-weighted spatial averages for each of the 30 unevenly spaced depths of the NAOSIM model. In addition, averages over the whole water column were computed by using the thicknesses of the layers as weights.



Figure 3.15. Visualisation of regions given in Table 3.1. Estimated water activity concentrations for these regions have been used for the dose calculations made in the present work.

Table 3.1 summarises these water activity concentrations for different regions (see Figure 3.15) which have been further used in all dose estimations made in this study.

Table 3.1. Geographic coordinates and concentration values for regions showing highest water activity concentrations for each release location and all considered release years. All values are based on considering instantaneous release scenarios.

Stepovogo Fjord (A)				
N1 72.80 E1 5 6.80 N2 72.95 E2 57.55				
Year		1983	1988	1998
Surface (Bq/l)	Max	19.3	16.6	18.3
	Mean	1.3	1.4	1.6
Depth Average (Bq/l)	Max	1.1	0.9	1.1
	Mean	0.1	0.2	0.2
Gremikha Bay (C)				
N1 68.20 E1 39.10 N2 68.50 E2 39.70				
Year		1983	1988	1998
Surface (Bq/l)	Max	20.5	17.2	15.6
	Mean	0.9	0.9	0.9
Depth Average (Bq/l)	Max	3.0	2.6	2.3
	Mean	0.2	0.2	0.2
Barents Sea (B)				
N1 70.00 E1 47.10 N2 70.30 E2 48.00				
Year		1983	1988	1998
Surface (Bq/l)	Max	12.7	13.4	13.3
	Mean	0.6	0.5	0.6
Depth Average (Bq/l)	Max	2.0	2.1	2.0
	Mean	0.1	0.1	0.1

4. Atmospheric dispersion

As discussed in Hosseini et al. (2015), accident scenarios have been considered which could result in releases to the atmosphere. Such scenarios represent accidents with and without involvement of a Spontaneous Chain Reaction (SCR).

To evaluate atmospheric transport and deposition of radioactive debris on Norwegian territory as a consequence of a hypothetical accident during possible recovery of K-27, three locations were considered as potential accident sites: Stepovogo Fjord, Gremikha Bay and one position en route between these locations (see Figure 3.15).

The time period considered was August-September. Releases are assumed to only occur at the surface (or within 10 m of the surface) and at a height of 100 m (such as after a fire). The releases at each location are assumed to be either “instantaneous” releases or as having occurred over a period of some hours (such as after a fire).

4.1 SNAP: the atmospheric dispersion model

A model called SNAP (Severe Nuclear Accident Program) was used to simulate the atmospheric dispersion of radionuclide debris in this study. SNAP is a Lagrangian particle model which was developed at the Norwegian Meteorological Institute (MET) (Bartnicki et al., 2011) for simulating atmospheric dispersion of radioactive debris in an emergency situation such as nuclear accidents and /or nuclear explosions. For more details regarding the SNAP model, see Appendix C.

The basic concept of a Lagrangian particle model is as follows: The released mass of radioactive debris is distributed among a large number of model particles. After the release, each model particle carries a given mass of selected pollutant which can be in the form of gas, aerosol or particulate matter. A model particle in this approach is given an abstract mathematical definition, rather than a physical air parcel containing a given pollutant. It is used in SNAP as a vehicle to carry the information about the pollutant emitted from the source. The model particle is not given a definite size and cannot be subdivided or split into parts. On the other hand, the mass carried by the particle can be subdivided and partly removed during the transport.

4.1.1 Model domain and meteorological data

The SNAP model is flexible concerning both model domain and meteorological data. The spatial and vertical structure of the SNAP model domain is in fact defined by the meteorological input. In this study, a meteorological database, especially developed for the purpose of this work and called NORA10-EI, was employed. The NORA10-EI database has a horizontal resolution of approximately 11 km. Surface fields are stored every hour, while model level fields are stored every third hour. The database covers the 33 year period between January 1980 and December 2012. There are 40 vertical layers with meteorological data. The model domain in this database is shown in Figure 4.1.

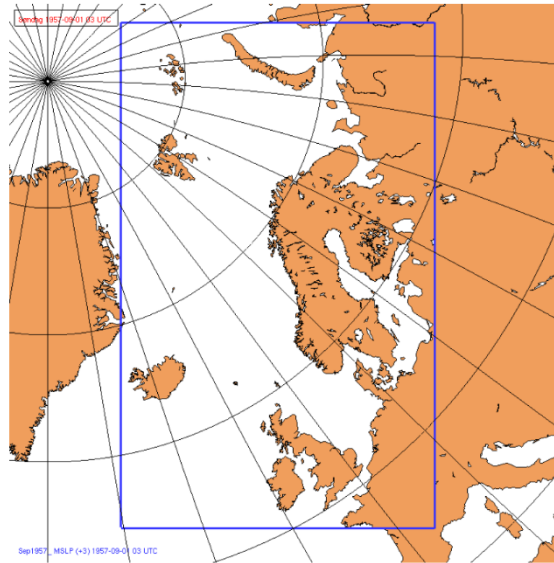


Figure 4.1. Domain (within blue frame) with meteorological data for the period 1980-2012 used in this study.

4.2 Selection of the worst case meteorological scenario

After compiling the aforementioned meteorological database, the next step towards identifying the worst case meteorological scenarios for Norway was to use these data as input and run the SNAP model. A preliminary source term with only one radionuclide was used for selecting meteorological situations of interest. The compiled meteorological database was also used for statistical analysis of the radioactivity transport to Norway in which the probability of arrival was the parameter of main interest.

4.3 Selection procedure

It is not straight forward to define a set of general and objective criteria for selecting the worst case meteorological scenario for the atmospheric transport of radioactive pollutants as the definition of a worst case can depend on many factors. Parameters such as deposition (wet or dry), arrival time, accident time (growing season or not), type of radionuclides (gaseous, particulate), type of receptors (human, non-human), type of area (urban, agricultural or others) have to be taken into consideration.

4.3.1 Source term for the selection procedure

In principle, three accident scenarios with three different source terms corresponding to the three selected locations had to be considered. However, mainly due to computational time limits, only one simplified source term has been used for all accident locations. Table 4.1 shows the derived source term that was used only for selection of the worst case meteorological scenarios. The particle size and density are taken from the ARGOS database. ARGOS is a decision support system which is used by radiation protection authorities in Scandinavian countries. The particle dimensions are amongst the smallest in this database, which are subject to the longest atmospheric transport and the least affected by wet deposition. The release rate and period, as well as vertical range, are in a good agreement with what is typically used in exercises conducted by all Scandinavian countries in the frame of a long term project called MetNet (Persson et al., 2007).

Table 4.1. Specification of the preliminary source term used for the selection procedure.

Parameter	Value
Initial location	72.5N, 55.5E
Intermediate location	69.5N, 47.0E
Final location	68.04N, 39.33E
Radionuclide	Cs-137 in the particle form
Particle radius	0.55 μm
Particle density	2.3 g cm^{-3}
Release rate	$2.0 \times 10^{11} \text{ Bq s}^{-1}$
Release period	12 hours
Vertical range	0-500 m

The SNAP model was run for all three accident locations, twice a day at 00:00 UTC and 12:00 UTC, for two months (August and September) for the entire period of 33 years available in the collated meteorological database. In total, this resulted in more than 12000 model runs.

As such a large number of runs makes it impracticable to examine the results of each individual run visually, a simple automatic algorithm was used for the selection purpose. It was applied to each of the three considered accident locations separately. In the algorithm, the total deposition of Cs-137 on Norwegian territory was calculated for each model run and the release date. In the next step of the selection procedure, the output files were sorted according to the deposition values and the situations with highest depositions were highlighted. The top cases on the sorted list were then inspected visually for selection of the worst case meteorological scenarios. An extract of the results of the selection procedure for all three release locations are shown in Table 4.2. Top four cases and the last case - with lowest average deposition over Norway are shown in Table 4.2.

The number of cases with deposition above zero decreases with the distance between the release location and Norway. For releases at Stepovogo Fjord, during transport (Barents Sea) and at the final destination (Gremikha), the probability of radioactive contamination reaching Norwegian Territory is 17%, 25% and 37%, respectively.

Also, the average deposition over Norway is clearly dependant on the distance from the release location, with the largest depositions for the accidental release occurring at Gremikha. There is an exception however with highest deposition being observed for the release located on the transport route and the case from 7 September 1986 at 12 UTC. This exceptional case is discussed in Section 4.4.2. The final selection of the worst case meteorological scenarios is discussed in the following sections.

Table 4.2. Results of the selection procedure for the worst case meteorological scenarios for all three releases locations. The time of accident start is shown as year, month, day and hour (UTC). Average deposition over Norway is given in $Bq m^{-2}$.

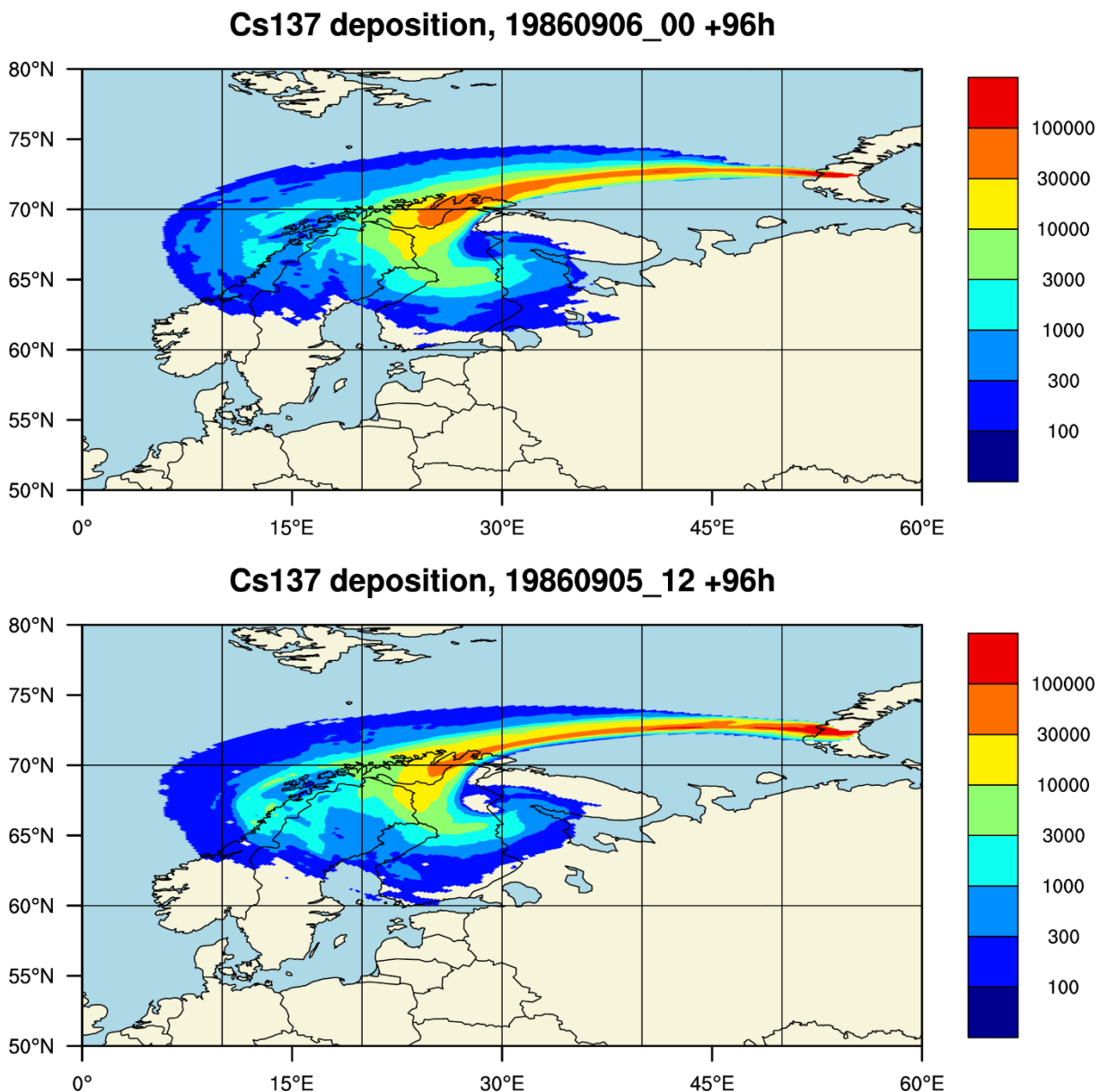
Stepovogo Fjord		
<i>Rank</i>	<i>Date</i>	<i>Average deposition</i>
1	1986 09 06 00	4878
2	1986 09 05 12	3272
3	1998 08 26 00	3146
4	1986 09 06 12	2933
.
620	1983 09 19 12	0.0003
Barents Sea		
<i>Rank</i>	<i>Date</i>	<i>Average deposition</i>
1	1986 09 07 12	6425
2	1986 09 07 00	4970
3	1998 09 17 00	4278
4	1999 08 15 12	4258
.
930	2009 08 20 00	0.0003
Gremikha Bay		
<i>Rank</i>	<i>Date</i>	<i>Average deposition</i>
1	2009 08 23 12	6185
2	2004 09 22 00	6000
3	2004 09 22 12	5993
4	2006 08 16 00	5645
.
1342	1983 09 07 12	0.0007

4.4 Worst case meteorological scenarios

In the following, the resultant worst case meteorological scenarios are discussed separately for each location of the considered hypothetical accident. Upon selection of the worst case meteorological scenario, use was made of not only absolute values of the average deposition for Norway but also the spatial distribution of the deposition over Norwegian territory. It is important to bear in mind that the deposition levels shown in this section (Figures 4.2 – 4.4) are for illustrative purpose only. They have been based on an elevated source term and used only in the process of selecting worst case meteorological scenarios.

4.4.1 Worst case scenario related to an accident at Stepovogo Fjord

Deposition maps corresponding to the top four meteorological cases listed in Table 4.2, for an accident at the current location of K-27 in Novaya Zemlya, are shown in Figure 4.2. For three of the top four meteorological cases identified for this location, only the northern and central part of Norway is affected by the deposition (mostly the Northern part). Average deposition in case nr. three is approximately 35% lower than average deposition in case nr. one, but almost the entire territory of Norway, including Oslo, is affected by the deposition in the former case. Therefore, case nr. three was selected as the worst case meteorological scenario for a hypothetical accident at Stepovogo Fjord with the accident starting on 26 August 1998 at 00 UTC.



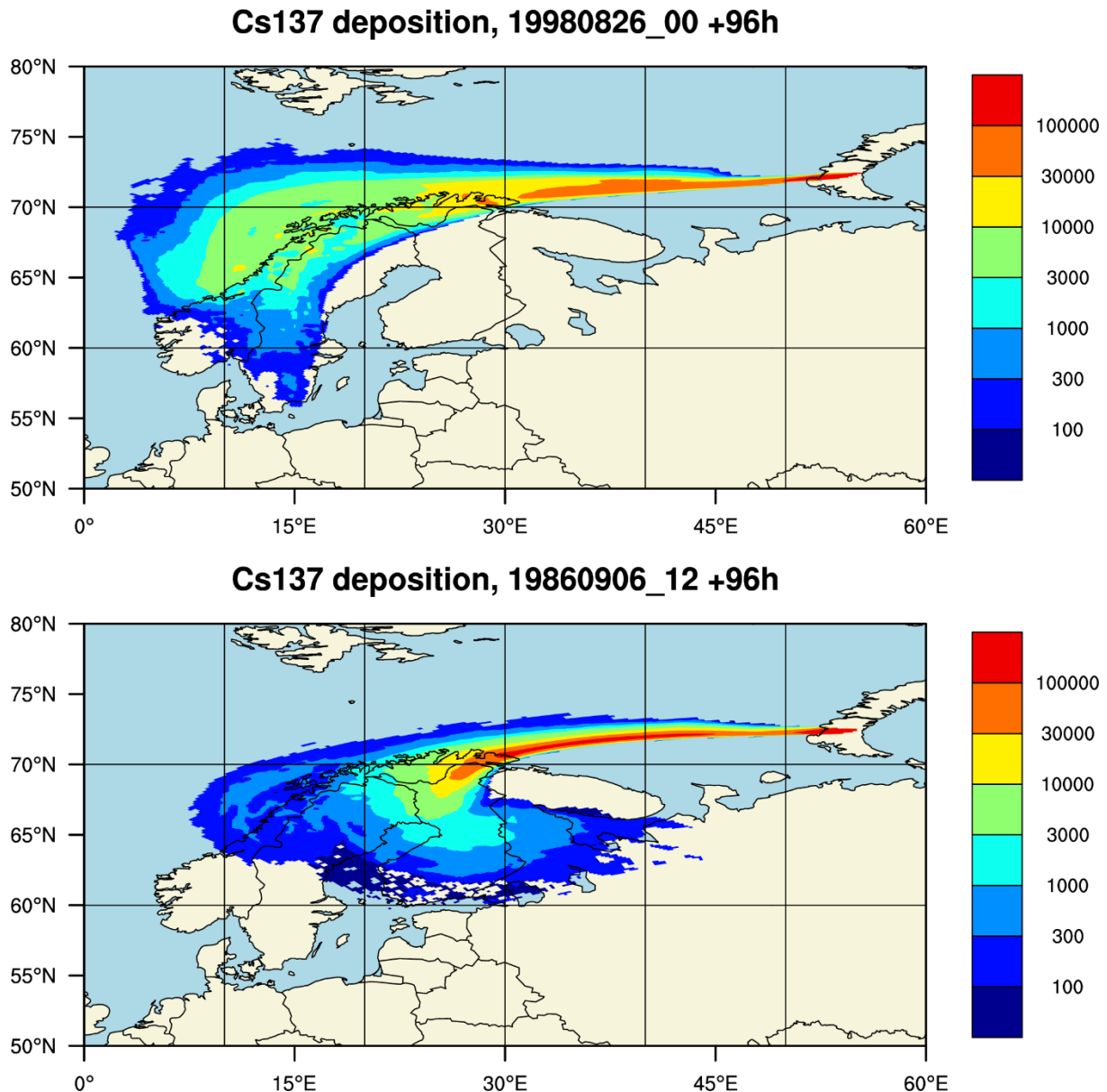
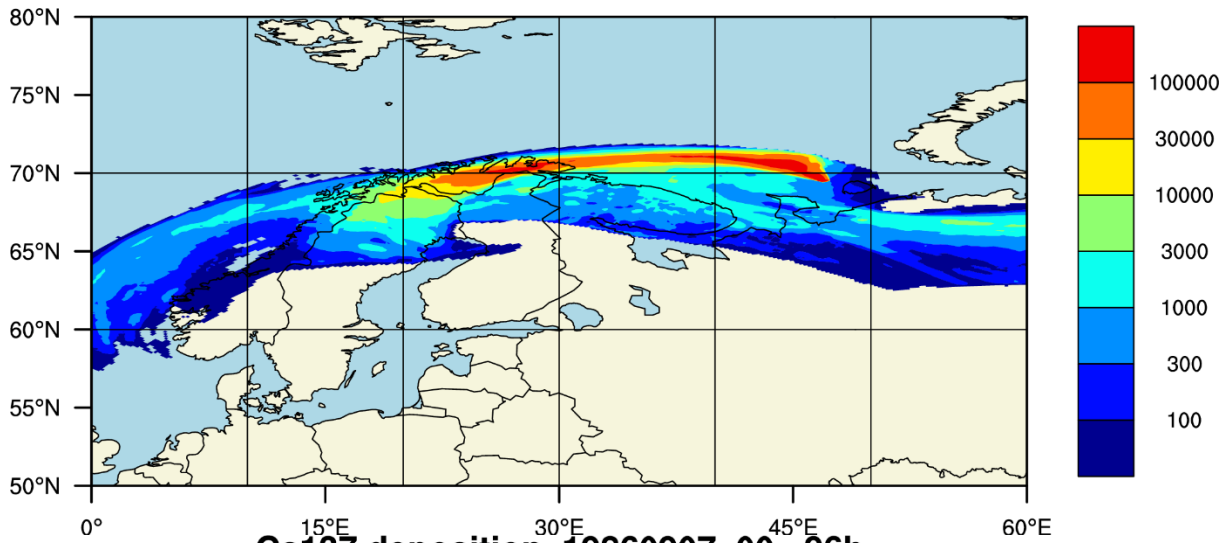


Figure 4.2. Deposition maps of Cs-137 for accident at the current location of K-27, 96 hours after the accident start. The date and hour of the accident start are shown above each map. Top four meteorological cases from Table 4.2. Units: Bq m⁻². The deposition levels here are for illustrative purpose only, having been based on an elevated source term.

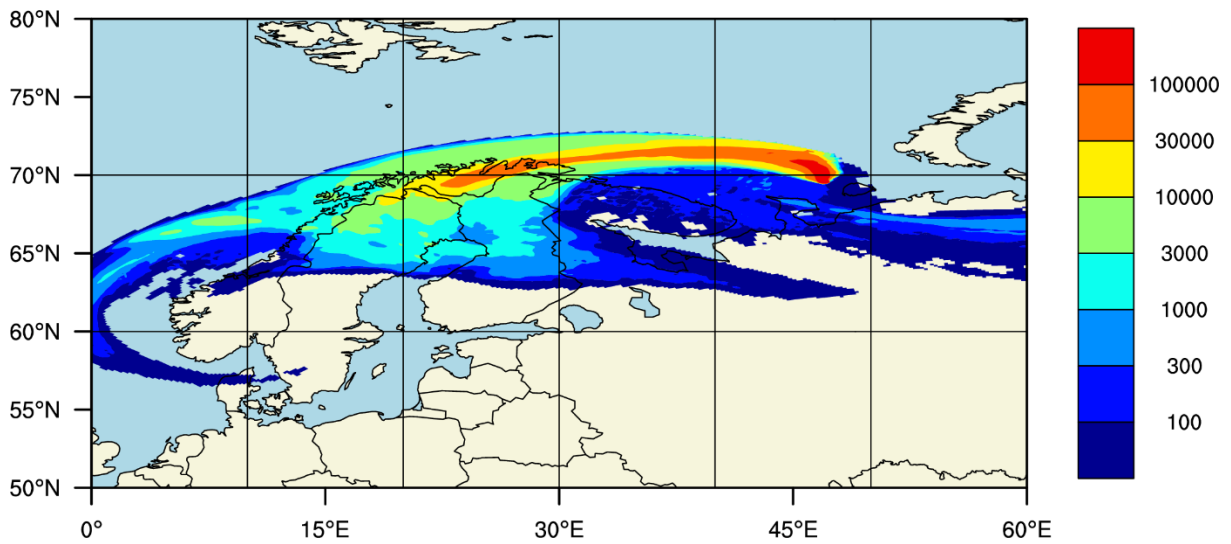
4.4.2 Worst case scenario related to an accident during transport

Deposition maps corresponding to the top four meteorological cases listed in Table 4.2, for an accident on the way from Novaya Zemlya to Gremikha Bay near Murmansk, are shown in Figure 4.3. For this release location, none of the four cases reach the south of Norway, but the top case in Table 4.2, with the release starting on 7 September 1986 at 12 UTC, covers the entire coast of Western Norway and a large part of Central Norway. This is also the case with highest average deposition over Norway for all three accident locations. These were the main reasons for selecting this case as the worst case meteorological scenario for an accident during transport. It is interesting to consider case nr. three with the release starting on 17 September 1998. In this case, the radioactive cloud passes only the very northern part of Norway and then turns north towards Svalbard. This gives very high deposition in the north of Norway but no deposition in the remaining parts of Norway.

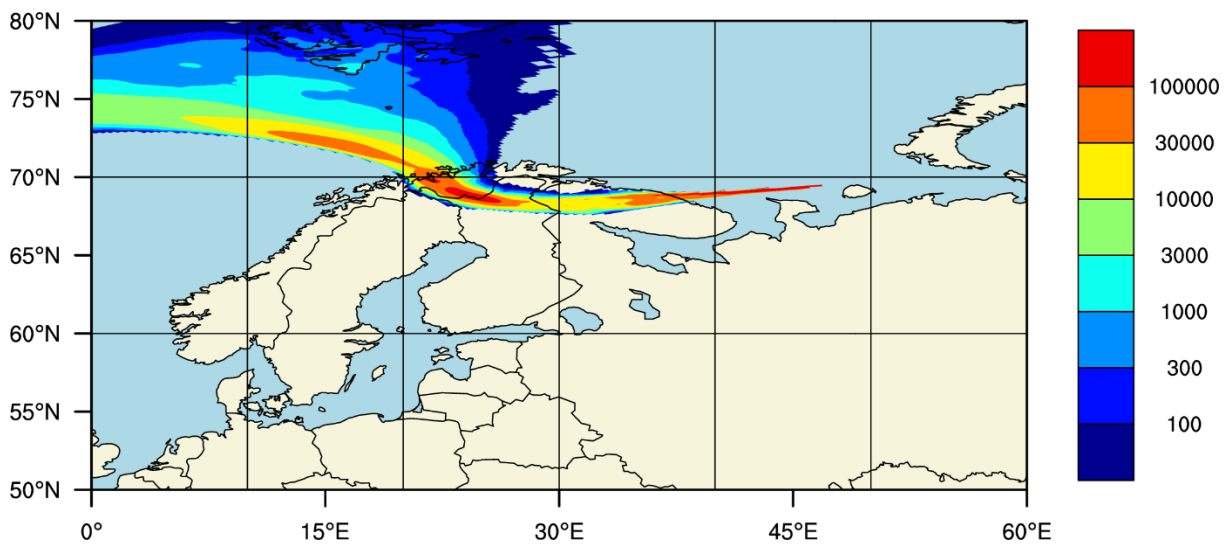
Cs137 deposition, 19860907_12 +96h



Cs137 deposition, 19860907_00 +96h



Cs137 deposition, 19980917_00 +96h



Cs137 deposition, 19990815_12 +96h

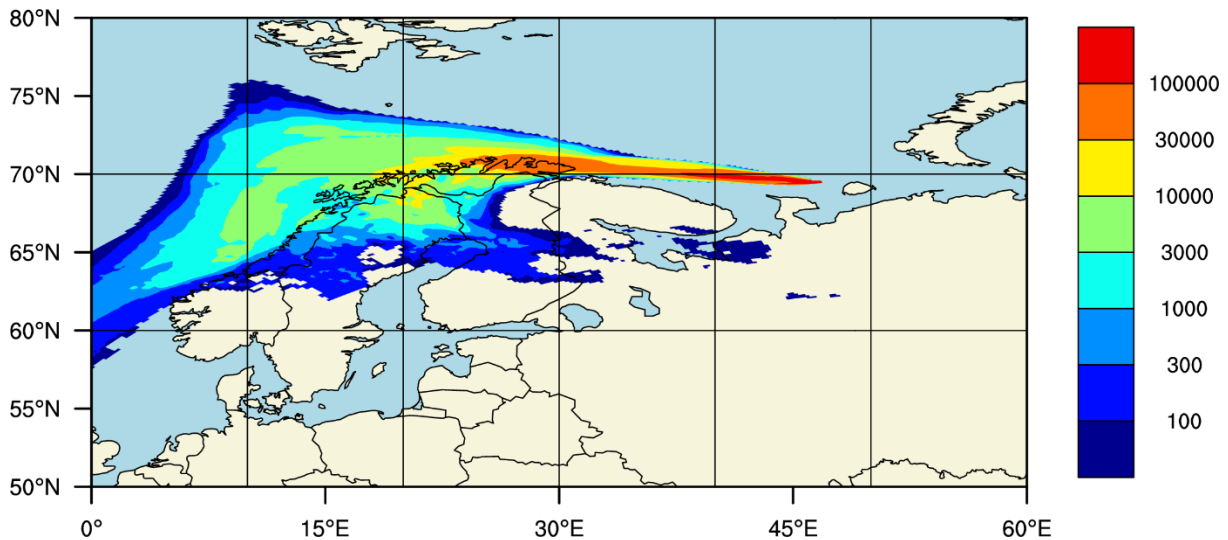
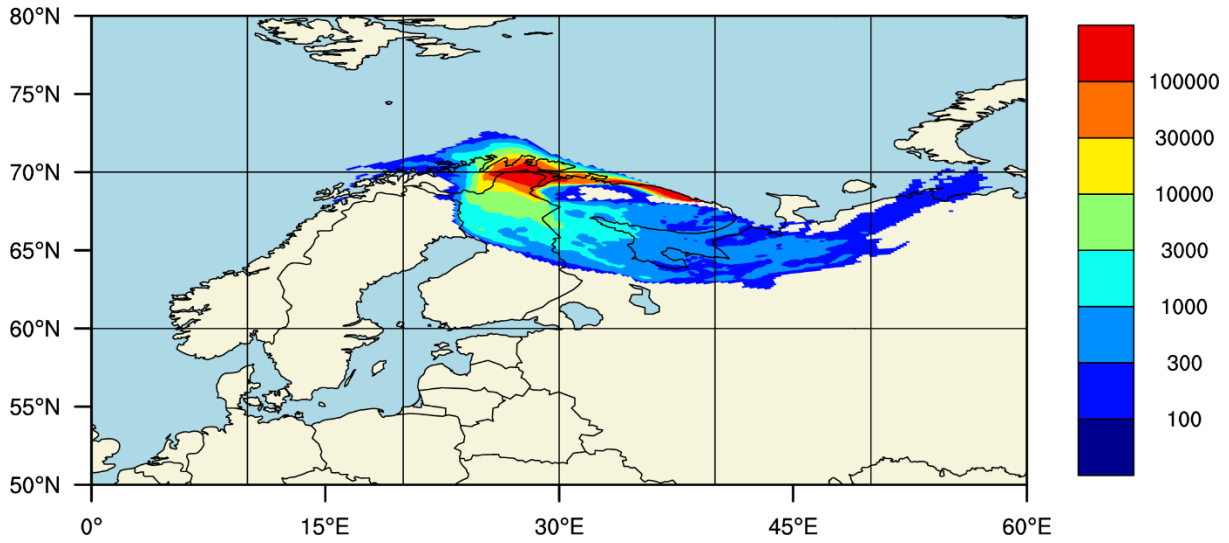


Figure 4.3. Deposition maps of Cs-137 for accident during the transport, 96 hours after the accident start. The date and hour of the accident start are shown above each map. Top four meteorological cases from Table 4.2. Units: $Bq\ m^{-2}$. The deposition levels here are for illustrative purpose only, having been based on an elevated source term.

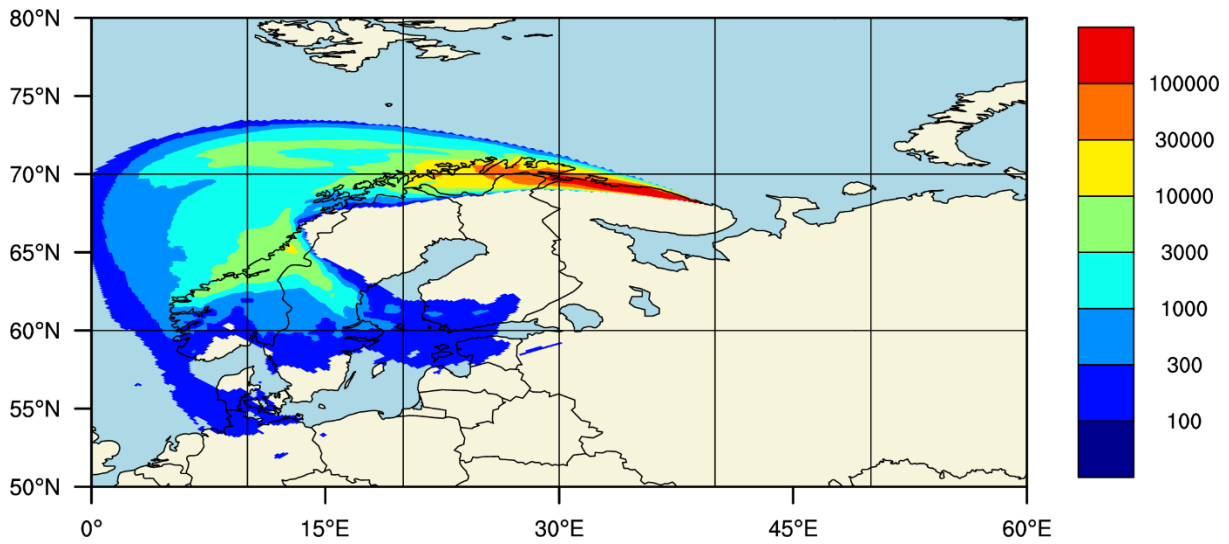
4.4.3 Worst case scenario for a release at Gremikha

For a release located at the final destination of the submarine, all four cases in Table 4.2 show very high levels of average deposition. The spatial pattern of the deposition in cases nr. two and nr. three is quite similar, however in case three, deposition over southern Norway is higher (see Figure 4.4). Since the average deposition in case three (with the release starting on 22 September 2004 at 12 UTC) is only 5% lower than the average deposition in the worst case, this case was selected as the worst case meteorological scenario for a release at the final destination. It should be mentioned that this meteorological worst case scenario is also the worst case among the three release locations from the Norwegian perspective. The main reason for this would be the proximity of the release site to Norway, but there is one additional factor which makes the final destination different from the other two locations and this is the potential for an accidental release during the entire year and not only during the two months considered for the other two accident locations.

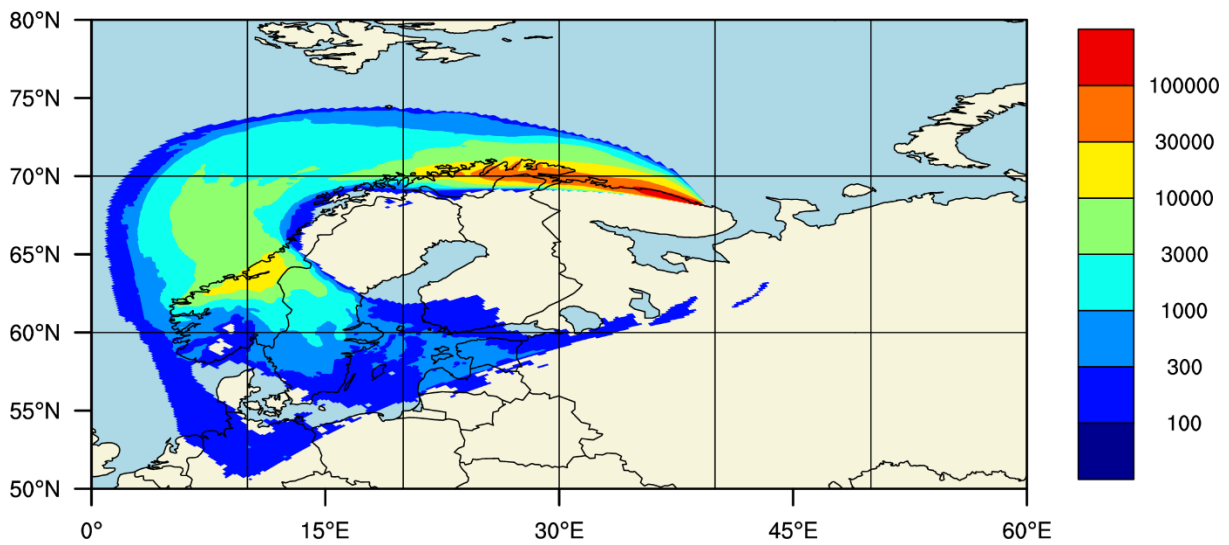
Cs137 deposition, 20090823_12 +96h



Cs137 deposition, 20040922_00 +96h



Cs137 deposition, 20040922_12 +96h



Cs137 deposition, 20060816_00 +96h

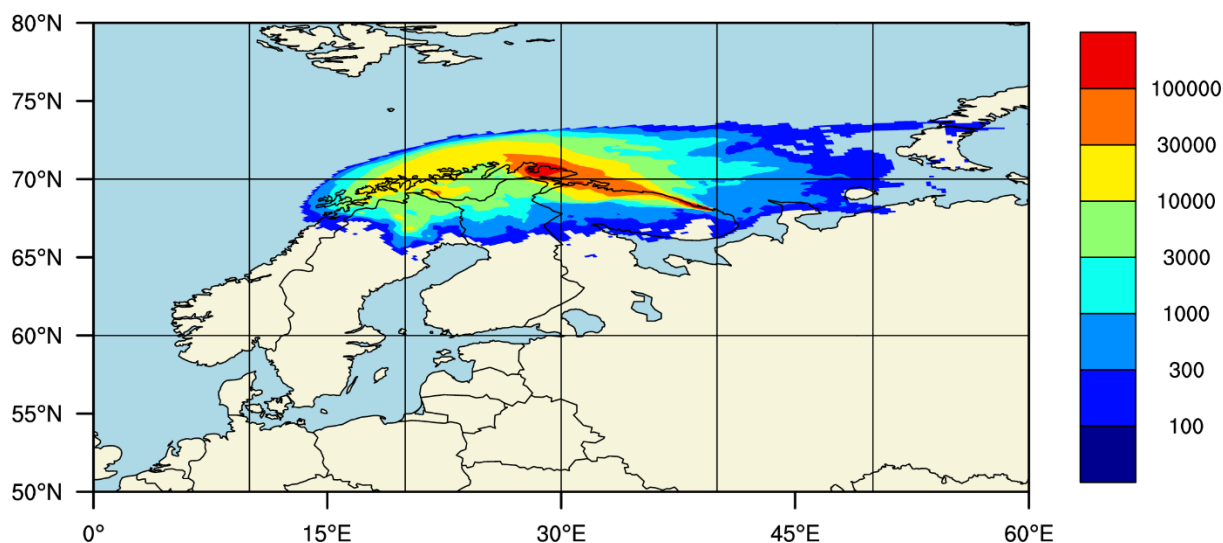


Figure 4.4. Deposition maps of Cs-137 for release at the final destination, 96 hours after the accident start. The date and hour of the accident start are shown above each map. Top four meteorological cases from Table 4.2. Units: $Bq\ m^{-2}$. The deposition levels here are for illustrative purpose only, having been based on an elevated source term.

4.5 Statistical analysis

The results of all model runs for the entire 33 years period was statistically analysed in order to estimate the total deposition and probability of arrival for each model grid for the territory of Norway. This analysis is computationally very time consuming and hence was performed just for Cs-137. Statistical analyses were performed separately for each of the three accident locations.

4.5.1 Meteorological cases which results in deposition in Norway

The percentiles for the deposition to Norwegian territory (excluding Svalbard) is shown in Figure 4.5. It is not surprising that an accident at Gremikha would result in more possible instances where contaminants arrive over Norway as the release source is located close to Norway.

A single case exists that is related to the transport scenario, where deposition over Norway is slightly higher than in the worst case related to the Gremikha scenario, and this is the reason for the anomaly observed at the far right of the histogram displayed in Figure 4.5.

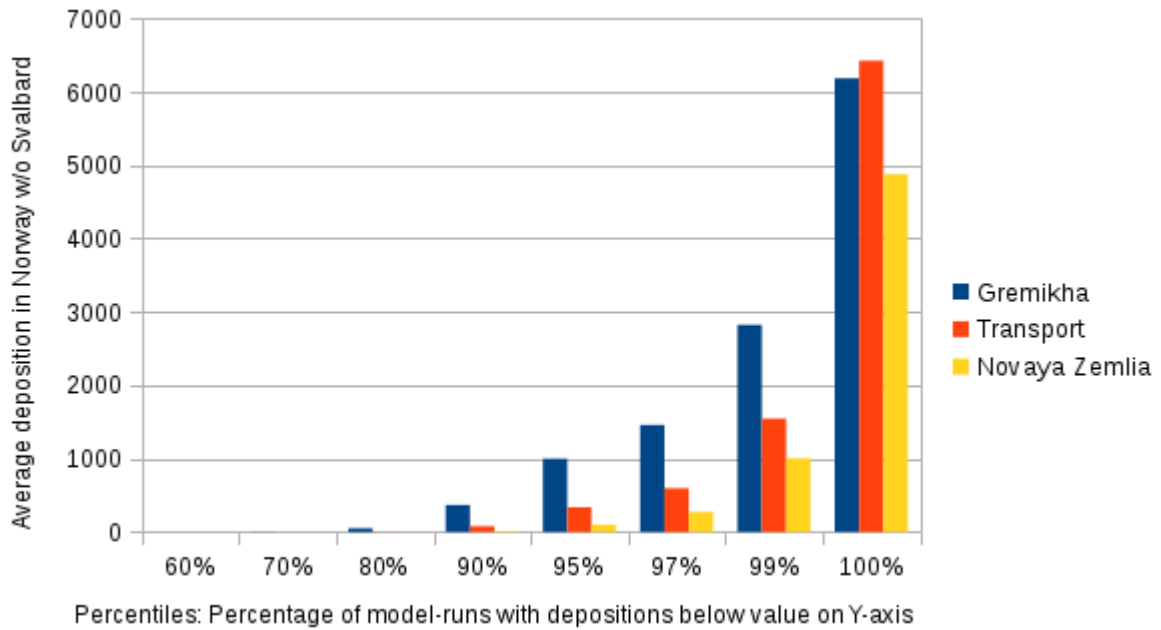


Figure 4.5. Percentages of cases with positive deposition to Norway from all model runs in the entire period. The territory of Svalbard was excluded from these calculations. Deposition units: Bq m⁻².

4.5.2 Probability of arrival

Probability of arrival is another piece of important information which can be used in the process of evaluation of an impact. Probability of arrival to a given model grid was calculated as the ratio of model runs with non-zero concentrations in the given grid to total number of model runs. The maps of the probability of arrival to each model grid are shown in Figure 4.6 for all three accident locations. Probability of arrival to Norway is clearly higher for the hypothetical accident in Gremikha Bay than for releases at the other two locations. This probability has a maximum in the very northern part of Norway with the following ranges 10-15%, 15-25% (closer to 15%) and 15-25% (closer to 25%) for an accident occurring at Stepovogo Fjord, under transport (Barents Sea) and at Gremikha, respectively. These probabilities are much lower for southern Norway, being below 1% for a release at the initial location and below 3% for releases at the remaining 2 locations.

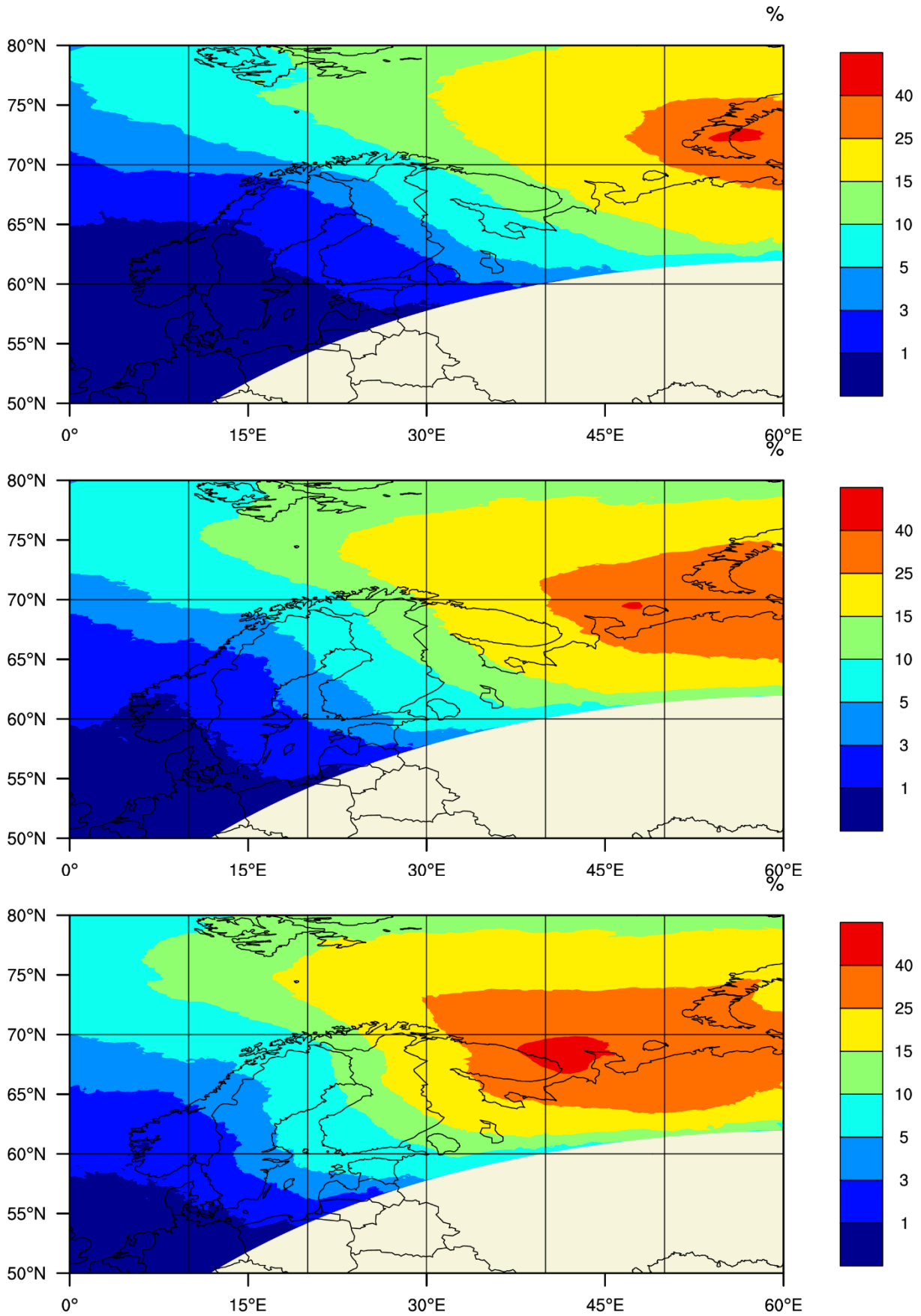


Figure 4.6: Maps of probability of arrival to each model grid from releases: at initial location - top, on the way to Gremikha Bay - in the middle and at the final destination - bottom.

4.6 Source term for selected scenarios

As previously discussed, the simplified, preliminary source term was used for the model runs in the selection procedure. A more advanced and elaborate source term was developed for the final SNAP runs with the selected worst case meteorological scenarios. This source term was used for all three potential release locations. Activities in the source term were calculated based on considering the inventory of the submarine as of 2013 and the assumption of 30% damage of the fuel rods upon the occurrence of a criticality event with a power of $10E+20$ fissions (for more details, see Hosseini et al. 2015).

Furthermore, it was assumed that a fire breaks out which would result in the release of 20% of the original inventory of the submarine to the atmosphere. Four particle classes with different densities and sizes and iodine gas were taken into account in determining the source term for the final model runs. There were some common features of the source for all classes of particles and iodine gas. These were:

- a release time of one hour
- a release height of 100 m
- a release radius of 25 m

Specification of the “accident” source term for four classes of particles as well as iodine gas is presented in Table 4.3. The total releases given in Table 4.3 is based on considerations and assumptions made earlier (see Hosseini et al. 2015, section 8.5).

4.6.1 Source term for the SNAP runs

In the SNAP model the properties of real particles and gases are included in the so-called “model particles” (see section 4.1). According to specification in Table 4.3, if each real particle and gas is represented, we would need 24 model particles for the UO_2 -Be group, 32 in Bitumen group, 24 in Metal group and 6 in Ru-106 group. In addition, two model particles should represent I-131 and I-133. Altogether this approach would require 86 model particles.

Table 4.3. Source term for the worst case accident scenario for K-27 submarine.

UO ₂ Be, density=2.1 g cm ⁻³ , size classes: 0.1, 0.5, 1.0, 5.0, 10.0, 20.0, 50.0, 100.0 µm		
Component	Half-life	Total release (Bq)
¹³⁷ Cs	30.17 years	7.10E+12
⁹⁰ Sr	28.8 years	6.20E+12
²³⁸ Pu	no decay	1.60E+11
<i>Total</i>		1.346E+13
Bitumen, density=1 g cm ⁻³ , size classes: 0.1, 0.5, 1.0, 5.0, 10.0, 20.0, 50.0, 100.0 µm		
Component	Half-life	Total release (Bq)
¹³⁷ Cs	30.17 years	4.40E+11
⁹⁰ Sr	28.8 years	3.90E+11
²³⁸ Pu + ²⁴⁰ Pu	no decay	1.00E+10
¹³¹ I	8.04 days	1.40E+11
<i>Total</i>		9.80E+11
Metal coolant, density=10.5 g cm ⁻³ , size classes: 0.1, 0.5, 1.0, 5.0, 10.0, 20.0, 50.0, 100.0 µm		
Component	Half-life	Total release (Bq)
¹³⁷ Cs	30.17 years	4.40E+11
⁹⁰ Sr	28.8 years	3.90E+11
²³⁸ Pu	no decay	1.00E+10
<i>Total</i>		8.40E+11
Ru-106, density=3.3 g cm ⁻³ , size classes: 0.1, 0.5, 1.0, 5.0, 10.0, 20.0 µm		
Component	Half-life	Total release (Bq)
¹⁰⁶ Ru	1.02 years	1.90E+09
I-131, gas, density=0.0113 g cm ⁻³		
Component	Half-life	Total release (Bq)
¹³¹ I	8.04 days	1.40E+11
¹³³ I	20.04 hours	5.20E+12
<i>Total</i>		5.34E+12

However, based on similarities with regards to size and density which are the most important properties of model particles in the context of SNAP simulations, it was decided to model each group rather than modelling each component. In this manner the number of model particles for simulating the source term specified in Table 4.3 could be reduced to 32 cases. The specification of the considered model particles in the SNAP runs for the worst case scenarios is presented in Table 4.4.

Table 4.4. Specification of the model particles representing the real particles and gases for the worst case SNAP model runs. The symbol "●" indicates the type of the model particle used in the simulations.

Group	Density g cm ⁻³	Radius in μm								Release Bq	Decay (h)
		0.1	0.5	1.0	5.0	10	20	50	100		
UO ₂ Be	2.1	●	●	●	●	●	●	●	●	1.35×10 ¹³	No
Bitumen	1.0	●	●	●	●	●	●	●	●	9.8×10 ¹¹	No
Metal	10.5	●	●	●	●	●	●			8.4×10 ¹¹	No
¹⁰⁶ Ru	3.3	●	●	●	●	●	●			1.9×10 ⁹	No
¹³¹ I	0.0113					●				1.4×10 ¹¹	192.96
¹³³ I	0.0113					●				5.2×10 ¹²	20.04

The release rate for each model particle was specified in the *snap.input* file according to Table 4.4. It was assumed that the accident takes place as a rapid release of radionuclides to the atmosphere. a one hour release duration was adopted.

As information regarding the distribution of radioactivity among different size classes were missing, an equal distribution of radioactivity for each of the size classes was assumed upon running SNAP.

The heat generated during the accident lifts the radioactive pollutants into the air. Usually the upper limit for vertical distribution of pollutants in such a case is the top of the mixing layer. For the chosen locations and the time of the year when the potential releases can happen, the typical range of the mixing layer is 200 m. Therefore, we have assumed the release to be placed in the middle of this typical mixing layer – at an altitude of 100 m. The horizontal spread of radionuclides during the release was assumed to take place in the cylinder with the radius of 25 m.

4.7 Model runs for the worst case scenarios

The results of the SNAP model runs with the final source term as specified in Table 4.4 are presented here. These results are presented separately for each of the three considered release locations; Stepovogo Fjord, the Barents Sea and Gremikha.

4.7.1 Accident at the Stepovogo Fjord

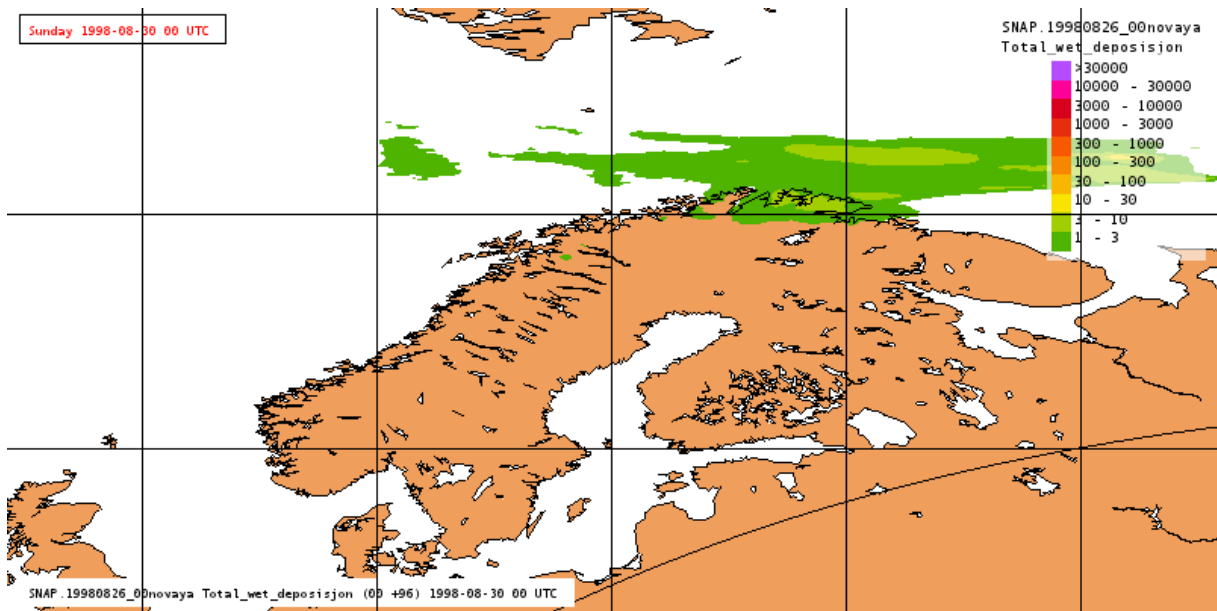
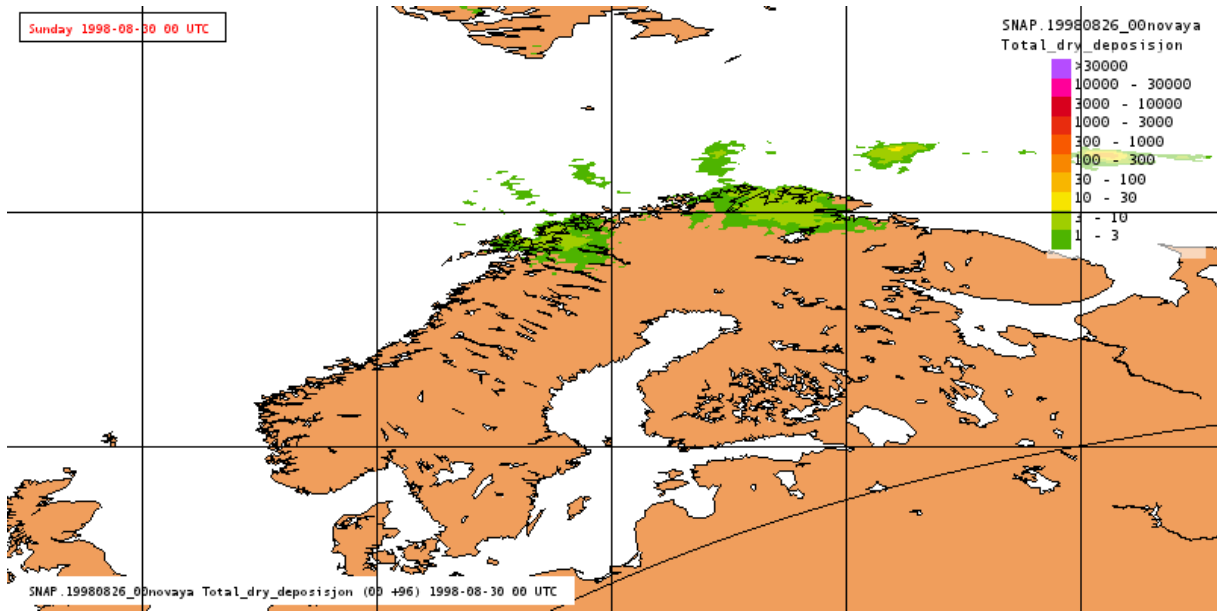
To simulate the worst case scenario for a release at the initial location, the SNAP model was run with a release starting on 26 August 1998 at 00 UTC. The model simulation was performed for 96 hours, which means that deposition and concentration fields were calculated until 30 August 1998 at 00 UTC. In Figure 4.7 the results of the model simulation are shown as maps of dry, wet and total deposition.

These depositions were calculated as a sum of depositions from all particle classes and iodine gas. Usually, wet deposition dominates compared to dry deposition in the atmospheric transport of radioactive particles. However, in the considered meteorological scenario, with the release occurring in the Stepovogo Fjord, Norway is more affected by dry than wet deposition, except for a very northern part of Finnmark where both types of deposition contribute almost equally to the total deposition. There is also a second area with visible deposition located between Nordland and Troms counties, but this time only dry deposition is present. The maximum values of total deposition in the northern part of Finnmark are in the range of 10-30 Bq m⁻². A range of maximum total deposition in the region between Nordland and Troms is slightly lower, 3-10 Bq m⁻².

4.7.2 Accident on the way to Gremikha

For simulation of the hypothetical release on the way from Novaya Zemlya to Gremikha Bay, the identified worst case meteorological scenario was used, with the start of the release being on 7 September 1986 at 12 UTC. For this meteorological scenario, the SNAP model was again run for 96 hours. The calculated maps of dry, wet and total depositions - 96 hours later, on 11 September 1986 at 12 UTC are shown in Figure 4.8. These maps also include complete deposition, as a sum from all particle classes and iodine gas.

Compared to the previous simulation (release at Stepovogo Fjord), the landscape is completely different with regards to the proportions of dry and wet deposition. The dry deposition pattern is very narrow indicating relatively low turbulence and lateral mixing close to the ground. The pattern of wet deposition is much wider indicating more mixing in the upper parts of the atmosphere. Dry deposition is apparent only in Finnmark with relatively low values of 1- 3 Bq m⁻². Wet deposition has maximum values also in Finnmark, with much higher range of 100-300 Bq m⁻², but it is also present in Troms and Nordland counties. The shape of total (dry and wet) deposition is very similar to the wet deposition pattern with maximum in the northern part of Finnmark close to 300 Bq m⁻². Also in this case, the central and southern part of Norway is not affected by the accident.



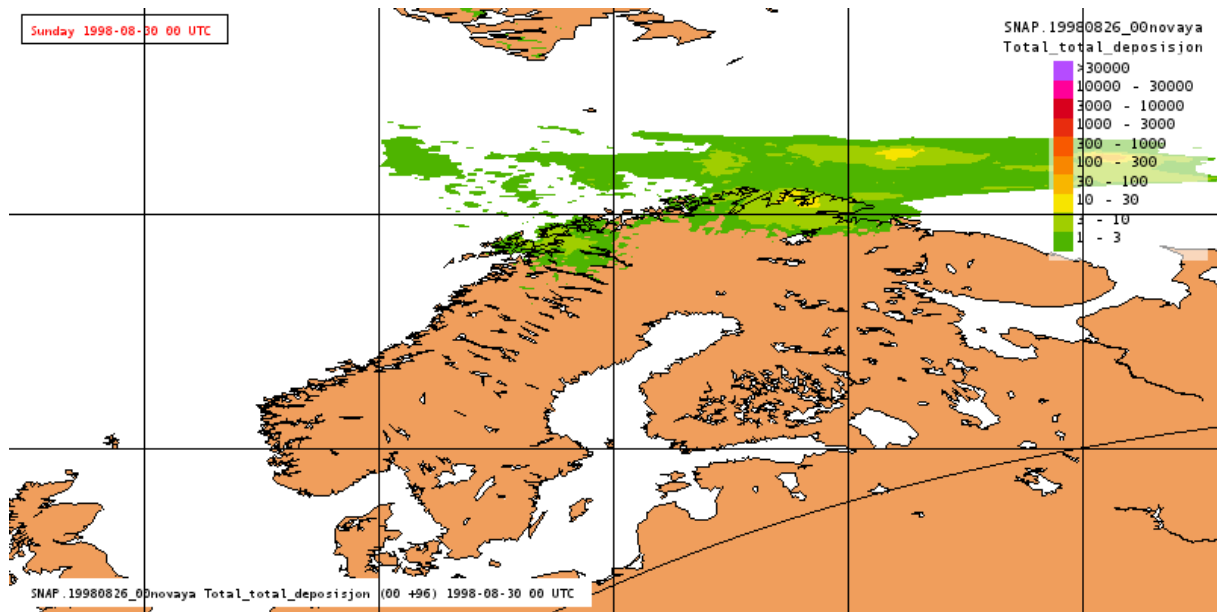
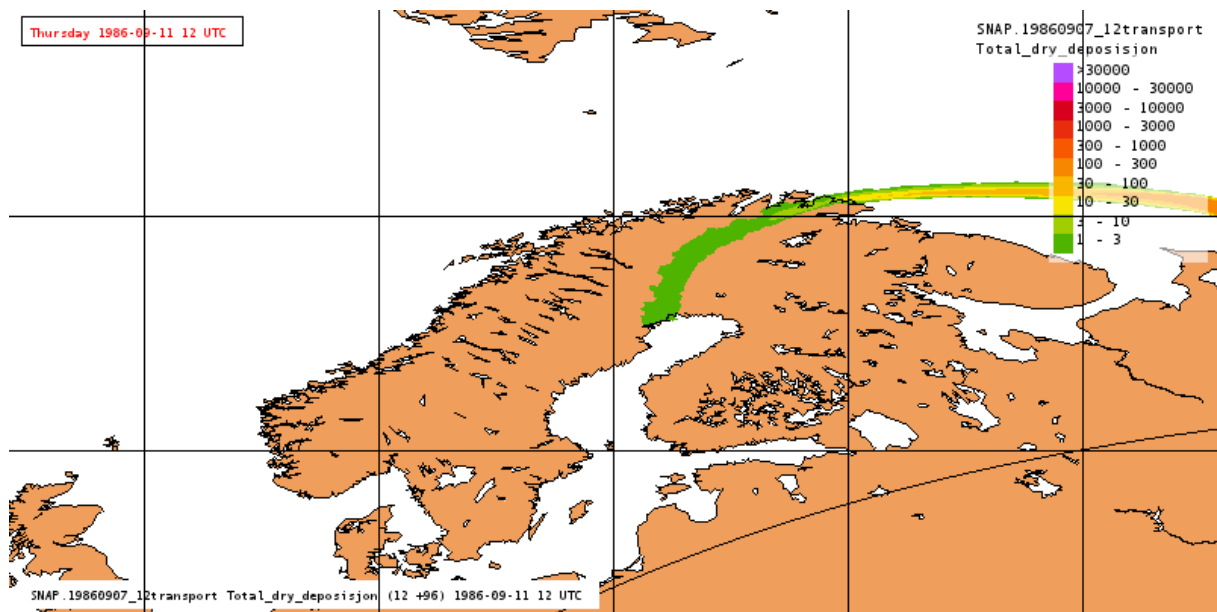


Figure 4.7. Deposition maps from SNAP run with the source term specified in Table 4.4 and accident at the initial location. Dry deposition - at the top, wet deposition – in the middle and total deposition (dry and wet) at the bottom. Units: Bq m⁻².



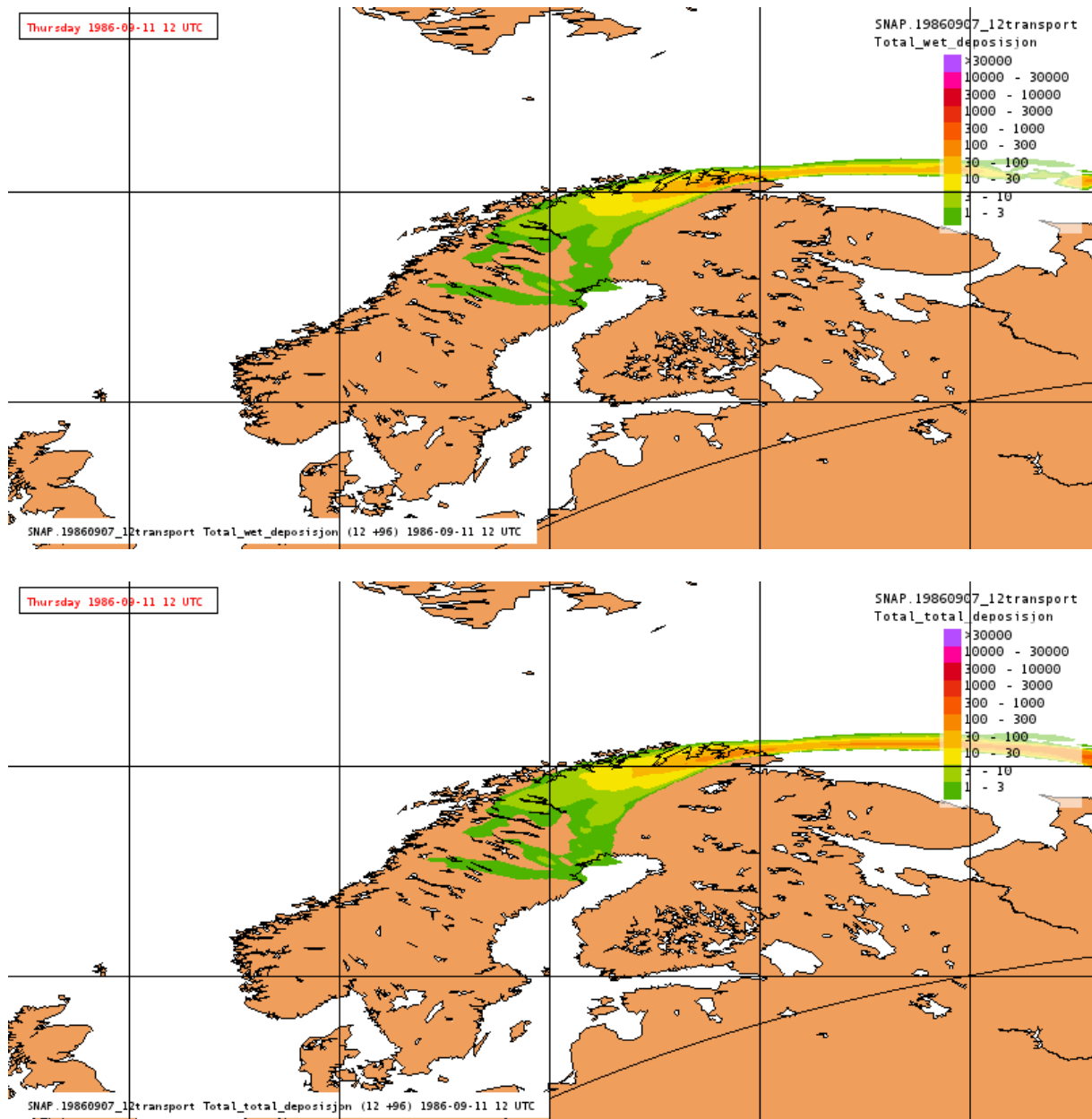


Figure 4.8. Deposition maps from SNAP run with the source term specified in Table 4.4 and accident on the way to Gremikha. Dry deposition - at the top, wet deposition - in the middle and total deposition (dry and wet) at the bottom. Units: $Bq\ m^{-2}$.

4.7.3 Release at Gremikha Bay - general worst case scenario

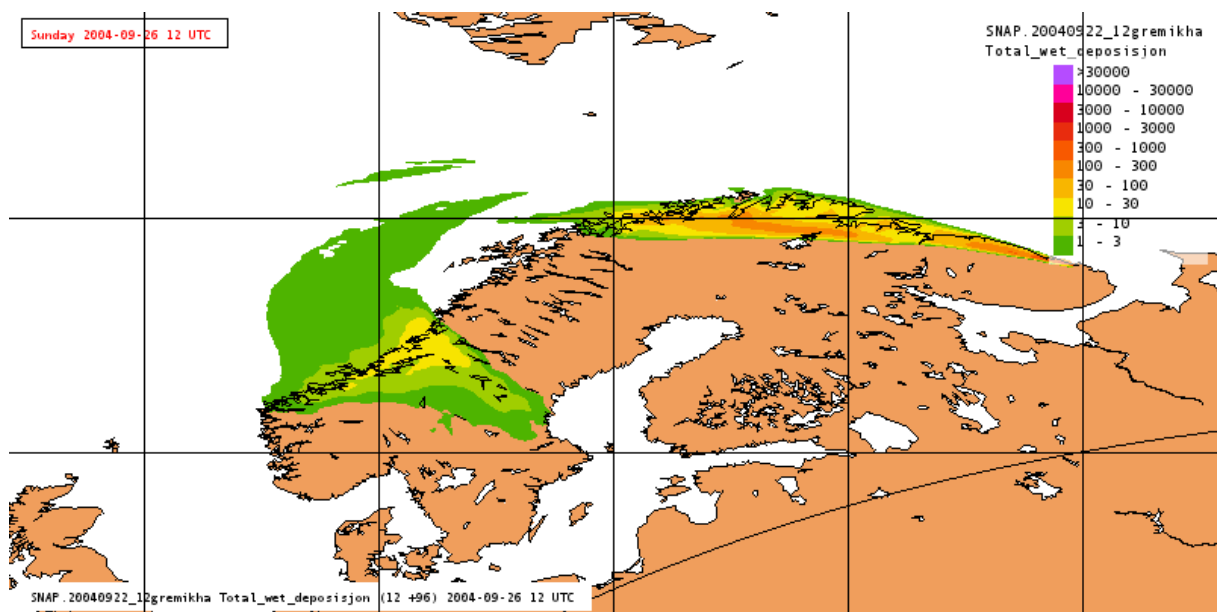
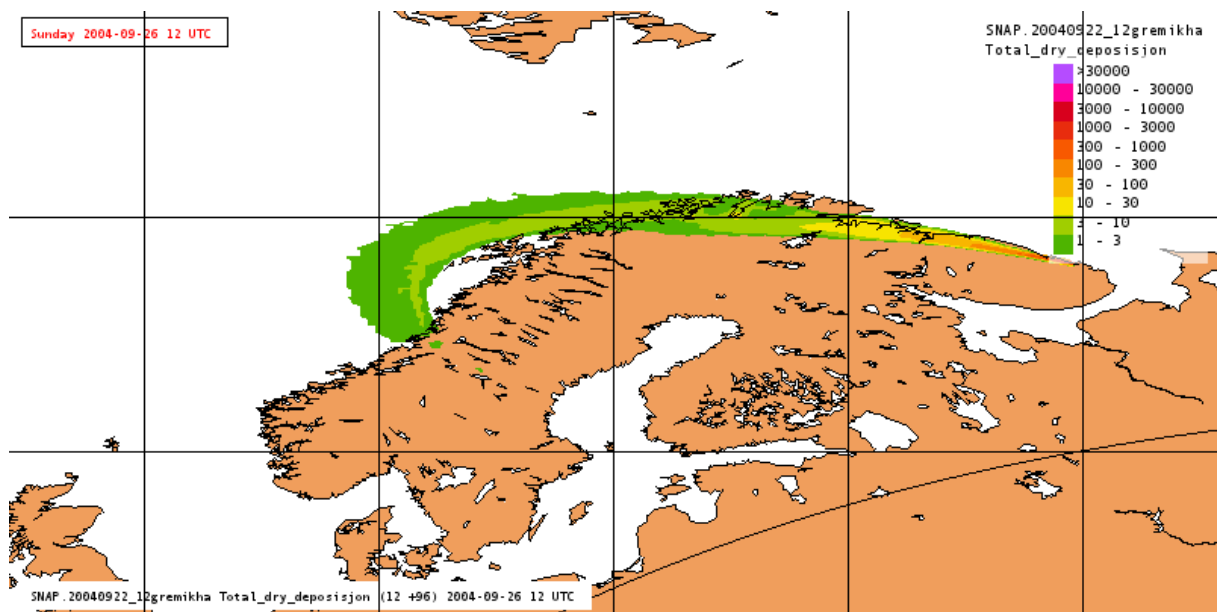
The SNAP model was run again with the source term as specified in Table 4.4 to simulate the worst case meteorological scenario for a release at the final destination, at Gremikha Bay. The release started on 22 September 2004 at 12 UTC. Depositions and concentrations were calculated 96 hours from the release start on 22 September 2004 at 12 UTC. In Figure 4.9, the maps with dry, wet and total depositions are shown. These depositions were calculated as a sum of all considered particle classes and iodine gas.

The range of the deposition and the extent of the Norwegian area which is affected by it is significantly larger in this case compared to the two previous cases. It applies to dry, wet and total deposition. The dry deposition pattern is in the form of relatively narrow and long tongue reaching the coast of central

Norway, but affecting only Finnmark, Troms and to very small extent Nordland counties. The maximum dry deposition of close to 30 Bq m^{-2} can be found in the far North, close to Kirkenes.

The wet deposition pattern is much wider and more irregular compared to dry deposition. There are two local maxima, one in the North reaching 300 Bq m^{-2} and one in central Norway (Nord Trondelag county) in the range $10\text{-}30 \text{ Bq m}^{-2}$.

The same local maxima are also visible in the pattern of total (dry and wet) deposition, which affects three counties in the North (Finnmark, Troms and Nordland), but in addition several counties in central Norway (Nord Trondelag, Sør Trondelag, Møre og Romsdal, Opland and Hedmark). The levels of local maxima are similar to the levels of wet deposition $100\text{-}300 \text{ Bq m}^{-2}$ in the North and $10\text{-}30 \text{ Bq m}^{-2}$ in central Norway. Due to the proximity of the accident location to Norwegian territory, this is the worst case among three locations of the potential accident which have been considered in this study.



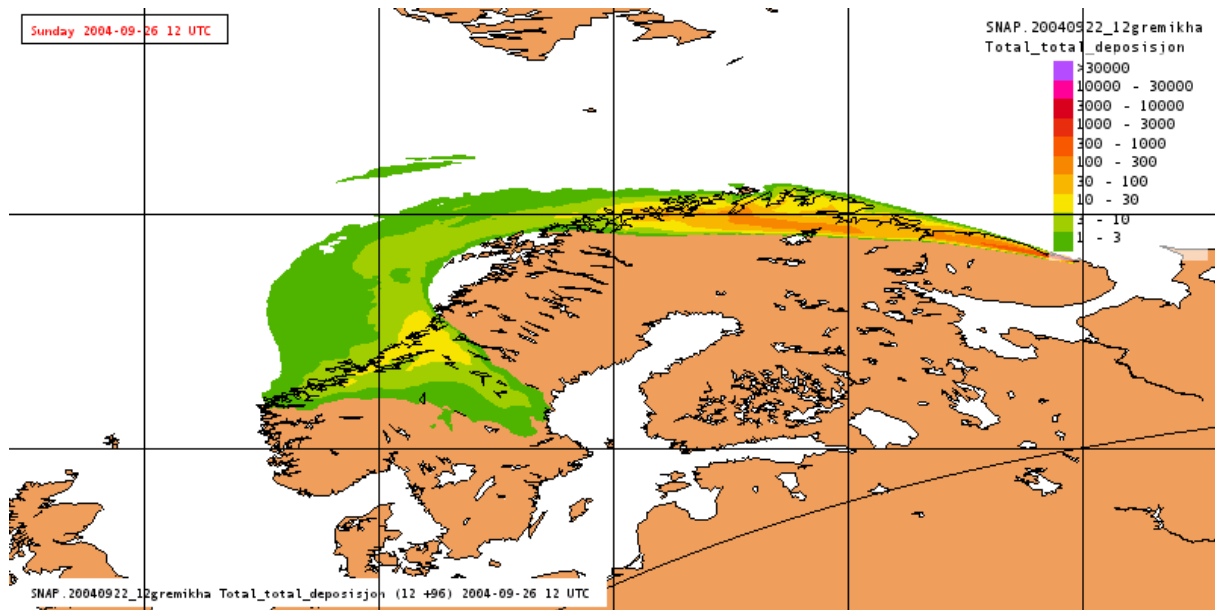


Figure 4.9. Deposition maps from SNAP run with the source term specified in Table 4.4 and accident at the final destination. Dry deposition - at the top, wet deposition – in the middle and total deposition (dry and wet) at the bottom. Units: Bq m^{-2} .

4.7.4 Depositions from individual components

Total deposition from all components together was presented and discussed in the previous section. Here we will discuss the individual impact of all 32 model particles or components included in Table 4.4.

Among four groups of particles which were included in the SNAP runs for the worst case scenario, the difference in total releases between the highest ($\text{UO}_2\text{-Be}$ group) and the lowest (Ru-106) was four orders of magnitude. The total releases of iodine gases were about $5.3\text{E}+12$ Bq and the releases from I-133 were more than that for I-131 by a factor of 37.

These differences in total releases for the groups are clearly reflected in the deposition maps. Also, differences in particle sizes for individual components within each group are quite significant and probably the most important. Deposition from $\text{UO}_2\text{-Be}$ components is higher than deposition from the Bitumen group and slightly lower than deposition from the Metal group. The main reason for this, despite a similar level of release, is the higher density of particles in the metal group compare to the Bitumen group.

The difference in total release is so large that deposition from the last group, Ru-106, is hardly visible on the maps except for areas close to the source, since the same deposition scale is used for all groups. There are some similarities for all groups of particles. Namely, long range transport is most effective when the particle size is below $1\ \mu\text{m}$. For $\text{UO}_2\text{-Be}$ group deposition fields for particles with the size 0.1, 0.2 and $1.0\ \mu\text{m}$, deposition fields are very similar. Above $1\ \mu\text{m}$, the transport range rapidly decreases and for particles with the size above $20\ \mu\text{m}$ (50 and $100\ \mu\text{m}$) only the immediate local area is affected in practice. Deposition fields for iodine and especially for I-133 are similar to those with particle size below $1\ \mu\text{m}$.

4.7.5 Dynamics of transport

The radioactive cloud resulting from a potential accident originating at Gremikha Bay was rapidly transported to Norway in the worst case scenario. After 8-9 hours, the Norwegian cities of Vadso, Vardø and Kirkenes were contaminated with deposition during modelling. In the next 1-2 hours Mehamn and Hammerfest were also contaminated. After 18-20 hours, Tromsø was also affected by the deposition.

Later, during the next 15-16 hours, deposition from the radioactive cloud only affected maritime areas. Approximately 35-36 hours after the worst case accident started, Namsos and Stejnckjer were affected by deposition and after a further 9 hours, Trondheim was as well. In the next stage, the radioactive cloud was transported to Sweden reaching the Baltic Sea after 51 hours.

4.7.6 Time integrated concentrations

The doses to populations can be calculated from the time integrated air concentrations at the surface level. A map of time integrated concentrations from all components together is presented in Figure 4.10. The integration period starts with the beginning of the release. The range of time integrated concentrations is less than the range of deposition. This is not surprising since the wind speeds are much lower at the surface than in the upper part of the mixing layer and above. In addition, wet deposition is a major contributor to total deposition and radionuclides can washout from a high elevation. Very often wet deposition from a nuclear accident can be observed before a significant increase of ground concentration. Mainly, the northern part of Norway is affected by time integrated concentrations in addition to cities such as Vadso, Vardø and Kirkenes. Theoretically some ships on the Norwegian Sea may be affected. In addition, the level of time integrated concentrations can be slightly elevated in Namsos.

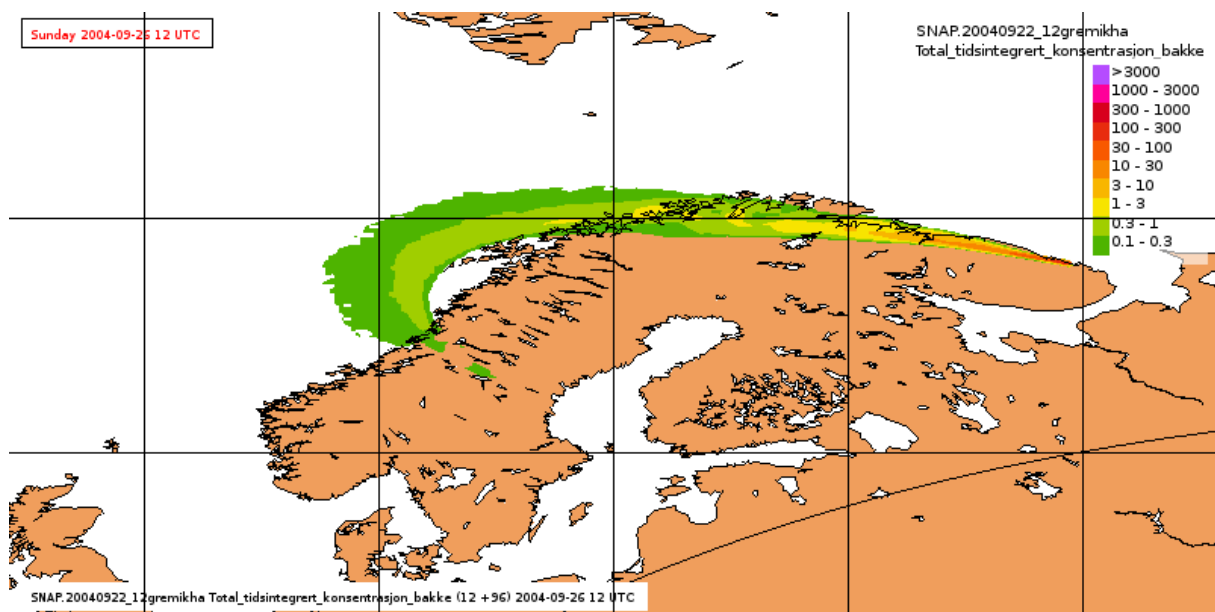


Figure 4.10. Map of time integrated air concentration from the SNAP run with the source term specified in Table 4.4 and Gremikha as accident location. Units: Bq m⁻³.

4.7.7 Comparison with Chernobyl Accident

The relatively low level of total deposition over Norway in this study is also confirmed by comparison with total deposition from the Chernobyl accident as presented in Figure 4.11. In the case of the Chernobyl accident, the entire area of Western Norway and especially mountain regions showed high levels of deposition. The maximum, above 30000 Bq m⁻² is noticeable in the Jotunheimen area and in southern Norway in general. The maximum deposition from a potential K-27 release is only in the range 100-300 Bq m⁻² and can be found in northern Norway. In case of K-27, deposition in southern Norway is insignificant. Further information can be found in Bartnicki et al. (2016).

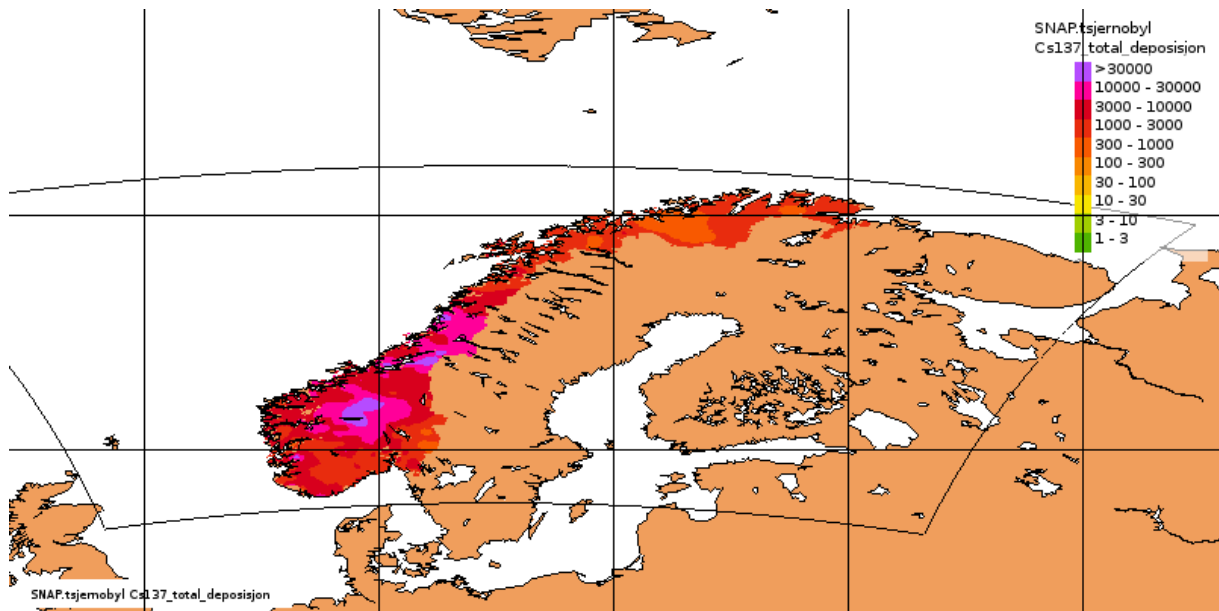
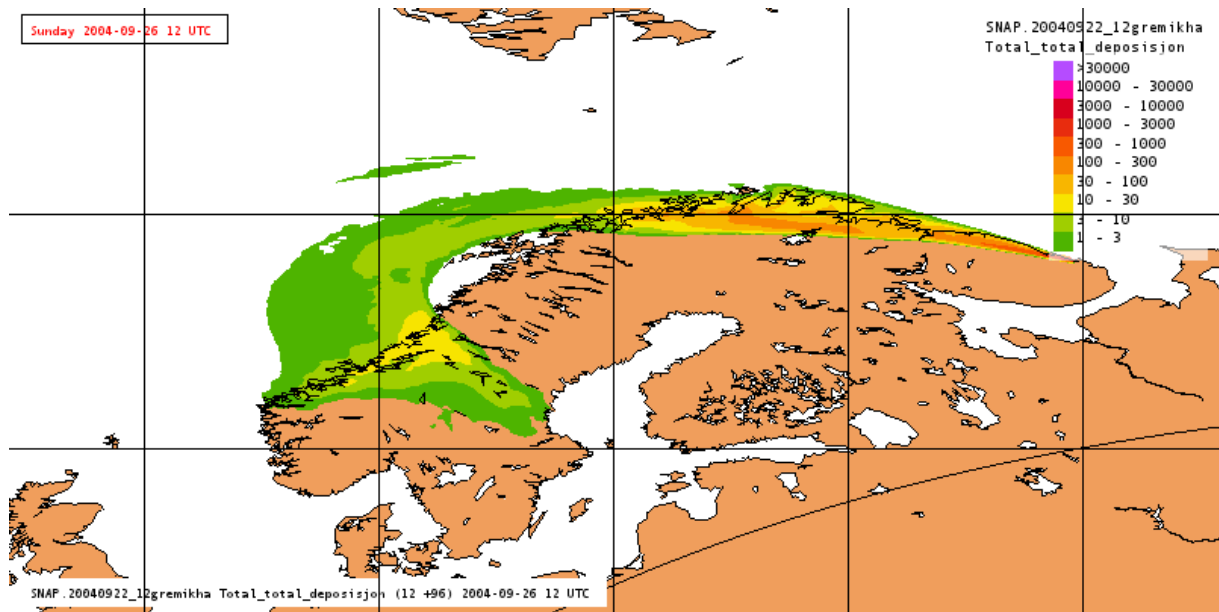


Figure 4.11. Comparison of a deposition map from the K-27 worst case scenario with a deposition map from the Chernobyl accident. The same scale is used on both maps. Units: Bq m⁻².

5. New considerations regarding release scenarios

In general, two release types have been considered in the present work; one to the marine environment and the other to the atmosphere. In this section the rationale behind the two considered release scenarios, which have been used in all dose calculations and estimations presented in this report, are fully discussed.

5.1 Release scenario for marine dispersion

The starting point for any release to the marine environment is the consideration of an SCR accident which would take place underwater either at the current location of the submarine or somewhere else en route. The latter situation would be possible in case of an accident during transport which could result in losing the submarine and its consequent sinking.

As mentioned earlier (Section 3.1), the marine dispersion modelling which has been conducted in this work utilizes NAOSIM which is a large scale numerical model and a model "tracer" to evaluate the marine dispersion of potentially released soluble radionuclides. The model assumed a release of 1 PBq of the tracer which begins in July for each release experiment, because the summer is the most likely time period for a potential recovery of the submarine. However, bearing in mind the inventory of the submarine and possible scenarios for release, some adjustments had to be made to the amount of released activity before starting the evaluation of any radiological consequences.

In the case of a criticality event, in addition to the long-lived radionuclides, newly generated fission products (comprising both long- and short-lived radionuclides) have to be considered.

Different possible scenarios that could be considered in relation to releases to the marine environment are presented in Table 5.1.

Table 5.1. Considered possible scenarios relevant to releases to the marine environment. PSR and SBR stand for portside reactor and starboard reactor, respectively.

Scenarios	Reactors	Long-lived (as of 2015)		Short-lived	
		Inventory	Released	Generated*	Released
Con1: SCR in both reactors	PSR	1.49E+14	1.49E+14	1.86E+14	1.86E+14
	SBR	1.59E+14	1.59E+14	2.32E+14**	2.32E+14
Total		7.26E+14			
Con2: SCR in SBR plus releases from PSR	PSR	1.49E+14	1.49E+14		
	SBR	1.59E+14	1.59E+14	2.32E+14	2.32E+14
Total		5.4E+14			
Con3: SCR in SBR and no releases from PSR	SBR	1.59E+14	1.59E+14	2.32E+14	2.32E+14
Total		3.91E+14			
Most plausible: SCR in SBR and fractional release	SBR	1.59E+14	4.80E+12	2.32E+14	2.75E+13
Total		3.23E+13			

*After 24 hours.

**As the inventory of the portside reactor is about 0.8 of the other reactor, we have assumed that the generated short-lived activities are also 80% of that from the starboard reactor.

The first three scenarios listed in Table 5.1, represent three possibilities calculated based on very conservative assumptions. The last scenario is the one which can be assumed as the most plausible release scenario and is based on estimates and prognoses provided by the Russian Energy Safety Analysis Centre of IBRAE.

However, for the estimation of any possible consequences of a potential release from the submarine, a compromise has to be made between conservatism and realism such that the considered release scenario is not only conservative but also plausible. These considerations led us to the third scenario, i.e. **Con3** (see Table 5.1) and the assumption of the maximum total release of 0.4 PBq. That is, it has been assumed that a total release, which is one order of magnitude higher than the “most plausible” scenario, as being conservative enough to accommodate several possibilities of accidental releases from the submarine and at the same time to encompass some of the uncertainty involved. This is still a conservative assumption and the total amount of release is very close to the total inventory of the submarine.

5.2 New analysis of atmospheric dispersion based on different assumptions and more “realistic” considerations

As has been stated previously, the transport of radioactive debris caused by a hypothetical release related to a potential recovery of the K-27 submarine was analyzed by the Norwegian Meteorological Institute (Bartnicki et al. (2013), Bartnicki et al. (2016)). The meteorological worst case scenario was determined by analyzing total deposition of ¹³⁷Cs on Norwegian land territory, and then selecting the most stable weather situation by visualizing the 4 cases with most deposition (see section 4.2). The weather situation of 22nd September 2004 at 12UTC was then selected as worst case for atmospheric transport to Norway, with a worst case for accident location being Gremikha Bay. The transport modelling started with strong

winds from east, blowing contamination over Northern Norway and to the Atlantic/ the Norwegian Sea. When the radioactive material is over the North Atlantic, the wind-direction changes to northern wind and thus transport to Nordland and Trøndelag regions occurs, where the contamination is deposited again over land as can be seen in Figure 5.1.

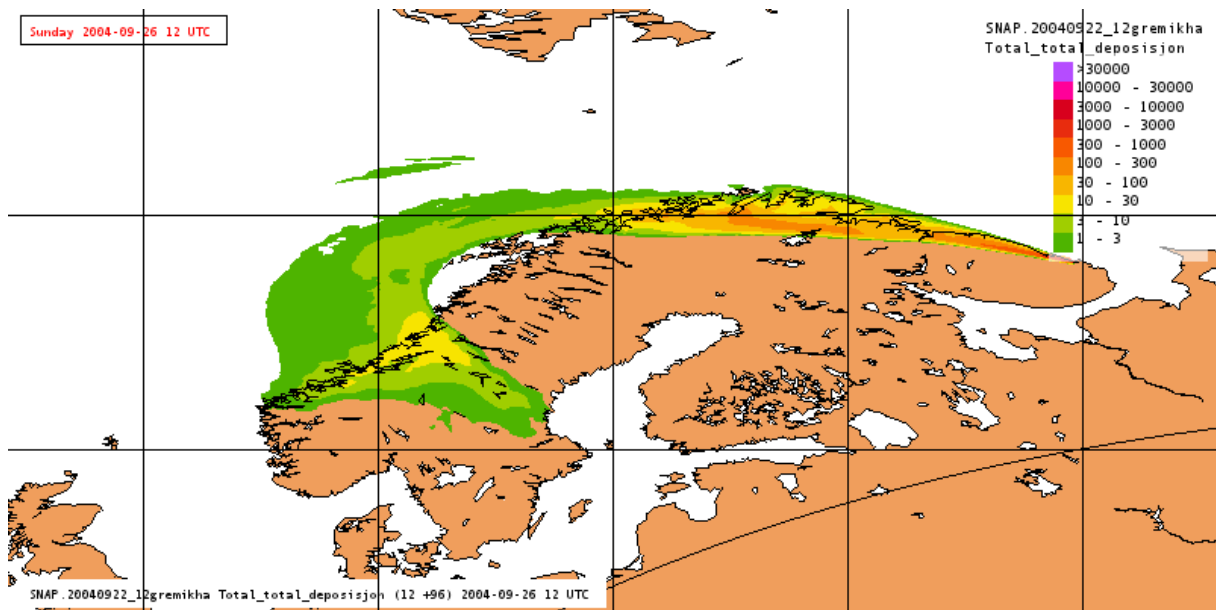


Figure 5.1. Deposition of nuclear debris from a hypothetical accident at Gremikha, 22nd September 2004, 12UTC. Units: $Bq\ m^{-2}$.

As described in previous chapter, a detailed source term with varying particle sizes and densities was used in the analysis of atmospheric dispersion. The particle sizes ranged from 0.1 to 100 μm . It was assumed a constant distribution of radioactive material to all particle classes, i.e. the same amount of radioactive material has been transported by particles with size 0.1 μm and density 1g/cm³ as with particles of size 100 μm and density of 10g/cm³. Upon analyzing the transport distance of various particle classes from Gremikha Bay, it was observed that larger particles (>10 μm) had significantly lower transport distances compared to smaller and lower density ones, i.e., usually below 200km (see Figure 5.2). Since one of the main objectives of this study was to identify and further explore the worst case scenarios for Norway, large heavy particles (> 1 μm) with limited transport distances were not considered in later runs of SNAP as they mainly affect a limited area at the vicinity of the accident location. In these runs (i.e. those discussed here in this chapter) aerosols with size and density of 0.55 μm and 2.3g/cm³, as used by ARGOS for emergency atmospheric dispersion, was used. These new considerations were also more in line with the assessment methodologies to hand (primarily those related to food-chain transfer) as these are not parametrized to incorporate the physical attributes of particles such as size and density.

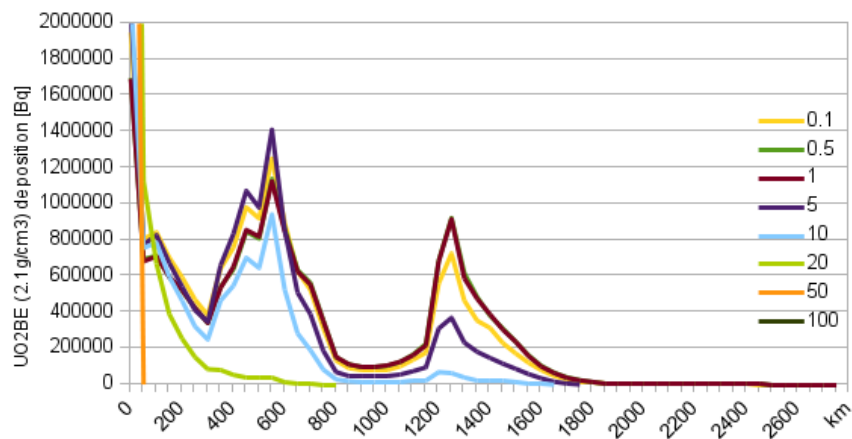


Figure 5.2. Analysis of flight distance from Gremikha Bay for particles of density 2.1 g cm^{-3} and sizes varying between $0.1 \mu\text{m}$ and $100 \mu\text{m}$.

5.2.1 New source term

For the refined and final runs a revised source term was developed based on the following considerations.

According to IBRAE (personal correspondence) it is not possible to have a fire as a result of an SCR event. The argument being that the total temperature increase in the bitumen as a result of maximum SCR (10^{20} fissions) would be about 10 degrees Celsius and this is not enough to ignite the surrounding bitumen. Based on such considerations decision was made to take into account two accident scenarios related to the atmospheric releases: one related to the occurrence of a maximum SCR at the Stepovogo Fjord at the depth of 30 m. And the other scenario was based on outbreak of fire at Gremikha when the submarine is on land and during the retrieval of its spent removable core.

Table 5.2. An overview of the two considered scenarios related to the atmospheric release.

Release to atmosphere	Max SCR in Stepovogo and /Barents Sea*	Fire at Gremikha
Short lived fission products	Assume that all released radioactivity end up in the atmosphere	
Long-lived fission products	Assume that all released radioactivity end up in the atmosphere	Assume that all released radioactivity end up in the atmosphere

*this same scenario can be assumed for "en route" accident but should have in mind that this scenario take place at the Barents and at much deeper depths.

5.2.2 Considerations regarding the fire scenario at Gremikha

In case of fire, it is not only long-lived fission products which need to be considered but other types of radionuclides such as activation products might also be released. Furthermore, it is also possible that both reactors are involved (and damaged) in an event of this type. Hence, following the suggestion of 15% release (see Hosseini et al. 2015) and taking into account the potentiality of damage to the portside reactor, this value has been increased to 20%. In addition, as the number of released radionuclides would be far more than the ones considered here, some adjustment (upscaling) should be made for activities of

radionuclide considered here reflecting the total activity released. Having these assumptions in mind, consulting Table A2 in the first report (Hosseini et al. 2015) resulted in the activities given in Table 5.3 which have been used in a new round of calculations.

Table 5.3. Long lived fission products and activities considered in the new model runs for the case of the Gremikha accident.

Radioisotope	Inventory (Bq)	Assumed released activity (Bq)
Kr-85	1.06E+12	3.18E+11
Sr-90	3.90E+13	1.17E+13
Y-90	3.90E+13	1.17E+13
Cs-137	4.43E+13	1.33E+13
Eu-155	7.81E+10	2.34E+10
Total (Bq)		3.70E+13

It is important to mention that the activities used are for the end of 2013. This is to accord with earlier estimates (as described in Chapter 4) and also to include a degree of conservatism.

The information used for the new runs is given in Table 5.4, noting some differences to the previous model runs (see chapter 4) in brackets.

Table 5.4. Specification of the new source term used for the final SNAP runs. Values in brackets refer to what is used in the previous model runs (see chapter 4).

Height	0 m (0-100 m)
Radius	50 m (25 m)
Time	1 h, starting 2004-09-22 12 UTC
Runtime	96 h
Particles	Aerosols with 2.3 g/cm ³ and 0.55 µm and constant gravity of 0.0002 m/s, and decay enabled. Passive tracer for Krypton.
¹³⁷ Cs	3.69E+09 Bq/s
⁸⁵ Kr	8.8E+07 Bq/s
⁹⁰ Sr	3.25E+09 Bq/s
⁴¹ Y	3.25E+09 Bq/s
¹⁵⁵ Eu	6.5E+06 Bq/s

The distribution map for accumulated deposition of ¹³⁷Cs can be seen in Figure 5.3.

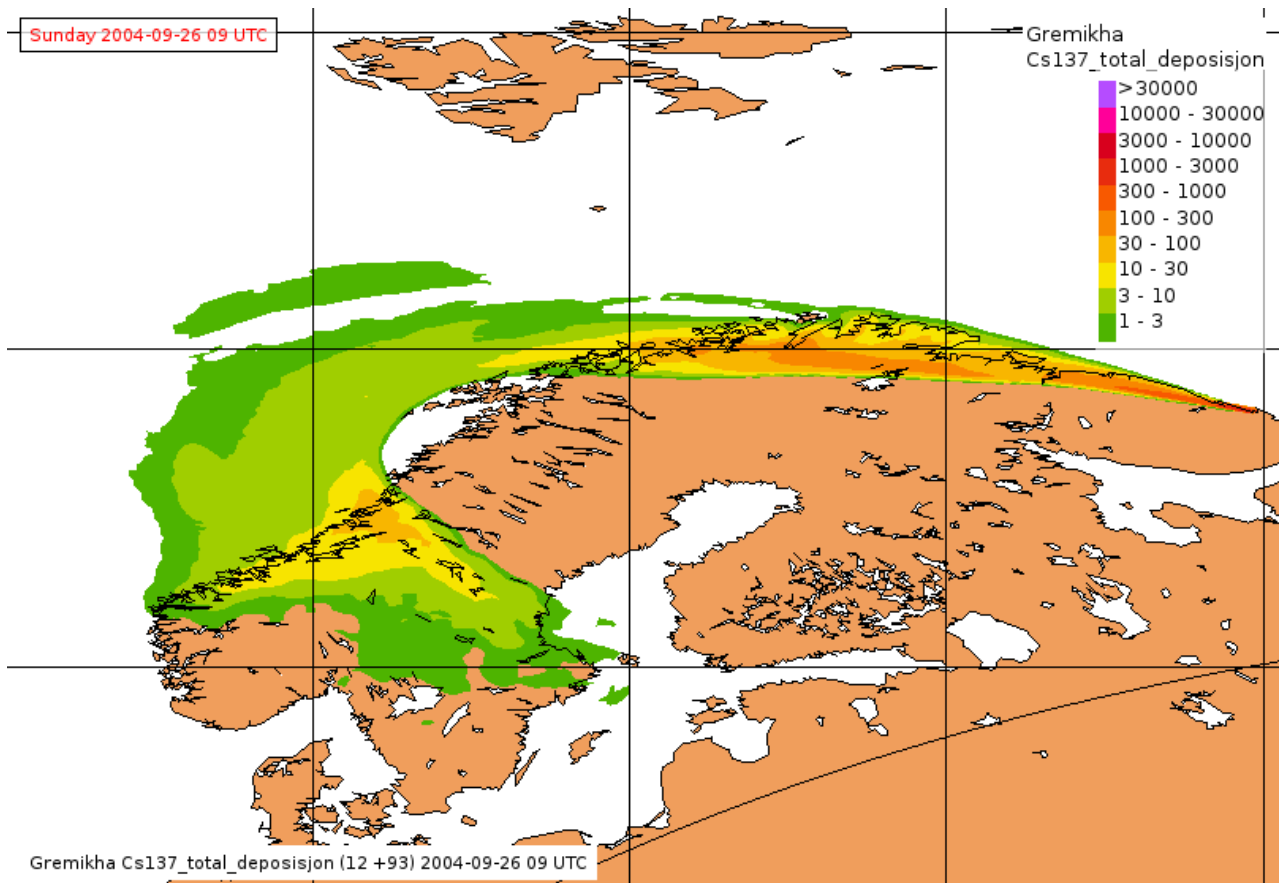


Figure 5.3. Accumulated deposition (Bq m^{-2}) of ^{137}Cs as used in this report.

5.2.3 Considerations regarding maximum SCR scenario at Stepovogo Fjord

As discussed previously, the occurrence of a maximum SCR is most probable as the submarine is under water. To be conservative, we have assumed that the fraction of radioactivity which would be released to water upon an accident involving an SCR, would eventually enter the atmosphere. According to Hosseini et al. (2015) as a result of a maximum SCR $4.82\text{E}+14$ Bq of short-lived (see Table 9.4 in Hosseini et al. (2015)) and $4.80\text{E}+12$ Bq of long-lived isotopes (see Table 9.5 in Hosseini et al. (2015)) would be released to the sea. In constructing the source term, the constraining element has been the total releases to the marine environment. As the number of actual radionuclides released to the sea is much higher than the few considered here some upscaling of individual activities was made to match the total releases. Bearing these assumptions in mind, and taking into account only radioisotopes of relatively high importance with regards to potential impact, the short-lived and long-lived radioisotopes presented in Tables 5.6 and 5.7, respectively, have been used in the new model runs for a potential accident at Stepovogo Fjord.

Table 5.6. Short-lived radioisotopes released to atmosphere for the maximum SCR scenario at Stepovogo Fjord.

Individual isotopes	Half-life	Activity (after 1 hour), Bq
Xe-133	5.24 d	2.65E+12
Xe-135	9.4 h	2.39E+14
I-131	8 d	4.48E+12
I-133	20.8 h	1.65E+14
Te-132	3.2 d	4.77E+13
Ru-103	39.26 d	2.92E+12
Sr-91	9.63 h	1.71E+12
Total		4.63E+14

Table 5.7. Long-lived radioisotopes assumed released to the atmosphere for the maximum SCR scenario at Stepovogo Fjord. Adapted from Table 9.5 of Hosseini et al. 2015.

Isotope	Half-life	Activity (after 1 hour), Bq
Kr-85	10.72 y	3.18E+11
Sr-90	29.2 y	5.85E+11
Y-90	64.26 h	5.85E+11
Cs-137	30 y	2.66E+12
Eu-155	4.68 y	1.17E+09
Total		4.14E+12

5.2.3.1 Estimating local deposition and air concentrations

As described in chapter 6 (section 6.3), a critical group which represents military personnel working at the site is considered for dose assessments. In this scenario, the Urban Dispersion Model (URD) (Andersson et al., 2008) was used to simulate the releases. URD is an integrated part of the ARGOS Decision Support System. This model was originally made for simulating releases in an urban area, and takes into account the effect that buildings have on the dispersion of airborne radionuclides. In this case, URD was used because it can model on a local level with high spatial (meters) and temporal (seconds) resolutions which allow to determine the air concentration and deposition close to the release point. The effect of buildings was not included since no building data was available.

Weather scenario was steady 3 m/s wind for East-North-East. The release was set to last for one minute to simulate a short release. Release height was set to 100 meters. The total release per isotope is given in Tables 5.6 and 5.7.

After running the model, maximum air concentration and deposition for each isotope was found by reading the values directly from the display in ARGOS. For air concentration, maximum overall value and maximum value at 350 meters was recorded (see tables given in subsection 8.1.1). For deposition the maximum values were found at 350 meters from the source.

6. Considerations regarding dose assessment methodology

6.1 Quantifying exposures and consequent impacts to man and the environment

The initial part of this report deals with the processes of physical transport that lead to the advection and dispersion of contaminants in the atmosphere and marine environment following release. The output from these models, in the form of radionuclide activity concentrations in seawater and air (and concomitant deposition to land), provides the basis for subsequent quantifications of impact on humans and the environment.

The standard means of quantifying exposure and interpreting what the estimates mean, in terms of an impact or risk of harm, involves several steps:

- Analysis of potential exposure pathways
- Derivation of doses (effective doses for people, weighted absorbed doses for plants and animals)
- Contextualisation of the doses in terms of appropriate benchmarks

The ICRP advocate the use of several points of reference in moving from activity to exposure, exposure to dose and dose to effects (or risk of health detriment) for both humans and the environment (Figure 6.1)

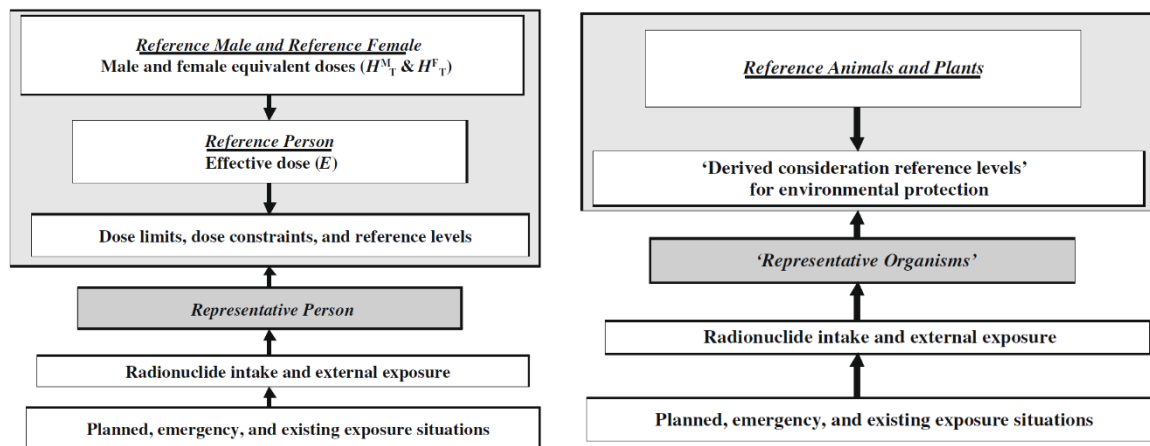


Figure 6.1. Relationships between various points of reference for protection of the environment (ICRP, 2008).

For the purposes of protection of the public, the Commission has used the 'critical group' concept to characterize an individual receiving a dose that is representative of the more highly exposed individuals in the population (ICRP, 1977). The Commission now recommends the use of the 'Representative Person' for the purpose of radiological protection of the public instead of the earlier critical group concept (ICRP, 2007). For protection of the environment the ICRP uses the related concept of Reference Animals and Plants (ICRP, 2008).

Much effort has been expended on the selection of suitable representative organisms for Arctic ecosystems (Brown et al., 2003a). Various criteria have previously been applied in making this selection including: (i) organisms that are typical or ubiquitous (ii) importance for the functioning of the ecosystem (iii) potential for high internal and external exposure from radiation, (iv) the availability of radiobiological information (v) the radiosensitivity of the organism (vi) amenability to future research. For the methodology adopted here, a somewhat simplified approach was taken that, whilst considering previous analyses, also placed emphasis on there being a reasonable likelihood that kinetic transfer models could be developed for the selected organism(s). The final list ended up as being for marine ecosystems: fish,

sea birds and seal and for terrestrial ecosystems lichen, grass, shrub, small/burrowing mammal and large mammal.

With regards to exposure pathways for both human and environmental dose assessments there is an immediate requirement to simulate transfer of radionuclides through food-chains. There are commonly adopted standard methodologies used for implementing this based on the application of concentration ratios (or factors), aggregated transfer factors (see IAEA, 2004, IAEA, 2010) but the applicability of such parameters is evidently more suited to either planned exposure situations or conditions existing some time following a release of radioactivity when steady state conditions are more prevalent. For conditions under which environmental activity concentrations are changing rapidly with time, models which account for the dynamics of the situation are more appropriate (Vives I Batlle et al, 2008). For this reason, marine and terrestrial food-chain models have been applied in the analyses presented in this report. There is a clear commonality in the approach in the sense that the assessment endpoints for the human and environmental assessment are often related. For example, for the environmental impact assessment with fish having been selected as a representative organism the food-chain model should be developed to provide activity concentrations associated with this organism group. As fish form a large component of the diet of some relatively highly exposed human groups, the same data might then be used to derive doses to humans through the application of appropriate dosimetric models. Similar considerations hold for the modelling undertaken for the terrestrial environment.

Clearly, in conducting an assessment, the selection of an appropriate point or region in geographical space is an issue requiring resolution. For humans, this might be the area covered by a fishery (as being a potential source of an ingestion dose) and for environment, this might relate to the location or region wherein a colony of the representative organisms is located at the selected time of year. The issue of spatial averaging has been raised earlier a critical feature relating to the spatial extent of various biota populations (Hosseini et al., 2010).

A web-based tool has been used for the purpose of extracting data from the marine simulations explained earlier (Section 3.5) allowing estimates of radionuclide activity concentrations with time to be derived at a point (strictly speaking within a given grid cell from the NAOSIM model) or in relation to a defined area. More details concerning the rationale for the selection of given locations or areas in the various assessment are provided within the more detailed descriptions given below (sections 6.3)

Both humans and plants and animals are exposed directly from radionuclides present in a contaminated environment (e.g. from radionuclides in water and soil) and appropriate dose conversion factors (themselves based on detailed dosimetric models) are available for the derivation of exposures from this pathway. Furthermore, for human (but not for environmental) assessments it is common practice to quantify explicitly the contribution of exposure pathways pertaining to inhalation of contaminated air and exposure from the passage of a contaminated plume in the period following an accidental release of radioactivity.

The models and parameters applied for various exposure pathways are outlined below. The radionuclides of interest are selected from knowledge of the source term i.e. largest amounts released, and the radionuclides' radiological significance. For food-chain modelling focus was placed upon ^{137}Cs with the addition of ^{90}Sr for the terrestrial environment.

6.2 Modelling transfer of radionuclides through food-chains

For the purpose of deriving activity concentrations in representative plants and animals and for human foodstuffs, food-chain models have been applied. For convenience these have been split into marine (Appendix D1) and terrestrial models (Appendix D2).

The suite of equations describing the systems (as described below) has been constructed within the modelling platform software ECOLEGO-6. ECOLEGO is a simulation software tool that is used for creating dynamic models and performing deterministic and probabilistic simulations. Further details are reported in Avila et al. (2005).

6.3 Modelling doses to humans and the environment

Once activity concentrations are derived, models are required to derive dose estimates for both a representative person and representative plants and animals.

6.3.1 Models used for human dose assessment

Standard methodologies were used for the calculation of human exposures (see e.g. IAEA, 2003) from various exposure pathways. The pathways of exposure considered were:

- Ingestion from contaminated foodstuffs
- Inhalation of radionuclides
- Exposure arising from a passing plume of contamination - cloud-shine
- Exposure from contaminated soil or shore sediments

The total annual effective dose from the ingestion of food, $E_{ing, food, public}$ (in Sv/a), has been calculated using equation:

$$E_{ing, food, public} = \sum_k H_B(k) \sum_j [C_B(j, k) DC_{ing, j}(j)] \quad (1)$$

where:

$H_B(k)$ is the rate of human consumption of foodstuff k (in kg/a);

$DC_{ing}(j)$ is the dose coefficient for ingestion of radionuclide j (in Sv/Bq); these values will be taken from ICRP publication (ICRP, 1995a)

$C_B(j, k)$ is the concentration of radionuclide j in the edible fraction of foodstuff k (in Bq/kg, fresh weight)

The activity concentrations in foodstuffs (for either marine or terrestrial products) were obtained via the kinetic models described in Appendix D and where this is not possible (e.g. parameters not available for a particular radionuclide) via the use of concentration ratios.

The (annual) effective dose (Sv) to an individual from inhalation of radionuclides from a passing plume, $E_{inh, pers}$ (in Sv/a), has been calculated using the equation:

$$E_{inh, pers} = \sum [C_{a, time-int}(j) DF_a(j) BR_{pers}] \quad (2)$$

where:

$DF_a(j)$ is the dose coefficient for inhalation of radionuclide j (in Sv per Bq); from ICRP (1995b)

$C_{a, time-int}(j)$ is the time integrated air concentration of radionuclide j in air (in Bq h/m³).

BR_{pers} = breathing rate adult (m³/h)

The exposure arising from cloud-shine has been derived as follows:

$$E_{cs, pers} = \sum [C_{a, time-int}(j) DF_{a, cs}(j)] \quad (3)$$

where:

$DF_{a, cs}(j)$ is the dose coefficient for cloud shine : (Sv h⁻¹ Bq⁻¹ m³);

$C_{a, time-int}(j)$ is the time integrated air concentration of radionuclide j in air (in Bq h/m³).

Finally, the annual effective dose to people from external exposure to radionuclides deposited on soil or sediment/shore line, $E_{ext, public}$ (in Sv/a), can be calculated using the equation

$$E_{ext, pers} = t_{pers} \sum [C_s(j) DF_{gr}(j)] \quad (4)$$

where:

t_{pers} is the time spent by person in contact with the contaminated soil/shore-sediment in a year (in h);

$DF_{gr}(j)$ is the dose coefficient for ground contamination of radionuclide j (in Sv/h per Bq m⁻²);

$C_s(j)$ is the surface contamination of radionuclide j in the shore sediments (in Bq m⁻²).

6.3.1.1 Parametrisation of the human dose assessment models in relation to various exposed groups

The human dose assessment has been split into 2 main parts – the first relating to the local area and region surrounding the dumping site and the second for the Norwegian representative person.

Marine food webs in the Arctic are short, with only two to three carbon transfers between diatoms and top predators (IAEA 1998). The great extent of ice coverage in the Arctic Basin put a limitation with regards to production and energy transfer through the existing food webs. This is especially the case in the central zone of the Kara Sea where few and small sized fish can be found. However, close to the shore and at the mouths of the great rivers Ob, Yenisey and Pyasina, the situation is different and fish are far more abundant. Actually, industrial fisheries have been developed in the relatively productive Ob–Yenisey sector (Krinitsyn, 1989). The southern part of the Kara Sea, off the mainland and along the coast of Novaya Zemlya provide suitable conditions for local brackish water fisheries (IAEA 1998).

Figure 6.2 illustrates the food web of the upper trophic levels relevant for the more coastal environment of the Kara Sea. It highlights the major energy flows in the shallow waters of the Sea, the potential seafood sources for humans and the paths through which radionuclide or other contaminants in the environment may reach humans.

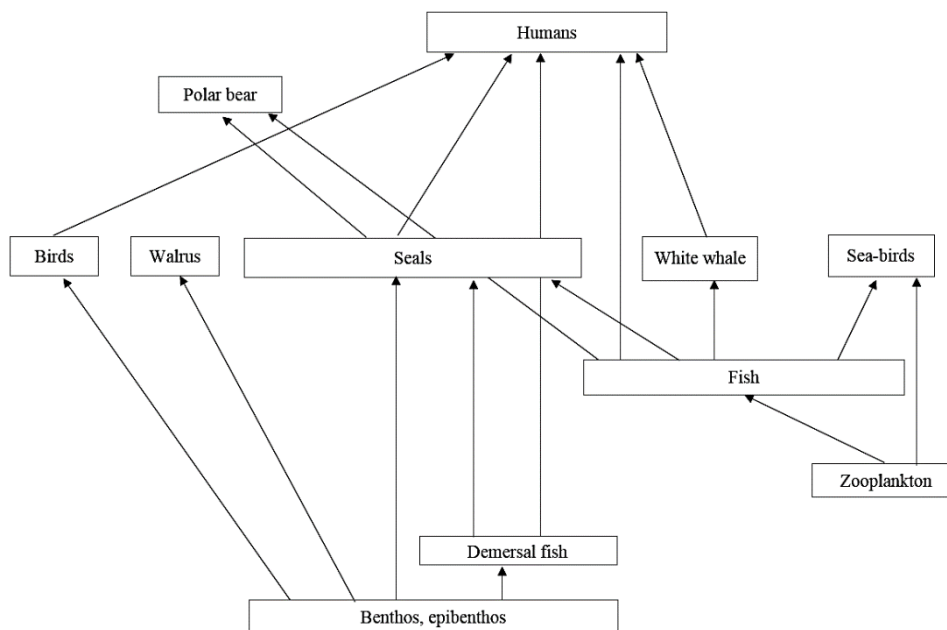


Figure 6.2. Food web of the upper trophic levels in the shallow Kara Sea and potential food sources for humans. Adapted from IAEA 1998.

1. Area surrounding the dumping site

a. Yamal/Northern Yenisey - subsistence fishing communities

It has been assumed that ingestion of marine product was the dominant exposure pathway IASAP (International Arctic Seas Assessment Project) considered subsistence fishing communities in other countries bordering the Arctic. The dietary habits postulated for these populations were:

- Sea fish, 500 g/d
- Sea mammals, 80 g/d
- Seabirds, 20 g/d
- Seabird eggs, 20 g/d

The same dietary data has been used for the calculations presented in this report.

In view of its proximity to the subsistence fishing communities being considered, the hypothetical release point in Stepovogo Fjord was selected for further analysis. The area selected for analyses (i.e. area for which time series seawater concentrations have been used as input data for models) encompasses fish stock and marine mammal populations. The activity concentrations of ¹³⁷Cs in pelagic fish and marine mammals have been derived using the marine food chain models described in Appendix D1.

b. Military personnel close to the dumped site

IASAP also considered another critical group represented by individuals occupying the foreshore of the fjords containing dumped radioactive materials. These individuals were considered likely to be military personnel to whom food was supplied from elsewhere. The pathways IASAP considered include external exposure and inhalation of sea spray and resuspended sediment.

Because a criticality with concomitant atmospheric releases of contaminants has been analyzed in this assessment, it was considered justified to replace the exposure pathways considered (by IASAP) for inhalation sea spray and resuspended sediment with direct inhalation of the contaminated plume, cloud shine and exposure from shore line sediment. These pathways would presumably dominate in the event of an accident.

The hypothetical release point in Stepovogo fjord has been selected for further analysis.

2. European/Norwegian assessment

a. Representative person (I) marine – high rate consumers of seafood

Standard calculation methods are used as presented above (Equation (1)). The EFSA (European Food Safety Authority) Comprehensive European Food Consumption Database (EFSA, 2011) has been used as a source of dietary information.

It is still necessary to consider a representative person in Norway. Pragmatically this may be considered to be a high percentile (e.g. 99th percentile) consumer from the statistics based on the entire country. The consumption data used for the calculations are given in Table 6.1.

Table 6.1. Consumption of marine foodstuffs per individual adult (g/d) (EFSA, 2011).

Foodstuff	Average	99 th percentile
Fish and seafood	63 (67,5)*	250

*the value in the bracket refers to the assumption of seafood for a Norwegian adult (Komperød, 2015).

The Reference publication of the national food consumption survey from EFSA appears to be from the publication of Johansson et al. (1997) and thus the data would appear to predate the mid-1990s. Since no

differentiation is made between fish and seafood, the activity concentrations from the former category has been used in all dose calculations.

The activity concentrations in seafood have been obtained via the kinetic models described in Appendix D1 and where this was not possible (e.g. parameters not available for a particular radionuclide) via the use of concentration ratios.

Some consideration was given to the appropriate area for spatial averaging of the activity concentrations in seafood to be used. Main fishery stocks such as cod, haddock and capelin were focused upon as these are important species for fisheries in the Barents Sea (Wienerroither et al., 2011).

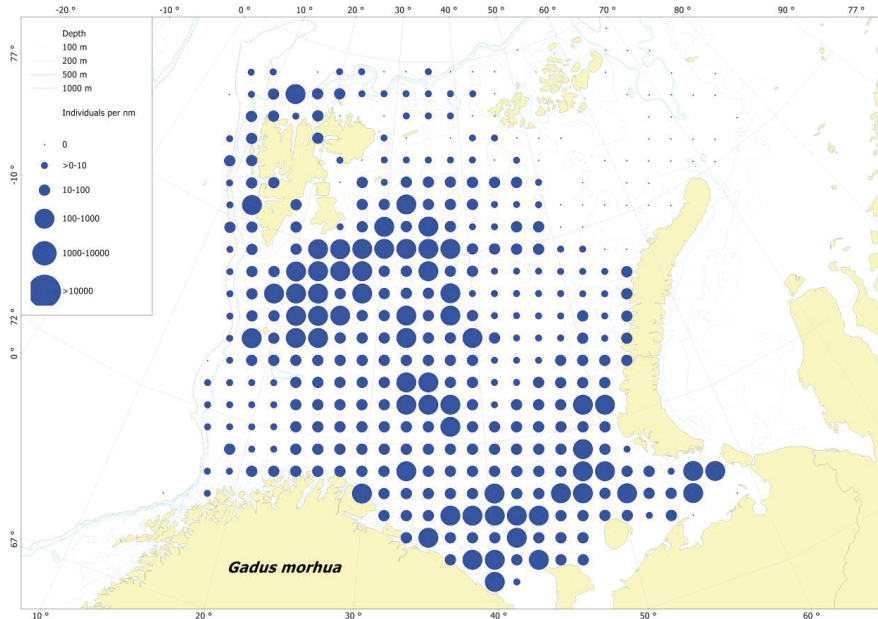


Figure 6.3. Map showing the distribution of cod in the Barents Sea. Taken from Wienerroither et al. (2011).

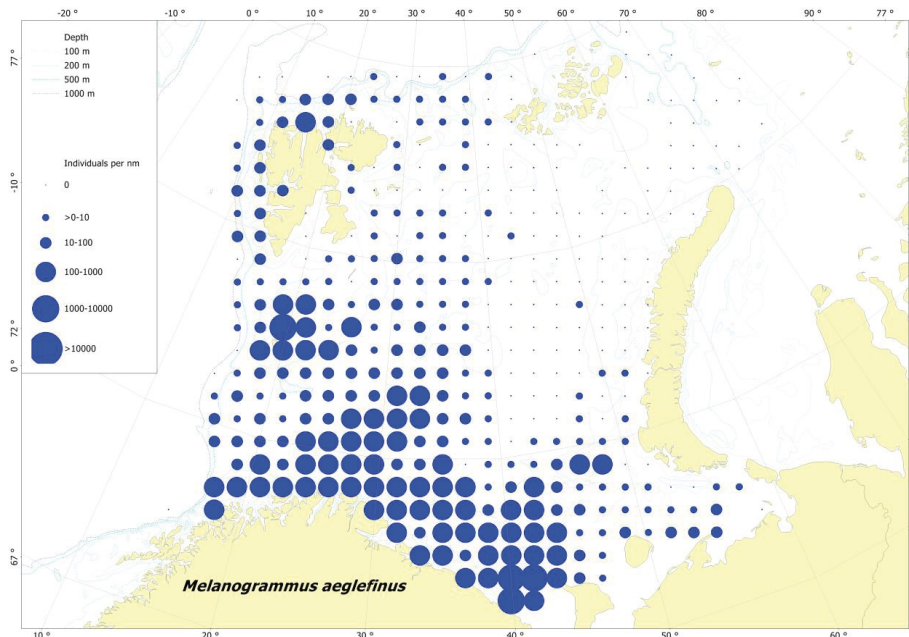


Figure 6.4. Map showing the distribution of haddock in the Barents Sea. Taken from Wienerroither et al. (2011).

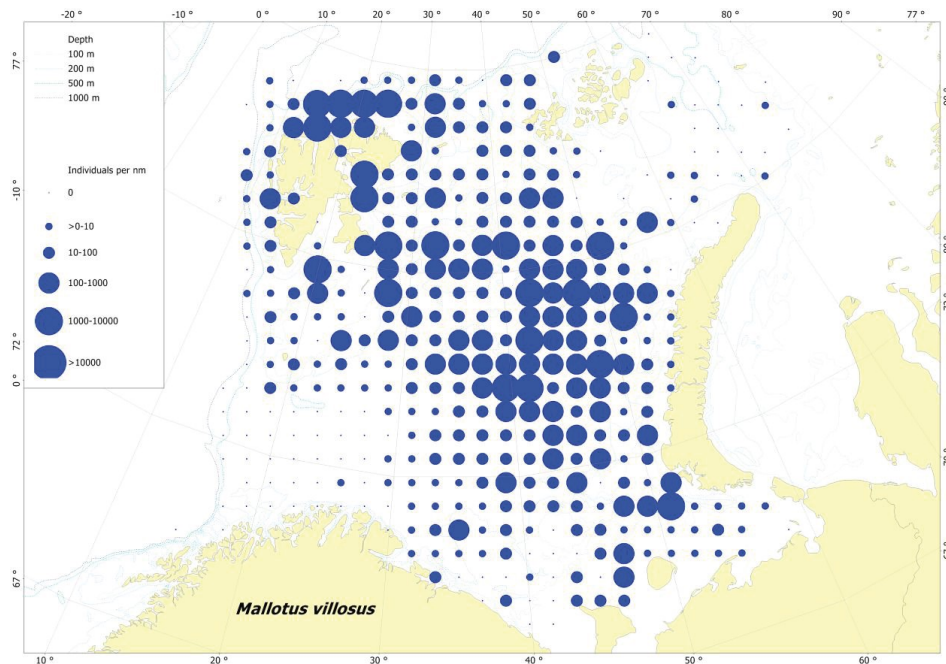


Figure 6.5. Map showing the distribution of capelin in the Barents Sea. Taken from Wienerroither et al. (2011).

In view of this uncertainty regarding where the fish have been prior to capture, a conservative assumption was made that the fish caught were in a small area commensurate with the resolution of the marine model used (28 x 28 km) and in close proximity to the accident site. The time series data for activity concentration in seawater for this area from the NAOSIM model has been taken as input to food-chain transfer models. The output from the modelling work is activity concentrations in fish with time. For the sake of conservatism the maximum value from this data series was used.

2. Representative person (II) terrestrial – consumers of natural products in high deposition areas in Finnmark exposed to initial plume and deposition

For the sake of conservatism, the maximum values from model simulations (see Section 5.2) for the time integrated activity concentrations of radionuclides in air over Norwegian territory (in Finnmark) were used for inhalation and cloud-shine dose estimates applying the equations given above (Equations 2 and 3).

Exposure from contaminated soil has been derived using the maximum deposition levels of radionuclides in Finnmark County. For this it was conservatively assumed that a person is found in continual contact with contaminated soil over a 1 year period. The reality, even in the absence of orders to shelter or evacuate, would be that individuals are shielded from ground contamination for prolonged periods as people spend a great deal of time indoors.

Finally, ingestion doses for people have been derived using various assumptions concerning diet.

The kinetic model described in Appendix D2 was used where possible to derive activity concentrations in various foodstuffs. The maximum deposition levels of radionuclides in Finnmark County have been used as input to the model and appropriate-activity concentration from the time series data generated in this process are then used for subsequent ingestion dose calculations.

Dietary surveys have been carried out in the Kautokeino area of Finnmark in 1999 and 2002 (Thørring et al., 2004). The survey included those foodstuffs that were believed to contribute the highest proportions to Cs-137 body burdens. The most recent (i.e. from 2002) ingestion rates for individual based questionnaires as oppose to household consumption data have been used because the former are believed to more closely reflect the actual amounts of food ingested by people. The information is summarized in Table 6.2. The average consumption rate has been selected as oppose to the 99th percentile (as adopted for the marine foodstuffs dose calculations) because the tabulated data already

pertain to high rate consumers (or a critical group) and as such do not require the selection of an upper percentile ingestion value.

Table 6.2. Consumption of various foodstuffs per individual adult (g/d) (Thørring et al., 2004).

Foodstuff	Average	Range
Reindeer	89	1.1 – 330
Game meat	12	0 – 120
Berries	34	1.5 – 140

With regards to fruit from semi natural systems, harvesting will depend on the type of berry but for some species, such as Cloud berry (*Rubus chamaemorus*) harvesting can start as early as July. By the end of September the main berry picking season will be over for most species. For the sake of the human ingestion dose assessment there is no requirement to model the change in activity concentration with time beyond that point. The input to the dose calculations was taken as the integrated (or average) activity concentration in berries in the 2 months following the initial deposition event.

Finally, considerations for reindeer were required. During the autumn season (September-December) in Finnmark, Reindeer are slaughtered for sale and to some degree for domestic consumption. This practice has been used to screen for infectious diseases in semi-domesticated reindeer in Finnmark culled during this period (Åsbakk et al., 1999). To avoid the requirement to develop a more sophisticated model to account for a change in the reindeers' diet as the seasons change, the simulation was truncated after 3 months. The activity concentration at 3 months (when the levels in reindeer meat attained a maximum) were selected as input for the human dose assessment. This might be considered a rather conservative approach in the sense that only the highest available values have been used but in fact such an evaluation is not entirely unambiguous. Following the Chernobyl accident, activity concentrations in reindeer in parts of Scandinavia were seen to increase in the winter months (Åhman, 2007) no doubt reflecting the change in diet of reindeer from one dominated by grass to one dominated by lichen. Although the simulation as set up will partly capture the influence of the ingestion of contaminated lichen on reindeer radiocaesium body burdens, there is no guarantee that the model prognoses will capture the extreme levels that could feasibly occur in the event of an accident.

6.3.2 Models used for environmental impact assessment

The methodology that was used in parallel for terrestrial and aquatic ecosystems was based around the ERICA Integrated Approach (Larsson, 2008). The approach was designed to provide guidance on impacts of radioactivity on the environment to ensure that decisions on environmental issues give appropriate weight to the exposure, effects and risks from ionising radiation. Emphasis was placed on protecting the structure and function of ecosystems from radionuclides (Larsson, 2008), and supporting software (the ERICA Tool) was developed to serve this purpose (Brown et al., 2008).

Once activity concentrations in environmental media and biota have been collated and calculated, dose-rates will be derived through application of the ERICA Tool.

The basic underlying equations (Equations 5 and 6) utilise activity concentration data in order to derive internal (D_{int}) and external (D_{ext}) absorbed dose-rates (in units of $\mu\text{Gy h}^{-1}$). The total absorbed dose-rate is the sum of these components, through the application of dose conversion coefficients (DCCs).

$$\dot{D}_{int}^b = \sum_i C_i^b * DCC_{int,j}^b \quad (5)$$

where:

C_i^b is the average concentration of radionuclide i in the reference organism b (Bq kg^{-1} fresh weight),

$DCC_{int,j}^b$ is the radionuclide-specific dose conversion coefficient (DCC) for internal exposure defined as the ratio between the average activity concentration of radionuclide i in the organism j and the dose rate to the organism b ($\mu\text{Gy h}^{-1}$ per Bq kg^{-1} fresh weight).

$$\dot{D}_{ext}^b = \sum_z v_z \sum_i C_{zi}^{ref} * DCC_{ext,zi}^b \quad (6)$$

where:

v_z is the occupancy factor, i.e. fraction of the time that the organism b spends at a specified position z in its habitat.

C_{zi}^{ref} is the average concentration of radionuclide i in the reference media of a given location z (Bq kg^{-1} fresh weight or dry weight (soil or sediment) or Bq l^{-1} (water)),

$DCC_{ext,zi}$ is the dose conversion coefficient for external exposure defined as the ratio between the average activity concentration of radionuclide i in the reference media corresponding to the location z and the dose rate to organism b ($\mu\text{Gy h}^{-1}$ per Bq kg^{-1} fresh weight or Bq l^{-1}).

The DCCs used correspond to those reported in ICRP (2008). Occupancy factors for organisms have been selected such that they might characterise a simplified yet realistic exposure geometry (Table 6.3).

Table 6.3. Summarised source target exposure geometry for selected organisms

Organism	Exposure geometry assumption
Rat/burrowing mammal	In soil, volumetric source
Deer/herbivorous mammal	On soil, volumetric source

Weighted total dose rates (in $\mu\text{Gy h}^{-1}$) are derived through the application of weighting factors (dimensionless) for alpha, low beta and high beta-gamma radiation (Equations 7 and 8).

$$DCC_{int} = wf_{low\beta} \cdot DCC_{int,low\beta} + wf_{\beta+\gamma} \cdot DCC_{int,\beta+\gamma} + wf_{\alpha} \cdot DCC_{int,\alpha} \quad (7)$$

$$DCC_{ext} = wf_{low\beta} \cdot DCC_{ext,low\beta} + wf_{\beta+\gamma} \cdot DCC_{ext,\beta+\gamma} \quad (8)$$

where:

wf = weighting factors for various components of radiation (low β , $\beta + \gamma$ and α)

DCC = dose conversion coefficients in $\mu\text{Gy h}^{-1}$ per Bq l^{-1} or Bq kg^{-1}

Default radiation weighting factors of 10 for alpha radiation, 1 for low energy beta and 1 for (high energy) beta and gamma radiation are applied in this assessment in line with those applied in UNSCEAR (2008).

The dosimetric calculation underpinning the derivation of DCCs is dealt with in detail elsewhere (Ulanovsky and Pröhl, 2006; Ulanovsky et al., 2008). Radioactive progeny are included in the DCCs of their parent if their half-lives are shorter than 10 days. DCCs for internal exposure were derived assuming a homogeneous distribution of the radionuclide in the organism; the error introduced by this assumption is, in view of the assessment goals, considered to be of minor significance (Gómez-Ros et al., 2008).

6.3.2.1 Parametrisation of the environmental dose assessment models

No specific information was required with regards to detailed parametrisation of the environmental dose models applied. For the terrestrial food-chain models the locations of maximum deposition were selected as input for the subsequent dose calculations.

For the marine system, surface and depth-averaged activity concentrations of ^{137}Cs in seawater and biota were selected for an area encompassing the most elevated levels associated with the main plume of contamination for the release scenarios. Although these data correspond to a single grid cell in the modelling domain, the spatial averaging involved is nonetheless quite substantial covering an area of

approximately 900 km² (as inferred from the 28 x 28 km² dimensions of the grid cells). A spatial averaging of this magnitude might over compensate for the migratory/peripatetic nature of the animal and fish species covered (Sazykina 1998 and Wienerroither et al., 2011), but no higher resolution was available for the model. This observation provided the rationale for additionally considering the surface water only (to a depth of 10 m) in the model output, and for which activity concentrations were at a maximum, to more robustly characterise the potential levels in the environment that could be attained for the release.

6.4 Contextualising impacts to humans and the environment

6.4.1 Humans

One way of contextualizing potential impact to humans is through direct comparison of predicted activity concentrations in foodstuffs with corresponding levels derived from various pertinent, e.g. radiological, criteria. For example, in a study exploring the potential impact of releases from the sunken submarine K-159 and the Komsomolets in Arctic seas, Heldal et al. (2013) used the intervention level of 600 Bq kg⁻¹ f.w., as currently applied by Norwegian authorities, to contextualize activity concentration data derived for commercial fish species. By considering cod and capelin abundance data, the authors were also able to define the % of a given population (in the Barents Sea) which exceeded a level of 0.2 Bq kg⁻¹ Cs-137 commensurate with the current contamination level in cod in the Norwegian and Barents Seas. In a conceptually similar approach, Thørring et al. (2010) considered impacts to the Norwegian environment following a hypothetical release to air from the Sellafield plant in the UK by utilising information from atmospheric advection-dispersion and deposition models and linking this with data on transfer to the food chains and statistics on production and hunting to assess the ‘consequences for foodstuffs’. Through comparison with food intervention levels as applied by Norwegian authorities it was then possible to identify areas for animal production where intervention would then be necessary accounting for a range in (empirically derived) transfer factors. Although these aforementioned approaches have clear practical merit and as such might have been suitably adopted for the current analysis, a decision was made not to focus on criteria based on foodstuffs as a sole indication of radiological significance. However, a cursory comparison with intervention levels such as the one mentioned above is a straightforward exercise. The reason it has not been adopted in this analyses is because the setting of intervention levels is arguably ambiguous, cf. the 100 Bq kg⁻¹ f.w. applied by Japanese authorities to foodstuffs such as fish following the Fukushima accident (Buessler, 2012) with the 600 Bq kg⁻¹ f.w. noted above, is subject to amendment and provides only indirect information on potential impact (as intervention levels are at some level circuitously derived from the levels at which doses are known to pose some risk) compared to the more rigorously elaborated metric of committed effective dose for humans. Furthermore, there is the issue of consistency with the approach adopted to assess impacts on the environment, *per se*, which also relies on dose-based criteria. Defining direct environmental impacts in terms of radiological criteria based on activity concentrations in ‘foodstuffs’, because of its obvious anthropocentric origins, would, furthermore, make little sense. For this reason focus has been placed upon dose-based radiological criteria.

Kocher (1987) introduced the concept of a *de minimis* dose defining a level below which control of radiation exposures would be deliberately and specifically curtailed. Such a dose would need to be set well below established limits on acceptable dose from all sources of exposure and, furthermore, be below any established dose limit for specific practices. In the context of setting criteria to allow or forbid the dumping of radioactive material at sea, the IAEA (1999a, 2015a) have used a *de minimis* dose of 10 μSv per annum. This effective dose (in tandem with a defined collective effective dose) to a representative person would allow a practice to be exempted from further regulatory consideration. Although not strictly applicable because of its development specifically for the London Convention, the *de minimis* level specified above provides a robust indication of what might be widely considered to be a trivial radiation dose and as such provides an appropriate benchmark with which the doses calculated in this assessment might be compared.

For emergency (and existing) exposure situations, the source-related restriction recommended by the ICRP is termed a “reference level” (ICRP, 2007). The concept of a reference level is used in the process of

optimisation of protection to assist in ensuring that all exposures are kept as low as reasonably achievable, societal and economic factors being taken into account.

The ICRP are quick to emphasise that reference levels do not represent a demarcation between 'safe' and 'dangerous' or reflect a step change in the associated health risk for individuals. Nonetheless, the recommended levels may be used in the current assessment as (essentially and upper-bound) benchmark with which to contextualize calculated committed effective doses to humans.

In emergency or existing controllable exposure situations, the reference levels represent the level of dose or risk, above which it is judged to be inappropriate to plan to allow exposures to occur, and for which therefore protective actions should be planned and optimised. At doses higher than 100 mSv, there is an increased likelihood of deterministic effects and a significant risk of cancer. For these reasons, the ICRP considers that the maximum value for a reference level is 100 mSv incurred either acutely or in a year. The ICRP set a Reference level band of 20 to 100 mSv set for the highest planned residual dose from a radiological emergency.

6.4.2 Environment

Although in a strict sense there are activity concentration based criteria available with which to contextualize the impact of given levels of radionuclides in seawater or soil, in the form of Environmental Media concentration Limits (see Brown et al., 2008), the standard methodology for making inferences about potential environmental effects involves the application of dose-based criteria.

The ICRP (ICRP, 2008) recommend the application of a set of derived consideration reference levels (DCRLs) for particular categories of Reference Plants and animals (Figure 6.6). These are defined (see ICRP, 2009) as "A band of dose rate within which there is likely to be some chance of deleterious effects of ionising radiation occurring to individuals of that type of Reference Animal or Plant (derived from a knowledge of defined expected biological effects for that type of organism) that, when considered together with other relevant information, can be used as a point of reference to optimise the level of effort expended on environmental protection, dependent upon the overall management objectives and the relevant exposure situation."

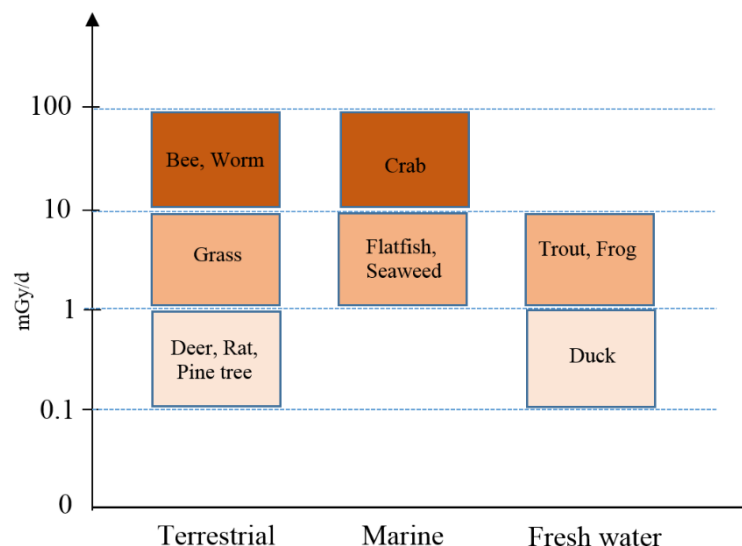


Figure 6.6. Derived Consideration Reference Levels (DCRLs) for environmental protection for each Reference Animal or Plant (RAP), the RAPs being grouped according to their terrestrial, freshwater, or marine habitat. Reproduced from ICRP (2014).

In the recent report ICRP-124 (ICRP, 2014), the Commission has begun to elaborate on the application of these criteria under cases other than planned exposure situations (for which the original criteria were developed). For existing emergency exposure situations where control of the source has not been obtained, if the dose rates are above the relevant DCRL band, the ICRP recommends that the aim should be to reduce exposures to levels that are within the DCRL bands for the relevant populations, with full

consideration of the radiological and non-radiological consequences of so doing. If dose rates are within the bands, the ICRP recommends that consideration should be given to reduce exposures, assuming that the costs and benefits are such that further efforts are warranted.

7. Results: Activity concentrations

It is important to note that the ^{137}Cs activity concentrations in plants and animals derived for the given scenarios would be in addition to the levels already present in the environment from various historical sources of contamination. For the locations of interest in these studies, the primary sources of “background” ^{137}Cs contamination can be attributed to the global fallout arising from atmospheric weapons testing (primarily in the 1950s and early 1960s), the Chernobyl accident (to a much lesser extent) and, for the marine environment, releases from western European reprocessing plants (AMAP, 1998). These historical contamination levels will be considered below in the text where it is pertinent to do so.

7.1 Terrestrial ecosystem

The dynamics of ^{137}Cs and ^{90}Sr activity concentrations in vegetation (Shrubs and Grass) at the location of maximum deposition in Finnmark, following releases from the Gremikha scenario, are presented in Figure 7.1. The levels of both radionuclides are simulated to fall quite rapidly from levels of approximately 270 and 360 Bq kg^{-1} f.w. for ^{137}Cs and ^{90}Sr , respectively, in the initial days after fallout to levels in the order of 1- 2 Bq kg^{-1} f.w. for both radionuclides when the time elapsed approaches 100 days. This period would correspond to mid-November by which time many areas in Finnmark could conceivably be covered in snow and temperatures could be sub-zero. The dynamic model has not been parameterised for these conditions. Nonetheless, processes dominated by the rapid loss of radionuclides, reflecting substantial wash-off of contaminants from shrubs and grass, is expected to transition towards processes characterised by steady-state but lower transfer to vegetation in the long term. This occurs as root uptake and translocation become more dominant processes, months and years after the fallout event, than interception and surficial retention.

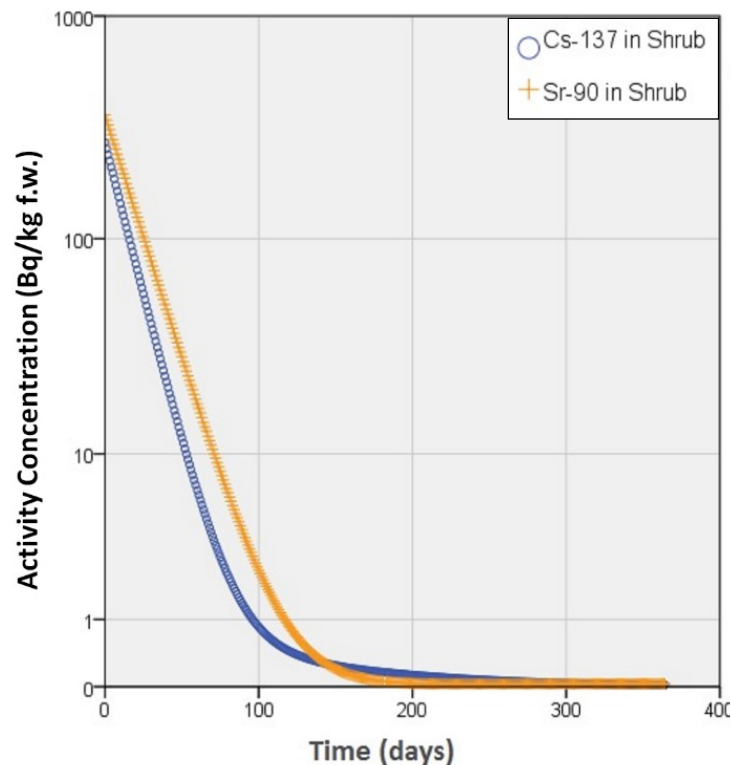


Figure 7.1. Activity concentrations (Bq/kg f.w.) of ^{137}Cs and ^{90}Sr in shrub (including *Vaccinium spp.*) for the area of maximum deposition in Finnmark for the Gremikha release scenario.

The dynamics of ^{137}Cs and ^{90}Sr activity in small (burrowing) mammals (taken to include game animals) at the location of maximum deposition in Finnmark following releases from the Gremikha scenario are presented in Figure 7.2. As considered for vegetation, the output, post 2-3 months, needs to be appraised with due caution because the model was not configured to account for changing environmental conditions (such as snowfall) with the seasons. However, the prognoses for the first months are considered to be robust in the sense of providing reasonable conservatism. The activity concentrations of both ^{137}Cs and ^{90}Sr are simulated to increase following the initial deposition event with ^{137}Cs attaining a maximum activity concentration of ca. $580 \text{ Bq kg}^{-1} \text{ f.w.}$ within the first month before falling moderately rapidly to a level slightly in excess of $300 \text{ Bq kg}^{-1} \text{ f.w.}$ by 100 days. The behaviour of ^{90}Sr contrasts to radiocaesium in that the maximum $550 \text{ Bq kg}^{-1} \text{ f.w.}$ occurs somewhat later, at around 90 days, and thereafter levels decrease less dramatically. Levels are, in fact, still close to $500 \text{ Bq kg}^{-1} \text{ f.w.}$ by the end of the simulation period. Although the output result for the period post 3 months are quite uncertain (because of the limitation expressed above), there is an expectation that ^{90}Sr will be lost relatively slowly from the body of mammals following assimilation because the radionuclide rapidly becomes associated with bone (see Coughtrey & Thorne, 1983). Once sequestered by bone the retention of radiostrontium within the animal's body can be protracted, reflecting the skeletal turnover of analogous elements such as calcium.

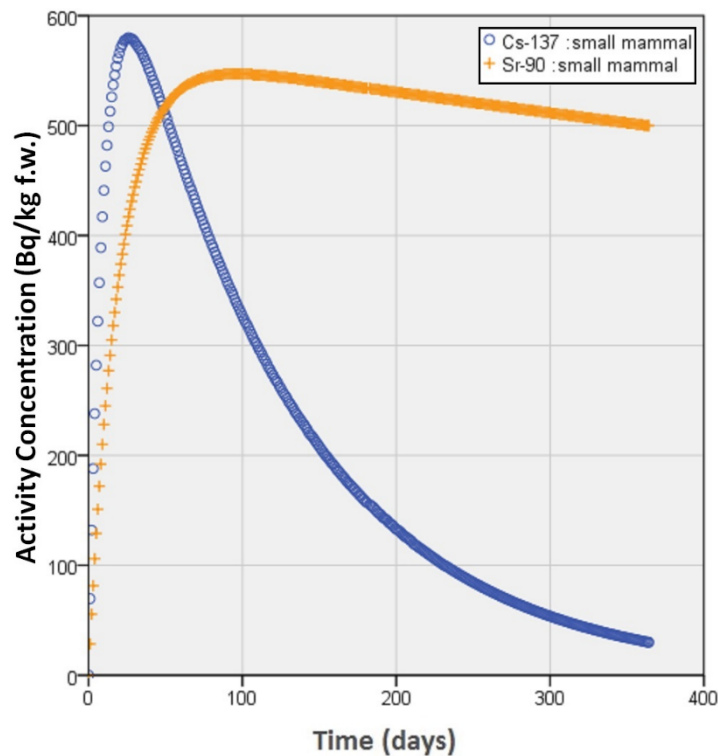


Figure 7.2. Activity concentrations ($\text{Bq kg}^{-1} \text{ f.w.}$) of ^{137}Cs and ^{90}Sr in small burrowing mammal (including game animals) for the area of maximum deposition in Finnmark for the Gremikha release scenario.

The kinetics of ^{137}Cs and ^{90}Sr in deer-reindeer (Figure 7.3), unsurprisingly, follow a similar pattern to those observed for small mammals with regards to an observed build up of activity with time following the initial deposition event. However, the biological half-lives characterising the retention of ^{137}Cs and ^{90}Sr in the whole body of deer are protracted compared to the much smaller burrowing mammal. This simply reflects the employment of allometric relationships in the derivation of biological half-lives for model parameterisation – the larger the animal, the longer the biological half-life. The activity concentration of ^{137}Cs in deer attain a maximum of ca. $175 \text{ Bq kg}^{-1} \text{ f.w.}$ some 2 months following the initial fallout event. The values for ^{90}Sr are striking in the sense that no equilibrium is attained over the 1-year simulation period. This may reflect poor parameterisation of the model. For example, in the case of reindeer, the diet and the biological half-lives (for radiocaesium and by proxy conceivably for other radionuclides) are known to vary throughout the year (Åhman, 2007) but these considerations are not accounted for in the

model. Despite the acknowledgment that the configuration of the model is limited after the first few months, it is not unrealistic to expect a continued build-up of ^{90}Sr during later periods. This is based on the assumption that ^{90}Sr is strongly retained on lichen thus leading to a relatively slow decline in levels with time as suggested by Golikov et al. (2004) and the knowledge that lichen do form a large part of the reindeer's diet at some periods of the year. Under such conditions, considerable time would be required to attain anything approaching equilibrium. Having said this, the appropriateness of using an approximately 5 year weathering half-time value for ^{90}Sr may be questionable in view of evidence to the contrary where (more or less corresponding) effective half-times of about 1.0 year for ^{90}Sr in lichen have been apportioned (Skuterud et al., 2005). Although the value of 5 years has been retained for the sake of conservatism, the effect of applying a lower weathering half-time for ^{90}Sr in lichen would be to observe a more rapid attainment of a maximum activity concentrations in reindeer.

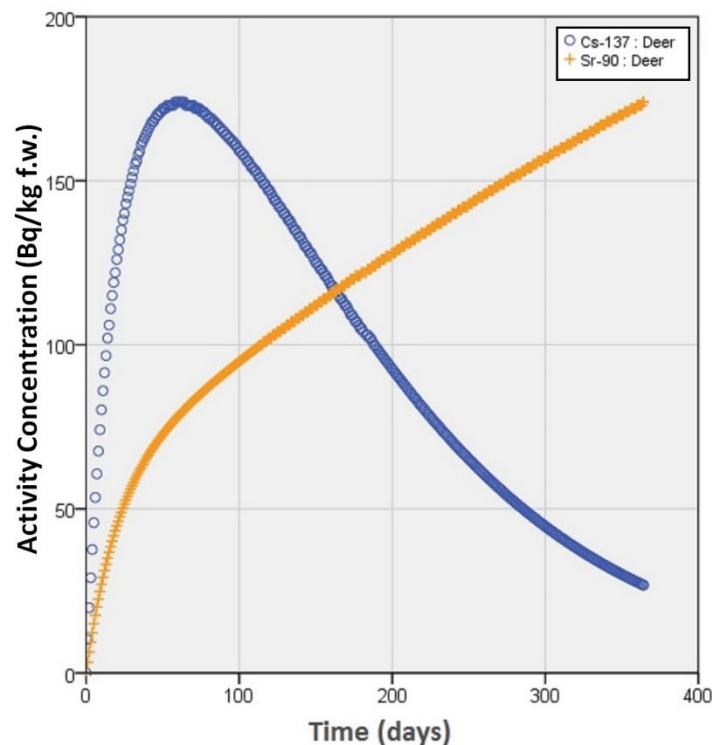


Figure 7.3. Activity concentrations ($\text{Bq kg}^{-1} \text{ f.w.}$) of ^{137}Cs and ^{90}Sr in Deer (as exemplified by Reindeer) for the area of maximum deposition in Finnmark for the Gremikha release scenario.

Because there was a certain degree of uncertainty associated with the application of this relatively untested model to the scenario and conditions outlined above, a check was made against a published model (Åhman, 2007) applied, in Sweden, after the Chernobyl accident to simulate contamination levels of ^{137}Cs in the long term. The maximum activity concentrations determined are reassuringly similar between simulations (cf. $175 \text{ Bq kg}^{-1} \text{ f.w.}$ for the bespoke model with ca. $150 \text{ Bq kg}^{-1} \text{ f.w.}$ from the model of Åhman, (2007)) but the published model of Åhman provides the additional advantage by providing a quantification of activity levels in the years following a deposition event. The model developed in the present report was not developed with such an objective in mind. An interesting feature of Åhman's model is the closeness with which the observed high amplitude sinusoidal form of ^{137}Cs levels in reindeer can be simulated by accounting for factors such as the animal's changing diet and metabolism over the season. Although ^{137}Cs activity concentrations might be expected to fall quite rapidly after the initial peak, as predicted in the simplified model developed in the current study, it is quite evident that new peak activities, coinciding with subsequent winter periods, would be expected (Figure 7.4). These subsequent peaks with quite elevated activity concentrations, for the first few years at least, fall at levels that are not dramatically lower than the initial maximum.

As noted in a general sense above, the predicted ^{137}Cs activity concentrations in reindeer in Finnmark, for the given scenario, would occur in addition to quite elevated levels which still persist from global fallout. As of 2005, average activity concentrations of ^{137}Cs were still in the region of 100 Bq kg^{-1} (Thørring and Skuterud, 2012). Even accounting for (the long component) of an effective half-life of approximately 11 years for Kautokeino reindeer meat (IAEA, 2010), this would mean the “background activity” would still be at a level of ca. 50 Bq kg^{-1} , i.e. only a factor of 3 or so lower than the peak activities predicted from the prognoses provided for the release scenario.

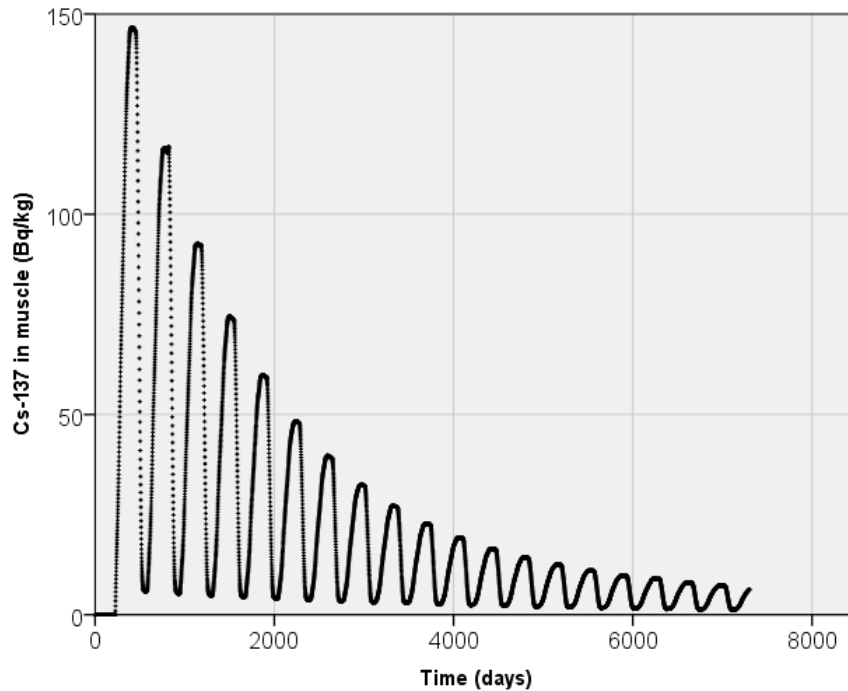


Figure 7.4. Activity concentrations (Bq kg^{-1} f.w.) of ^{137}Cs in reindeer in the long term (20 years) following an accident based upon the model of Åhman (2007).

Howard et al. (2004) determined doses to population groups in Trøms and Finnmark from a hypothetical accident at the Kola nuclear power plant that draws upon a number of similar methodologies to those applied in the current terrestrial assessment for K-27. However, Howard et al. (2004) did not use kinetic food-chain transfer models but instead applied aggregated transfer factors (Tags) and effective half-lives to derive activity concentrations of ^{137}Cs and ^{90}Sr in foodstuffs. The initial Tags used were 1.4 and $1.4 \times 10^{-3} \text{ m}^2 \text{ kg}^{-1}$ for ^{137}Cs and ^{90}Sr , respectively, in reindeer and 3×10^{-2} and $6 \times 10^{-3} \text{ m}^2 \text{ kg}^{-1}$ for ^{137}Cs and ^{90}Sr respectively in berries. Applying such transfer coefficients to the initial deposition data we have would generate initial activity concentrations of approximately 350 and 7.5 Bq kg^{-1} ^{137}Cs in reindeer and berries and 0.3 Bq kg^{-1} and 1.3 Bq kg^{-1} ^{90}Sr in reindeer (meat) and berries. The ^{137}Cs activity concentrations prognosis using the simple Tag approach actually generates values that are only a factor of 2 higher than those using a dynamic approach but the transfer of ^{137}Cs to berries using a Tag approach does not capture the potentially highly elevated concentrations that might be observed immediately after a deposition event. A similar observation can be made for ^{90}Sr where the initial concentrations using the dynamic approach exceed 100 Bq kg^{-1} compared to the prognosis from the Tag approach yielding values around 1 Bq kg^{-1} . Prognoses for ^{90}Sr in reindeer meat are also quite different with results from the dynamic model (note a factor of 0.1 was applied to the values presented above to convert from whole body to muscle activity concentrations) providing values approximately a factor of 50 greater than the Tag approach (cf. activity concentrations $>15 \text{ Bq kg}^{-1}$ at 300 days for the dynamic model with 0.3 Bq kg^{-1} from the Tag approach).

The activity levels for small burrowing mammals and deer can be compared to the current relevant Norwegian intervention level of 3000 Bq kg^{-1} f.w for radiocaesium (Thørring et al., 2010). In neither case would the intervention level for ^{137}Cs be exceeded. As for shrubs (used as a proxy for berries) the situation

is less clear-cut, as the highest predicted levels are only a factor of 2 below the Norwegian intervention level for basic foodstuffs of 600 Bq kg⁻¹ f.w for radiocaesium (Liland et al., 2009; Thørring et al., 2010). Aside from discussions as to whether berries constitute a basic foodstuff, the fact that activity concentrations in berries fall quite rapidly would render any potential concerns ephemeral.

7.2 Marine ecosystem

7.2.1 Gremikha release scenario

Depth-averaged activity concentrations of ¹³⁷Cs in seawater, fish and seal are presented in Figure 7.5a for an area encompassing the most elevated levels associated with the main plume of contamination for the Gremikha release scenario.

The pulsed nature of activity concentrations of ¹³⁷Cs in seawater are quite evident with maximum depth-averaged activity concentration of ca. 3 Bq/l occurring within the first 7 days of simulation. The levels are then predicted (by application of NAOSIM) to decrease rapidly to levels below 1 Bq/l once a period of 25 days has elapsed. For sake of comparison, Heldal et al. (2013), using a 3D numerical ocean model, predicted maximum (essentially depth averaged) levels of around 0.5 Bq/l ¹³⁷Cs in seawater for a 5.2 PBq instantaneous input (compared to our input of 0.4 PBq) and corresponding to a release occurring at a nearby (notably sea-bed) coastal location in the Barents Sea.

Maximum activity concentrations simulated to occur in fish and seal, in contrast to those for seawater, build up slowly with maximum ¹³⁷Cs levels attained at approximately 2 months for fish and 3½ months for seal using the depth averaged seawater concentrations as input (Figure 7.5a). The maximum levels in fish and seal based on depth averaged ¹³⁷Cs activity concentrations in seawater were ca. 30 and 70 Bq kg⁻¹ (f.w.) for fish and seal respectively. These levels are substantially below the intervention level of 600 Bq kg⁻¹ applied for basic foodstuffs in Norway (Liland et al., 2009) but in the case of fish, are only a factor of 3 or so below the Japanese regulation value of 100 Bq kg⁻¹ (fresh weight) for sale and human consumption that was applied following the accident at Fukushima Daiichi (Buessler, 2012).

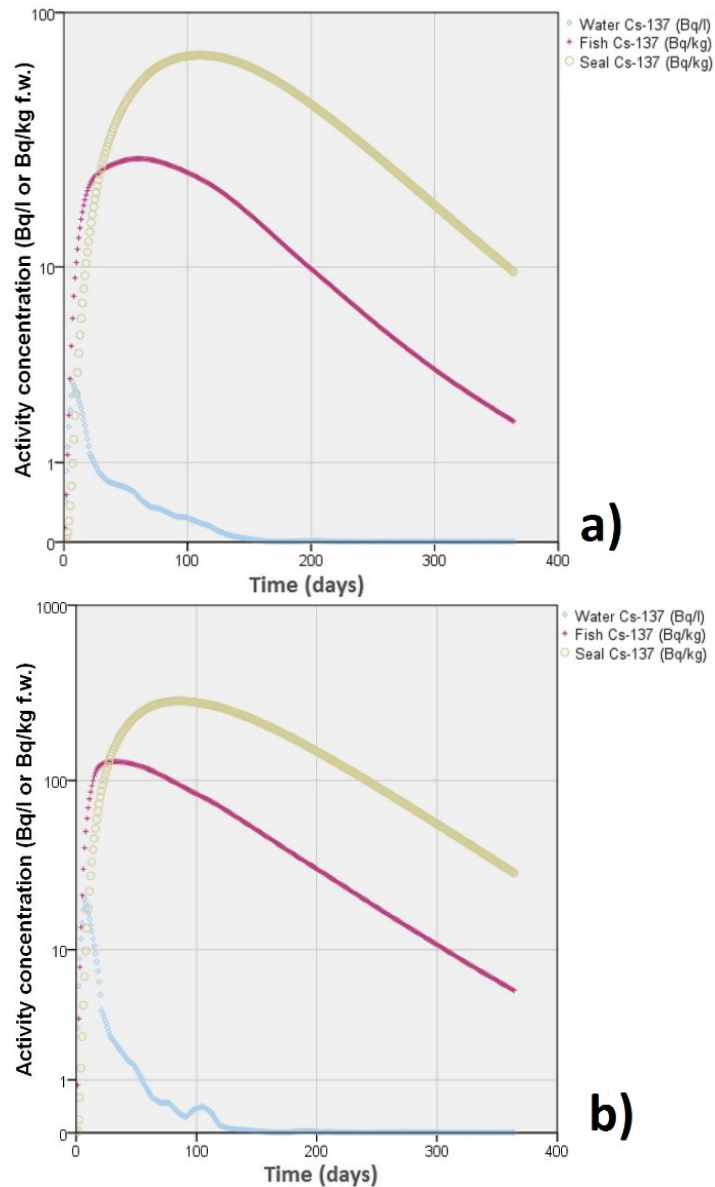


Figure 7.5. (a) Depth-averaged and (b) At surface activity concentrations of ^{137}Cs in sea water (Bq/l) fish (Bq kg $^{-1}$ f.w.) and seal (Bq/kg f.w.) based on releases to the marine environment for the Gremikha scenario.

Simulated surface activity concentrations of ^{137}Cs in seawater along with resultant levels of ^{137}Cs in fish and seal are presented in Figure 7.5b. Clearly the levels of contamination are substantially greater than those associated with depth averaged activity concentrations reflecting the initial presence of ^{137}Cs near the top of the water column under the conditions of a near surface release prior to the occurrence of substantial mixing. The maximum ^{137}Cs activity concentrations in seawater, forming a similar pulsed time profile to that seen for the depth averaged data series, attain levels of ca. 20 Bq/l within the first week of the release. To place these levels into context, similar ^{137}Cs activity concentration were measured 30 km offshore within the first few weeks following the Fukushima Dai-ichi accident for a substantially larger actual release of ^{137}Cs (IAEA, 2015b). As seen previously, there is a pronounced lag before the maximum levels in fish and seal are observed, these maxima of 130 and 285 Bq kg $^{-1}$ f.w. occurring within a period of 1 month and 3 months for fish and seal respectively. A tentative comparison can be made with the modelling work of Heldal et al. (2013) for a nearby source in the Barents Sea (assumed in that work to be about 13 times greater than the inventory used in the present study as considered above). In that study levels in fish (cod) were predicted to fall at around 63 and 123 Bq/kg f.w. in the near-surface and near-bottom layer, respectively. This rather large difference in view of the source term magnitudes applied can only be partly explained by the release conditions, i.e. near surface for the present study versus near-

bottom for the study of Heldal et al. (2013). The difference would have been even more pronounced had the option been taken, as it was in Heldal et al. (2013), to use seawater to fish concentration ratios as oppose to the kinetic models applied in the present work. Although the ^{137}Cs activity concentrations predicted for fish, strictly speaking, fall below the aforementioned 600 Bq/kg intervention limit by some margin, the levels are close enough to raise some concerns. In view of the uncertainties involved, not least those associated with the imposed degree of spatial averaging (essentially over an area of 900 km²), the levels in fish for an actual pulsed release of 0.4 PBq ^{137}Cs could conceivably exceed the intervention limit. Such an outcome would potentially require the imposition of fishing restrictions/fishery closures. Nonetheless, this expressed view is tempered by the knowledge that the actual release of ^{137}Cs would most probably be substantially less than 0.4 PBq even under extremely pessimistic conditions. Considering the total inventory of Cs-137 and its realistic released fraction (Hosseini et al. 2015), the actual release of Cs-137 would be less by two orders of magnitudes (ca. 2.7 TBq).

The predicted ^{137}Cs contamination levels in fish for the given scenarios would far exceed existing “background” contamination levels. According to Heldal et al. (2013), the levels of ^{137}Cs in cod (*Gadus morhua* L.) muscle in the Barents Sea in the period around 2010 were ca. 0.1-0.2 Bq/kg f.w. In contrast to the terrestrial analyses, the existing background contamination levels could essentially be ignored for ^{137}Cs inputs of the magnitude modelled in this scenario.

7.2.2 Stepovogo release scenario

Depth-averaged activity concentrations of ^{137}Cs in seawater, fish, seal and seabird are presented in Figure 7.6a for an area encompassing the most elevated levels associated with the main plume of contamination for the Stepovogo release scenario.

The time profile for the activity concentrations of ^{137}Cs in seawater is similar to the one described above for Gremikha. The elevated peak in levels occurs at a slightly later time point but within the first 2 weeks of the release and attains a slightly lower (depth-averaged) activity concentration, marginally in excess of 1 Bq/l. Cs-137 levels then decrease to below 0.5 Bq/l after the first month.

The levels of ^{137}Cs derived for marine organism were concomitantly lower than those derived for Gremikha, with predicted levels of 13 and 34 Bq/kg f.w. for fish and seal respectively. These are not values that would likely cause concern from a regulatory perspective as, even were factors to be applied to account for uncertainties, the activity concentrations fall at least an order of magnitude below commonly applied food intervention levels (as discussed in more detail above). The Stepovogo analysis differed from the one conducted for Gremikha with regards to the inclusion of a third biota group – seabird (included as it formed a potential ingestion exposure pathway for humans). The activity concentrations of ^{137}Cs in seabird actually exhibited the highest levels among all biota groups with predicted maxima falling just below 100 Bq/kg f.w. A prediction where transfer to seabirds is elevated compared to other organism types is in line with the pattern observed from collations of empirically based concentration ratio data (IAEA, 2014). Nonetheless, the uncertainties associated with this prediction are great, primarily reflecting the challenges in generating experimentally based transfer parameters for wild birds, and the prognosis provides only an approximate indication of activity concentrations that might be observed. The fact that ingestion of seabirds/seabird eggs is unlikely to form an important (human) exposure pathway renders this putative high uncertainty in prediction less critical than it might otherwise have been.

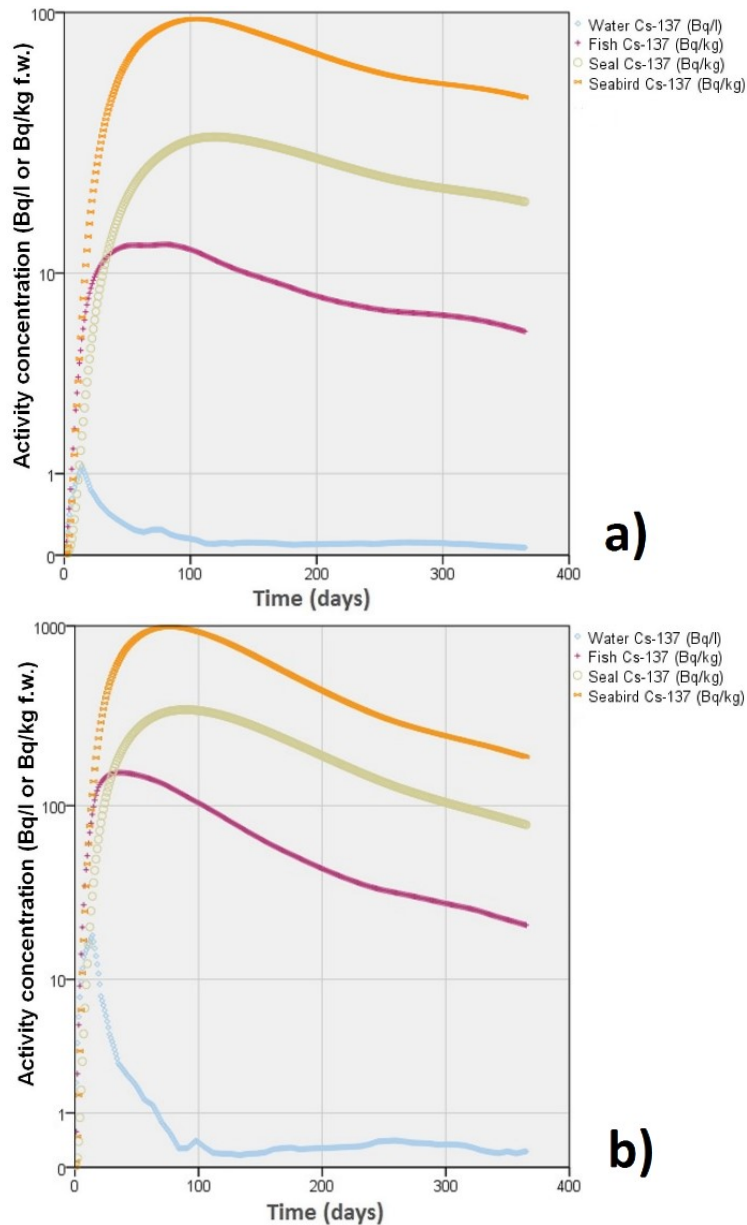


Figure 7.6. (a) Depth-averaged and (b) At surface activity concentrations of ^{137}Cs in sea water (Bq/l), fish (Bq/kg f.w.) seal (Bq/kg f.w.) and seabird (Bq/kg f.w.) based on releases to the marine environment for the Stepovogo scenario.

Although the maximum depth-averaged activity concentrations for the Stepovogo release scenario were substantially lower than those predicted for Gremikha, the maximum surface activities were similar for both cases. The maximum ^{137}Cs level in seawater at Stepovogo was calculated to be around 18 Bq/l (see Figure 7.6b), occurring at approximately 2 weeks into the simulation. As seen for the other cases the activity concentrations decrease rapidly falling below 1 Bq/l by the time 67 days have elapsed.

This particular simulation case yielded the highest of all peak ^{137}Cs activity concentrations in biota with levels of ca. 150 Bq/kg f.w. and 340 Bq/kg f.w. derived for fish and seal respectively (see Figure 7.6b). These elevations beyond those predicted for Gremikha plausibly reflect the protracted relatively high concentrations of ^{137}Cs in seawater for the Stepovogo scenario. Although levels fell rapidly in both cases, ^{137}Cs remained at levels above 5 Bq/l for almost 1 week longer at the selected measurement location for Stepovogo compared to the Gremikha scenario. The maximum activity concentration of ^{137}Cs predicted for seabird fell slightly below 1000 Bq/kg f.w.

The maxima occurred at 81, 119 and 105 days for fish, seal and seabird respectively. Such delays in exhibiting activity peaks are to be expected from an understanding of the general behaviour for the types of (bio)-kinetic models applied and with regards to how transfer parameters have been selected. In contrast, the application of concentration ratios to the time profile of ^{137}Cs activity concentrations in seawater would have led to highly elevated biota concentrations in the initial phase followed by relatively low values in the proceeding phase (weeks and months later). Application of such methods would arguably lead to a poor characterisation of the ^{137}Cs levels in the marine food-chain and provide misleading insights into the protracted nature of food contamination following an accidental release.

8. Results: Dose estimates

8.1 Estimation of doses to humans

For scenarios outlined above (see section 6.3), the annual effective doses have been calculated for the following pathways: inhalation, cloud shine, ground shine and ingestion. These exposure pathways have been defined based on the considered “critical group” (or representative person) in each scenario. The applied dose coefficients are taken from ICRP (2012) and Health Canada (1999) for intake (inhalation and ingestion) and external exposure (groundshine and cloudshine), respectively. Breathing rate values are taken from ICRP 71 (ICRP, 1995b).

8.1.1 Human Dose estimates for Stepovogo

Tables 8.1 – 8.4 show the estimated annual effective doses for individuals in identified population groups who could be affected by releases following a potential criticality accident at the current location of the submarine, i.e. Stepovogo Fjord.

Table 8.1. Estimated effective doses for inhalation pathway based on release scenario at Stepovogo Fjord.

Pathway	Radionuclide	Time integ. Air Conc. (Bq s/m ³)	Effective dose (mSv)
Inhalation	Sr-90	5.65E+06	5.2E-02
	Y-90	5.65E+06	2.2E-03
	Cs-137	2.57E+07	3.0E-02
	I-131	4.33E+07	8.2E-02
	I-133	1.59E+09	6.1E-01
	Te-132	4.61E+08	2.4E-01
	Ru-103	2.82E+07	1.7E-02
Total			1.0E+00

Table 8.2. Estimated effective doses from cloud-shine pathway based on release scenario at Stepovogo Fjord.

Pathway	Radionuclide	Time integ. Air Conc. (Bq s/m ³)	Effective dose (mSv)
Cloud shine	Kr-85	3.1E+06	7.8E-07
	Sr-90	5.7E+06	2.5E-06
	Y-90	5.7E+06	4.5E-06
	Cs-137	2.6E+07	6.6E-04
	Xe-133	2.6E+07	3.6E-05
	Xe-135	2.3E+09	2.6E-02
	I-131	4.3E+07	7.3E-04
	I-133	1.6E+09	4.4E-02
	Te-132	4.6E+08	5.4E-02
	Ru-103	2.8E+07	5.9E-04
	Sr-91	1.7E+07	5.7E-04
Total			1.3E-01

The doses from inhalation are approximately one order of magnitude greater than those from cloud-shine. The combined dose from these exposure pathways essentially for a person hypothetically standing some (short) distance downwind of a radioactive release would be in the region of 1 mSv. The dose from ground-shine is more substantial at approximately 26 mSv but this has not been combined with the other doses as the value pertains to the hypothetical exposure which could occur over a period of 1 year as opposed to the doses from inhalation and cloud shine pathways which would occur over time scales of hours and days. Assuming substantial contamination of shorelines did occur, the expectation would be that these areas would have access restrictions placed upon them, an intervention that would limit doses to humans over protracted periods.

The doses calculated in this work fall within the ICRP's (ICRP, 2007) band that is greater than 20 mSv but not more than 100 mSv (see section 6.5.1). This would be seen to apply in unusual, and often extreme, situations where actions taken to reduce exposures would be disruptive. The ICRP considers that a dose rising towards 100 mSv will almost always justify protective action and in view of uncertainties in the dose estimates given here, there would conceivably be actions taken to attempt to reduce the doses received by near-by military personnel, i.e. in the form of sheltering, movement restrictions etc.

Table 8.3. Estimated annual effective doses from ground shine pathway based on release scenario at Stepovogo Fjord.

Pathway	Radionuclide	Deposition (Bq/m ²)	Annual effective dose (mSv)
Ground shine	Sr-90	2.1E+03	1.1E-04
	Y-90	2.1E+03	7.4E-03
	Cs-137	9.7E+03	1.7E-01
	I-131	1.6E+04	1.9E-01
	I-133	6.0E+05	1.2E+01
	Te-132	1.7E+05	1.4E+01
	Ru-103	1.1E+04	1.5E-01
	Sr-91	6.2E+03	1.3E-01
Total			2.6E+01

The doses from subsistence fishing communities Yamal/Northern Yenisey are shown below (Table 8.4) and constitute a separate group, i.e. they would not receive doses of the same magnitude from other exposure pathways. The doses fall far below the reference level of 100 mSv (ICRP, 2007) applicable to emergency exposure situations but certainly well above a level that might be considered trivial. At these doses the ICRP recommends that general information on the level of exposure should be made available and that periodic checks should be made on the exposure pathways as to the level of exposure. As considered above the environmental management of this situation would be driven by restriction placed on foodstuffs because of applied intervention levels. In view of the activity concentrations that might hypothetically be attributed for foodstuffs for the pessimistic scenario considered it is not inconceivable that some restrictions on fishing etc. would need to be introduced.

Table 8.4. Estimated annual effective doses from ingestion of marine food for release scenario at Stepovogo Fjord.

Radionuclide	Activity in water (Bq/l)	Dose, fish (mSv)	Dose, seal (mSv)	Dose, sea bird (mSv)	Dose, sea bird egg (mSv)	Annual effective dose (mSv)
Cs-137	18.3 (Surface)	3.63E-01	1.30E-01	9.37E-02	1.39E-02	6.01E-01
	1.1 (Depth average)	3.09E-02	1.30E-02	8.98E-03	1.33E-03	5.41E-02

8.1.2 Human Dose estimates for Gremikha

The estimated annual effective doses for individuals in identified population group in Norway who could be affected by releases following a potential accident at the Gremikha Bay are shown in Tables 8.5– 8.9. In this scenario, it has been assumed that in case of any accident at Gremikha no criticality would be involved, hence there was no need to take into account any short-lived radionuclides.

Table 8.5. Estimated effective doses for inhalation pathway based on release scenario at Gremikha Bay.

Pathway	Radionuclide	Time Integ. Air Conc. (Bq s /m ³)	Effective dose (mSv)
Inhalation	Sr-90	1.2E+04	1.1E-04
	Y-90	1.1E+04	4.3E-06
	Cs-137	1.4E+04	1.7E-05
Total			1.3E-04

Table 8.6. Estimated effective doses for cloud shine pathway based on release scenario at Gremikha Bay.

Pathway	Radionuclide	Time Integ. Air Conc. (Bq s /m ³)	Effective dose (mSv)
Cloud shine	Kr-85	6.7E+02	1.7E-10
	Sr-90	1.2E+04	5.3E-09
	Y-90	1.1E+04	8.9E-09
	Cs-137	1.4E+04	3.6E-07
Total			3.7E-07

Table 8.7. Estimated annual effective doses for ground shine pathway based on release scenario at Gremikha Bay.

Pathway	Radionuclide	Deposition (Bq/m ²)	Annual effective dose (mSv)
Ground shine	Sr-90	2.2E+02	1.1E-05
	Y-90	7.8E+01	2.7E-04
	Cs-137	2.5E+02	4.4E-03
Total			4.7E-03

Table 8.8. Estimated annual effective doses from ingestion of terrestrial food for release scenario at Gremikha Bay.

Pathway	Radionuclide	Dose, reindeer (mSv)	Dose, Game (mSv)	Dose, Berries (mSv)	Annual effective dose (mSv)
Food ingestion	Sr-90	1.6E-02	6.7E-02	4.0E-02	1.2E-01
	Cs-137	8.0E-02	3.3E-02	1.2E-02	1.2E-01
Total					2.5E-01

Table 8.9. Estimated annual effective doses from ingestion of fish for release scenario at Gremikha Bay.

Radionuclide	Activity in water (Bq/l)	Activity in fish (Bq/kg)	Yearly intake (Bq/y)	Annual effective dose (mSv)
Cs-137	21 (Surface)	1.3E+02	1.2E+04	1.5E-01
	3 (Depth average)	2.7E+01	2.5E+03	3.0E-02

In the longer term (over the first year), ingestion from foodstuffs would have the potential to dominate the doses to a representative person in Finnmark Norway. The hypothetical dose from inhalation is orders of magnitude below 1 mSv and, as such, would not constitute a level of exposure where concerns would be high¹. Doses from ingestion pathways could be as high as 0.25 mSv for the ingestion of terrestrial foodstuffs. The doses fall within the ICRP's reference band below 1 mSv where a requirement for significant intervention would not be deemed appropriate. In any case, interventions in the form of food restrictions would be putatively driven by activity concentration based intervention levels. With the exception of berries, activity concentrations for radiocaesium appear to fall substantially below the apposite levels as described above.

The results shown in tables above provide a conservative measure of the potential exposures of human critical groups as a result of an accident at Stepovogo and Gremikha, respectively. It can be seen that of the two accident scenario considered the accident at Stepovogo Fjord gives the highest doses which arise primarily, in the longer term, through ground shine pathways. It should be noted that, the main contributors to the estimated doses for the Stepovogo scenario are short-lived radionuclides. Considering the food ingestion pathway, the Stepovogo scenario again results in higher doses through consumption of marine food. However, there is a caveat on direct comparison of the consequences of the two accident scenarios as they consider different types of accident and also different target population groups.

8.2 Dose estimation for non-human biota

8.2.1 Terrestrial

Dose rates to vegetation (shrub and grass), small burrowing mammals (considered to also characterise game animals harvested by hunting) and Deer/reindeer are presented in Figure 8.1. The highest exposures were calculated for small mammals with maximum dose rates slightly in excess of 0.4 μ Gy/h and accumulated doses for a 90 days period of 0.77 mGy. The dose rates fall slightly over the simulation period. A large component of the dose (> 70 % post day 30 of the simulation) for the periods considered is

¹ According to the Nordic "Flag book" (NFB, 2014), the dose criteria for operational intervention level for an internal dose via inhalation is a projected dose of 10 mSv in two days.

attributable to irradiation by beta particles from the decay of internally incorporated ^{90}Sr . External irradiation of the animal from ground deposition of ^{137}Cs (and to a negligible extent ^{90}Sr) is small in comparison. The dose-rates predicted for deer/reindeer in the earliest period of the accident are lower than those for small mammals with maximum dose rates slightly in excess of $0.1 \mu\text{Gy/h}$ and accumulated doses for a 90-day period of approximately 0.2 mGy . In contrast to the dynamics of small mammal exposures, the dose rates for Deer/reindeer actually increase slightly towards the end of the modelling period. This tenably reflects the growing importance of exposure from radionuclides in lichen with time via ingestion pathways.

The dose-rates for shrub decrease rapidly from a dose rate slightly in excess of $0.2 \mu\text{Gy/h}$, coinciding with the initial deposition event, to less than $0.1 \mu\text{Gy/h}$ within the first 15 days of simulation. The accumulated dose in the first month following the hypothetical release is a relatively low $84 \mu\text{Gy}$.

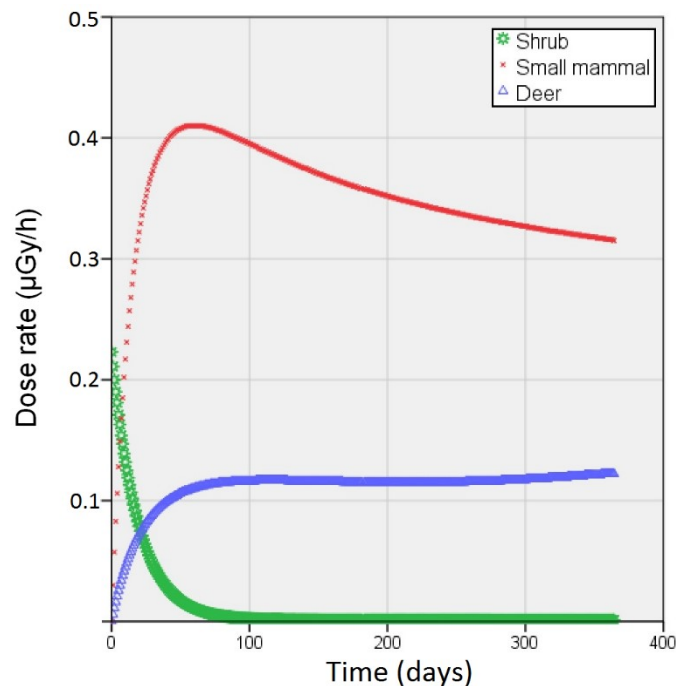


Figure 8.1. Dose-rate ($\mu\text{Gy/h}$) for Shrub (and other vegetation such as grass), small (burrowing) mammal, and Deer (as exemplified by Reindeer) for the area of maximum deposition in Finnmark for the Gremikha release scenario.

To place the exposures into some kind of context typical background dose rates (from terrestrial primordial radionuclides and excluding inhalation doses from ^{222}Rn) for terrestrial organisms have been reported in the range 0.07 to $0.6 \mu\text{Gy/h}$ (Beresford et al., 2008a).

Dose rates were far below the levels where even sub-lethal effects such as impairment of reproductive capacity or scoreable cytogenetic damage might be observed. Although strictly speaking accumulated doses are more appropriate to consider in the aftermath of an accident (see Strand et al., 2014), for sake of comparison, the lower end of DCRL bands are attributed by the ICRP (ICRP, 2008) to 0.1 mGy/d (or ca. $4 \mu\text{Gy/h}$) for (Pine) tree, and the mammals - Deer and Rat. At dose rates below this level, the likelihood of observing radiation-induced effects would be considered to be vanishingly small. The dose-rates generated for the given scenarios were, even at maximum exposure levels, an order of magnitude below this benchmark and would, therefore, be considered insignificant in terms of their potential impacts on wild organisms.

8.2.2 Marine

8.2.2.1 Gremikha release scenario

The dose rates for fish and seal predicted to arise from the Gremikha release scenario using the depth averaged activity concentration in seawater are presented in Figure 8.2a. The total dose rates essentially reflect the activity concentrations of ^{137}Cs in the organisms, per se, as oppose to ambient seawater concentrations with >95 % dose-rate attributable to internal body burdens of radiocesium at times after 1 month. The maximum dose rates calculated were slightly above $5 \times 10^{-3} \mu\text{Gy/h}$ for fish and slightly above $0.02 \mu\text{Gy/h}$ for seal. These are dose rates that are substantially below those derived as being characteristic of marine reference animals and plants (flatfish, crab and seaweed) exposed to naturally occurring primordial radionuclides (Hosseini et al., 2010). The accumulated doses (90 days) of ca. 9 and 27 μGy have been derived for fish and seal respectively. These are extremely low doses falling orders of magnitude below levels where any types of effect on organisms might be expected.

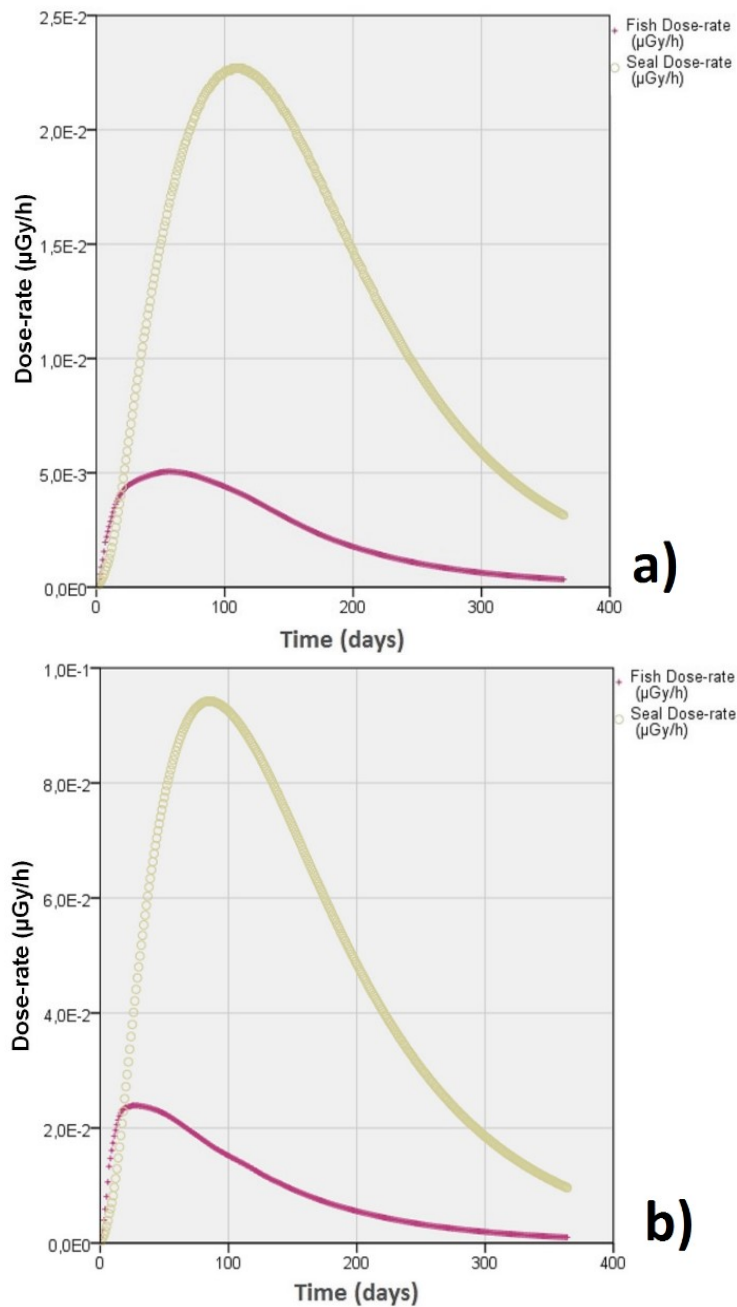


Figure 8.2. Dose-rate ($\mu\text{Gy/h}$) for fish and seal for the Gremikha scenario derived from (a) depth-averaged and (b) At surface activity concentrations of ^{137}Cs in sea water.

Using instead the surface seawater activity concentrations as input to the kinetic and dose rate model dose-rates elevated by approximately a factor of 4 to 5 (Figure 8.2b) were attained, commensurate with the difference between the activity concentrations of ^{137}Cs expressed as depth-averaged values compared to surface values. The dose rates were now within the same order of magnitude as those associated with exposure from naturally occurring radionuclides (cf. $0.15 \mu\text{Gy/h}$ for flatfish (see Hosseini et al., 2010) with the maximum of $0.024 \mu\text{Gy/h}$ for fish (present study) and $0.1 \mu\text{Gy/h}$ for marine mammals (Brown et al., 2004a) with the maximum of $0.094 \mu\text{Gy/h}$ for seal determined here). These dose-rates might furthermore be contextualised through consideration that the maximum (total including radionuclides in addition to ^{137}Cs) for fish in proximity to the main release point from the Fukushima Daiichi accident were (at an early stage post-accident) ca. $140 \mu\text{Gy/h}$ whereas dose rates determined at a later stage further offshore were in the range 0.10 to $0.17 \mu\text{Gy h}^{-1}$ (benthic fish, crustaceans and molluscs) (Vives i Batlle et al., 2014). The dose rates determined for the aforementioned Fukushima study were not considered to be at a level that might cause substantial impacts on populations of wild organisms.

The accumulated doses (over 90 days) of $43 \mu\text{Gy}$ and $130 \mu\text{Gy}$ have been determined for fish and seal respectively. These are very low doses, falling orders of magnitude below levels where pronounced effects on plants and animals might be expected. Furthermore, even at maximum dose-rates of ca. $2 \mu\text{Gy/day}$ for seals, the exposures are orders of magnitude below the $0.1\text{-}1 \text{ mGy/d}$ DCRL band recommended for application to mammals (strictly speaking Reference Deer and Rat but mammals are known to exhibit similar radiosensitivity) by the ICRP (2008). This band is considered to correspond to dose-rates where the probability of radiation-induced effects occurring is very low.

8.2.2.2 Stepovogo release scenario

The dose rates for fish, seal and seabird predicted to arise from the Stepovogo release scenario using the depth-averaged activity concentration in seawater are presented in Figure 8.3a. As for Gremikha, internal dose-rates dominate following the initial 30 days period reflecting the gradual uptake and transfer through the marine food-chain. Maximum dose rates at around 100 days for seal and seabirds with an absolute maximum of just under $0.02 \mu\text{Gy/h}$ being derived for the latter. As for Gremikha, the dose rates for all organism groups fall far below the dose-rates attributable to the presence of naturally occurring radionuclides (Brown et al., 2004a; Hosseini et al., 2010) and the lower end of comparable DCRL values the lowest of which falls at ca. $4 \mu\text{Gy/h}$ (Duck and the mammals Rat and Deer). Accumulated doses of ca. $1 \mu\text{Gy}$ for both fish and mammal and ca. $2 \mu\text{Gy}$ for seabirds have been derived. These are low doses and would have no conceivable impact on wild organisms.

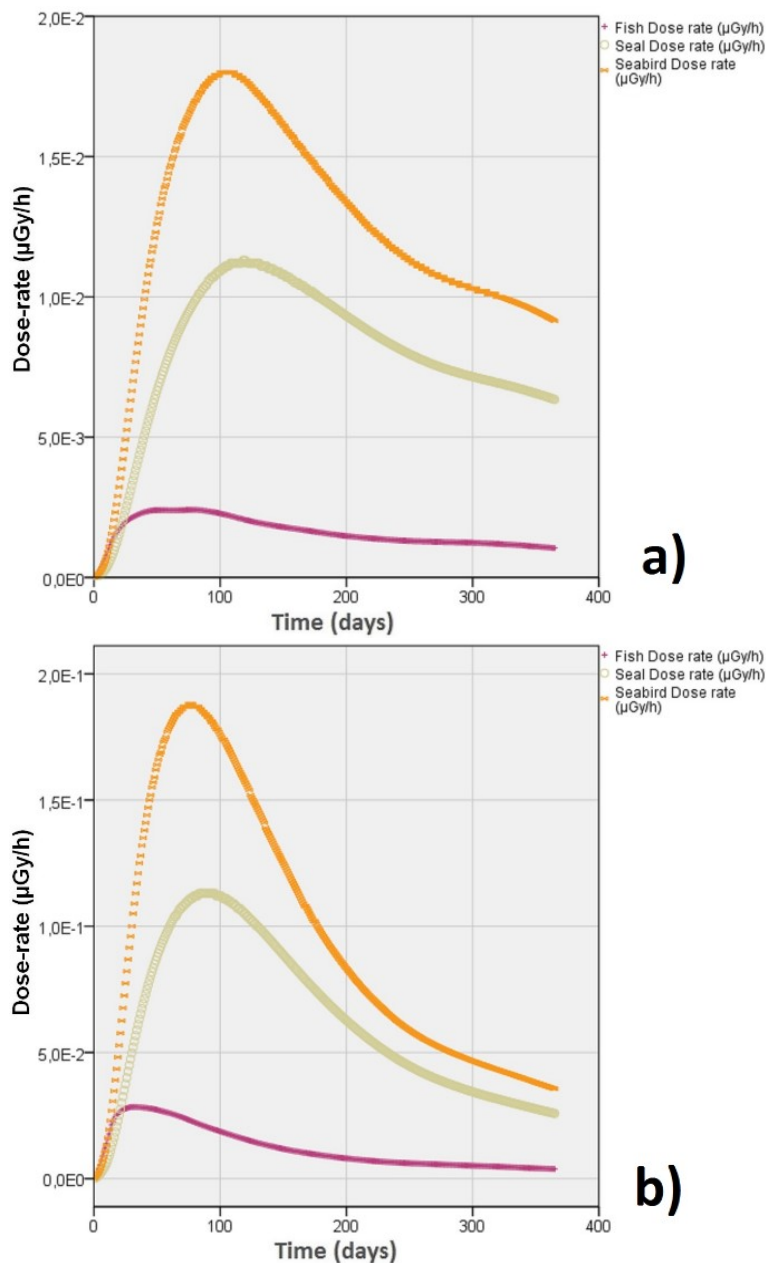


Figure 8.3. Dose-rate ($\mu\text{Gy/h}$) for fish and seal for the Stepovogo scenario derived from (a) depth-averaged and (b) At surface activity concentrations of ^{137}Cs in sea water.

Dose-rates pertaining to surface activity concentrations of ^{137}Cs for the Stepovogo scenario are shown in Figure 8.3b. A similar time profile to that observed for calculations based on depth-averaged seawater ^{137}Cs activity concentrations, although the timing of the maximum dose-rate occurs at a slightly earlier stage for all organism types. Seabirds are, again, predicted to experience the most elevated exposures with dose rates of around $0.19 \mu\text{Gy/h}$. The dose rates for fish and seal were of a similar order of magnitude to the dose rates associated with exposures for corresponding groups of organisms from naturally occurring radionuclides (Brown et al., 2004a; Hosseini et al., 2010). A cursory comparison with ICRP's DCRLs show predicted values falling more than an order of magnitude below a dose rate where some chance of observable radiobiological effects would be present.

Accumulated doses (30 days) of ca. $14 \mu\text{Gy}$ for both fish and mammal and ca. $28 \mu\text{Gy}$ for seabirds have been derived. These are relatively low doses for which the observation of effects would not be plausible.

9. Dealing with uncertainties

It is apparent that any assessment of risk (to both humans and the environment) requires the specification and inclusion of many elements. In our case, these elements comprise of problem formulation, models, scenarios, assumptions, data, expert judgement and the various tools employed. In dealing with any of these components, we eventually have to face situations of inadequate information and uncertainty (Van der Sluijs, 2007). However, uncertainty may not simply reflect a lack of knowledge, it can also arise due to variability inherent to the system under discussion. The distinction between these two types of uncertainty is often of great importance (Frey, 1992).

Walker et al. (2003) defined uncertainty as a three dimensional concept. They argued that in discussing the uncertainty related to model-based studies, we have to distinguish between three dimensions of uncertainty: location, level and nature. The first dimension refers to relevant locations where uncertainty can manifest itself e.g. context, model structure, inputs, parameters, and model outcome (result). The second dimension represent what we know and ranges from perfect knowledge to total ignorance. However, to distinguish between various levels of uncertainty, they employed the following concepts which define the transition from determinism to total ignorance: Statistical Uncertainty (known probability distributions), Scenario Uncertainty (range of the possible outcomes known, but no credible basis for the assignment of probability distributions), and Identified Ignorance (unknown bounds of the set of potential outcomes and unknown probabilities). Finally, the third dimension describes whether the uncertainty is due to the lack of knowledge or due to inherent variability of the phenomena being studied.

Hence, a thorough characterisation of uncertainty requires a critical analysis of all the components comprising the assessment (e.g. models, scenarios, underlying assumptions, underpinning data). Such a detailed analysis of uncertainty would require the allocation of considerable resources and effort and was considered beyond the scope of the present work.

We have to bear in mind that for the case of K-27 (or any other dumped or sunken object for which salvage is an option) there are factors which add extra layers to the existing uncertainty. Such factors might include, for example, the time and circumstances of lifting and the characteristics of the scenarios considered. When in the future a salvage operation would take place and which technology would be used has an impact on the applicability of the results arising from any concomitant impact assessment (NES, 2013). We cannot foresee the future but to indicate what might happen, we make use of scenarios. The latter implies making assumptions that often cannot be verified. Uncertainties of this kind most probably mask much of the efforts in characterising other types of uncertainties that could be described statistically. Conscious of these sources of great uncertainty, spending resources to characterise model and parameter uncertainties, measurement and sampling errors and other location relevant uncertainties would not be fully justified.

Hence, a resource efficient and pragmatic approach to deal with uncertainty and consequently lend credibility to the outcomes of a study of the kind we have conducted would be to apply conservative assumptions, consider extreme accident scenarios and employ high-end input values (IPCS 2014). We have adopted such an approach in this study. Application of a sensitivity analysis in order to identify the most important parameters/ factors (e.g. Avila et al., 2004) as well as determining their influence on the outputs would also be of a great use. However, this was considered as being beyond the scope of the current analysis.

Conservatism has been introduced at various points in the assessment. This has been done by looking for the worst case scenarios which represent extreme situations (e.g. different flow regimes in marine dispersion modelling and worst metrological cases), considering various accident scenarios (accident under water, at the surface and on the land), employing conservative parameters and assumptions (spontaneous release of total inventory, highest possible SCR), focusing on higher end input values (considering critical groups, using 95th percentiles). In addition, to reduce uncertainty, further attempts have been made to use best available knowledge/ information through consulting the most relevant sources and employing state of the art models.

Even using these highly pessimistic assumptions and considering worse cases, the calculated radiation doses for Norwegian territory would not lead to excessive concerns regarding impacts on human health or the environment from the exposure pathways considered here.

10. Summary and concluding remarks

There has been and continues to be concern over potential radioactive contamination of the Arctic. This is in large part due to the presence of a wide range of nuclear sources within, what is perceived to be, a pristine and vulnerable region of direct economic and socioeconomic importance for a number of countries. Dumped radioactive waste contributes the greatest proportion to the total activity found in the Arctic Seas, followed by inputs from European nuclear reprocessing facilities and global fallout from the nuclear weapons testing period. Of the dumped objects present within the Arctic, those containing Spent Nuclear Fuel (SNF) are of special importance given the nature of such materials. Amongst dumped objects in the Arctic, the submarine K-27 has been the focus of much attention due to particular concerns related to this vessel, primarily related to the fact that it contains two reactors with SNF, encapsulating highly enriched fuel, and lies at a shallow depth of about 30 m.

To address these concerns and to provide a better foundation for the evaluation of possible radiological impact, especially in the case of a potential recovery of the submarine, a health and environmental impact assessment has been undertaken. The study was based on the derivation of a number of hypothetical accident scenarios and the evaluation of possible consequences for humans and the environment as a result of these hypothetical scenarios. Three main scenarios were considered. The first was the “zero alternative”, i.e. an investigation of current and future impacts assuming no interventions. The second considered an accident scenario during the raising of the submarine and the third, an accident scenario related to the transportation of the submarine for defueling. The main focus was directed to those scenarios related to the raising and transportation of the submarine including situations under which spontaneous chain reaction (SCR) can take place. The work involved application of state of the art 3-dimensional hydrodynamic and atmospheric dispersion models to elucidate the transport, distribution and fate of relevant radionuclides in aquatic and terrestrial ecosystems following hypothetical accidents.

To evaluate the marine dispersion of potentially released radionuclides as a consequence of a possible recovery of K-27 as well as a prolonged stay under water, the model NAOSIM (North Atlantic/Arctic coupled Ocean Sea Ice Model) was employed. Accident scenarios during the following stages were considered:

- a) On-site; release at the surface (Stepovogo Fjord),
- b) Under transportation; release at two depths - surface and ~ 300 m (Barents Sea),
- c) At the final destination; release at the surface (Gremikha Bay),

For each stage, three different large scale atmospheric and oceanic circulation scenarios were studied: a weak and strong flushing of the Barents and Kara Seas and a special case exhibiting reverse flow through the Kara Gate. For each combination of accident scenario and oceanographic circulation scenarios, two hypothetical release situations - instantaneous and continuous – were considered. Hypothetical releases of 1 PBq and 1 TBq per year were utilised for the instantaneous and continuous releases, respectively.

Some key data pertaining to activity concentrations in biota are given in Tables 10.1 and 10.3.

Table 10.1. Maximum activity concentration in water and marine biota at different accident locations considered in the study along with the estimated associated doses to biota.

Accident location	Maximum activity concentration, Cs-137			Maximum dose ($\mu\text{Gy/h}$)
	Water (Bq/l)	Biota (Bq/kg f.w.)		
Stepovogo Fjord	18	Fish	153	0.03
		Seal	342	0.12
		Seabird	987	0.19
Barents Sea	13	Fish	72	0.013
		Seal	164	0.054
		Seabird	470	0.09
Gremikha Bay	21	Fish	129	0.024
		Seal	285	0.094

To place the simulated and predicted activity levels (both in seawater and in biota) into context, the measured ^{137}Cs activity concentrations at the areas of interest are summarized in Table 10.2.

Table 10.1. Measured activity concentrations of ^{137}Cs in seawater and biota based on samples collected in the Stepovogo Fjord, Barents Sea and Norwegian Sea in recent years.

Location	Measured activity concentration, Cs-137			Reference
	Water (Bq/l)	Biota (Bq/kg f.w.)		
Stepovogo Fjord	1.5E-03 – 1.8E-03	Fish	<0.3	JNREG 2014
		Seal	<0.2	
Barents Sea	1.6E-03 – 2.0E-03	Fish	<0.3	(Gwynn et al. 2012)
Norwegian Sea	1.1E-03 – 5.9E-03	Fish*	<0.5	NRPA (2011) & NRPA (2015)

* Caught at coastal waters of Finnmark and Troms.

To evaluate atmospheric dispersion of radionuclides in a way that was compatible for exposure calculations pertaining to a critical group in Stepovogo Fjord, a local dispersion Model was used in tandem with a source term based on a SCR. For regional level atmospheric dispersion involving long range transport of radionuclides, the Norwegian Meteorological Institute's SNAP (Severe Nuclear Accident Program) model was employed using a source term based upon the outbreak of fire at Gremikha when the submarine is on land and during the retrieval of SNF.

Table 10.3. Maximum activity concentration in terrestrial biota at Gremikha Bay along with the estimated associated doses to biota.

Accident location	Maximum activity, Bq/kg (f.w.)			Maximum dose ($\mu\text{Gy/h}$)
	Biota	Cs-137	Sr-90	
Gremikha Bay	Vegetation	270	360	0.23
	Small mammals	580	550	0.4
	Deer	175	175*	0.13*

*highest value observed during the simulation time (1 year).

The output data (see Tables 10.1 and 10.3) from the various models deployed were used as inputs to ingestion dose calculations with other exposure pathways for humans (e.g. cloud shine, ground shine and inhalation). These in turn are calculated via outputs (radionuclide air concentration and deposition levels) from atmospheric dispersion models. Doses to both humans and biota were then evaluated (see Tables 10.1 and 10.3 -10.5). Because of the uncertainties involved in modelling work of this type, a degree of conservatism was introduced at various points in the assessment. Bearing such conservatism in mind, it remains apparent that serious impacts on either human health or environmental integrity, as a result of releases from the hypothetical scenarios studied, would not be expected. Nonetheless, potential doses, primarily due to ground shine, to a group of personnel on-site at Stepovogo resulting from a SCR could require preventative measures where decision to be based on ICRP recommendations. The hypothetical terrestrial-based dose calculated to a critical group in Finnmark was estimated to be below 1 mSv and as such would not constitute a level of exposure where concerns would be extreme (see Table 10.4). Nonetheless, the doses are non-trivial and there would conceivably be attempts made to reduce doses as far as possible with due regard to social and economic perspectives.

Table 10.4. Estimated effective doses to human for various pathways based on releases to atmosphere at Stepovogo Fjord and Gremikha Bay.

<i>Accident location</i>	<i>Pathway</i>	<i>Effective dose* (mSv)</i>	<i>Comments</i>
Stepovogo Fjord	Inhalation	1.0E+00	Military personnel on site
	Cloud shine	1.3E-01	
	Ground shine	2.6E+01**	
	Total	2.7E+01	
Gremikha Bay	Inhalation	1.3E-04	individuals in identified population group in Norway
	Cloud shine	3.7E-07	
	Ground shine	4.7E-03**	
	Ingestion (terrestrial food)	2.5E-01**	
	Total	2.6E-01	

* Doses are based on consideration of various radionuclides the composition of which depends on the considered scenario.

** Annual effective dose.

The doses for humans for the Gremikha release scenario derived for the ingestion of contaminated marine foodstuffs are only slightly lower (see Table 10.5) than the potential doses from ingestion of contaminated terrestrial foodstuffs. The levels of ¹³⁷Cs derived for marine organism in areas close to Norway were not values that would likely cause concern from a regulatory perspective although for subsistence fishing communities Yamal/Northern Yenisey, it is not inconceivable that some restrictions on fishing etc. would need to be introduced.

Table 10.5. Estimated annual effective doses to human for various pathways based on releases to the sea at Stepovogo Fjord and Gremikha Bay.

<i>Accident location</i>	<i>Pathway</i>	<i>Annual effective dose (mSv)</i>	<i>Comments</i>
Stepovogo Fjord	Ingestion of seafood	6.0E-01	Subsistence fishing communities
Barents Sea	Ingestion of seafood	2.8E-01	Subsistence fishing communities
Gremikha Bay	Ingestion of fish	1.5E-01	individuals in identified population group in Norway, high rate consumers of fish

Bearing in mind the socio-economic impacts of other accidents involving nuclear and radiological materials, such as the sinking of the Kursk, as well as public unease evident in relation to the Fukushima accident, there remains a cause for concern. The study indicates the potential for significant and widespread contamination of the Arctic environment with radionuclides in the event of an incident involving a SCR. Such contamination and public perception of the significance of its extent and magnitude is difficult to predict but previous incidents serve to indicate that there would be a potential impact with respect to consumer confidence in marine products and presumably concomitant consequences for the production and export industries of such products.

11. Acknowledgments

This work was (partly) supported by the Research Council of Norway through its Centre's of Excellence funding scheme, project number 223268/F50.

Appendix A: Previous studies: Near and far field dispersion modelling

A1 Near field dispersion modelling

In this section, the issue of near field dispersion has been addressed by considering earlier studies. Three different scenarios have been considered: i) idealized flushing time scenarios which provide basic estimates for the retention times of radioactivity in the fjord, ii) idealized release scenarios for continuous releases in a homogeneous fjord under constant forcing and iii) release rate scenarios with realistic transient forcing.

A1.1 Flushing time scenarios

In order to evaluate the retention time of radioactivity in Stepovogo Fjord, an idealized flushing scenario was considered by Harms (Harms, 1997). The scenario was developed based on the following assumptions: the fjord was ice-free and wind was the most important driving force for circulation with a moderated wind speed of 5 m/s blowing in two longitudinal directions (on- and offshore winds). Simulations based on such a scenario indicated that an offshore wind flushes the Stepovogo Fjord by 90% after 15 days and an onshore wind flushes the fjord after 30 days (for more details see Hosseini et al., 2015).

Based on volume estimates for Stepovogo Fjord it can be expected that an instantaneous release of 1 TBq would result in water concentrations (on site) in the range of $10^4 - 10^5$ Bq/m³. The above flushing time scenario suggests that a high contamination load would start affecting the outer parts of the fjord and the adjacent coastal waters of Novaya Zemlya within a few days; an almost complete displacement of the contamination (assuming in dissolved phase) onto the western Kara Sea is possible in two weeks time.

However, the flushing times depend strongly on the presence of ice cover. Sea ice in small Arctic fjords is mostly land fast (i.e. immobile) which means that the transfer of momentum from wind to the water surface is largely inhibited. The aforementioned flushing time scenario was carried out without any ice module and with homogeneous density. Results from Koziy et al. (1998) indicate that ice and vertical density stratification may prolong the flushing time considerably. The given flushing times can thus be regarded as worst-case estimates.

A1.2 Release rate scenarios with simplified forcing

The following release rate scenarios (Baxter et al., 1998) use the same conditions as for the previous flushing time scenarios, i.e. constant winds, homogeneous density (no horizontal or vertical density gradients), no ice cover. Based on stationary flow fields, the authors simulated the dispersion in the fjord considering a continuous release.

The wind forcing comprises constant winds from the south-east and south west which represent the prevailing wind directions in the southern Kara Sea (Pavlov et al., 1993). For the eastern Novaya Zemlya coast, easterly winds would have on-shore components whereas south-westerly winds would have off-shore components. The general circulation patterns in Stepovogo Fjord following on- and off-shore winds can be described briefly in the following way (Figure A1): on-shore winds cause an inflow into the fjords in the surface layers. This inflow is compensated by a downwelling in the innermost parts and a resulting outflow in the bottom layers. Off-shore winds lead to a surface outflow with a compensatory inflow over the sill at depth, and an upwelling at the shore. Accordingly, the release of a tracer from a source at the bottom of the fjord would lead to an export from the fjord and a contamination of surface or bottom waters of the western Kara Sea, respectively, depending on the direction of the wind. An onshore wind situation would lead to export of contaminated water at the bottom, an offshore wind situation would lead to an export with the surface waters.

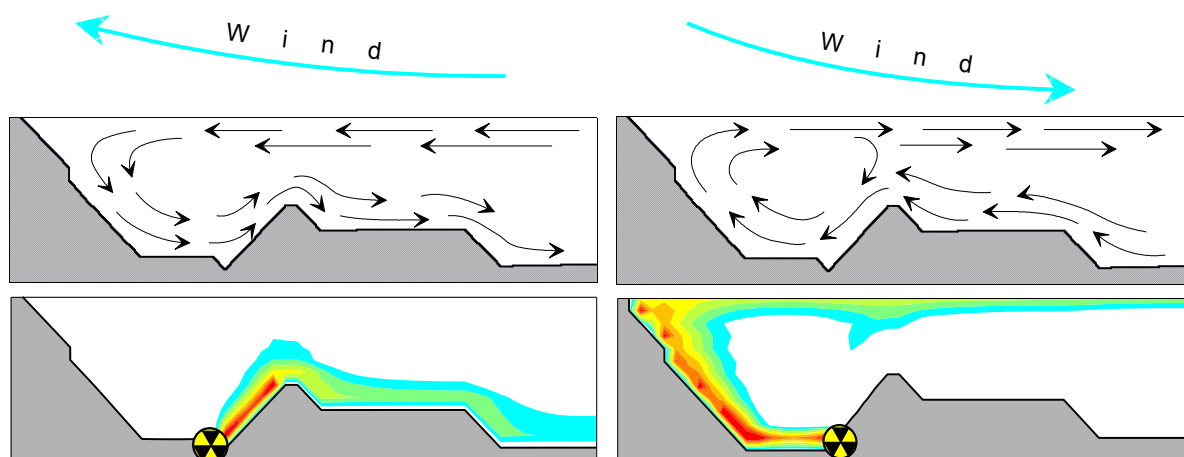


Figure A1. Simplified sketch for on-shore (left) and off-shore (right) wind induced circulation types in Stepovogo Fjord (upper panels). The resulting dispersion from a continuously emitting source is depicted in the lower panels.

In Stepovogo Fjord, the considered source was placed just behind the sill in the inner part. The dispersion from the source reflects the principle circulation pattern (Figure A1): in case of an onshore wind, the outflow of dispersion is close to the bottom which keeps the overall contamination in the fjord at a much lower level than in the off-shore case. In the latter case, the contamination from the source is carried to the surface via upwelling before it leaves the fjord. This type of circulation causes a much more widespread contamination in the inner fjord and at the surface.

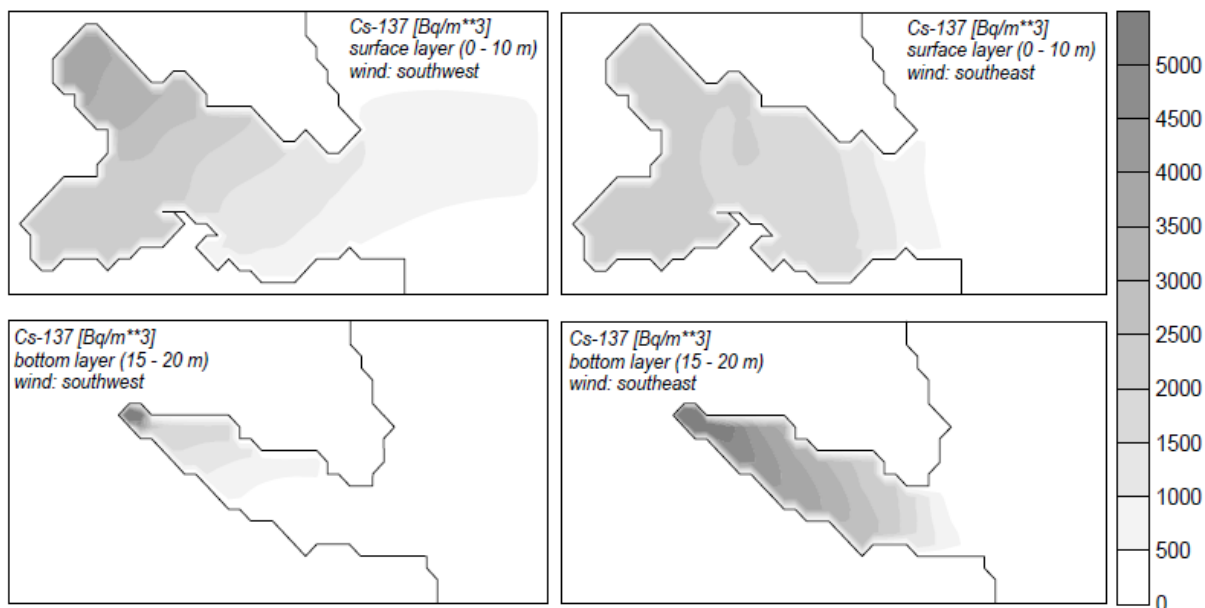


Figure A2. Concentrations of radioactivity at the surface and the bottom of Abrasimov Bay. Applied release rate: 1TBq/y ^{137}Cs in the inner part. Applied winds: south west (left) and south-east (right). Baxter et al. (1998).

This simplified release rate scenario was also used in simulations for Abrasimov Bay applying the same south-easterly and south-westerly winds, as described above. The source is assumed to emit ^{137}Cs tracers equivalent to a release rate of 1 TBq/y. The stationary state with respect to ^{137}Cs concentrations due to both wind directions is depicted in Figure A2. Similarly to Stepovogo Fjord, the outflow of contaminated waters in Abrasimov Bay for south-westerly winds is predominantly in the surface layer with activity

concentrations ranging from 3500 Bq/m³ in the inner bay up to 500 Bq/m³ at the opening. For south-easterly winds the bottom layer carries the outflow signal, ranging from 4500 Bq/m³ in the inner bay up to 500 Bq/m³ at the mouth of the bay. In both cases, vertical mixing leads to contamination of the entire water column in the bay. The maximum concentration in a layer might exceed 4000 Bq/m³ but averaged over the entire water column depth levels do not exceed 1000 Bq/m³.

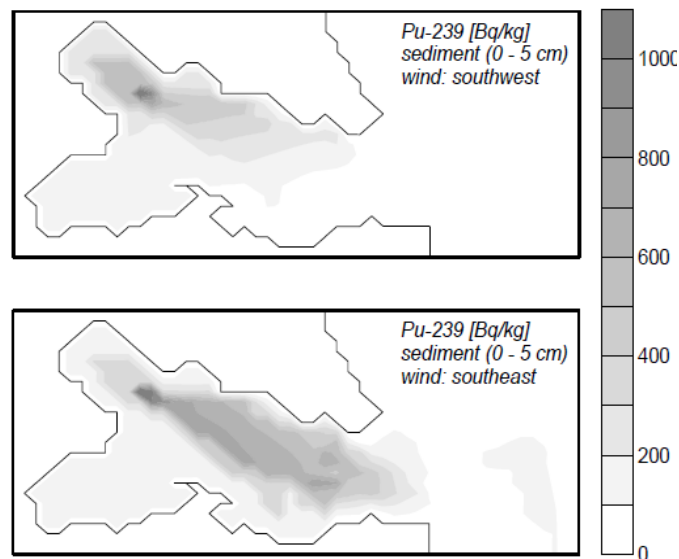


Figure A3. Concentrations of ²³⁹Pu in the sediment of Abrasimov Bay. Applied release rate: 1TBq/y in the inner part. Applied winds: south west and south-east. Baxter et al. (1998).

The application of a constant forcing leads to stationary circulation and dispersion patterns which allows for an estimation of sediment concentrations based on the algorithm described in Appendix B2 (for this scenario, the suspended load was set to 0.024 kg/m³). Concentrations in the upper 5 cm of the sediment were estimated for a 1TBq/y release of ²³⁹Pu (Figure A3). It is obvious that higher sediment concentrations of ²³⁹Pu occur for the south-easterly wind case. This is due to less effective flushing, which leads to higher contamination of the out flowing water in the bottom layers. In this scenario the concentrations in sediment might exceed 500 Bq/kg over large parts of the bay, although locally, at locations in proximity to the source, levels can be much higher. In this case at the mouth of the bay concentrations in the sediment are of the order of 300 Bq/kg.

A1.3 Release rate scenarios with realistic forcing

In the following scenarios (Harms and Povinec, 1999) the topography, model domain and grid size were identical to the previous model studies (A1.1 and A1.2). The resolution for the grid was kept to 1/10 nautical mile (185.2 m) on the horizontal scale. In order to incorporate the density stratification of the water body, the vertical scale was resolved with seven layers, each of which was 5 m thick. Other important differences from the previous scenarios were the application of realistic forcing data and the inclusion of an ice model as described in Appendix A2.3.

Ice drift in shallow regions or small fjords differs considerably from ice drift in open sea. However, calculating the ice motion in shallow areas can be done according to the free drift assumption but with an additional linear dependence on the depth, allowing for moderate ice velocities during spring and autumn, as is the case in the shallow areas of the fjord. During winter it must be assumed that the ice movement is totally blocked. Therefore, a land fast ice cover (i.e. no ice movement) is applied during January, February, March and April, for depths of less than 20 m.

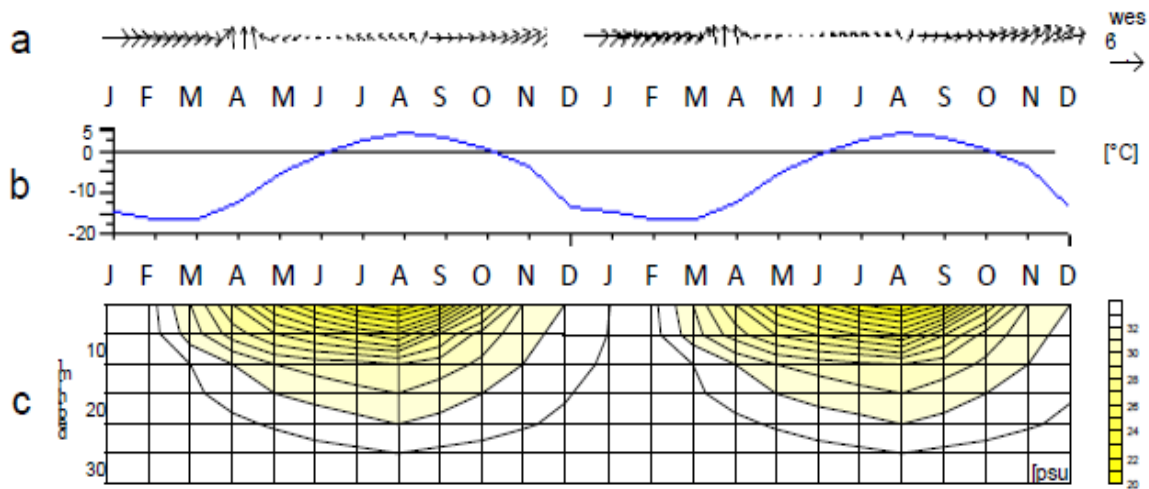


Figure A4. a) Stick plot of wind direction and speed, b) time series of air temperatures and c) Hovmöller diagram of the seasonal development of vertical stratification of salinity. Taken from Harms and Povinec (1999).

In contrast to previous applications, the model simulations discussed here use transient winds and air temperatures which were derived from monthly mean climatological ECMWF1-data. Figure A4 shows a stick plot of the applied winds (a), and the air temperatures (b) for a time span of 2 years. Surface heat fluxes at the ocean/ice/atmosphere interfaces are calculated on the basis of air temperatures with standard bulk formulae (Maykut, 1986). These heat fluxes encompass the atmospheric latent and sensible heat flux, the conductive heat flux through the ice, the turbulent heat flux under the ice, the long-wave radiation and the incoming short-wave radiation. The oceanic gain and loss of heat is used to determine the sea surface temperature which in turn affects the ice formation. Additionally, a three-dimensional advection scheme is applied in order to treat the water temperature as a free 'prognostic' variable that is not constrained by given data.

Salinity was treated by considering 10-day mean vertical profiles representing the seasonal stratification in Novaya Zemlya fjords. These vertical profiles were derived from typical summer and winter situations using a linear interpolation to ensure a smooth transition. Information on the summer stratification was taken from the Joint Norwegian-Russian Expert Group (JNREG, 1994), Føyn and Nikitin (1994) and IAEA (1999b). For a late winter situation, a homogeneous salinity profile was assumed, based on the fact that vertical mixing and convection due to cooling and ice formation leads to complete vertical mixing in winter. The summer situation was characterised by salinities around 20 near the surface and 33 at the bottom. This corresponds well with the descriptions of Stepovogo Fjord from the IAEA TecDoc 1075 (IAEA 1999b) and vertical profiles described by Koziy et al. (1998) and Stepanets et al. (2006). The interpolation between summer and winter profiles leads to an idealized cyclic stationary stratification as depicted in the Hovmöller diagram in Figure A4c.

The vertical distribution of the tracer does not only depend on the wind energy input, the density stratification also playing a role. For the present investigation of a rather small Arctic fjord, it is important to include the vertical distribution of density. The stratification of the water column controls the transfer of momentum and the diffusion of matter between different depth horizons. A strong stratification for example reduces the momentum as well as the vertical mixing and allows different water masses to remain almost unaffected above each other as long as the stability is ensured. On the other hand, a weak or even neutral stratification enhances the transfer of momentum which might result in rather homogeneous vertical profiles of velocity or matter.

These effects play an important role in Arctic fjords because vertical stratification shows a strong seasonal signal. In particular in summer, when the wind speeds are low, the density stratification influences the tracer distribution. Atmospheric warming and ice melt create a thin, warm and low saline surface layer above much colder and more saline 'deeper' waters (see Figure A4c). The boundary in between reduces

the vertical exchange and allows for an accumulation of tracers near the bottom. In autumn and winter, the density stratification is eroded due to cooling, ice formation and wind mixing. Strong vertical mixing together with accelerated dynamics lead to lowest concentration levels and almost no stratification of radioactivity in autumn.

Due to a persisting lack of information on space and time distributions of temperature and salinity properties in the bay, a verification of the obtained temperature and salinity fields remains difficult, if not impossible. For this reason, horizontal gradients in salinity, which play only a minor role in the bay circulation, were omitted. The described handling of temperature and salinity in the model represents a compromise between a more realistic vertical stratification and poor knowledge that still exists on the hydrography of the bay.

The circulation model includes a transport algorithm for passive tracers based on the advection / diffusion transport equation (see Section B2).

The model was started at rest with no ice and run for a 1-year spin-up time. After reaching a cyclostationary state of circulation, the simulations were continued for 2 more years applying tracer releases in the bay. Our results from the second and third year confirm the view that time dependent tracer variations in both, wind fields and ice cover cause a pronounced seasonality in the water circulation of the bay. This is reflected first of all in the surface layers where wind and ice affect the circulation directly.

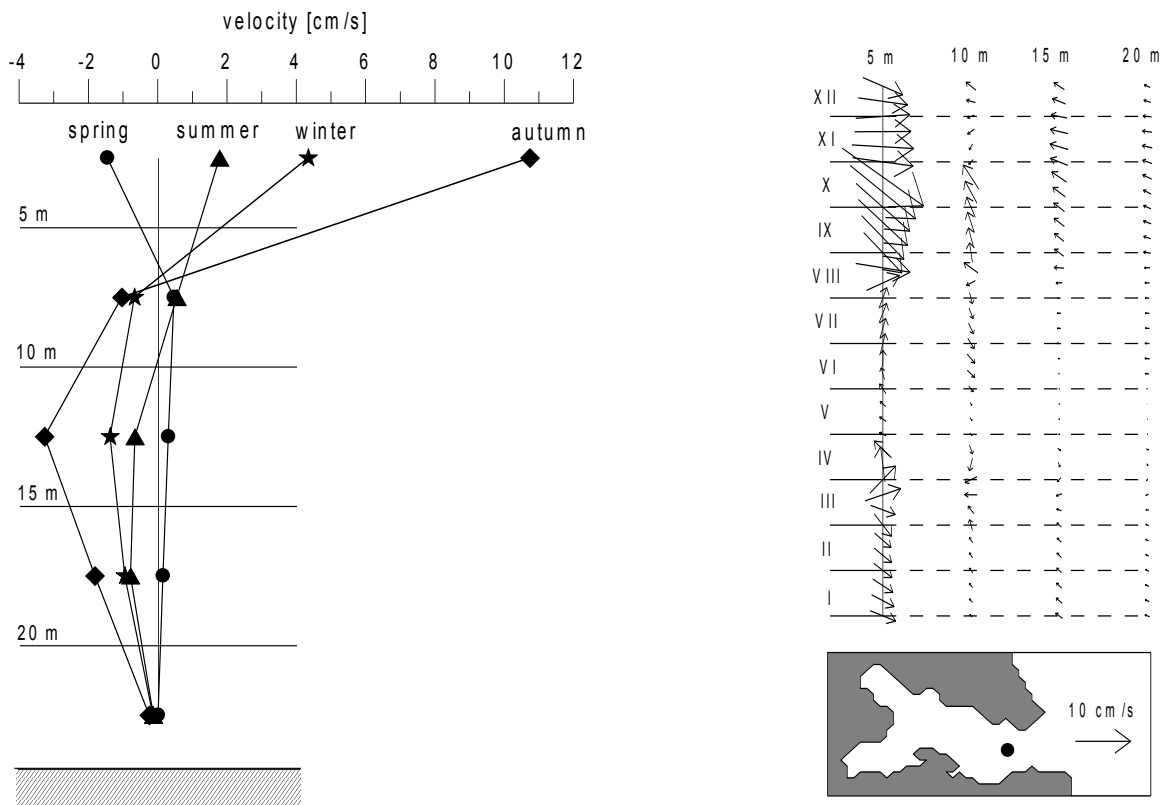


Figure A5. Left: Vertical profile of current speeds at the entrance of the fjord (dot). Right: 10-day interval stick plot of horizontal current directions at four different depth horizons. Roman numbers on the y-axis denote the month. Harms and Povinec (1999).

Figure A5 reveals that surface currents in early spring, autumn and winter are directed out of the bay with highest velocities in September and October. For conservation of mass, this surface outflow requires a compensation through a returning inflow in lower layers which is also strongest during this time. However, in November and December, the ice cover becomes established leading to a reduction in the effect that wind has at the surface. In spite of the fact that the wind speeds increase during that time, the surface velocities decrease during these months.

In winter, when the ice drift in the bay is totally blocked, the driving forces for the water are reduced largely to external and internal pressure gradients stemming from the density field. Since the ice is not moving, the friction below the ice leads to dissipation of kinetic energy. For this reason, surface velocities in late winter are quite low in spite of high wind speeds.

In spring and early summer (April, May, June, July), the wind changes from offshore to onshore directions, however, at much lower wind speeds. This results in a reversed water circulation in the bay but with considerable lower current speeds. Ice is transported into the bay where it melts due to short-wave radiation and increasing surface water temperatures.

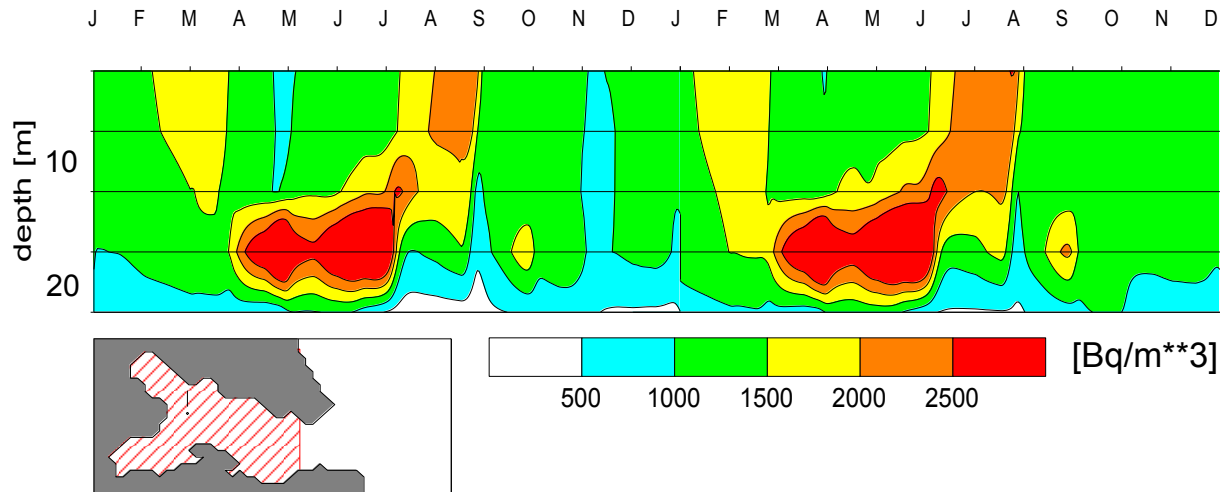


Figure A6. Two years Hovmöller diagram of the average vertical concentration of radioactivity in the inner fjord area (red) due to a constant release of 1 TBq/y; Harms and Povinec (1999).

Based on these transient circulation patterns, a 2-year long simulation was carried out assuming a constant 1 TBq/y release of radioactivity in the inner bay. The vertical distribution of radioactive tracer concentration is depicted in Figure A6 for a time span of 2 years. The values represent a spatial average for each layer in the inner bay (red area).

A pronounced seasonal signal in the intensity of the flushing is visible: highest concentrations can be observed in spring and early summer at a depth of 15 m. This accumulation occurs because of low dynamics due to weak summer wind conditions. Land-fast ice which hampers the transfer of momentum from the atmosphere to the ocean contributes to this effect. A weak uncontaminated inflow at the surface dilutes upper layer concentrations while in the bottom layers concentrations increase.

In autumn, however, the situation changes rapidly. Strong winds and the absence of ice cause a pronounced flushing and significantly lower tracer concentrations in the whole water column. Lowest tracer concentrations in the bay occur therefore in November and December.

Examples for the two circulation types together with concentration levels are given in Figure A7. The autumn / winter circulation pattern that prevails during most of the ice free season is shown in the left panel. Here we find highest concentrations together with the outflow at the surface, whereas the lower layers are flushed by uncontaminated inflow from the open boundaries. The spring and summer situation is given in the right panel. The uncontaminated inflow occurs at the surface, whereas, in lower layers, high concentrations and contaminated outflow prevails. However, due to weak winds and the presence of ice, the flushing is generally less pronounced.

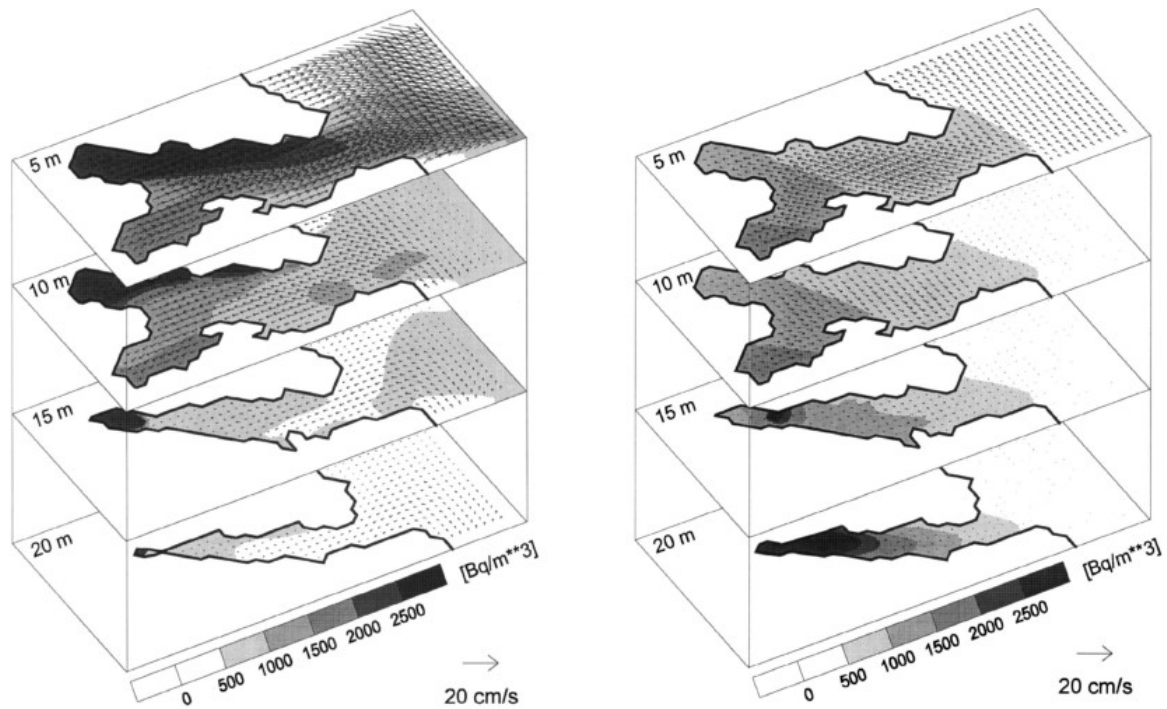


Figure A7. Circulation patterns and concentrations of radioactivity for autumn / winter (left panel) and spring / summer (right panel); Harms and Povinec (1999).

The situation a few miles off-shore at the entrance of the fjord is different from within the bay (Figure A8). In the coastal outer bay concentrations at the surface (blue line) are mostly lower than in deeper layers around 30 m (red line). This is apparent in particular in summer due to moderate on-shore winds bringing uncontaminated waters towards the coast. The compensating outflow in summer is mostly at the bottom where accumulated concentrations leave the bay in sporadic events (arrows).

In late autumn however, the situation reverses. Surface concentrations significantly increase, partly above levels in the deeper outflow (shaded areas). This surface 'outburst' stems from accumulated bottom radioactivity in summer, brought to the surface by upwelling due to strong off-shore winds. Since there is no ice during that time of the year, the concentrations are flushed out of the bay by surface currents, thereby enhancing levels in coastal areas off Novaya Zemlya.

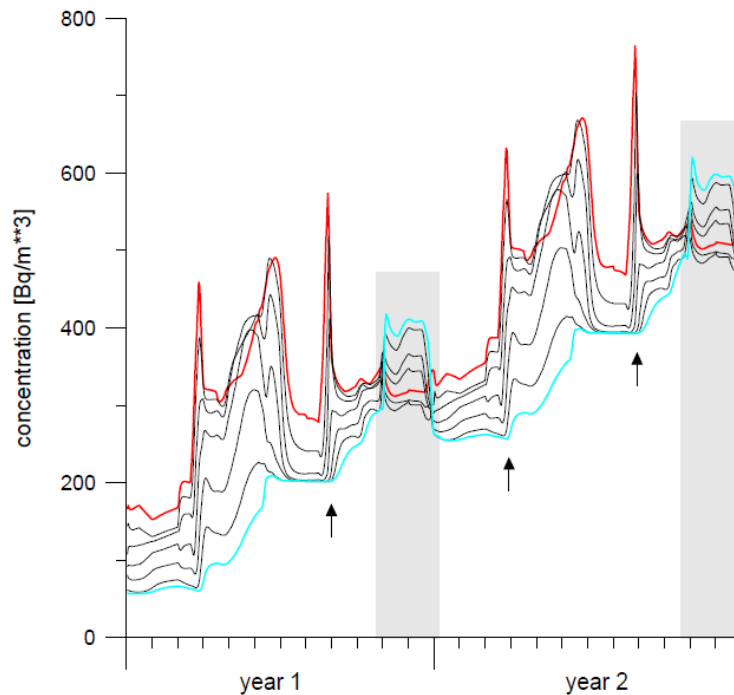


Figure A8. Concentrations of Cs^{137} in different depth horizons at the entrance of Abrasimov Bay following a continuous release of 1 TBq / year. The blue line denotes surface concentrations, the red line are concentration in 30 m depth. The black lines in between are 5 m intervals. Shaded areas denote strong surface outflow situations.

A2 Far Field Assessment: a perspective view

A2.1 Far field dispersion from radioactive sources in the Kara Sea

In large scale dispersion studies by Nies et al., (1997, 1998) and (Karcher et al., 1998) an activity of 1 TBq/year of ^{137}Cs was used to simulate release from the nuclear dumpsites along the eastern coast of Novaya Zemlya in the Kara Sea. The release was driven with oceanic circulation fields which were a result of climatological forcing (i.e. no inter-annual variability was assumed). The scenario experiments concluded that the contaminated surface plume leaves the Kara Sea towards the north-east and is advected by water masses of Atlantic origin and also towards the east with a coastal current into the Laptev Sea Figure A9. In the mixed layer, the contaminants were advected pole-wards until they were picked up by the transpolar drift stream. The radioactivity reached Fram Strait after 7 to 8 years and after 12 years the Denmark Strait was reached. Concentration levels decreased from 1 to 0.1 Bq/m³ in the Kara Sea down to 10⁻² Bq/m³ in the East Greenland Current along the eastern Greenland coast. On the northern Kara Sea Shelf significant fractions of the contamination were mixed down to the bottom water layers, where it finally fed into the halocline of the central Arctic Ocean (100 – 200m depth). These contaminated water masses travelled below the Polar Mixed Layer in the upper ocean and reached the Fram Strait after approximately 18 years. The densest water formed on the shelf is also contaminated and after entering the central basins at the depth of the so-called 'Atlantic Water Layer' at 200-800m it crossed the Lomonosov Ridge to enter the Canadian basin. It reached the Canadian Archipelago after 30 years, however, at very low contamination levels of 10⁻² to 10⁻³ Bq/m³. A very low probability 'worst case' scenario, simulating an instantaneous release of 1 PBq in the Kara Sea led to no significant contamination of the Arctic Ocean: on the wider scale, computed values of 50 Bq/m³ were in the range of existing background levels for the mid 1990s. These background levels were mostly due to long range transport of discharges from the nuclear reprocessing facility Sellafield, which became evident when comparing the 'worst case scenario' results with a 'Sellafield hindcast scenario'. The pathways and dilution factors found in the aforementioned study are comparable to those from a similar study of Preller and Cheng (1999).

**Source: Kara Sea
dump site**

depth: surface

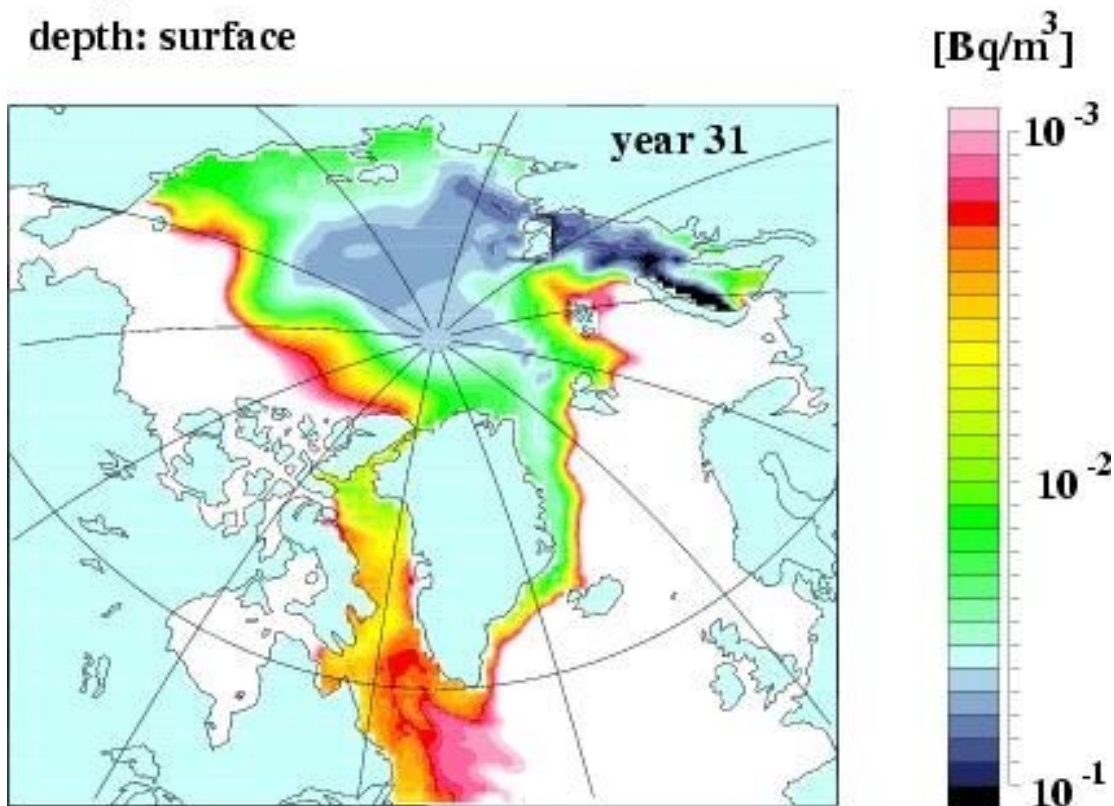


Figure A9. Simulated concentrations of ^{137}Cs , following a continuous 1 TBq/y release at Kara Sea dump sites. The picture shows concentrations at the surface, 31 years after release. Nies et al. (1999).

A2.2 Release scenarios for the sunken submarine 'Kursk'

The nuclear submarine 'Kursk' sank on August 12th 2000 in the Barents Sea, some 100 km north-east of Murmansk. It has since been recovered and transported to Murmansk. Nevertheless, reviewing a model study on potential dispersion from its original location which had been performed for different atmospheric and oceanic circulation conditions remains illustrative for the K-27 case.

The release study for the Kursk submarine (Gerdes et al., 2001) was performed with the coupled ice-ocean model NAOSIM, in a set-up similar to the one used in the present study (see chapter 3). Driven by daily mean atmospheric forcing from the period 1979-1993, Gerdes et al. (2001) simulated a potential instantaneous release of 1 PBq of ^{137}Cs from the inventory of the sunken vessel. To evaluate the potential effects of different circulation patterns in the Barents and Kara Sea on the pathways and concentration levels, two three year periods with different intensity of ventilation on the Barents Sea Shelf were picked as dispersion scenarios. The choice of two forcing periods of three years duration each was based on an Empirical Orthogonal Function (EOF) analysis of a frequency distribution in EOF space for the (barotropic) stream function of the vertically integrated transport in the Barents Sea. Thus the respective periods were chosen depending on the oceanic reaction to the forcing, namely the predominant flow regimes in the Barents Sea. With 83% and 11% of the variance described, the first two EOFs captured the bulk of the variability. The first EOF described a change in strength of the flow through the Barents Sea, the second EOF described a longitudinal shift of the stream axis. Based on this analysis two three years periods were selected that span maximally distinct areas in the space of the EOF coefficients, i.e. maximally different flow regimes. The periods selected are 1983–1986 and 1988–1991. During 1983–1986 a weak throughflow through the Barents Sea was dominant, while a strong throughflow was predominant during 1988–1991.

The general direction of the dispersion in both regimes was towards the north-east (Figure A10 a and b). A longer flushing time of the Kara Sea and south-eastern Barents Sea in the 'weak' regime (Figure A10 a) results in higher concentrations, compared to the 'strong' regime (Figure A10 b). The 'strong' regime leads to concentrations up to 1 Bq/m^3 in the interior Arctic Ocean beyond the Lomonossov Ridge. The western Eurasian Basin and the vicinity of the North Pole are almost unaffected, however. In contrast, the 'weak' regime leads to a more direct path towards the Fram Strait, which has reached most of the western Eurasian Basin after 3 years. A filament of elevated contaminant concentration reaches westward north of Greenland while another filament extends south with the East Greenland Current.

At the sea surface, 5 years after release during the "weak" regime (not shown, see Harms and Karcher, 2003) maximum concentrations in the Kara Sea are still slightly above 10 Bq/m^3 . When reaching the northern Fram Strait, the signal divides into a major branch moving southward with the East Greenland Current and a minor branch which follows the northern Greenland and Canadian coastlines westward. North of Alaska, this branch feeds into the anticyclonic Beaufort Gyre of the Canadian Basin. Concentrations in the northern East Greenland Current are up to 1 Bq/m^3 , in the western Arctic branch 10^{-1} - 10^{-2} Bq/m^3 .

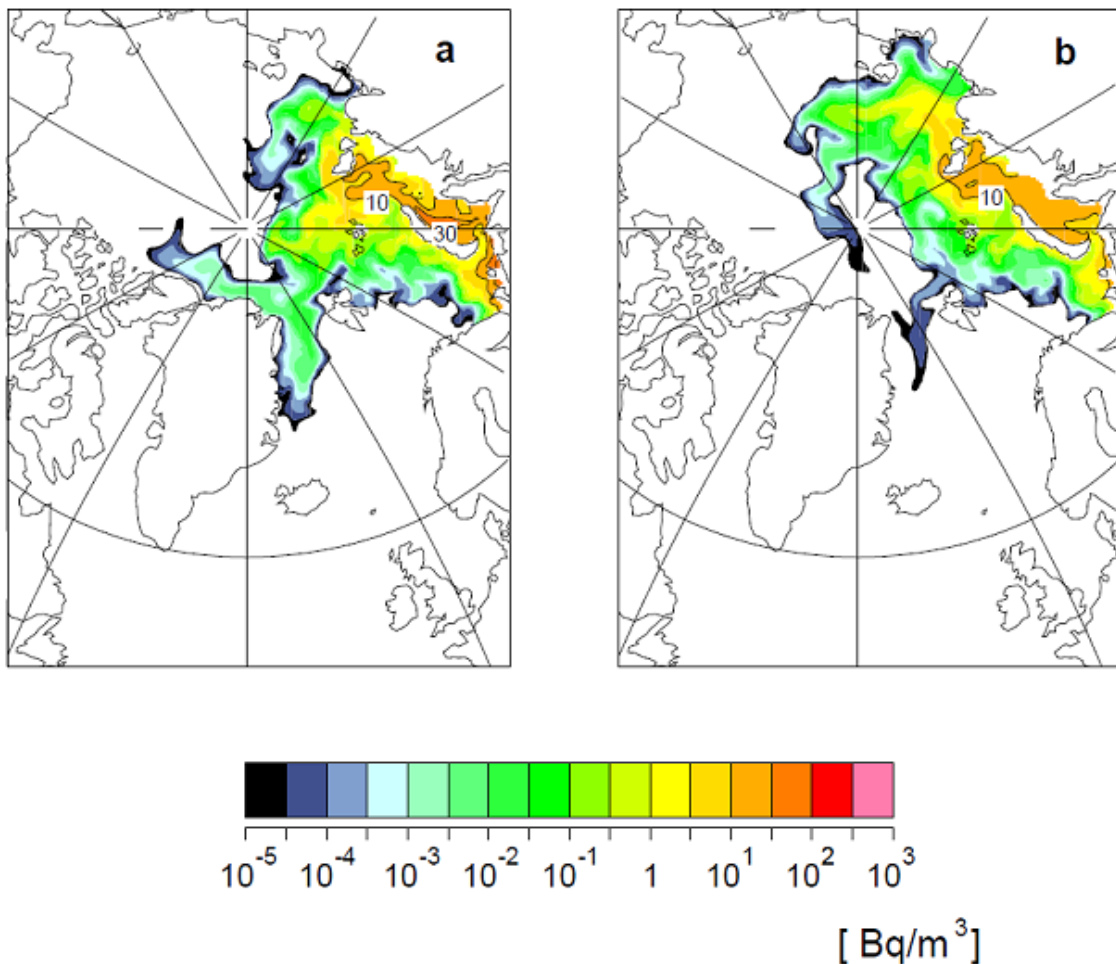


Figure A10. Concentration of ^{137}Cs at 10 m depth after a release of 1 PB of ^{137}Cs in the Barents Sea off Murmansk 3 years after the release. Two different ocean circulation states, depending on the atmospheric forcing are shown: Panel a) gives the results for a 'weak regime' period (1983–1986), panel b) for a 'strong regime' period (1988–1991) (Gerdes et al., 2001).

A2.3 Transport of radioactivity by Arctic sea ice

Sea ice plays a special role in the transport of radionuclides in the Arctic. In general, radionuclide concentrations in sea ice itself are very low. Like salt, most of the dissolved radionuclides are excluded from the ice due to brine rejection, a filtration process that occurs when ice is forming. This means sea ice is usually very 'clean' or at least less contaminated than the water from which it is formed (Pfirman et al., 1995).

However, several radionuclides are particle reactive which means they tend to attach to particles or suspended matter in the water column or to the sediment. Arctic sea ice very often carries loads of sediment and, if this is contaminated, the ice drift may play an important role in the long-range redistribution of radioactivity (Pfirman et al., 1995; Pfirman et al., 1997a and 1997b).

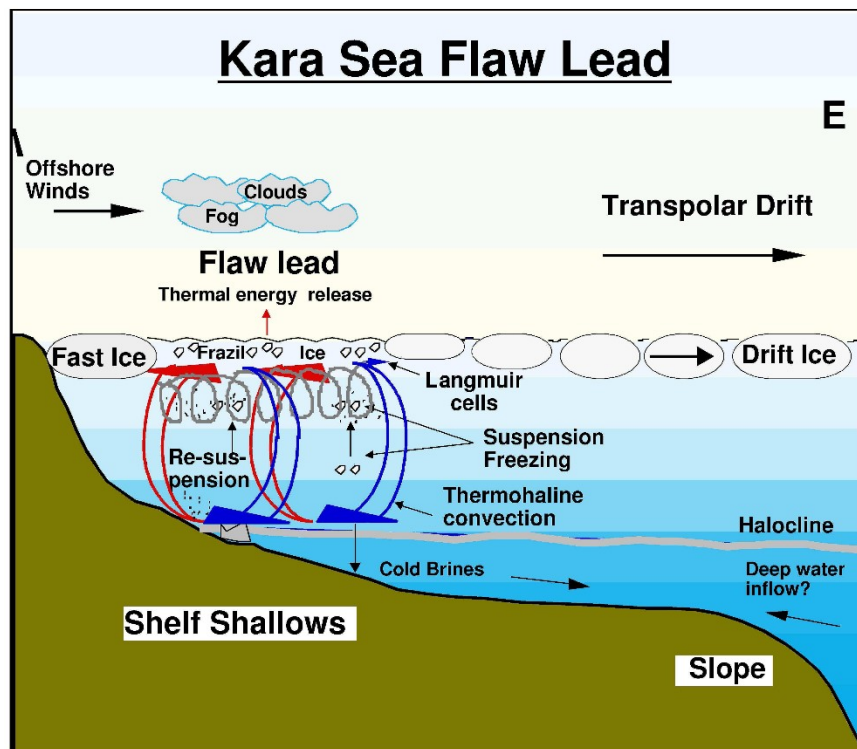


Figure A11. Mechanisms for the incorporation of sediment into sea ice:

- suspension freezing, i.e. the scavenging of sediment from the water column during ice formation,
- flooding of fast ice by sediment laden river water,
- the formation of anchor ice,
- the ad freezing of bottom sediments to grounded or shore-fast ice,
- Eolian transport by off-shore winds from Siberia ('Arctic Haze') (from Dethleff, 1995)

The east coast of Novaya Zemlya is characterised by recurrent open water between fast and drifting ice, which are driven by offshore winds (Figure A11). In an overview which evaluated possible processes of entraining sediments into sea ice, Nürnberg et al. (1994) stated that suspension freezing is the most important process. Suspension freezing is thought to happen in so called 'flaw leads' (Dethleff, 1995). These 'flaw leads' produce large amounts of new ice through the mechanism of leeward advection (Martin and Cavalieri, 1989; Dethleff et al., 1998). Strong heat loss and enhanced ice formation provide a turbulent, convectively mixed, water column which enhances resuspension of fine grained material. Under these conditions, the sea water becomes supercooled by a fraction of a degree and frazil ice forms. The underwater ice crystals interact and mechanically interlock with sedimentary particles in the water and lift fine-grained particulate matter to the surface. The accumulation at the ice surface is due to the fact that the ice melts at the top and freezes at the bottom. In multiyear cycles, the sediment 'migrates' to the ice surface.

Model results from a regional scale model application are used to detect at which time and in which areas the incorporation of particles into newly forming sea ice is most likely. The particles are released under ice-free conditions in August and drift in the following months along the Novaya Zemlya coast and towards the central Kara Sea (Figure A12). The simulated particle patterns suggest that sediment incorporation is very likely from October to December in the Kara Sea and generally during winter in recurrent flow leads along the coast.

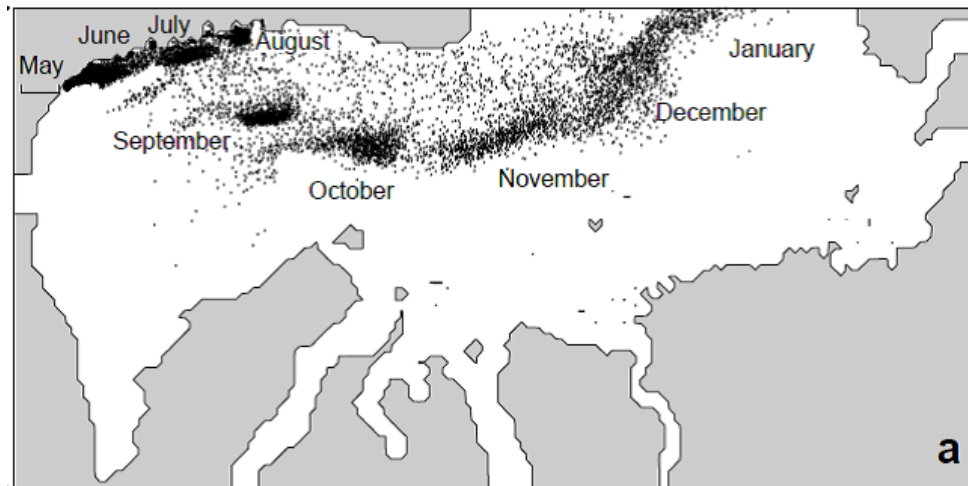


Figure A12. Simulated particle dispersion in the Kara Sea. Particles are released in May in Novaya Zemlya fjords and traced for the following months. Dethleff et al. (1998).

Sediment laden sea-ice may leave the Kara Sea to be part of the transpolar drift. The ice movement in the Arctic Ocean is dominated by the Transpolar Drift (TPD) and the Beaufort Gyre. The TPD crosses the Arctic Ocean in two branches: the Siberian branch which is closer to the Siberian coast, and the polar branch on the side facing the North American continent. In particular the Siberian branch is fed by large ice production areas located in the East Siberian, Kara and Laptev Seas. The TPD is responsible for the transport of sediment-laden sea ice from Arctic Shelf areas through the Fram Strait towards the Greenland Sea (e.g. Dethleff et al., 1994; Eicken et al., 1997). Through ice melting, the material is released to the marine environment of the Nordic Seas, Europe's most important fishing ground. Since the North Atlantic ice-melt period coincides with the locally increasing biological activity during spring bloom, the pollutants may easily enter the food web (AMAP, 1998).

Large scale drift studies of possibly contaminated sediments, incorporated in Siberian flaw lead ice, were presented by Nies et al. (1998), Dethleff et al. (2000) and Harms et al. (2000). Ice drift, thickness and concentration from a 3-D coupled ice-ocean model of the Arctic Ocean and Nordic Seas were used to simulate ice trajectories for several subsequent years from ice formation to ice melt. These studies suggested that trajectories from the northern and central Kara Sea are able to reach the Arctic TPD within one winter cycle. However, trajectories started in the southern Kara Sea usually melt in the following spring before they can leave the formation area. A direct link between Novaya Zemlya / Kara Sea and the Fram Strait via the TPD is unlikely, at least for the southernmost coasts. Trajectories started in the central and eastern Kara Sea, however, showed a strong tendency to leave north-westward into the Barents Sea or the Arctic Ocean. Some of the eastern trajectories, close to the Ob and Yenisei estuaries, leave the Kara Sea between Franz-Josef-Land and Novaya Zemlya before they ended up in the Barents Sea. The most eastern trajectories pass north of Franz-Josef-Land and join the TPD. For these trajectories, the transit time from the Kara Sea towards Fram Strait can be very fast, between 1 and 3 years. Figure A13 shows examples for this ice-drift from the northern Kara Sea for a three years period for different start years, as calculated with a coupled ice ocean model (e.g. Karcher et al., 2003b). The different trajectories for the different timeperiods reflect the atmospheric circulation and thus sea ice drift regimes at different times and highlight the possibility of fast (O (1 year)) transport of potentially contaminated sea ice from the Kara Sea into the Barents Seas.

The model findings are supported by sea ice backward trajectories calculated by Pfirman et al. (1997b) and drift buoy data from King et al. (1997), as well as ice drift estimates by Pavlov et al. (2004). The latter estimated that contaminated sea ice from the Kara and the Laptev Sea could reach the Fram Strait in about 2-4 years. They also showed that depending on the local circulation situation it can easily end in the Barents Sea after 1 year. Other model estimates (c.f. Nies et al., 1998; Dethleff, 2000) reveal that at maximum 10 % of the ice formed in the southern parts leave the Kara Sea towards the central Arctic Ocean before summer melt. The ice formed in the northern parts left the Kara Sea with a probability of almost 100%. Colony and Thorndike (1985) estimated a 79% probability for ice formed in the Kara Sea to drift into the Arctic Ocean. These observations showed that simulated ice trajectories are quite reliable and that the time and space variability of ice formation and ice melt are well reproduced. Model simulations thus provide very useful information on pathways and transit times of sediments in sea ice.

However, realistic export rates of radioactively contaminated sea ice are difficult to deduce because of the significant lack of sedimentological data and uncertain parametrisations. In a simple conservative approach, Harms (1997) estimated the possible radionuclide export by sea ice from the Kara Sea to the Arctic Ocean to be of the order of 0.03 TBq/y. This calculation assumes an ice volume flux from the Kara Sea into the Arctic Ocean of 150 km³/y (Pavlov and Pfirman, 1995), a sediment load in sea ice of 3 mg/l (IAEA, 1994) and a radionuclide concentration in sea ice sediment of 70 Bq/kg (Meese et al., 1997). The estimated export rate is at least one order of magnitude lower than the corresponding export rate through the water column but probably still overestimated. A wide range of possible export rates was also presented in a more detailed study by Dethleff et al. (2000).

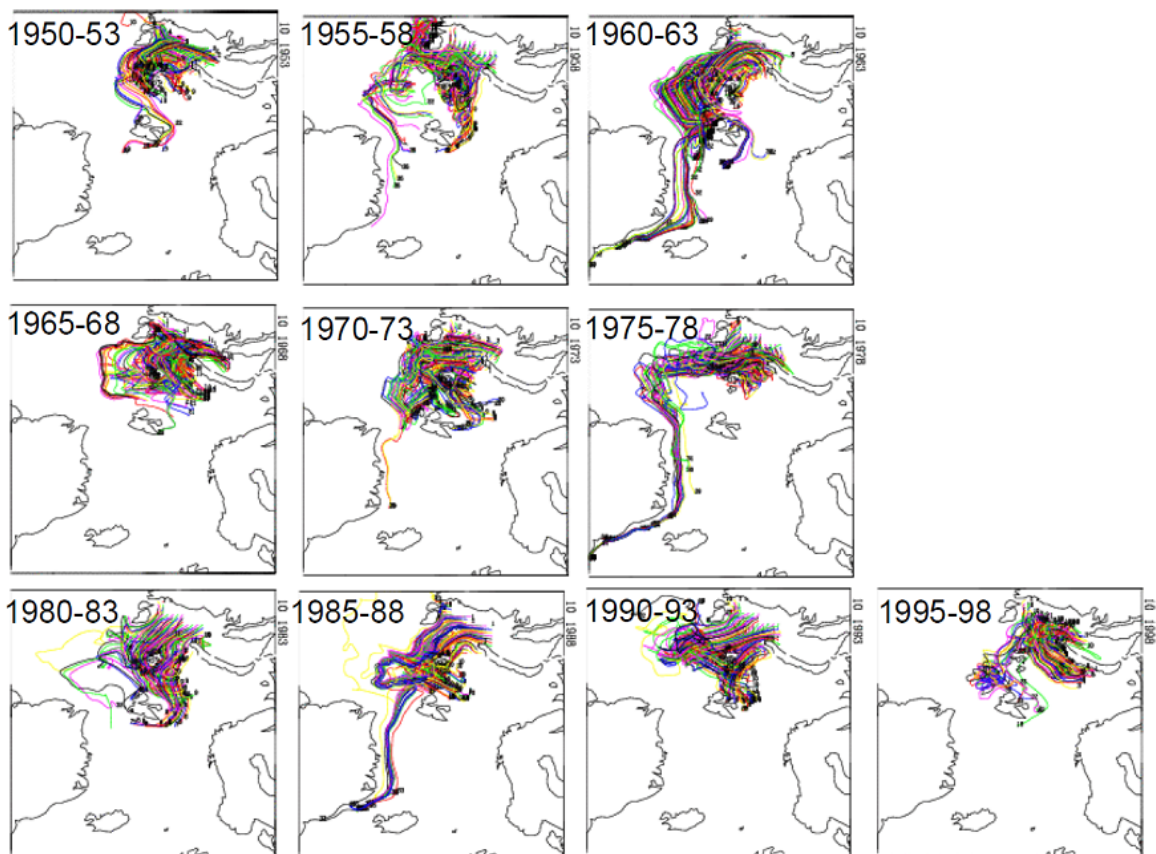


Figure A13. Ice-drift trajectories starting in the northern Kara Sea during freeze-up in October. Duration of drift is 3 years or until melt.

Appendix B: Marine dispersion modelling

B1 Hydrodynamics

The hydrodynamic circulation model applied to the fjords is based on the well documented **Hamburg Shelf Ocean Model (HamSOM)** which is a three-dimensional, baroclinic, circulation model, developed at the Institute of Oceanography, University Hamburg for investigations of shelf sea processes (Backhaus, 1985). The model is based on non-linear primitive equations of motion, invoking the Boussinesq-approximation. Furthermore, the hydrostatic approximation and the equation of continuity are applied which serves to predict the elevation of the free surface from the divergence of the depth mean transport. The numerical scheme of the circulation model is semi-implicit which allows for economic time steps. The equations are discretised as finite differences on an Arakawa C-grid. A detailed description of the circulation model can be found in Stronach et al. (1993).

B2 Transport modelling

The dispersion of radioactivity in the water is determined by using three-dimensional transport equations in an Eulerian system. Radionuclides are treated as passive tracers which drift in a soluble form in the water column. A half-life decay for radioactivity was omitted since the simulated time of forecast is in general much smaller than the half-life time for considered radioactivity.

Horizontal advection is calculated with a numerical upstream algorithm based on the previously simulated flow field. Horizontal diffusion was omitted due to a high amount of numerical (artificial) diffusion caused by this method. In spite of this disadvantage, the upstream scheme proves to be a rather robust algorithm that avoids over-shootings even if strong releases into 'clean' environments are performed. It therefore presents a reasonable tool for preliminary order-of-magnitude estimations. According to Roache (1972), the artificial horizontal diffusion is related to the advection velocity, the average grid size and the time step. For small and moderate velocities (< 0.5 m/s) typical for the simulated fjord circulation, the artificial diffusion remains below $10^3 \text{ m}^2/\text{s}$.

The simulation of vertical diffusion is included to account for considerable differences between summer and winter stratification. The vertical eddy diffusivity coefficients (E_d) are calculated in the same way as the eddy viscosity coefficients (E_v) which in the present study depend on the shear production of the velocity field and the stability, expressed by the Brunt-Väisälä frequency (i.e. the Richardson number).

At open boundaries, a zero gradient condition is applied, which allows for an export of radionuclide concentrations out of the model domain.

The removal of radioactivity from water to suspended particles is estimated by applying a partition coefficient P to the total simulated radionuclide concentration. For stationary solutions it can be assumed that the concentration of radioactivity in the surface sediment is equal to that of suspended particles in the water. This could imply that the suspended particles sink down onto the sediment.

The application of a partition coefficient P is based on the assumption that the distribution of radionuclide activity on suspended particles and in the water is in an equilibrium state. To comply with this requirement, 3.6 and 3.7 are applied only to stationary solutions, where $dR_i/dt = 0$ (eq. 3.2). Only for this case it is assumed that the concentration in sediment is equal to that on suspended particles. Even if this approach is rather simple, it is a good first guess of specific radionuclide concentrations in sediment, in particular if essential geochemical and sedimentological data for a more sophisticated sedimentological model are not available. During an intensive benchmarking exercise that was undertaken within the IASAP 'modelling task group' (Scott et. al, 1997), the present model approach reveals a remarkable good agreement for calculated concentrations in Kara Sea sediment with corresponding results from other model approaches.

Particle reactive and non-reactive radionuclides are classified according to a radionuclide specific distribution coefficient, $K_d = C_s / C_w$, which is defined as the ratio of the concentration of radionuclides in sediment C_s and in sea water C_w in an equilibrium state (Duursma & Carroll, 1996). K_d values are usually

determined in laboratory experiments using sediments, collected from the sea bed. Recommendations for K_d values can be found e.g. in IAEA (1998).

The conservative model approach is only applicable to the dispersion of dissolved radionuclides with low distribution coefficients ($K_d < 10$ [m³/kg], e.g. ¹³⁷Cs). As a first approximation it may be justified to treat these radionuclides as conservative.

There are several ways to include particle reaction and simulate the dispersion of non-conservative radionuclides. Our simulations use a simple approach from box modelling to determine the fraction of activity in water A_w and sediment A_s (Carroll and Harms, 1999) via the partition coefficient P :

$$P_w = A_w / A_t = 1 / (1 + K_d \cdot C_s)$$

$$P_s = A_s / A_t = K_d \cdot C_s / (1 + K_d \cdot C_s)$$

A_t is the total activity consisting of $A_w + A_s$. P_w gives the fraction of activity in water that remains dissolved whereas the reciprocal or P_s gives the fraction that sorbs onto particles. The activity with particles in suspension, A_s is thus given by $A_s = A_t P_s$ and the reduced activity in water is $A_w = A_t P_w$.

The partition coefficient P ranges from zero to one and is a function of the distribution coefficient K_d in m³/kg and the suspended load C_s in kg/m³. For low K_d and suspended load values, P_w will not differ much from unity and P_s remains close to zero. In this case, the major fraction of activity remains in a dissolved phase. Conversely, high K_d and suspended load values will cause a considerable transfer of activity onto particles or the sediment.

The application of a K_d based partition coefficient P is based on the assumption that the distribution of radionuclide activity on suspended particles and in the water is in an equilibrium state. Box models may fulfil this requirement due to their large time steps (days or more). However, this is usually not the case with hydrodynamic models. Short time steps (minutes, hours) do not allow for an equilibrium assumption between the dissolved and the particulate phase. An exception from this may be in the case of stationary dispersion patterns where some sort of equilibrium can be assumed. We therefore applied the above mentioned approach only to stationary solutions. Even if this approach is rather simple, it may be a good first guess of radionuclide concentrations in dissolved or particulate phase, in particular if essential geo-chemical or sedimentological data for a more sophisticated approach are not available.

B3 Thermodynamics / Sea Ice

The circulation model is coupled to a thermodynamic and dynamic sea ice model in order to derive realistic forcing fields for temperature and salinity. The ice model consists of dynamic and thermodynamic components which calculate space and time dependent variations of ice thickness and ice compactness. The basic configuration follows Hibler's (1979) one layer sea ice model. Thermodynamic processes are based mainly on the ideas of Maykut and Untersteiner (1971), Semtner (1976) and Parkinson and Washington (1979). According to these modules the coupled ice-ocean model accounts for:

- Sea surface temperature variations which depend on the surface heat fluxes, calculated with standard bulk formulae (Maykut, 1986),
- thermodynamic ice growth, determined from heat flux balance equations for the top and bottom of the ice cover (Parkinson and Washington, 1979) and
- sea surface salt fluxes (brine or freshwater release) which are proportional to thermodynamic ice growth (Lemke et al., 1990).

The dynamic component of the model consists of a free ice drift algorithm (no rheology) that includes the advection of ice thickness and compactness due to wind and water stress. A detailed description of the ice model and the coupling to the circulation model can be found in Harms (1994).

Appendix C: Atmospheric dispersion modelling: SNAP model

C1 Parametrization of the source term

The source term can be specified individually for each SNAP application. The source geometry is time dependent in the SNAP model and can be specified differently for each time segment of the release. However, the number of model particles released at each model time step is the same for the entire period of the release. The source term can be also specified separately for each substance which is released into the atmosphere. Gases, noble gases and particles can be included for dispersion simulation in SNAP. The individual radionuclides are represented in the model by different model particles which can have different properties. The release rate is separate for each component included in the model run and can vary in time.

C2 Mixing Height

As good as possible determination of the mixing height, which represents in the model the depth of atmospheric boundary layer (ABL), is very important for modelling atmospheric transport and deposition of air pollution. The turbulent diffusion is significantly more intensive in the ABL and only pollution in the boundary layer is a subject of dry deposition. The procedure to identify and calculate the mixing height is based on critical Richardson Number.

C3 Advection, diffusion and gravitational settling

The advective displacement of each model particle is calculated at each model time step, which is equal to 5 minutes in the present SNAP version. For this calculation, three-dimensional velocity is interpolated to particle position from the eight nearest nodes in the model grid. Bilinear interpolation in space is applied to horizontal components of the velocity field and linear interpolation for the vertical component. In addition, linear interpolation in time is applied between sequential meteorological input fields. The vertical component of the velocity field used for calculation of advective displacement includes gravitational settling velocity which is very important for larger particles.

The gravitational settling velocity is calculated for each model particle at each time step based on actual meteorological data (air pressure and temperature) and particle characteristics (size and density). Cunningham correction factor for small particles is calculated, as well as, correction to account for high Reynolds number (Seinfeld, 1986). This approach requires a numerical solution of the set of two non-linear equations at each model time step (Bartnicki et al, 2004).

Random walk technique is used to simulate atmospheric diffusion in the SNAP model. The Wiener type of process used here is governed by a length scale, the sequence of steps following the description by Mayron (1991). A slightly different parametrization is used for particles located within boundary layer and for those above, but can be described by the same equations.

In the algorithm, model particle is displaced randomly. The random displacement amount is proportional to magnitude of diffusion and is calculated as a product of random number from sampled from the range (-0.5, +0.5) - generated from uniform distribution, and the length scales from the horizontal and vertical turbulent motion. The horizontal length scale increases with the wind speed, but the vertical scale is kept constant and is lower above the ABL than below.

C4 Boundary conditions

When displaced, particles can reach the boundaries of the model domain. Since SNAP is a model of the Lagrangian type, formulation of boundary conditions is relatively simple. For particles with larger diameter like 10 μm and above, the mechanism of gravitational settling can be effective in moving them

quickly to the ground. If the position of model particle in the next time step is lower than the ground level, the entire particle is removed from the further computations and its entire mass is added to dry deposition matrix.

In the random walk process, the model particles cannot penetrate the surface - the bottom boundary of the model domain. If the particle hits the ground in the random walk procedure, it is reflected back into the boundary layer.

A similar procedure is applied to the model particles reaching the upper boundary of the model domain. At the top of the model domain, there is no exchange of particles. This assumption implies the closed upper boundary conditions.

Particles can flow out of the lateral boundaries of the model domain, but none can enter the model domain from the outside. This implies open lateral boundary conditions.

C5 Dry deposition

Many particles of different size are released into the atmosphere during a nuclear accident. For the relatively large particles, the dry deposition process is dominated by the gravitational settling. However, for the relatively small particles with the diameter below 3 μm , other processes are dominating the removal of particles from the air. Therefore, not only gravitational settling, but also other surface related processes are included in the parametrization of dry deposition.

A key parameter in the dry deposition process is the dry deposition velocity, which can be calculated based on the resistance analogy (Seinfeld, 1986). The dry deposition velocity is different for gases and particles, but for both it is a function of actual meteorological conditions. The gravitational settling velocity is dominating dry deposition process for large particles. For very large particles, emitted into the atmosphere during a nuclear accident, the dry deposition velocity is practically the same as gravitational settling velocity.

In our calculations, we assumed that the model particles located above the surface layer are not affected by the dry deposition process. The height of the surface layer is defined as 10% of the mixing height. Reduction of the particle activity, due to dry deposition in one time step, for each model particle located within the surface layer can be calculated as a function of dry deposition velocity and surface level height.

C6 Wet deposition

Wet deposition is the most effective process in removing soluble gases and particles of different size from the atmosphere. This process includes absorption of particles into the droplets in the clouds (rain-out) and then droplet removal by precipitation (washout). Wet deposition process depends on many complicated factors, which are difficult to take into account, like for example occult deposition related to fog, scavenging by snow, effect of convective precipitation and orographic effects.

In the present version of the model, we have assumed that the mass of particle, affected by precipitation is reduced during one model time step depends on the coefficient of wet deposition. Following Baklanov and Sørensen (2001), the coefficient of wet deposition is a function of the particle radius and the precipitation intensity. In below cloud scavenging, the coefficient of wet deposition is calculated differently for three classes of particles. In this parameterization, the wet deposition coefficient for small particles ($r \leq 1.4\mu\text{m}$) and for large particles ($10.0\mu\text{m} < r$) does not depend on the particle size, but on precipitation intensity only. For particles in the range ($1.4\mu\text{m} < r \leq 10.0\mu\text{m}$), the wet deposition coefficient is a function of both particle size and precipitation intensity.

Wet deposition process between cloud base and cloud top (rain-out) depends on the type of precipitation - dynamic or convective. The wet deposition coefficient for dynamic precipitation is close to wet deposition coefficient below the cloud. The wet deposition is more effective for convective than dynamic precipitation. Therefore, wet deposition coefficient for convective precipitation between cloud base and top is estimated according to Maryon et al. (1996).

In many cases and in convective situation especially, precipitation does not occur in the entire model grid square. The area of the model grid square covered by precipitation as a function of precipitation intensity was originally estimated in Haga, (1991). In the SNAP model we use a probability curve based on this estimation. From the probability curve we can find the probability of the model particle to be affected by precipitation in a given model grid as a function of precipitation intensity.

C7 Radioactive decay

All isotopes included in the SNAP model are subject to radioactive decay. The half-life time for arbitrary radionuclide can be specified in input file for the model run. The radioactive decay is also affecting a part of each isotope already deposited to the ground, so the same approach is applied to matrices of wet and dry deposition for each isotope at each model time step.

Appendix D: Modelling transfer of radionuclides through food-chains

D1 Marine food-chain model description

A model, based on the work of Thomann (1981), Landrum et al. (1992), and Fisher (2002), was used to simulate the uptake of radionuclides via food and water by aquatic organisms and transfer through marine food-chains. Excretion/ elimination rates were assumed to be independent of the uptake route, the assimilation efficiency was assumed to be independent of food type, and predators were assumed not to assimilate the activity concentration in the gut content of their prey. Further assumptions were that the zooplankton were a homogeneous group, described by specified parameter values rather than by ranges, and that the growth rate for all organisms was 0. This last assumption may be a less robust than the others (Thomann, 1981), but the complexity of the weight dynamics for the organisms in question would require further, more detailed study and were anticipated as adding little in terms of yielding more accurate prognoses. The time-dependent transfer of radionuclides to fish within the food chain can be described by simple, first-order differential equations. This approach was adopted as opposed to using only equilibrium based concentration ratios because kinetic models are much better suited to simulating transfer through food-chains when seawater concentrations are changing rapidly as in the case of accidental releases (i.e. steady state/equilibrium conditions are not prevalent). An earlier version of the model is described in Brown et al. (2004b) with a condensed explanation provided below:

For Zooplankton (prey species), steady state conditions between radionuclide activity concentrations in biota and water are assumed, allowing the application of concentration ratios²:

$$C_p = CR_p \cdot C_w \quad [1]$$

Where:

C_p is the radionuclide activity concentration in prey species (Bq kg⁻¹ f.w.);

CR_p is the concentration ratio for prey species (l kg⁻¹); and

C_w is the radionuclide activity concentration in sea water (Bq l⁻¹).

For Fish, accounting for radionuclide uptake via water and food, the following equation is applied:

$$\frac{dC_f}{dt} = AE_f \cdot IR_f \cdot C_p + k_{uf} \cdot C_w - C_f \cdot k_{ef} \quad [2]$$

Where:

AE_f is the assimilation efficiency (dimensionless) for fish;

IR_f is the ingestion rate per unit mass of fish (kg f.w. d⁻¹ per kg f.w.);

k_{uf} is the uptake rate of radionuclide to fish directly from water column (d⁻¹);

C_f is the activity concentration in fish (Bq kg⁻¹ f.w.);

k_{ef} is the depuration rate from fish (d⁻¹).

CR values (arithmetic means) for zooplankton were taken from IAEA (2014), Fish depuration rates (based on biological half-lives) from ICRP (2009), all other parameters were taken from Thomann (1981).

One way to consider radionuclide transfer to seals, based on the work of Brown et al. (2004b), is through Equation 3.

² Concentration ratios = Activity concentration within an organism relative to that in (normally filtered) water.

$$\frac{dC_s}{dt} = \sum_1^n (x_i \cdot AE_s \cdot IR_s \cdot C_i) - C_s \cdot k_{es} \quad [3]$$

Where:

x_i is the fraction of the diet associated with dietary component “i”

$AE_{r,i}$ is the assimilation efficiency (dimensionless) for dietary component “i”

IR is the ingestion rate per unit mass of seal (kg f.w. d⁻¹ per kg f.w.)

C_i is the activity concentration in the dietary component “i” (Bq kg⁻¹ f.w.)

C_s is the “whole body” activity concentration in the seal (Bq kg⁻¹ f.w.)

k_{es} is the effective loss rate from seal (d⁻¹) – incorporating both excretion rate and physical decay of the radionuclide

A similar approach can be adopted to model the time varying activity concentrations in seabirds, C_b , with a requirement to then provide specific values for the parameters IR_b (the ingestion rate per unit mass for seabirds), AE_b (the assimilation efficiency of radiocaesium for seabirds) and k_{eb} (the effective loss rate of radiocaesium for seabirds).

An ingestion rate, IR_s , of 0.072 kg f.w. day⁻¹ per kg f.w. seal was derived by Gwynn et al. (2006) using allometric relationships (Nagy, 2001) for carnivora (Equation 4)

$$FMI = 0.348M^{0.859} \quad [4]$$

where FMI is the fresh matter intake (g/day) and M is the mass of the seal (g).

In a similar way, Nagy (2001) provides the allometric relationship for marine birds (Equation 5):

$$FMI = 3.221M^{0.658} \quad [5]$$

where FMI is the fresh matter intake (g/day) and M is the mass of the bird (g).

A representative mass of 1.26 kg commensurate with the value used for marine birds in the ERICA Tool (Brown et al., 2008) was used as a default for calculations. This yields an IR_b of 0.28 kg f.w. day⁻¹ per kg f.w. seabird.

For seals and sea birds, the assimilation efficiencies for ¹³⁷Cs were set to unity commensurate with generic values that are normally applied for mammals (Brown et al., 2003b). For the sake of simplicity it was also assumed that the seals and seabirds live entirely off fish. The term $x_i = 1$ in equation 3 and C_i is equal to the (time varying) activity concentration in fish derived using the approach outlined earlier. Harp seals, for example, have a varied diet of fish including species such as capelin, polar and Arctic cod and herring. Although they also are known to consume crustaceans, the simplification of the diet was not considered to be unduly problematic. Since a generic group was also being considered in the case of seabirds, similar contentions are valid – assuming the entire diet is based on fish would appear to be a reasonable assumption.

A whole-body biological half-life of 29 days was derived by Gwynn et al. (2006) for ¹³⁷Cs in an adult ringed seal. This compares to values for grey and harbour seals of 20 days from the Baltic Sea (Holm et al., 2005) and 28 days from the UK and Ireland (Watson et al., 1999). A value of 29 days was adopted in this work as a conservative approximation, i.e. the longer the retention time of a given radionuclide for a specified intake the greater will be the concomitant internal exposure. Deriving biological half-lives for sea birds is a more uncertain process in which recourse was made to the allometric relationships for biological loss provided by Whicker and Shultz (1982) for caesium. The following formula can be applied.

$$k_a = \frac{\ln 2}{18.36 M^{0.24}} \quad [6]$$

where k_a = the effective loss rate for the animal (d^{-1}), M = mass of animal (kg, f.w.).

This gave a k_b of $0.036 d^{-1}$ corresponding to a biological half-life of radiocaesium in birds of ca. 19 days. This value appears to be a little on the high side (in view of information concerning other organism groups) but was likely to provide a conservative estimate of transfer in keeping with accepted approaches to err on the side of caution when model parameters are considered to be uncertain.

An overview of all of the parameters used in the (bio-) kinetic models is presented in Table D1.

Table D1: Parameters used in the kinetic model for ^{137}Cs in the marine environment

Parameter	Value (units)	Reference/comment
CR_p	130	IAEA (2014); Arithmetic mean value for zooplankton
AE_f	0.5 (dimensionless)	Brown et al. (2004b)
k_{uf}	0.01 (d^{-1})	Brown et al. (2004b)
AE_s	1 (dimensionless)	Gwynn et al. (2006)
AE_b	1 (dimensionless)	Assumed to be equal to seal
IR_f	0.009 (kg f.w. d^{-1} per kg f.w.)	Brown et al. (2004b)/Large fish
IR_s	0.072 (kg f.w. d^{-1} per kg f.w.)	Gwynn et al. (2006)
IR_b	0.28 (kg f.w. d^{-1} per kg f.w.)	Derived allometrically – see main text
k_{ef}	0.0107 (d^{-1})	ICRP (2009)
k_{es}	0.0239 (d^{-1})	Gwynn et al. (2006)
k_{eb}	0.036 (d^{-1})	Derived allometrically – see main text

D2 Terrestrial food-chain Model description

A terrestrial food-chain model was used to provide input for both the derivation of ingestion doses for humans and for the assessment of doses to wild plants and animals.

In view of available data, it was most appropriate to split the modeling into flora (Wild grass/grasses, herbs and shrub) and fauna (Deer/herbivorous mammal and rat/burrowing mammal) partly based on the classifications given in UNSCEAR (2008).

Using a variant of the methodology given in UNSCEAR (2008, 2014), the activity concentration in flora can be derived from the total deposition using an expression accounting for interception by foliage, direct deposition onto soil, weathering losses of radionuclides from vegetation and uptake from soil to plant.

In case of an acute deposition the radionuclide content on vegetation at time 't', accumulated via direct deposition from the air, can be calculated (as outlined in Brown et al., 2003b) as:

$$C_{flora,r}^{air} = \frac{f_{flora} \cdot D_{tot,r}}{b_{flora}} \cdot [e^{-(\lambda_{flora,r} + \lambda_r)t}] \quad [7]$$

where

$C_{flora,r}$ is the radionuclide activity concentration in flora from air deposition (Bq kg^{-1} f.w.)

f_{flora} is the interception fraction for a given flora (dimensionless)

$D_{tot,r}$ is the total deposition of radionuclide 'r' ($Bq\ m^{-2}$)

$\lambda_{flw,r}$ is the weathering constant for a given flora for radionuclide r (d^{-1})

λ_r is the decay constant for radionuclide r (d^{-1})

b is standing biomass of the flora ($kg\ m^{-2}$)

t is time (d)

For the same acute deposition, at time 't', there is also a component of contamination that arises from soil to plant transfer. In this case an assumption is made that for this fraction of the contamination in the plant attributable to root uptake, equilibrium exists between the activity concentration in the plant and the soil.

$$C_{flora,r}^{soil} = \left[\frac{D_{tot,r} \cdot \left[(1 - f_{flora}) + f_{flora} \cdot (1 - e^{-\lambda_{flw,r}t}) \right] \cdot e^{-\lambda_r t}}{\rho_{soil} \cdot d_{soil}} \right] \cdot CR_{flora,r} \quad [8]$$

where

ρ_{soil} is the dry soil density ($kg\ m^{-3}$ d.m.) d_{soil} is the depth of soil within which radionuclide r has become mixed (m) $CR_{flora,r}$ is the soil to plant concentration ratio for radionuclide r (dimensionless)

All other parameters have been described above in equation (7). Application of this model also allows for time varying deposition rates to be considered. For this more complex situation, the problem can be solved numerically.

There is an assumption in this model that a representative interception fraction 'f' for a given flora type can be applied for the entire simulation period. Data compilations for agricultural systems in relation to this parameter (IAEA, 2010) indicate that the interception fraction depends on whether dry or wet deposition is occurring, the stage of development of the plant and plant type in question, the capacity of the canopy to retain water, elemental properties of the radionuclide, and other factors such as amount and intensity of rainfall in the case of wet deposition and particle sizes of the deposited material. The approach taken here was, therefore, arguably simplistic but in view of the numerous uncertainties involved should at least provide an indication of contamination levels in food-chains following deposition of contamination and at least constitutes an attempt to model the dynamics of interception and loss from flora in contrast to approaches considering soil to plant transfer only. In addition to the interception fraction, biomass, which clearly relates to the stage of development of the plant, also requires further consideration as an important model parameter.

Tømmervik et al. (2009) reported a biomass of 4.13 tonnes/hectare for a 'Field layer' (forbs and grasses) in Northern Finland. This understory biomass would appear to be fairly typical for many other categories of shrub, field, bottom (moss and lichen) layers in mountain birch forests and mountain heaths in this region: Tømmervik et al. (2009) report 1.5 to 5.35 tonnes/hectare for such categories from northern Fennoscandia, including Finnmark). A biomass of 4 tonnes/hectare corresponds to $400\ g/m^2$. Although Schino et al. (2003) studied grasslands in mountainous areas of central Italy, the work provides an indication of variations in grass biomass that can arise from seasonality and the presence of different species. The recorded range of grass biomass in this aforementioned study was approximately 60 to almost $700\ g\ m^{-2}$ providing a useful context for our selection of an appropriate biomass value for 'Wild grass/grasses' and for shrubs.

The start and end of the growing seasons (based on data for the period 1982–2002) in the Arctic/Alpine and Northern boreal zones to which large areas of Finnmark belong, are June 4–20th and 21–24th September respectively (Karlsen et al., 2006) with a peak in growth occurring towards the end of July/beginning of August. The period selected for the hypothetical release from K-27 was August and September, coinciding with the period where any salvage activity is likely to take place from practical considerations. The deposition would thus occur in the middle of the growing season but following peak

growth removing the requirement to model the effect of growth dilution on radionuclide levels. Modelling of this phenomenon would be required were determinations needed for the period coinciding with rapid vegetation biomass increases early in the growing season.

The interception fraction, f , for Cs and grass varies from 0.84 (dry deposition) to 0.027 (wet deposition heavy rain) (IAEA, 2010). A default of 0.43 has been selected for this analysis simply based on the value falling midpoint between the maximum and minimum values reported above. This yields a mass interception fraction f_b of $1.1 \text{ (m}^2 \text{ kg}^{-1}\text{)}$ a value which was considered as being typical for Cs deposited on grass following the Chernobyl accident (IAEA, 2010). Owing to the lack of specific information on shrubs, the same default values as grass have been used. As noted by Tømmervik et al. (2009), the shrub layer has a biomass of a similar order of magnitude to the field layer in mid growing season. Although leaf area and surface roughness etc. might be expected to be different between grasses and shrubs the similarity purely in terms of above ground mass available to intercept contaminants render the assumption of similar mass interception fractions a reasonable one. The differences in interception between different elements reflect their different valencies. Plant surfaces are negatively charged and thus may be considered as analogous to a cation exchanger (IAEA, 2009). Therefore, the initial retention of anions such as iodide is less than for polyvalent cations, which seem to be very effectively retained on plant surface. For analyses of data for Chernobyl deposition in Germany, the mass interception factors increase in the order ^{106}Ru , ^{131}I , ^{137}Cs , ^{140}Ba , with these radionuclides having been deposited during the same rainfall event (IAEA, 2009). The highest values were observed for ^{140}Ba , which behaves similarly to strontium. Barium is a bivalent cation, and seems to be more strongly retained on the negatively charged plant surface than the monovalent caesium cation.

A mass interception of 1.4 and $0.7 \text{ (m}^2 \text{ kg}^{-1}\text{)}$ for ^{137}Cs and ^{90}Sr has been used by Golikov et al. (2004) in modelling the interception by lichen and subsequent transfer of these radionuclides through Arctic foodchains. Aside from the apparent discrepancy with observation for plants – where the magnitude of f_b is linked with valency – these values constitute a seldom characterization of the apposite process of interception for lichens. Using an assumed lichen biomass of 400 g m^{-2} based loosely on the information of Tømmervik et al. (2009), this information yields interception fractions, of 0.56 and 0.28 for Cs and Sr respectively.

Weathering rates for grass have been derived from the extensive analyses of data undertaken elsewhere (IAEA, 1996). Mitchell (2001) provides an overview of models concerning the transfer radionuclides to fruits. In order to model weathering of radionuclides on plant surfaces, an effective retention half-time was derived for use in the FARMLAND model. A single value of 11 d gave the best fit to experimental data giving a radionuclide independent rate constant of $6.3 \times 10^{-2} \text{ d}^{-1}$. The similarity of this value with those applied for grass has led to the application of the same default values for both vegetation categories. Golikov et al. (2004) modelled the loss of Cs-137 and Sr-90 from lichen using short-term and long-term ecological half-lives. For both radionuclides the short-term ecological half-life (1 and 2 years for ^{90}Sr and ^{137}Cs respectively) accounted for losses from the predominant fraction of deposited activity. Longer retention half-lives for Cs-137 in lichen have been reported by Kirchner & Daillant (2002), from their own and other studies, falling between 2.6 to 4.9 years. In view of these data and consideration of the fact that the long-term ecological half-life from Golikov et al. (2004) is ca. 20 years for ^{137}Cs and ^{90}Sr , a default weathering loss rate of 5 years, corresponding to the upper end of the values reported by Kirchner & Daillant (2002), has been applied for both radionuclides in our model.

The parameters have been assigned different default values as shown in Table D2. Two categories of flora – Wild grass/grasses, and shrubs – taken to be representative of berry plants such as *Vaccinium* spp.

Table D2. Parameters used in Terrestrial food-chain model.

Parameter	Dependencies : flora, radionuclide	Value	Units and notes	References
ρ_{soil}		1550	kg m ⁻³ typical soil densities for Finnmarksvidda range between 1.4 and 1.7 g cm ⁻³	Uhlig et al. (2004)
d_{soil}		0.05	m, Assumed depth of initial contamination following a deposition event	
f	Wild grass/grasses, Cs	0.43	(Unitless) f varies from 0.84 (dry deposition) to 0.027 (wet deposition heavy rain) (IAEA, 2010)	IAEA, 2010
f	Wild grass/grasses, Sr	0.66	Bivalent Sr-90 will have a higher f than monovalent Cs (see main text)	IAEA, 2009
f	Shrub, Cs	0.43	As for grass	
f	Shrub, Sr	0.66	As for grass	
f	Lichen, Cs	0.56		Golikov et al. (2004)
f	Lichen, Sr	0.28		
b	Wild grass/grasses	0.4	kg m ⁻²	Tømmervik et al. (2009)
b	Shrub	0.4	kg m ⁻²	
b	Lichen	0.4	kg m ⁻²	
$\lambda_{\text{flw,r}}$	Wild grass/grasses, Cs	5 x10 ⁻²	d ⁻¹ , Table VIII, p.37 (IAEA, 1996)	IAEA (1996)
$\lambda_{\text{flw,r}}$	Wild grass/grasses, Sr	5 x10 ⁻²	d ⁻¹ , As for Cs (see main text)	
$\lambda_{\text{flw,r}}$	Shrub, Cs	5 x10 ⁻²	d ⁻¹ , As for grass	
$\lambda_{\text{flw,r}}$	Shrub, Sr	5 x10 ⁻²	d ⁻¹ , As for grass and Cs	
$\lambda_{\text{flw,r}}$	Lichen, Cs	4 x10 ⁻⁴	d ⁻¹ ,	Kirchner & Daillant (2002)
$\lambda_{\text{flw,r}}$	Lichen, Sr	4 x10 ⁻⁴	d ⁻¹ ,	Kirchner & Daillant (2002)

The interception of Sr-90 has been taken to be a factor of (1.7/1.1) based upon the ratio of Ba-140 to Cs-137 for Chernobyl from IAEA (2009). According to Andersson et al. (2011), there are no clear differences between the weathering rates for grass that can be attributed to radiocesium and radiostrontium. From this observation the same default value has been used for both radionuclides.

Limitations to the use of concentration ratios³, CRs, arise from an incompatibility of the application of empirical data based on the long term post depositional conditions to the period directly following an accident. The CR values used (Table D3) are based on empirical datasets from field investigations collated to avoid inclusion of data pertaining to the period directly following depositional events (global fallout and Chernobyl accident deposition for some radionuclides such as Cs, Pu, Sr and Am) and thus should omit values pertaining to surface contamination of vegetation (Beresford et al., 2008b). These default CR data are generally assumed to correspond to, and thus are applicable for, a contaminated soil depth of 10

³ Concentration ratio = activity concentration in whole organism divided by activity concentration in soil

cm. There is thus an inconsistency with the observed distributions of radionuclides shortly following deposition. Using the Fukushima accident by way of example, Kato et al., (2012) reported that greater than 86% of total radiocaesium and 79% of total ^{131}I were absorbed in the upper 2.0 cm in a soil profile from a relatively contaminated cultivated area sampled, at the end of April 2011, in proximity to (< 50 km distant, in a northeasterly direction) the Fukushima Dai-ichi site. A default value of 5 cm has been used for the calculations undertaken in the current assessment. Furthermore, bioavailability of radiocaesium has been observed to decrease with time following its introduction to soils (Vidal et al., 1995) with the implication that CRs based upon long term post depositional datasets might not reflect the transfer occurring in the early phase depositional environment appropriately. Indeed this contention is evidenced by reviews of published information on Cs-137 in the soil-plant system shortly after the Chernobyl accident (Fesenko et al., 2009). Finally, soil type, as defined by various soil properties, strongly influences transfer to plants (IAEA, 2010) and there will undoubtedly be differences in the soil types upon which the default data are based and the soil types in Finnmark for which the transfer parameters are applied.

Table D3. CRs for terrestrial ecosystem from IAEA (2014) – arithmetic mean values.

Element	Organism	CR (Bq kg ⁻¹ f.w. per Bq kg ⁻¹ d.w)
Cs	Wildgrass/grasses	1.8
Sr	Wildgrass/grasses	1.8
Cs	Shrubs	2.3
Sr	Shrubs	0.5
Cs	Lichen	4.1
Sr	Lichen	4.8

Although some information exists on soil to grass transfer for the short term after accidents (Fesenko et al., 2009) these data are, by the author's own admission, insufficient for adequate (CR) estimation. This, coupled to the knowledge that, with the model constructed and parameterized in its current configuration, direct contamination by fallout dominates the total activity concentration in vegetation in the initial weeks of simulation renders the application of highly uncertain CR values relatively unimportant.

Contaminated lichens may be an important source of radiocaesium to reindeer during summer (Staaland et al., 1995). For this reason the CR data for this biota category is also included in Table D3 and for subsequent modelling calculations (see section 8.2.1).

It is important to note that output data for shrubs have been used as input to the assessment of ingestion doses for humans by assuming that shrub contamination levels provide a reasonable proxy for edible berries.

Finally, translocation is often accounted for in assessments with agricultural systems. Translocation is the process leading to the redistribution of a chemical substance deposited on the aerial parts of a plant to other parts that have not been contaminated directly (IAEA, 2010). Since the hypothetical accident has been assumed to coincide with the time of year when berries might be harvested the requirement to account for this process was not obvious and was therefore not attempted.

For mammals, examples of (bio)kinetic model for terrestrial environments have been published in the open literature and one of these, the so-called FASTer model, has been selected for further application (Brown et al., 2003b; Beresford et al., 2010). For herbivorous mammals, the input data used can be those specifying the activity concentrations in grass as expressed above. Details are required regarding biokinetic parameters for various representative animals/fauna as described below.

$$\frac{dC_{r,a}}{dt} = \sum_{i=1}^{i=n} \left(x_i \cdot AE_{r,i} \cdot \frac{FMI}{M} \cdot C_{r,i} \right) - C_{r,a} \cdot \lambda_{r,a}$$

[9]

Where :

x_i is the fraction of the diet associated with dietary component "i";

$AE_{r,i}$ is the assimilation efficiency (dimensionless) for radionuclide "r" within dietary component "i";

FMI/M is the ingestion rate per unit mass of animal (kg f.w. day^{-1} per kg f.w.);

$C_{r,i}$ is the activity concentration of radionuclide "r" in dietary component "i" (Bq kg^{-1} f.w.);

$C_{r,a}$ is the "whole-body" activity concentration of radionuclide "r" in the animal (Bq kg^{-1} f.w.); and

$\lambda_{r,a}$ is the effective loss rate of radionuclide "r" from animal (day^{-1}) incorporating both excretion rate and physical decay of the radionuclide.

This model has been applied to determine the transfer to deer/herbivorous mammal and rat/burrowing mammal.

A special note should be made of the use of output data from the FASTer model. As the activity concentrations predicted pertain to the whole body of reindeer some account needs to be taken of the consideration that people are not eating the entire animal, for example bone should be excluded. For this reason an additional factor was considered to account for the fraction of total body activity that is in the soft tissues of herbivores (relative units). A value of 1 for Cs and 0.1 for Sr was used in line with the assumption made in Beresford et al. (2008 b).

Fresh matter ingestion rates, FMI have been derived using allometric relationships of the form given in equation (10) as shown in Table D4. The masses for Rat/burrowing mammal have been extracted from ICRP (2008). Since for Deer/herbivorous mammal, the obvious candidate for analyses would be Reindeer (*Rangifer tarandus*), it is possible to be more specific with the appropriate masses to be used. Although selecting a representative mass for an adult of a particular species is not uncontentious, because of uncertainties associated with seasonal changes and differences between the sexes, a value of 100 kg, based on a cursory synthesis of the data collated by Finstad & Prichard (2000), might not be considered entirely groundless. The following allometric relationship can thus be applied:

$$\text{FMI} = a \cdot M^b \quad [10]$$

where

a is the multiplication constant in the allometric relationship for fresh matter intake for animal [kg d^{-1}] b is the exponent in the allometric relationship for fresh matter intake for animal [relative units] M is mass of the animal (kg)

Table D4. Fresh matter ingestion rates, FMI, for the various animals selected for study

Organism	FMI (kg/d)	Comments and references
Deer/herbivorous mammal	3.6E+00	Mass = 100 kg (Finstad. & Prichard (2000)); FMI for herbivores (kg d^{-1}) = $0.1995M^{0.628}$ from Nagy (2001)
Rat/burrowing mammal	8.4E-02	Mass = 0.314 kg (ICRP, 2008); FMI for Rodentia (kg d^{-1}) = $0.2296M^{0.864}$ from Nagy (2001)

Similarly, $\lambda_{r,a}$ the effective loss rate of radionuclide "r" from animal, a, can be derived using allometric relationships along with the animal masses specified above (Table D4).

Table D5. Allometric equations used to derive effective loss rates (d^{-1}) for studied animals from mass of animals (kg) (Brown et al., 2003b).

Radionuclide	Allometric equ.s
Cs	$\lambda_{r,a} = \frac{\ln 2}{18.36 M^{0.24}}$
Sr	$\lambda_{r,a} = \frac{\ln 2}{645 W^{0.26}}$

The various parameters required in the model runs are thus specified in Table D6.

Table D6. Parameters used in dynamic model runs.

Parameter	Dependencies : fauna, flora,radionuclide	Value	Units	Notes (references)
x_i	Grass (Deer)	0.75	dimensionless	Åhman (2007)
	Lichen (Deer)	0.25	dimensionless	
AE	Deer, Cs	1	dimensionless	USDoE (2002); USDoE(2002), ICRP 1979 (Part 1)
	Deer, Sr	0.3	dimensionless	
FMI/M	Deer	3.6E-02	kg f.w. day ⁻¹ per kg	(FMI/M)
	Rat	2.7E-01	kg f.w. day ⁻¹ per kg	(FMI/M)
$\lambda_{r,a}$	Deer, Cs	1.3E-02	d ⁻¹	Table vv; Mass = 100 kg
	Deer, Sr	3.2E-04	d ⁻¹	Table vv; Mass = 100 kg
	Rat, Cs	5.0E-02	d ⁻¹	Table vv; Mass = 0.314 kg
	Rat, Sr	1.5E-03	d ⁻¹	Table vv; Mass = 0.314 kg

The fraction dietary intake of lichen, grass and other vegetation in the diet of reindeer for the period in question is of course unknown but an assumption of 75 % grass intake by mass for September, as adopted by Åhman (2007), and assuming the rest of the diet comprises of lichen can be considered a reasonable first estimate. The inclusion of lichen in the summer diet will have the tendency to yield a conservative estimate of transfer to reindeer.

Glossary

Aggregated transfer factor

The ratio of the mass activity density (Bq kg^{-1}) in a specified object to the unit area activity density (Bq m^{-2}).

Allometric

The allometric approach is based on the observation that many metabolic parameters, including basal metabolic rates, ingestion rates, biological half times etc., are related (as power functions) to the masses of organisms.

Arctic Oscillation (AO)

The Arctic Oscillation (AO) can be described as changes in pressure between the arctic and mid-latitudes.

Assimilation efficiency

The efficiency by which animals convert the food they ingest into energy for growth and reproduction.

Barotropy

Barotropy is the condition and type of motion in which pressure is constant on surfaces of constant density, e.g. surface tides. Barotropic flow occurs when levels of constant pressure in the ocean are parallel to the surfaces of constant density.

Beaufort Gyre

The Beaufort Gyre is a wind-driven ocean current located in the Arctic Ocean polar region. It is a slowly swirling bowl of icy water covering an area of about $5.80\text{E}+05 \text{ km}^2$).

Biological half life

The time required for a biological system (e.g. animal or animal tissue) to eliminate, by natural processes, half the amount of a substance that has been absorbed into that system.

Concentration ratio (CR)

The ratio of the radionuclide concentration in the receptor biota tissue (fresh weight) from all exposure pathways (including water, sediment and ingestion/dietary pathways) to that in water.

Distribution coefficient (k_d)

Is the ratio of the mass of solute species absorbed or precipitated on the soil or sediment to the solute concentration in the water.

Dose conversion coefficient (DCC)

Represents the instantaneous dose rate per unit activity concentration of the radionuclide in an organism or in the environment.

Dynamic model

A mathematical model which incorporates time as an independent variable.

ECMWF

European Centre for Medium-Range Weather Forecasts

Empirical Orthogonal Function analysis

A method for decomposition of data which is often used to study possible spatial modes (i.e. patterns) of variability and how they change with time (e.g., The Arctic Oscillation).

Eolian process

Eolian processes are processes of relief formation resulting from the action of wind.

ERICA

The model developed under the ERICA project (Environmental Risks from Ionising Contaminants: Assessment and management).

Eulerian and Lagrangian approach

There are two ways to characterize a flow mathematically. One way is to indicate the velocity, as a function of time, for each individual fluid parcel (i.e., for each little bit of mass in the fluid) and follow each parcel as they move through space and time (Lagrangian approach). Another approach would be to define coordinates that are fixed in a reference frame and then to indicate the velocity of the fluid parcel that is flowing past a given point in that coordinate system, at a given time (Eulerian approach).

Exposure pathways

A route by which radiation or radionuclides can reach humans and cause exposure.

An exposure pathway may be very simple, e.g. external exposure from airborne radionuclides, or a more complex chain, e.g. internal exposure from drinking milk from cows that ate grass contaminated with deposited radionuclides.

Food chain

A linear series of species linked by specific *trophic* or feeding relationships, e.g. plant-herbivore-carnivore.

Frazil ice

Small pieces of ice that form in water moving turbulently enough to prevent the formation of a sheet of ice.

Kinetic model

A mathematical model which incorporates rate equations and is dynamic (time-dependent).

NAOSIM

North Atlantic/Arctic coupled Ocean Sea Ice Model

NetCDF

Network Common Data Form Is a set of software libraries and self-describing, machine-independent data formats that support the creation, access, and sharing of array-oriented scientific data.

NORA10-EI

NORwegian ReAnalysis 10km – Era Interim. A meteorological database developed for the purpose of this work using data from ECMWF Era-Interim project:

<http://www.ecmwf.int/en/research/climate-reanalysis/era-interim>

Occupancy factor

Refers to the fraction of the time that an organism spends in a specified habitat.

Radiation weighting factor

Its value represent the *relative biological effectiveness* of the different radiation types, relative to X- or gamma-rays, in producing endpoints of ecological significance.

Reference organisms

A series of entities that provide a basis for the estimation of radiation dose rate to a range of organisms that are typical, or representative, of a contaminated environment. These estimates, in turn, would provide a basis for assessing the likelihood and degree of radiation effects.

Resuspension

The physical transport of soil particles into the air by wind or other physical disturbance, or of bottom sediment particles into suspension by water currents or other physical disturbance.

Source term

Source term defines the amount and isotopic composition of radioactive material released (or postulated to be released following an accident) from an object /facility.

Spontaneous chain reaction

A reaction that initiates its own repetition is called chain reaction. A spontaneous chain reaction is a nuclear reaction which occurs spontaneously upon the presence of the right composition of nuclear fuel and water.

Sverdrup (Sv)

A measure of volume transport $1.0E+06 \text{ m}^3/\text{s}$. Used to measure the volumetric rate of transport of ocean currents.

Transfer factor (TF)

Is defined as the ratio of the activity density (Bq/kg or Bq/l) of a radionuclide in the receptor compartment to that in the donor compartment. In this report the term transfer factor is used as a generic term that includes CRs, CFs and activity concentration relative to annual deposited activity.

Transpolar Drift current

The Transpolar Drift Stream is a major ocean current of the Arctic Ocean, transporting sea ice from the Laptev Sea and the East Siberian Sea towards Fram Strait.

Trophic level

Functional classification of organisms in an ecosystem according to feeding relationships from first level autotrophs through succeeding levels of herbivores and carnivores.

References

- AMAP (1998). AMAP assessment report: Arctic pollution issues. Oslo: Arctic Monitoring and assessment programme (AMAP), 1998.
- Andersson KG, Mikkelsen T, Astrup P et al (2008). Estimation of health hazards resulting from a radiological terrorist attack in a city. *Radiation Protection Dosimetry* (2008); 131(3): 297-307.
- Andersson KG, Nielsen SP, Thørring H et al (2011). Revision of deposition and weathering parameters for the ingestion dose module (ECOSYS) of the ARGOS and RODOS decision support systems. *Journal of Environmental Radioactivity* 2011; 102(11): 1024-1031.
- Avila R, Beresford, NA, Aguero, A et al (2004). Study of the uncertainty in estimation of the exposure of non-human biota to ionising radiation. *J. Radiol. Prot.* 24, A105–A122.
- Avila R, Broed R, Pereira A (2005). ECOLEGO - a toolbox for radioecological risk assessment. In: *Protection of the environment from the effects of ionizing radiation: Proceedings of an international conference Stockholm, 6-10 October 2003*. STI/PUB/1229. Vienna: IAEA, 2005: 229-232.
- Backhaus JO (1985). A three-dimensional model for simulation of shelf sea dynamics. *Deutsche Hydrographische Zeitschrift* 1985; 38(4): 165-187.
- Baklanov A, Sørensen JH (2001). Parameterisation of radionuclide deposition in atmospheric long-range transport modeling. *Physics and Chemistry of the Earth (B)* 2001; 26(10): 787-799.
- Bartnicki J, Amundsen I, Brown J et al (2016). Atmospheric transport of radioactive debris to Norway in case of a hypothetical accident related to the possible recovery of the Russian submarine K-27. *Journal of Environmental Radioactivity* 2016; 151(part 2): 404-416.
- Bartnicki J, Salbu B, Saltbones J et al (2004). Long-range transport of large particles in case of nuclear accident or explosion. In: *Borrego C, Incencik S (eds.). Air pollution modelling and its application XVI*. New York: Springer, 2004: 77-86.
- Bartnicki J, Haakenstad H, Hov Ø (2011). Operational SNAP model for remote applications from NRPA. MET Report 12/2011. Oslo: Norwegian Meteorological Institute, 2011.
- Bartnicki J, Heiko K, Hosseini A et al (2013). Atmospheric transport of radioactive debris to Norway in case of a hypothetical accident related to the possible recovery of K-27 submarine. MET Report 21/2013. Oslo: Norwegian Meteorological Institute, 2013.
- Baxter MS, Harms IH, Osvath I et al (1998). Modelling the potential radiological consequences of radioactive waste dumping in the Kara Sea. *Journal of Environmental Radioactivity* 1998; 39(2): 161-181.
- Beresford NA, Barnett CL, Brown JE et al (2010). Predicting the radiation exposure of terrestrial wildlife in the Chernobyl exclusion zone: an international comparison of approaches. *Journal of Radiological Protection* 2010; 30(2): 341–373.
- Beresford NA, Barnett CL, Jones DG et al (2008a). Background exposure rates of terrestrial wildlife in England and Wales. *Journal of Environmental Radioactivity* 2008; 99(9): 1430–1439.
- Beresford NA, Barnett CL, Howard BJ et al (2008b). Derivation of transfer parameters for use within the ERICA Tool and the default concentration ratios for terrestrial biota. *Journal of Environmental Radioactivity* 2008; 99(9), 1393-1407.
- Brown J, Hosseini A, Børretzen P et al (2003a). Environmental impact assessments for the marine environment – transfer and uptake of radionuclides. *StrålevernRapport* 2003:7. Østerås: Norwegian Radiation Protection Authority, 2003.
- Brown J, Strand P, Hosseini A et al (2003b). Handbook for assessment of the exposure of biota to ionising radiation from radionuclides in the environment. FASSET deliverable 5. <https://wiki.ceh.ac.uk/display/rpemain/FASSET+reports> (22.03.2016)
- Brown JE, Alfonso B, Avila R et al (2008). The ERICA tool. *Journal of Environmental Radioactivity* 2008; 99(9): 1371-1383.
- Brown JE, Jones SR, Saxén R et al (2004a). Radiation doses to aquatic organisms from natural radionuclides. *Journal of Radiological Protection* 2004; 24(4A): A63-A77.
- Brown J, Børretzen P, Dowdall M et al. (2004b). The derivation of transfer parameters in the Assessment of Radiological Impacts to Arctic Marine Biota. *Arctic*, 57 (No.3), pp. 279-289.
- Buesseler KO (2012). Fishing for answers off Fukushima. *Science* 2012; 338(6106): 480-482.
- Carroll J, Harms IH (1999). Uncertainty analysis of partition coefficients in a radionuclide transport model. *Water Research* 1999; 33(11): 2617-2626.
- Colony R, Thorndike AS (1985). Sea ice motion as a drunkard's walk. *Journal of Geophysical Research* 1985; 90(C1): 965-974.

- Coughtrey PJ, Thorne MC (1983). Radionuclide distribution and transport in terrestrial and aquatic ecosystems: a critical review of data. Volume 1. Rotterdam: A.A. Balkema, 1983.
- Dethleff D, Nies H, Harms IH et al (2000). Transport of radionuclides by sea-ice and dense-water formed in western Kara Sea flaw leads. *Journal of Marine Systems* 2000; 24(3-4): 233-248.
- Dethleff D (1995). Sea ice and sediment export from the Laptev Sea flaw lead during 1991/92 winter season. In: Kassens H et al (eds.). Russian-German cooperation: Laptev Sea system. Reports on Polar Research 176. Bremerhaven: Kamlot, 1995: 78-93.
- Dethleff D, Kleine E, Loewe P (1994). Oceanic heat loss, sea ice formation and sediment dynamics in a turbulent Siberian flaw lead. In: Vihma T (ed.). Evening sessions of the summer school on physics of ice-covered seas, Savonlinna, Finland. Report series in geophysics 28. Helsinki: Department of Geophysics, University of Helsinki, 1994: 35-40.
- Dethleff D, Loewe P, Kleine E (1998). The Laptev Sea flaw lead - detailed investigation on ice formation and export during 1991/92 winter season. *Cold Regions Science and Technology* 1998; 27(3): 225-243.
- Duursma EK, Carroll J (1996). Environmental compartments: equilibria and assessments of processes between air, water, sediments and biota. Berlin: Springer-Verlag, 1996.
- EFSA (European Food Safety Authority) (2011). Use of the EFSA comprehensive European food consumption database in exposure assessment. *EFSA Journal* 2011; 9(3): 2097.
- Eicken H, Reimnitz E, Alexandrov V et al (1997). Sea-ice processes in the Laptev Sea and their importance for sediment export. *Continental Shelf Research* 1997; 17(2): 205-233.
- Fesenko S, Sanzharova N, Tagami K (2009). Evolution of plant contamination with time. In: Quantification of radionuclide transfer in terrestrial and freshwater environments for radiological assessments. IAEA-TECDOC 1616. Vienna: International Atomic Energy Agency (IAEA), 2009: 259-263.
- Finstad GL, Prichard AK (2000). Growth and body weight of free-range reindeer in western Alaska. *Rangifer* 2000; 20(4): 221-227.
- Fisher NS (2002). Advantages and problems in the application of radiotracers for determining bioaccumulation of contaminants in aquatic organisms. In: Børretzen P, Jølle T, Strand P (eds). Proceedings of the International conference on radioactivity in the environment, Monaco 1–5 September 2002. Østerås: Norwegian Radiation Protection Authority, 2002: 573–576.
- Frey, H.C. (1992). Quantitative Analysis of uncertainty and variability in environmental policy making. Research Associate Centre for Energy and Environmental Studies, Department of Engineering and Public Policy, Carnegie Mellon University, Pittsburgh.
- Føyn L, Nikitin A (1994). The joint Norwegian-Russian expedition to the dump sites for radioactive waste in the Abrosimov Fjord and the Stepovogo Fjord, August-September 1994. Bergen: Institute of Marine Research, 1994.
- Gerdes R., Karcher M, Kauker F et al (2001). Prediction for the spreading of radioactive substances from the Kursk. *EOS transactions* 2001; 82(23): 253, 256-257.
- Gerdes R., Hurka J, Karcher M et al (2005). Simulated history of convection in the Greenland and Labrador seas 1948-2001. In: Drange H, Dokken T, Furevik T et al. The Nordic seas: an integrated perspective. Washington DC: American Geophysical Union (AGU): 2005: 221-238.
- Golikov V, Logacheva I, Bruk G et al (2004). Modelling of long-term behaviour of caesium and strontium radionuclides in the Arctic environment and human exposure. *Journal of Environmental Radioactivity* 2004; 74(1-3): 159–169.
- Gómez-Ros JM, Pröhl G, Ulanovsky A et al (2008). Uncertainties of internal dose assessment for animals and plants due to non-homogeneously distributed radionuclides. *Journal of Environmental Radioactivity* 2008; 99(9): 1449-1455.
- Gwynn JP, Brown J, Kovacs KM et al (2006). The derivation of radionuclide transfer parameters for and dose-rates to an adult ringed seal (*Phoca hispida*) in an Arctic environment. *Journal of Environmental Radioactivity* 2006; 90(3): 197-209.
- Gwynn JP, Heldal HE, Gäfvert, T, et al (2012). Radiological status of the marine environment in the Barents Sea. *Journal of Environmental Radioactivity*, 2012; 113: 155–162.
- Haga PE (1991). Hvordan influerer nedbørprosessers tids- og romskala på langtransport av svoveldioksyd og partikulært sulfat? Master thesis. Oslo: Oslo University, 1991.
- Harms IH (1997). Modelling the dispersion of ¹³⁷Cs and ²³⁹Pu released from dumped waste in the Kara Sea. *Journal of Marine Systems* 1997; 13(1-4): 1-19.
- Harms IH, Karcher MJ (2003). Pathways of anthropogenic radionuclides in the Northern Oceans. In: Scott EM (ed.). Modelling radioactivity in the environment. Amsterdam: Elsevier, 2003: 287-314.
- Harms IH, Povinec PP (1999). The outflow of radionuclides from Novaya Zemlya bays: modelling and monitoring strategies. *Science of the Total Environment* 1999; 237-238: 193 – 201.

- Harms IH (1994). Numerische Modellstudie zur winterlichen Wassermassenformation in der Barentssee. Dissertation. Berichte aus dem Zentrum fuer Meeres- und Klimaforschung. Reihe B: Ozeanographie 7. Hamburg: Institut für Meereskunde, 1994.
- Harms IH, Karcher MJ, Dethleff D (2000). Modelling Siberian river runoff : implications for contaminant transport in the Arctic Ocean. *Journal of Marine Systems* 2000; 27(1-3): 95–115.
- Harms IH, Karcher MJ, Burchard H (2003). Modelling radioactivity in the environment: the application of hydrodynamic circulation models for simulating oceanic dispersion of radioactivity. In: Scott EM (ed.). *Modelling radioactivity in the environment*. Amsterdam: Elsevier, 2003: 55-86.
- Harms IH, Karcher M (2005). Kara Sea freshwater dispersion and export in the late 1990s. *Journal of Geophysical Research: Oceans* 2005; 110(C8). doi:[10.1029/2004JC002744](https://doi.org/10.1029/2004JC002744)
- Health Canada (1999). Recommendations on dose coefficients for assessing doses from accidental radionuclide releases to the environment. Ottawa: Radiation Protection Bureau, Health Canada, 1999.
- Heldal HE, Vikebø F, Johansen GO (2013). Dispersal of the radionuclide caesium-137 (¹³⁷Cs) from point sources in the Barents and Norwegian Seas and its potential contamination of the Arctic marine food chain: coupling numerical ocean models with geographical fish distribution data. *Environmental Pollution* 2013; 180: 190-198.
- Hibler WD III (1979). A dynamic thermodynamic sea ice model. *Journal of Physical Oceanography* 1979; 9(4): 815-846.
- Holloway G, Dupont F, Golubeva E et al (2007). Water properties and circulation in Arctic Ocean models. *Journal of Geophysical Research: Oceans* 2007; 112(C4): C04S03. doi:[10.1029/2006JC003642](https://doi.org/10.1029/2006JC003642).
- Holm E, Leisvik M, Ranebo Y et al (2005). Radioactivity in seals from the Swedish coast. In: Bréchnignac F, Howard BJ (eds.). *Scientific trends in radiological protection of the environment*. ECORAD 2004. Paris: Lavoisier, 2005: 85-95.
- Hosseini A, Amundsen I, Brown J et al (2015). Inventory and source term evaluation of the dumped nuclear submarine K-27. *StrålevernRapport 2015:6*. Østerås: Norwegian Radiation Protection Authority, 2015.
- Hosseini A, Beresford NA, Brown JE et al (2010). Background dose-rates to reference animals and plants arising from exposure to naturally occurring radionuclides in aquatic environments. *Journal of Radiological Protection* 2010; 30(2): 235–264.
- Howard BJ, Wright SM, Salbu B et al (2004). Long-term consequences for Northern Norway of a hypothetical release from the Kola nuclear power plant. *Science of the Total Environment* 2004; 327(1-3): 53–68.
- IAEA (1994). CRP on modelling of the radiological impact of radioactive waste dumping in the Arctic Seas: benchmarking scenarios: working material on the International Arctic Seas Assessment (IASAP). Vienna: IAEA, 1994.
- IAEA (1996). Modelling of radionuclide interception and loss processes in vegetation and of transfer in semi-natural ecosystems: second report of the VAMP Terrestrial Working Group. IAEA-TECDOC-857. Vienna: IAEA, 1996.
- IAEA (1998). Radiological conditions of the Western Kara Sea: assessment of the radiological impact of the dumping of radioactive waste ion the Arctic Seas. Radiological assessment reports series 4. Vienna: IAEA, 1998.
- IAEA (1999a). Inventory of radioactive waste disposals at sea. IAEA-TECDOC-1105. Vienna: IAEA, 1999.
- IAEA (1999b). Radioactivity in the Arctic Seas: report for the International Arctic Seas Assessment Project (IASAP). IAEA-TECDOC-1075. Vienna: IAEA, 1999.
- IAEA (2003). Determining the suitability of materials for disposal at sea under the London Convention 1972: a radiological assessment procedure. IAEA-TECDOC-1375. Vienna: IAEA, 2003.
- IAEA (2004). Sediment distribution coefficients and concentration factors for biota in the marine environment. Technical reports series 422. Vienna: IAEA, 2004.
- IAEA (2009). Quantification of radionuclide transfer in terrestrial and freshwater environments for radiological assessments. IAEA-TECDOC-1616. Vienna: IAEA, 2009.
- IAEA (2010). Handbook of parameter values for the prediction of radionuclide transfer in terrestrial and freshwater environments. IAEA technical report series 472. Vienna: IAEA, 2010.
- IAEA (2014). Handbook of parameter values for the prediction of radionuclide transfer to wildlife. Technical report series 479. Vienna: IAEA, 2014.
- IAEA (2015a). Determining the suitability of materials for disposal at sea under the London Convention 1972 and London Protocol 1996: a radiological assessment procedure. IAEA-TECDOC-1759. Vienna: IAEA, 2015.
- IAEA (2015b). The Fukushima Daiichi consequences: radiological consequences. Technical volume 4/5. Vienna: IAEA, 2015. <http://www-pub.iaea.org/MTCD/Publications/PDF/AdditionalVolumes/P1710/Pub1710-TV4-Web.pdf> (01.04.2016).
- ICRP (1977). Recommendations of the International Commission on Radiological Protection. ICRP publication 26. *Annals of the ICRP* 1977; 1(3).
- ICRP (1979). Limits for intakes of radionuclides by workers. ICRP publication 30 (Part 1). *Annals of the ICRP* 1979; 2(3-4).

- ICRP (2009). Environmental protection: transfer parameters for reference animals and plants. ICRP publication 114. *Annals of the ICRP* 2009; 39(6).
- ICRP (2012). Compendium of dose coefficients based on ICRP Publication 60. ICRP publication 119. *Annals of the ICRP* 2012; 41(Suppl.).
- ICRP (2014). Protection of the environment under different exposure situations. ICRP publication 124. *Annals of the ICRP* 2014; 43(1).
- ICRP (1995a). Age-dependent doses to members of the public from intake of radionuclides - part 3 ingestion dose coefficients. ICRP publication 69. *Annals of the ICRP* 1995; 25(1).
- ICRP (1995b). Age-dependent doses to members of the public from intake of radionuclides - part 4 inhalation dose coefficients. ICRP publication 71. *Annals of the ICRP* 1995; 25(3-4).
- ICRP (2007). The 2007 recommendations of the International Commission on Radiological Protection. ICRP publication 103. *Annals of the ICRP* 2007; 37(2-4).
- ICRP (2008). Environmental protection: the concept and use of reference animals and plants. ICRP publication 108. *Annals of the ICRP* 2008; 38(4-6).
- IPCS (2014). Guidance document on evaluating and expressing uncertainty in hazard characterization. The International Programme on Chemical Safety (IPCS). Harmonization Project Document 11. World Health Organization, ISBN 978 92 4 150761 5.
- Johansson L, Solvoll K, Bjørneboe G-E A et al (1997). Dietary habits among Norwegian men and women. *Scandinavian Journal of Nutrition* 1997; 41(1):63-70.
- JNREG (1994). Radioactive contamination at dumping sites for nuclear waste in the Kara Sea: results from the Russian Norwegian 1993 expedition to the Kara Sea. Østerås: Norwegian Radiation Protection Authority, 1994.
- JNREG (2014). Investigation into the radioecological status of Stepovogo Fjord. The dumping site of the nuclear submarine K-27 and solid radioactive waste. Results from the 2012 research cruise. Edited by Justin P. Gwynn and Alexander I. Nikitin. Norwegian Radiation Protection Authority, Østerås.
- Kalnay E, Kanamitsu M, Kistler R et al (1996). The NCEP/NCAR 40-year reanalysis project. *Bulletin of the American Meteorological Society* 1996; 77(3): 437-495.
- Karcher MJ, Harms IH, Smith JM (1998): Long range transport of ¹²⁹I and ¹³⁷Cs in the Nordic Seas and the Arctic Ocean. In: *Marine pollution: proceedings of a symposium held in Monaco, 5-9 October 1998*. IAEA-TECHDOC-1094. Vienna: IAEA, 1999: 193-198.
- Karcher MJ, Gerdes R., Kauker F et al (2003a). Arctic warming: evolution and spreading of the 1990s warm event in the Nordic Seas and the Arctic Ocean. *Journal of Geophysical Research* 2003; 108(C2): 3034.
- Karcher M, Gerdes R., Kauker F (2008). Long-term variability of Atlantic water inflow to the Northern Seas: insights from model experiments. In: Dickson B, Meincke J, Rhines P (eds.). *Arctic-Subarctic ocean fluxes: defining the role of the Northern Seas in climate*. Dordrecht: Springer, 2008: 1-13.
- Karcher M, Harms I, Standing WJ et al (2010). On the potential for climate change impacts on marine anthropogenic radioactivity in the Arctic regions. *Marine Pollution Bulletin* 2010; 60(8): 1151-1159.
- Karcher M, Gerdes R, Kauker F (2006). Modeling of delta 18O and 99 Tc dispersion in Arctic and subarctic seas. *ASOF Newsletter* 2006; 5: 19-20.
- Karcher M, Smith JN, Kauker F et al (2012). Recent changes in Arctic Ocean circulation revealed by iodine-129 observations and modelling. *Journal of Geophysical Research: Oceans* 2012; 117(C8).
- Karcher MJ, Kulakov M, Pivovarov S et al (2003b). Atlantic water flow to the Kara Sea: comparing model results with observations. In: Stein R, Fahl K, Fütterer DK et al (eds.). *Siberian River runoff in the Kara Sea: characterisation, quantification, variability and environmental significance*. *Proceedings in Marine Science* 6. Burlington, Elsevier Science, 2003: 47-69.
- Karcher MJ, Gerland S, Harms IH et al (2004). The dispersion of ⁹⁹Tc in the Nordic Seas and the Arctic Ocean: a comparison of model results and observations. *Journal of Environmental Radioactivity* 2004; 74(1-3): 185-198.
- Karlsen SR, Elvebakk A, Høgdal KA et al (2006). Satellite based mapping of the growing season and bioclimatic zones in Fennoscandia. *Global Ecology and Biogeography* 2006; 15(4): 416-430.
- Kato H, Onda Y, Teramaga M (2012). Depth distribution of ¹³⁷Cs, ¹³⁴Cs, and ¹³¹I in soil profile after Fukushima Dai-ichi nuclear power plant accident. *Journal of Environmental Radioactivity* 2012; 111: 59-64.
- King SE, Carroll J, Johnson JR et al (1997). Transport of caesium in the Kara Sea. In: Germain P, Guray JC, Guegueniat P et al (eds.). *Radionuclides in the oceans : RADOCS 96-97 Proceedings: Part 1 Inventories, behaviour and processes*. RADOCS 96-97 Cherbourg-Octeville 1996 Symposium. Radioprotection – colloquies, volume 32(C2). Les Ulis, France: Les éditions de physique (EDP sciences), 1997: 231.

- Kirchner G, Daillat O (2002). The potential of lichens as long-term biomonitors of natural and artificial radionuclides. *Environmental Pollution* 2002; 120(2002): 145–150.
- Krinitzky VS (1989). Peculiarities of biology and distribution of commercial fish in the Yenisey Gulf. *GOSNIORH: Collated scientific papers* 296: 130-141. (In Russian)
- Köberle C, Gerdes R (2003). Mechanisms determining the variability of Arctic sea ice conditions and export. *Journal of Climate* 2003; 16(17): 2843–2858.
- Kocher DC (1987). A proposal for a generally applicable de minimis dose. *Health Physics* 1987; 53(2): 117-121.
- Komperød M, Rudjord AL, Skuterud L et al (2015). Radiation doses from the environment. Calculations of the public's exposure to radiation from the environment in Norway. *StrålevernRapport 2015:11*. Østerås: Norwegian Radiation Protection Authority, 2015 (In Norwegian).
- Koziy L, Maderich V, Margvelashvili N et al (1998). Three-dimensional model of radionuclide dispersion in estuaries and shelf seas. *Environmental Modelling & Software* 1998; 13(5-6): 413–420.
- Landrum PF, Lee H, Lydy MJ (1992). Toxicokinetics in aquatic systems: model comparison and use in hazard assessment. *Environmental Toxicology and Chemistry* 1992; 11(12): 1709–1725.
- Larsson CM (2008). An overview of the ERICA Integrated Approach to the assessment and management of environmental risks from ionising contaminants. *Journal of Environmental Radioactivity* 2008; 99(9): 1364-1370.
- Lemke P, Owens WB, Hibler WD (1990). A coupled sea ice-mixed layer-pycnocline model for the Weddell Sea. *Journal of Geophysical Research* 1990; 95(C6): 9513-9525.
- Liland A, Lochard J, Skuterud L (2009). How long is long-term? Reflections based on over 20 years of post-Chernobyl management in Norway. *Journal of Environmental Radioactivity* 2009; 100(7): 581-584.
- Martin S, Cavalieri DJ (1989). Contributions of the Siberian shelf polynyas to the Arctic Ocean intermediate and deep water. *Journal of Geophysical Research* 1989; 94(9): 12725-12738.
- Maryon RH, Smith JB, Conway BJ et al (1991). The UK nuclear accident model. *Progress in Nuclear Energy* 1991, 26(2): 85-104.
- Maryon RH, Saltbones J, Ryall DB et al (1996). An intercomparison of three long range dispersion models developed for the UK Meteorological Office, DNMI and EMEP. *Turbulence and diffusion note 234*. Bracknell, UK: Meteorological Office, 1996.
- Maykut GA (1986). The surface heat and mass balance. I: Untersteiner N (ed.). *Geophysics of sea ice*. NATO ASI series B 146. New York: Plenum Press, 1986: 395-463.
- Maykut GA, Untersteiner N (1971). Some results from a time dependent thermodynamic model of sea ice. *Journal of Geophysical Research* 1971; 76(6): 1550-1575.
- Meese DA, Reimnitz E, Tucker III WB et al (1997). Evidence for radionuclide transport by sea-ice. *Science of the Total Environment* 1997; 202(1-3): 267-278.
- Mitchell NG (2001). Models for radionuclide transfer to fruits and data requirements. *Journal of Environmental Radioactivity* 2001; 52(2-3): 291-307.
- Nagy KA (2001). Food requirements of wild animals: predictive equations for free-living mammals, reptiles, and birds. *Nutrition Abstracts and Reviews Series B Livestock Feeds and Feeding* 2001; 71(10): 21R–32R.
- NES, 2013. *Sunken K-27 Nuclear Submarine Recovery: Risk Overview*. Nuclear and Environmental Safety Magazine Nr. 1, 2013.
- Nies H, Bahe C, Dethleff D, Harms I et al (1997). Transport and dispersion of artificial radioactivity in the Arctic Ocean: model studies and observations. In: Germain P, Guray JC, Guegueniat, P et al (eds.). *Radionuclides in the oceans: RADOX 96-97 Proceedings: Part 1 Inventories, behaviour and processes*. RADOX 96-97 Cherbourg-Octeville 1996 Symposium. Radioprotection – colloquies, volume 32(C2). Les Ulis, France: Les éditions de physique (EDP sciences), 1997: 406-416.
- Nies H, Harms IH, Karcher M et al (1999). Anthropogenic radioactivity in the Arctic Ocean: review of the results from the joint German project. *Science of the Total Environment* 1999; 237/238: 181-191.
- Nies H, Harms IH, Karcher MJ et al (1998). Anthropogenic radioactivity in the Nordic Seas and the Arctic Ocean: Results from a joint project. *Deutsche Hydrographische Zeitschrift* 1998; 50(4): 313-343.
- NFB (2014). *Nordic "Flag Book": Protective measures in early and intermediate phases of a nuclear or radiological emergency. Nordic guidelines and recommendations*. The Radiation Protection Authorities in Denmark, Finland, Iceland, Norway and Sweden.
- NRPA (2011). *Radioactivity in the marine environment 2008 and 2009. Results from the Norwegian National Monitoring Programme (RAME)*. StrålevernRapport 2011:4. Østerås: Norwegian Radiation Protection Authority, 2011.
- NRPA (2015). *Radioactivity in the Marine Environment 2011. Results from the Norwegian Marine Monitoring Programme (RAME)*. StrålevernRapport 2015:3. Østerås: Norwegian Radiation Protection Authority, 2015.

- Nürnberg D, Wollenburg D, Dethleff D et al (1994). Sediments in Arctic sea ice: implications for entrainment, transport and release. *Marine Geology* 1994; 119(3-4): 185-214.
- Pacanowski RC (1995). MOM 2 Documentation, user's guide and reference manual. GFDL Ocean Group Technical Report 3. Princeton, NJ: Geophysical Fluid Dynamics Laboratory, 1995.
- Parkinson CL, Washington WM (1979). A large scale numerical model of sea ice. *Journal of Geophysical Research* 1979; 84(C1): 311-337.
- Pavlov VK, Kulakov MY, Stanovoy VV (1993). Oceanographical description of the Kara and Barents Sea. Report to the International Arctic Seas Assessment Program (IASAP). IAEA working material. Vienna: IAEA, 1993.
- Pavlov V, Pavlova O, Korsnes R (2004). Sea ice fluxes and drift trajectories from potential pollution sources, computed with a statistical sea ice model of the Arctic Ocean. *Journal of Marine Systems* 2004; 48(1): 133-157.
- Pavlov VK, Pfirman SL (1995). Hydrographic structure and variability of the Kara Sea: implications for pollutant distribution. *Deep Sea Research Part II* 1995; 42(6): 1369-1390.
- Persson C, Baklanov A, Sørensen H et al (2007). Nordic network of meteorological services engaged in nuclear emergency preparedness: NKS-MetNet. NKS-147. Roskilde: Nordic Nuclear Safety Research (NKS), 2007.
- Pfirman S, Colony R, Nürnberg D et al (1997b). Reconstructing the origin and trajectory of drifting Arctic sea-ice. *Journal of Geophysical Research* 1997; 102(C6): 12575-12586.
- Pfirman S, Eicken H, Bauch D et al (1995). The potential transport of pollutants by Arctic sea ice. *Science of the Total Environment* 1995; 159(2-3): 129-146.
- Pfirman S, Kögele JW, Rigor I (1997a). Potential for rapid transport of contaminants from the Kara Sea. *Science of the Total Environment* 1997; 202(1-3): 111-122.
- Preller RH, Cheng A (1999). Modelling the transport of radioactive contaminants in the arctic. *Marine Pollution Bulletin* 1999; 38(2): 71-91.
- Roache PJ (1972). On artificial viscosity. *Journal of Computational Physics* 1972; 10(2): 169-184.
- Sarkisov AA, Sivintsev YV, Vysotskiy VL et al (2009). Atomic legacy of the cold war at the Arctic seabed: radioecological consequences and technical and economic problems of radiation remediation at the Arctic Seas. Moscow: Nuclear Safety Institute, 2009.
- Sazykina TG (1998). Long-distance radionuclide transfer in the Arctic Seas related to fish migrations. *Radiation Protection Dosimetry* 1998; 75(1-4): 219-222.
- Schino G, Borfecchia F, De Cecco L, et al (2003). Satellite estimate of grass biomass in a mountainous range in central Italy. *Agroforestry Systems* 59: 157-162, 2003.
- Scott EM, Gurbutt P, Harms I et al (1997). Benchmarking of numerical models describing the dispersion of radionuclides in the Arctic Seas. *Science of the Total Environment* 1997; 202(1-3): 123-134.
- Seinfeld JH (1986). Atmospheric chemistry and physics of air pollution. New York: Wiley, 1986.
- Semtner AJ (1976). A model for the thermodynamic growth of sea ice in numerical investigations of climate. *Journal of Physical Oceanography* 1976; 6(3): 379-389.
- Skuterud L, Gwynn JP, Gaare E et al (2005). ⁹⁰Sr, ²¹⁰Po and ²¹⁰Pb in lichen and reindeer in Norway. *Journal of Environmental Radioactivity* 2005; 84(3): 441-456.
- Staaland H, Garmo TH, Hove K et al (1995). Feed selection and radiocaesium intake by reindeer, sheep and goats grazing alpine summer habitats in southern Norway. *Journal of Environmental Radioactivity* 1995; 29(1): 39-56.
- Steele M, Morley R, Ermold W (2001). PHC: a global ocean hydrography with a high quality Arctic Ocean. *Journal of Climate* 2001; 14(9): 2079-2087.
- Stepanets OV, Kodina LA, Ligaev AN et al (2006). Radiochemical studies of the features of radionuclide distribution at the sites of dumping of radioactive wastes of the Novaya Zemlya Archipelago. *Geochemistry International* 2006; 44(12): 1215-1224.
- Stevens DP (1991). *The open boundary condition in the United Kingdom fine-resolution Antarctic model*. *Journal of Physical Oceanography* 1991; 21(9): 1494-1499.
- Strand P, Aono T, Brown J et al. (2014). Assessment of Fukushima-derived radiation doses and effects on wildlife in Japan. *Environmental Science and Technology Letters* 2014; 1(3): 198-203.
- Stronach JA, Backhaus JO, Murty TS (1993). An update on the numerical simulation of oceanographic processes in the waters between Vancouver Island and the mainland: the GF8 model. *Oceanography and Marine Biology: an Annual Review* 1993; 31: 1-86.
- Thomann RV (1981). Equilibrium model of fate of microcontaminants in diverse aquatic food-chains. *Canadian Journal of Fisheries and Aquatic Sciences* 1981; 38(3): 280-296.

- Thørring H, Hosseini A, Skuterud L (2004). Kostholdsundersøkelser 1999 og 2002. Reindrifstutøvere i Midt-Norge. StrålevernRapport 2004:14. Østerås: Statens strålevern, 2004.
- Thørring H, Skuterud L (2012). Radioaktiv forurensning i befolkningen: reindrifstutøvere og andre personer i Kautokeino 1965-2010. StrålevernRapport 2012:11. Østerås: Statens strålevern, 2012.
- Thørring H, Ytre-Eide MA, Liland A (2010). Consequences in Norway after a hypothetical accident at Sellafield - Predicted impacts on the environment. StrålevernRapport 2010:13. Østerås: Statens strålevern, 2010.
- Tømmervik H, Johansen B, Riseth JA et al (2009). Above ground biomass changes in the mountain birch forests and mountain heaths of Finnmarksvidda, northern Norway, in the period 1957–2006. *Forest Ecology and Management* 2009; 257(1): 244–257.
- Uhlig C, Sveistrup TE, Schjelderup I (2004). Impacts of reindeer grazing on soil properties on Finnmarksvidda, northern Norway. *Rangifer* 2004; 24(Special Issue 15): 83-91.
- Ulanovsky A, Pröhl G, Gómez-Ros JM (2008). Methods for calculating dose conversion coefficients for terrestrial and aquatic biota. *Journal of Environmental Radioactivity* 2008; 99(9): 1440-1448.
- Ulanovsky A, Prohl G (2006). A practical method for assessment of dose conversion coefficients for aquatic biota. *Radiation and Environmental Biophysics* 2006; 45(3): 203-214.
- UNSCEAR (2008). Sources and effects of ionizing radiation, UNSCEAR 2008 report: Volume II: Annex E: Effects of ionizing radiation on non-human biota. New York: United Nations, 2008.
- UNSCEAR (2014). Sources, effects and risks of ionizing radiation, UNSCEAR 2013 report: Volume I: Annex A: Levels and effects of radiation exposure due to the nuclear accident after the 2011 great east-Japan earthquake and tsunami. New York: United Nations, 2014.
- USDoE (2002). A graded approach for evaluating radiation doses to aquatic and terrestrial biota. Technical Standard DOE-STD-1153-2002. Washington DC: U.S. Department of Energy, 2002.
- Van der Sluijs, J.P. (2007). Uncertainty and precaution in environmental management: Insights from the UPEM conference. *Environmental Modelling & Software* 22 (2007) 590 -598.
- Vidal M, Roig M, Rigol A et al (1995). Two approaches to the study of radiocaesium partitioning and mobility in agricultural soils from the Chernobyl area. *Analyst* 1995; 120(6): 1785-1791.
- Vives i Batlle J, Wilson RC, Watts SJ et al (2008). Dynamic model for the assessment of radiological exposure to marine biota. *Journal of Environmental Radioactivity* 2008; 99(11): 1711-1730.
- Vives i Batlle J, Aono T, Brown JE et al (2014). The impact of the Fukushima nuclear accident on marine biota: retrospective assessment of the first year and perspectives. *Science of the Total Environment* 2014; 487: 143-153.
- Walker, WE, Harremoës, P, Rotmans, J, et al (2003). Defining Uncertainty A Conceptual Basis for Uncertainty Management in Model-Based Decision Support. *Integrated Assessment*, 2003, Vol. 4, No. 1, pp. 5–17.
- Watson WS, Sumner DJ, Baker JR et al (1999). Radionuclides in seals and porpoises in the coastal waters around the UK. *Science of the Total Environment* 1999; 234(1-3): 1-13.
- Whicker FW, Schultz V (1982). Kinetics of compartment systems. In: *Radioecology: nuclear energy and the environment*, volume II. Boca Raton, FL: CRC Press, 1982: 64-117.
- Wienerroither R, Johannesen E, Dolgov A et al (2011). Atlas of the Barents Sea fishes. IMR/PINRO joint report series 1-2011. Bergen: Institute of Marine Research, 2011.
- Åhman B (2007). Modelling radiocaesium transfer and long-term changes in reindeer. *Journal of Environmental Radioactivity* 2007; 98(1-2): 153-165.
- Åsbakk K, Stuen S, Hansen H et al (1999). A serological survey for brucellosis in reindeer in Finnmark county, northern Norway. *Rangifer* 1999; 19(1): 19-24.



Statens strålevern
Norwegian Radiation Protection Authority

2016

StrålevernRapport 2016:1

Årsrapport

StrålevernRapport 2016:2

Scales for Post-closure Assessment Scenarios (SPACE)

StrålevernRapport 2016:3

Nettbasert tilsyn med industriell radiografi

StrålevernRapport 2016:4

Regulatory Cooperation Program between Norwegian Radiation Protection Authority and Russian Federation

StrålevernRapport 2016:5

Regulatory Supervision of Legacy Sites: from Recognition to Resolution

StrålevernRapport 2016:6

Kartlegging av radon på Svalbard og Jan Mayen

StrålevernRapport 2016:7

Regulatory support in radiation safety and radioactive waste management in Central Asia

StrålevernRapport 2016:8

Environmental modelling and radiological impact assessment associated with hypothetical accident scenarios for the nuclear submarine K-27

ISSN 1891-5191 (online)

ISSN 0804-4910 (print)